

**DUAL INHIBITORS OF FATTY ACID AMIDE HYDROLASE  
AND SOLUBLE EPOXIDE HYDROLASE ENZYMES  
AS POTENTIAL THERAPEUTICS FOR  
TREATING PULMONARY  
FIBROSIS**

**A Thesis By**

**STEPHANIE R. WILT  
ORCID iD: 0000-0002-4898-0250**

**California State University, Fullerton  
Spring, 2022**

---

**In partial fulfillment of the degree:**

Master of Science in Chemistry

**Department:**

Department of Chemistry and Biochemistry

**Committee:**

Stevan Pecic, Department of Chemistry and Biochemistry, Chair  
Nicholas Salzameda, Department of Chemistry and Biochemistry  
Peter de Lijser, Department of Chemistry and Biochemistry

**DOI:**

10.5281/zenodo.6578749

**Keywords:**

structure-activity relationship, enzyme inhibition, polypharmacology, microwave-assisted synthesis, docking experiments, ADMET predictions

**Abstract:**

Fatty acid amide hydrolase (FAAH) is a membrane protein that hydrolyzes endocannabinoids, such as anandamide, which possesses analgesic, anti-inflammatory, and anti-fibrotic properties, resulting in arachidonic acid. Arachidonic acid is involved in pro-inflammatory pathways, such as cyclooxygenase, lipoxygenase, and soluble epoxide hydrolase (sEH) pathways. sEH hydrolyzes anti-inflammatory and anti-fibrotic epoxyeicosatrienoic acids to pro-inflammatory dihydroxyeicosatetraenoic acids. Designed multiple ligands (DMLs) are small molecules specifically designed to interact with several biological targets involved in multifactorial diseases, such as pain, cancer, Alzheimer's disease, and pulmonary fibroses. In this project, we used DMLs strategies to design drugs that will simultaneously inhibit sEH and FAAH enzymes which could produce a therapeutic effect for those suffering from idiopathic pulmonary fibrosis and chronic pain related to it. Here using *in silico* methodologies, microwave-assisted green chemistry synthesis, and *in vitro* assays, we have designed, synthesized, and biologically evaluated over 60 compounds. In addition, the best inhibitor discovered in this study was evaluated *in vivo* in a rat model of acute pain. We were able to establish a clear structure-activity relationships and identified benzothiazole and 4-phenylthiazole moieties as the important groups to inhibit these two enzymes in the low nanomolar range as well showing favorable predictions of several pharmacokinetic/pharmacodynamic properties.

## TABLE OF CONTENTS

LIST OF TABLES .....	iv
LIST OF FIGURES .....	v
ACKNOWLEDGMENTS .....	viii
Chapter	
1. INTRODUCTION.....	1
Idiopathic Pulmonary Fibrosis (IPF) .....	1
Predisposition, Activation, and Progression .....	2
Treatments .....	4
IPF and COVID-19.....	8
Cannabinoids .....	8
Fatty Acid Amide Hydrolase .....	11
Arachidonic Acid and Cytochrome P450.....	14
Soluble Epoxide Hydrolase.....	15
Designed Multiple Ligands – A Polypharmacology Approach.....	18
Proposed Research and Design.....	21
2. RESULTS AND DISCUSSION .....	25
FAAH Inhibitors: 2-naphthyl and 4-phenylthiazoles.....	25
Design, Synthesis, and SAR .....	25
Homology Model.....	26
Docking Experiments .....	32
Predicting ADME-Tox Properties.....	40
Dual FAAH and sEH Inhibitors: Benzothiazoles .....	43
Design and Synthesis.....	43
Biological Evaluation and SAR.....	46
Molecular Modeling Studies .....	48
Predicting ADME-Tox Properties.....	63
Dual FAAH and sEH inhibitors: 4-phenylthiazoles.....	67
Design and Synthesis.....	67
Biological Evaluation and SAR.....	71
Molecular Modeling Studies .....	73
Predicting ADME-Tox Properties.....	84
<i>In vivo</i> Analysis of Antinociception.....	86
3. CONCLUSIONS.....	89
4. EXPERIMENTAL .....	90
Materials and Methods.....	90
Synthesis, Assay, and Modeling of 2-naphthyl and 4-phenylthiazoles Analogs.....	90
General Procedure (Figure 56) for the Preparation of Naphthyl Analogs 1-1 to 1-3.....	93
General Procedure (Figure 57) for the Preparation of 4-phenylthiazole Analogs 2-1 to 2-7	96
OMP Synthesis (Figure 58).....	99
Synthesis, Assay, and Modeling of Benzothiazole-phenyl Analogs.....	100
General Procedure for the Preparation of Benzothiazole-phenyl Analogs.....	100

sEH and FAAH IC50 Assay Conditions Human FAAH Enzyme Inhibition Assay .....	110
Synthesis, Assay, and Modeling Studies of Additional 4-phenylthiazole Analogs.....	111
General Procedure for the Preparation of 4-1 to 4-16.....	111
General Procedure for the Preparation of Anilines 5-12 to 5-16.....	117
Biological Evaluation .....	118
Molecular Modeling .....	119
Formalin Test .....	120
APPENDIX: NUCLEAR MAGNETIC RESONANCE DATA .....	121
REFERENCES .....	190

## LIST OF TABLES

<u>Table</u>	<u>Page</u>
1. IPF Genes.....	3
2. IPF Clinical Trials.....	5
3. What Check Results for Human FAAH Homology Model .....	31
4. FAAH Inhibitory Activity and Docking Scores of Analogs 1-1 to 1-3 and 2-1 to 2-7 .....	33
5. Non-covalent Interactions of 4-phenylthiazole Series .....	35
6. Predicted ADME-Tox Properties 1-1 to 1-3 and 2-1 to 2-7 .....	41
7. Inhibitory Activities and Docking Scores for Analogs 3-1 to 3-30 .....	48
8. a) FAAH Interactions of Docked Analogs for 4-1 to 4-30 .....	52
b) sEH Interactions of Docked Analogs for 4-1 to 4-30.....	55
9. Predicted ADMET Properties 4-1 to 4-30 .....	64
10. Inhibitory Activities and Docking Scores for 4-1 to 4-30.....	69
11. Effects of 60 Minutes Preincubation on Potency.....	73
12. FAAH Interactions of Docked Analogs 3-5 and 4-15 .....	78
13. sEH Interactions of Docked Analogs 3-5 and 4-15 .....	82
14. Predicted ADMET Properties for Selected Dual sEH/FAAH Inhibitors.....	85

## LIST OF FIGURES

<u>Figure</u>	<u>Page</u>
1. Normal Lung Tissues vs IPF Lung Tissue.....	3
2. Chemical Structure of THC .....	9
3. Cannabinoid Receptors.....	10
4. Chemical Structures for AEA, 2-AG, and AJA.....	11
5. Hydrolysis of AEA by FAAH .....	11
6. Catalytic Triad and Mechanism for FAAH .....	12
7. Various Known Types of Inhibitors for FAAH .....	14
8. Arachidonic Cascade .....	16
9. First Generation sEH Inhibitors.....	17
10. Second Generation sEH Inhibitors.....	17
11. Inhibitor TPPU's Impact on Bleomycin Induced Fibrosis .....	18
12. FDA Approval for Fixed vs Single Dose Medications.....	19
13. Endocannabinoid System.....	20
14. Multitarget Merged Ligands.....	21
15. Isobologram for TPPU and URB937.....	22
16. Benzothiazole FAAH Inhibitor .....	22
17. Known sEH Inhibitors and Their SAR Studies .....	23
18. Design of New FAAH Inhibitors .....	25
19. Multiple Sequence Alignment of FAAH Enzymes .....	27
20. Sequence Alignment of Rat and Human FAAH .....	27
21. Superimposed Homology Model of Human and Rat FAAH .....	28
22. Ramachandran Plot of Human FAAH Homology Model .....	29
23. Errat Analysis of Human FAAH Homology Model .....	30
24. Verify 3D Analysis of Human FAAH Homology Model.....	30
25. Z-score Results from Prove Test of Homology Model .....	31
26. Docking Results for Inhibitor 2-6.....	36

27.	Docking Results for Inhibitor 2-7.....	37
28.	Docking Results for Inhibitor 2-1.....	38
29.	Docking Results for Inhibitor 2-2.....	38
30.	Docking Results for Inhibitor 2-3.....	39
31.	Docking Results for Inhibitor 2-4.....	39
32.	Docking Results for Inhibitor 2-5.....	40
33.	Known FAAH and sEH Inhibitors.....	44
34.	Design Strategy for Synthesis of Dual sEH/FAAH Inhibitors .....	45
35.	Inhibitory Potency vs Docking Scores for FAAH Enzyme.....	59
36.	3D Docking Results for Inhibitor 3-5 in FAAH Enzyme.....	60
37.	2D Docking Results for Inhibitor 3-5 in FAAH Enzyme.....	60
38.	Inhibitory Potency vs Docking Scores for sEH Enzyme.....	61
39.	3D Docking Results for Inhibitor 3-5 in sEH Enzyme.....	62
40.	2D Docking Results for Inhibitor 3-5 in sEH Enzyme.....	63
41.	Design Strategy Used to Optimize New Dual Inhibitors.....	67
42.	2D Image of Inhibitor URB597 in Catalytic Site of Human FAAH.....	74
43.	3D Image of Inhibitor URB597 in Catalytic Site of Human FAAH.....	74
44.	2D Image of Inhibitor AUDA in Catalytic Site of Human FAAH .....	75
45.	3D Image of Inhibitor AUDA in Catalytic Site of Human FAAH .....	76
46.	2D Docking Results for Inhibitor 4-15 in FAAH Enzyme.....	77
47.	3D Docking Results for Inhibitor 4-15 in FAAH Enzyme.....	77
48.	2D Docking Results for Inhibitor 3-5 in FAAH Enzyme.....	79
49.	3D Docking Results for Inhibitor 3-5in FAAH Enzyme.....	79
50.	2D Docking Results for Inhibitor 4-15 in sEH Enzyme.....	80
51.	3D Docking Results for Inhibitor 4-15 in sEH Enzyme.....	81
52.	2D Docking Results for Inhibitor 3-5 in sEH Enzyme.....	83
53.	3D Docking Results for Inhibitor 3-5 in sEH Enzyme.....	83
54.	Proposed Pharmacophore for Dual Inhibitors Based on the Binding of 4-15.....	84

55.	Antinociceptive Effects of 3-5 Against Formalin-induced Inflammatory Pain .....	87
56.	Reaction Scheme for 1-1 to 1-3 .....	91
57.	Reaction Scheme for 2-1 to 2-7 .....	92
58.	Reaction Scheme for OMP .....	92
59.	Reaction Scheme for 4-1 to 4-16 .....	93
60.	Reaction Scheme for 5-12 to 5-16 .....	93

## **ACKNOWLEDGMENTS**

I would like to thank to our many collaborators: Dr. Bruce D. Hammock, Dr. Christophe Morisseau and Dr. Sean Kodani from UC Davis, Dr. Ram Kandasamy from CSU East Bay, Dr. Amir A. Zeki, MD from UC Davis School of Medicine and Dr. Paula K. Hudson for help with HRMS.

I would like to express my gratitude to my committee members: Dr. Peter de Lijser and Dr. Nicholas Salzameda, the Department of Chemistry and Biochemistry for the opportunity to study here, and my fellow graduate students for their support.

I also would like to thank my research advisor Dr. Stevan Pecic for all of his help, I could not have asked for a better mentor!

Finally, I wish to express my thanks to my husband for always supporting me, my son for uplifting me, and Montero for helping me focus.



## CHAPTER 1

### INTRODUCTION

Interstitial lung disease (ILD) is a broad term for different lung disorders that lead to scarring of lung tissue (Antoniou et al., 2014). Hallmarks of ILD are cell proliferation, inflammation, and/or fibrosis. These diseases are considered ILD if they are not due to infection or cancer (Lederer & Martinez, 2018). ILD can result in a decrease in quality of life and even death. These lung disorders are further classified as major, rare, and unclassified. Of the different lung disorders that are observed in this classification, idiopathic pulmonary fibrosis (IPF) is regarded as the most lethal (Antoniou et al., 2014).

#### **Idiopathic Pulmonary Fibrosis**

Idiopathic pulmonary fibrosis was first named in 1838 by DJ Corrigan who called it 'cirrhosis of the lung'. Next, in 1893, William Osler coined it 'chronic interstitial pneumonia' but kept cirrhosis of the lung as an alternate in the text *Principles and Practice of Medicine*. Finally, in 1948, Laurence L. Robbins used the term 'idiopathic pulmonary fibrosis'. All of these were associated with a condition in which the tissue in the lungs had fibrosis or thickening in the walls of the lungs (Wolters et al., 2018). IPF is not localized to one area of the world although it affects North America notably more than other regions of the world. In the United States, there was a reported rate of 10-60 cases per 100,000 people, but these numbers increase significantly for the elderly (494 cases per 100,000) (Esposito et al., 2015; Lederer & Martinez, 2018; Raghu et al., 2014; Raghu et al., 2016). Globally there is an estimated rate of 2.8-9.3 per 100,00 per year with Asian and South American countries being the least impacted (Barratt, Creamer, Hayton, & Chaudhuri, 2018; Hopkins, Burke, Fell, Dion, & Kolb, 2016; Navaratnam et al., 2011; Raghu et al., 2014). Symptoms include dry cough, abnormal lung sounds, reduced force vital capacity (FVC), and reduced total lung capacity. Diagnosis is normally determined after a high-resolution computerized tomography (CT) scan (Barratt et al., 2018; Lederer & Martinez, 2018). Prognosis is poor with half of sufferers succumbing to the disease or associated

illness in an average of 2 to 6 years, due to poor outcomes care which is generally directed towards slowing progression (Bjoraker et al., 1998; du Bois, 2012; Ley et al., 2011).

### **Predisposition, Activation, and Progression**

The word idiopathic for IPF can be misleading as it makes one think the disease pathway is unknown. While some aspects of IPF are unknown there have been many genes discovered in conjunction with the condition. In over eleven different regions in gene sequences, Table 1, multiple different genes have been identified as contributing to IPF: ABCA3, DKC1, MUC5B, PARN, RTEL1, SFTPC, SFTPA2, TERC, TERT, and TINF2. MUC5B, which encodes for mucin proteins, contains a promoter variant that was identified in eleven separate studies as being a risk indicator for IPF (Wolters et al., 2018). Three of these genes, ABCA3, SFTPC, and SFTPA2, correspond to alveolar stability by regulating surfactant proteins (Zhou et al., 2016). Telomeres, the protective ends of the chromosome, are maintained by telomerases. Telomeres lose material on their ends when cell division happens and telomerases help to keep these telomeres from shortening (Shammas, 2011). The genes TERT and TERC encode for telomerase and short telomere lengths were found in IPF patients due to mutations within these genes. DKC1 encodes for telomerases and is associated with dyskeratosis congenita (DC) which is found in about 20% of IPF patients. Dyskeratosis congenita is a rare condition one is born with wherein there is an irreversible degeneration of tissues and is also associated with the aforementioned genes: PARN, RTEL1, and TINF2 (Savage & Alter, 2009). RTEL1 specifically is found in the loci for DC as well and patients with mutations in RTEL1 were found to have shortened telomeres (Zhou et al., 2016).

There are also environmental and lifestyle factors that contribute to IPF. Inflammation and cell proliferation are common with IPF as collagen deposits in the lung tissue, as such, inhalants, infections, age, and other damage may cause this condition (Wolters et al., 2018). Activation of IPF can be due to disease affecting the lungs, exposures, and genetic factors such as some autoimmune disorders; although, these are not always found to be the cause (Lederer & Martinez, 2018). Typically one has a predisposition and exposure that activates the disease. During the progression of IPF, the

proliferation of cells occurs, fibrotic tissue starts to replace typical alveolar tissue, the tissue starts to build up, and stiffness occurs, see Figure 1 (Wolters et al., 2018). IPF is so lethal largely due to the progressive and irreversible nature of the disease which cumulates in an average life expectancy of only 3 to 5 years (Antonioni et al., 2014; Lederer & Martinez, 2018).

Table 1. Identified IPF related genes and their relevant associations

Gene	Abbreviation	Purpose
Adenosine Triphosphate (ATP) Binding Cassette Subfamily A Member 3	ABCA3	Provide alveolar stability by regulating surfactants proteins
Dyskerin Pseudouridine Synthase 1	DKC1	Telomere stabilization and maintenance, associated with dyskeratosis congenita
Mucin 5B	MUC5B	Major gel-forming mucin in mucus
Poly (A)-Specific Ribonuclease	PARN	Targets degradation of specific human mRNA, associated with dyskeratosis congenita
Regulator of Telomere Elongation Helicase 1	RTEL1	Associated with decreased telomere lengths and dyskeratosis congenita
Surfactant Protein C	SFTPC	Provide alveolar stability by regulating surfactants proteins
Surfactant Protein A2	SFTPA2	Provide alveolar stability by regulating surfactants proteins
Telomerase RNA Component	TERC	Encode for telomerase (maintains telomere length)
Telomerase Reverse Transcriptase	TERT	Encode for telomerase (maintains telomere length)
TERF Interacting Nuclear Factor 2	TINF2	Encodes for shelterin, one protein that protects telomeres, associated with dyskeratosis congenita

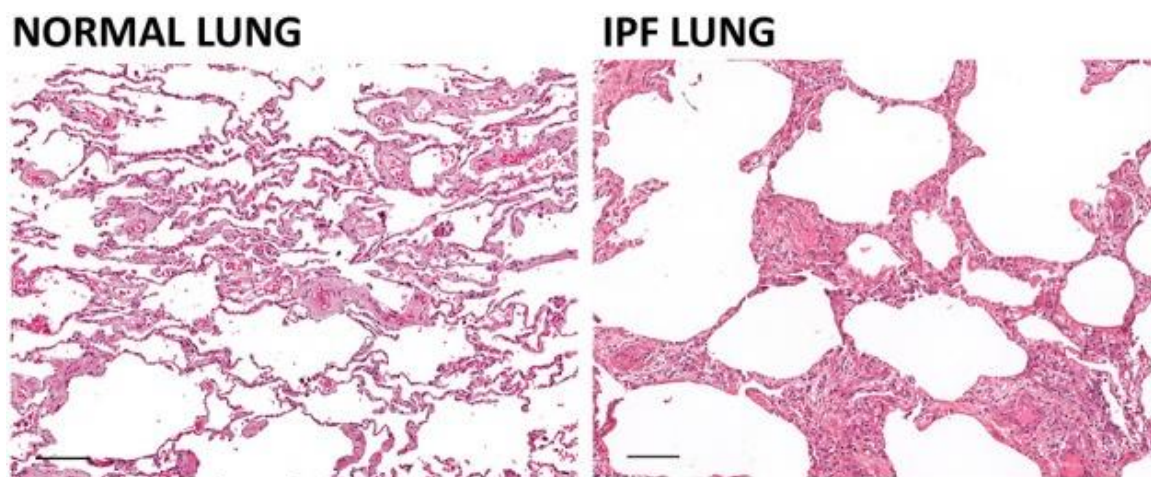


Figure 1. Comparison of normal lung tissue and tissue affected by IPF. IPF tissues show thickening due to fibrosis. Figure taken from Gardet et al., 2013.

## Treatments

Many different treatment options have been explored but most have moderate efficacy, adverse side effects, and/or are still in clinical trials (Somogyi et al., 2019). Combination therapies are commonly used to treat ailments and due to IPF's complicated nature, this approach is often utilized for treatment. In a 12-week study with 105 IPF patients, nintedanib alone was compared to a combination of nintedanib (kinase inhibitor) plus pirfenidone (pyridone). This study did not confirm efficacy but did find that the participants had similar side effects with the exception of the combination causing more nausea (Somogyi et al., 2019). In 2012 a study was published that concluded that the combination of antioxidant *N*-Acetylcysteine, the immunosuppressants prednisone, and azathioprine increased the risk of death and hospitalization (Idiopathic Pulmonary Fibrosis Clinical Research et al., 2012). Another study in 2016 found that the combination of these compounds after 12-months showed improved forced vital capacity in patients (King et al., 2011). Novel therapies on their own have been tried, such as the anti-inflammatory drug pirfenidone. Pooled data from two different phase-3 trials with pirfenidone showed the treatment increased the forced vital capacity in participants (King et al., 2011). Nintedanib and pirfenidone have been studied both together and independently with promising results to suggest that they ease suffering but also contribute to several adverse side effects such as gastrointestinal issues, photosensitivity, and increase liver function (Barratt et al., 2018). A trial utilizing Pentraxin (PRM-151), a protein that prevents differentiation of monocytes into pro-fibrotic fibrocytes, was done with positive outcomes as IPF patients have low levels of this protein naturally. Several different antibody-based therapies are currently being tested as well (Somogyi et al., 2019). Mesenchymal stem cell therapy has been explored for tissue regeneration but has not yet been tested in IPF patients, only in bleomycin-lung models (King et al., 2011). Lung transplantation and rehabilitation therapies can be used but these have limited efficacy (King et al., 2011; Somogyi et al., 2019). Currently, there are 33 registered phase 3 trials with the U.S. National Library of Medicine's ClinicalTrials.gov, for IPF treatments, Table 2 (NIH, 2021).

Table 2. Clinical trials registered with NIH for treatment of IPF with their location and current status.

	Study Name	Status	Intervention	Location
1	Minocycline Therapy for Lung Scarring in Patients With Idiopathic Pulmonary Fibrosis - a Pilot Study	Unknown	Drug: minocycline	UCLA Pulmonary Outpatient Clinic, Los Angeles, California, United States
2	Efficacy and Safety of Pirfenidone in Patients With Idiopathic Pulmonary Fibrosis (IPF)	Has Results	Drug: Pirfenidone, Placebo	InterMune Inc., Brisbane, California, United States
3	Open-Label Study of the Long Term Safety of Pirfenidone in Patients With Idiopathic Pulmonary Fibrosis (IPF)	Has Results	Drug: pirfenidone	Genentech, Inc., South San Francisco, California, United States
4	Safety and Efficacy of Pirfenidone in Patients With Idiopathic Pulmonary Fibrosis	Has Results	Drug: Pirfenidone, Placebo	InterMune, Inc., Brisbane, California, United States
5	Three-Arm Study of the Safety and Efficacy of Pirfenidone in Patients With Idiopathic Pulmonary Fibrosis	Has Results	Drug: Pirfenidone, Placebo	InterMune, Inc., Brisbane, California, United States
6	Treatment of Chronic Cough in Idiopathic Pulmonary Fibrosis With Thalidomide	Has Results	Drug: Thalidomide, Placebo	Johns Hopkins Bayview Medical Center, Baltimore, Maryland, United States
7	A Study of the Safety and Efficacy Interferon-Gamma 1b in Patients With Idiopathic Pulmonary Fibrosis (IPF)	Completed - Results Not Available	Drug: Interferon-gamma 1b	University of Washington Medical Center, Seattle, Washington, United States
8	The INSPIRE Trial: A Study of Interferon Gamma-1b for Idiopathic Pulmonary Fibrosis	Terminated - No Results Available	Drug: Interferon gamma-1b ("Actimmune")	InterMune, Inc., Brisbane, California, United States
9	Targeting Vascular Reactivity in Idiopathic Pulmonary Fibrosis	Terminated - Results Available	Drug: Sildenafil, Losartan, combination Sildenafil and Losartan, Placebo Oral Tablet	University of Iowa Hospitals and Clinics, Iowa City, Iowa, United States
10	An Open-Label Study of the Safety of Interferon Gamma-1b in Patients With IPF	Terminated - No Results Available	Drug: Interferon gamma-1b	InterMune Inc, Brisbane, California, United States
11	Evaluation of Efficacy and Safety of Pamrevlumab in Patients With Idiopathic Pulmonary Fibrosis	Recruiting	Drug: Pamrevlumab Drug: Placebo	Multiple Locations - Worldwide
12	A Study to Evaluate Long Term Safety and Efficacy of Recombinant Human Pentraxin-2 (rhPTX-2; PRM-151) in Participants With Idiopathic Pulmonary Fibrosis	Recruiting	Drug: PRM-151	Multiple Locations - Worldwide
13	A Study to Evaluate the Efficacy and Safety of Recombinant Human Pentraxin-2 (rhPTX-2; PRM-151) in Participants With Idiopathic Pulmonary Fibrosis	Recruiting	Drug: PRM-151, Placebo	Multiple Locations - Worldwide

	Study Name	Status	Intervention	Location
14	A Clinical Study to Test How Effective and Safe GLPG1690 is for Subjects With Idiopathic Pulmonary Fibrosis (IPF) When Used Together With Standard of Care	Terminated - No Results Available	Drug: GLPG1690, Placebo	Multiple Locations - Worldwide
15	A Clinical Study to Test How Effective and Safe GLPG1690 is for Subjects With Idiopathic Pulmonary Fibrosis (IPF) When Used Together With Standard of Care	Terminated - No Results Available	Drug: GLPG1690, Placebo	Multiple Locations - Worldwide
16	Efficacy and Safety of Nintedanib Co-administered With Sildenafil in Idiopathic Pulmonary Fibrosis Patients With Advanced Lung Function Impairment	Has Results	Drug: Nintedanib, Placebo, Sildenafil	Multiple Locations - Worldwide
17	Extension Trial of the Long Term Safety of BIBF 1120 in Patients With Idiopathic Pulmonary Fibrosis	Has Results	Drug: BIBF 1120	Multiple Locations - Worldwide
18	Nintedanib Twice Daily vs Placebo in Patients Diagnosed With Idiopathic Pulmonary Fibrosis (IPF)	Has Results	Drug: Matching Placebo, Nintedanib	Multiple Locations - Worldwide
19	AntiCoagulant Effectiveness in Idiopathic Pulmonary Fibrosis	Terminated - Results Available	Drug: warfarin, Placebo	Multiple Locations - USA
20	Open Label Extension Study in Patients With Idiopathic Pulmonary Fibrosis Who Completed Protocol AC-052-321/ BUILD 3 / NCT00391443	Has Results	Drug: Bosentan	Multiple Locations - Worldwide
21	Study of Efficacy and Safety of Inhaled Treprostinil in Subjects With Idiopathic Pulmonary Fibrosis	Recruiting	Drug: Placebo, Inhaled Treprostinil Device: Treprostinil Ultrasonic Nebulizer	Multiple Locations - USA
22	CleanUP IPF for the Pulmonary Trials Cooperative	Terminated - Results Available	Drug: Antimicrobial therapy: Co-trimoxazole or Doxycycline Other- No Intervention: Standard of Care	Multiple Locations - USA
23	(ARTEMIS-IPF) Randomized, Placebo-Controlled Study to Evaluate Safety and Effectiveness of Ambrisentan in IPF	Terminated - Results Available	Drug: Ambrisentan, Placebo	Multiple Locations - Worldwide
24	ARTEMIS-PH - Study of Ambrisentan in Subjects With Pulmonary Hypertension Associated With Idiopathic Pulmonary Fibrosis	Terminated - Results Available	Drug: Ambrisentan, Placebo	Multiple Locations - Worldwide
25	BUILD 3: Bosentan Use in Interstitial Lung Disease	Has Results	Drug: Bosentan, Placebo	Multiple Locations - Worldwide
26	Prospective Treatment Efficacy in IPF Using Genotype for Nac Selection (PRECISIONS) Trial	Recruiting	Drug: N-acetyl cysteine, Placebo	Multiple Locations - USA
27	Sildenafil Trial of Exercise Performance in Idiopathic Pulmonary Fibrosis	Has Results	Drug: Sildenafil Citrate, Placebo	Multiple Locations - USA

	Study Name	Status	Intervention	Location
28	Efficacy and Safety of Oral Bosentan in Patients With Idiopathic Pulmonary Fibrosis	Completed - Results Not Available	Drug: bosentan, Placebo	Multiple Locations - Worldwide
29	Safety and Efficacy of BIBF 1120 at High Dose in Idiopathic Pulmonary Fibrosis Patients	Has Results	Drug: Placebo, BIBF 1120	Multiple Locations - Worldwide
30	Safety and Efficacy of BIBF 1120 at High Dose in Idiopathic Pulmonary Fibrosis Patients II	Has Results	Drug: Placebo, BIBF 1121	Multiple Locations - Worldwide
31	EZ-2053 in the Prophylaxis of Acute Pulmonary Allograft Rejection	Has Results	Biological: Placebo, EZ-2053, EZ-2053 5mg/kg	Multiple Locations - Worldwide
32	Evaluating the Effectiveness of Prednisone, Azathioprine, and N-acetylcysteine in Patients With IPF	Has Results	Drug: N-acetylcysteine (NAC), Placebo	Multiple Locations - USA
33	Efficacy and Safety of Oral Bosentan in Pulmonary Fibrosis Associated With Scleroderma	Completed - Results Not Available	Drug: Bosentan	Multiple Locations - Worldwide

## IPF and COVID-19

Due to infection, injury, and age being contributing factors to IPF, there is reason to believe that a lasting outcome of COVID-19 exposure may be IPF. While at this point the full scope of long-term damage cannot be known, it is known that many of those infected with COVID-19 suffer from pneumonia and lung injury, both of which are associated with IPF. Another genetically comparable coronavirus, Severe Acute Respiratory Syndrome-1 (SARS-1), is known to have similar pulmonary effects and in a 15 year follow up study, 4.6% of the recovered showed lung abnormalities and decreased lung function. Another study of Middle East Respiratory Syndrome (MERS) patients showed lung fibrosis after an average of 43 days recovered, which is not long-term data, but does give evidence of potential lifelong consequences (George et al., 2020; Spagnolo et al., 2020). Early data shows that of 108 patients that have been discharged from the hospital, 25% had reduced lung capacity after having COVID-19 (George et al., 2020). It will take many years to know for certain if COVID-19 exposure may cause IPF but there is evidence to support that this could occur. Additionally, those with IPF are at increased risk for more severe complications if infected with COVID-19 (Prevention, 2021).

## Cannabinoids

There are two cannabinoid receptors, CB1 and CB2, which are located within neurons and within the immune system, respectively. These receptors are class A, G-protein coupled receptors (GPCR), with transmembrane alpha-helices which are believed to serve as the binding sites for ligands (Reggio, 2010). There are at least 60 cannabinoids in the *cannabis* plant but most do not activate CB1 or CB2. Phytocannabinoids are cannabinoids that are found in marijuana and contain  $\Delta^9$ -tetrahydrocannabivarin (THC), the psychoactive ingredient in marijuana (Figure 2). Phytocannabinoids are partial agonists to both CB1 and CB2 receptors providing inflammation and pain relief that is more powerful than many over-the-counter medications; however, they also bind other targets in mixed agonist-antagonist capacities which can result in unwanted psychotropic effects (Ahn et al., 2009; Howlett et al., 2002; Morales et al., 2017). Cannabidiol is an extract from



THC that does have anti-inflammatory effects by decreasing TNF-  $\alpha$  and reducing fatty acid amide hydrolase (FAAH) activity. Synthetic cannabinoids are chemically synthesized to be used as chemical agonists for disease treatments. Another category, endocannabinoids, is a class that activates CB1 and CB2 receptors (Zurier & Burstein, 2016). Synthetic cannabinoids can be problematic due to a lack of regulation and speed at which they can enter the market. They bind cannabinoid receptors as potent agonists, inducing the same psychotropic effects as THC, and can have dangerous side effects such as tachycardia, stroke, and death (Cha et al., 2019; Pertwee, 2010; Tait et al., 2016).

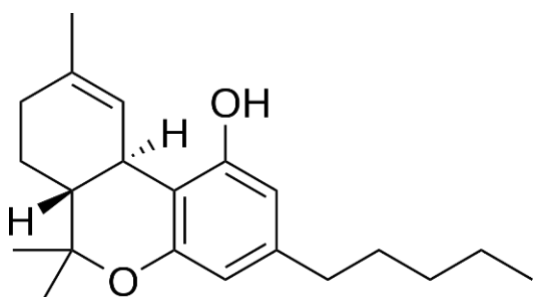
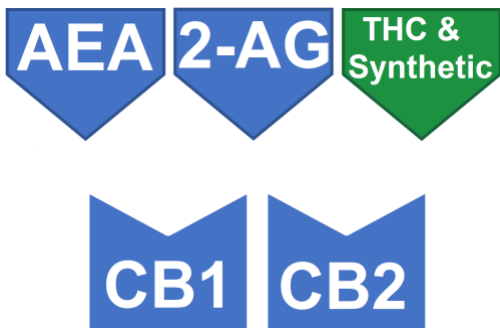


Figure 2. Chemical structure of THC

Endocannabinoids are endogenous cannabinoid lipids that are able to activate CB1 and CB2 receptors, see Figure 3. They are released by neurons through immune responses which put them in the prime location for the CB receptors. Two specific endocannabinoids, anandamide (AEA) and 2-arachidonoylglycerol (2-AG), are precursors for arachidonic acid, see Figure 4. Lipophilic regions of AEA bind the hydrophobic pocket of the transmembrane helices in the cannabinoid receptors and it is thought that 2-AG would bind in a similar manner, although AEA has a slightly higher affinity for CB1 than 2-AG does (Ashton et al., 2008; McAllister et al., 2003; Pertwee, 2010). The endogenous cannabinoid system is linked with several pathways and processes within the body, including but not limited to: cardiovascular disruptions such as hypertension and cardiogenic shock, liver cirrhosis, neurological disorders such as Alzheimer's, Parkinson's, and Huntington's disease, anxiety, and depression (Behl et al., 2020; Berry et al., 2020; Centonze et al., 2007; Giménez et al., 2018; Scotter et al., 2010). The wide reach of the endocannabinoid system shows there are a lot of avenues in which therapies may be explored with AEA and 2-AG displaying promise of relief without psychotropic

effects like synthetic cannabinoids and THC. AEA is able to help alleviate pain when available, but availability is an issue as it is activated on-demand from lipid precursors and is readily metabolized by FAAH (Bisogno & Maccarrone, 2013; Di Marzo, 2008; D. Piomelli, 2003).



*Figure 3.* Cannabinoid receptors 1 and 2 with endocannabinoids AEA, 2-AG, THC and synthetic potential ligands.

In a study by Zurier et al. (2016) a synthetic cannabinoid receptor for AEA, ajulemic acid (AJA) (Figure 4), was administered and it was determined to act on CB receptors stimulating necrosis factors, prostaglandin J2, and lipoxin A4, which in turn decreased inflammation. Furthermore, there was a decrease in transforming growth factor-beta (TGF $\beta$ ) production and signaling, leading to a decrease in collagen production in fibroblasts, resulting in a reduction of fibrotic material produced. When higher concentrations were administered there was also stimulation of peroxisome proliferator-activated receptor gamma (PPAR $\gamma$ ) also decreasing the amount of fibrotic collagen being produced (Zurier & Burstein, 2016). AEA is also be a key mediator in pulmonary hypoxia by increasing arterial tone (Wenzel et al., 2013). 2-AG plays a role in pain and inflammation as it has been seen that inhibition of receptors that remove 2-AG ameliorates symptoms (Alhouayek et al., 2014; Guindon & Beaulieu, 2009). This ligand can act on CB2 receptors, CB2 receptor activation causes a reduction in pro-inflammatory cytokine release (Leleu-Chavain et al., 2013; Patsenker et al., 2015).

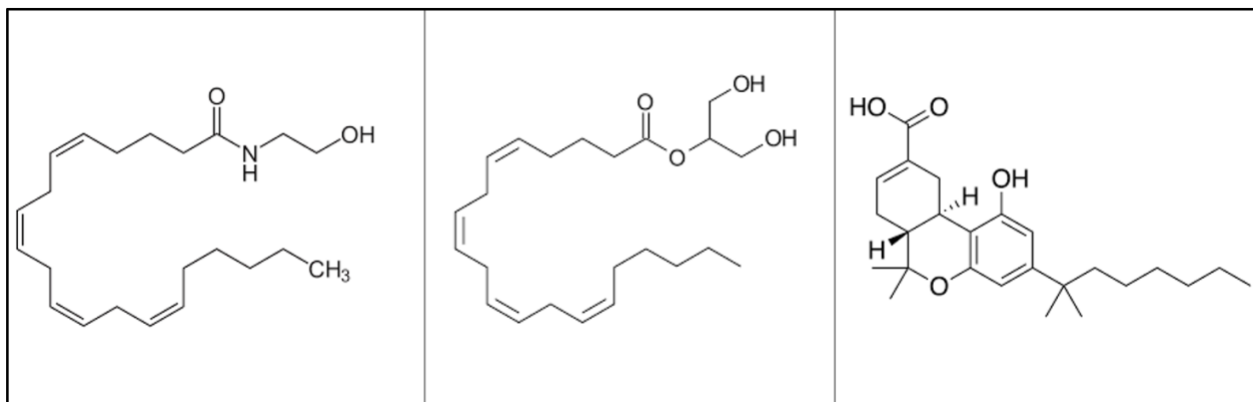


Figure 4. Chemical structures for AEA, 2-AG, and AJA respectively

### Fatty Acid Amide Hydrolase

AEA is hydrolyzed by the integral membrane enzyme, FAAH, forming arachidonic acid (AA) and ethanolamine, see Figure 5, and these metabolites do not activate the aforementioned CB receptors. FAAH knockout mice were found to be healthy despite FAAH gene interruption, furthermore, 50 to 100 fold hydrolysis reduction was achieved by this gene targeting (McKinney & Cravatt, 2003). FAAH enzyme can be found distributed throughout the body via the nervous system and is primarily found in intracellular membranes (Ahn et al., 2009). FAAH is part of the amidase family and is found in both prokaryotes and eukaryotes. FAAH is specifically different in that it has structural differences that likely contribute to its biochemical capabilities. FAAH has been extracted from rats and crystalized showing at least a dimeric configuration in the solution (McKinney & Cravatt, 2005).

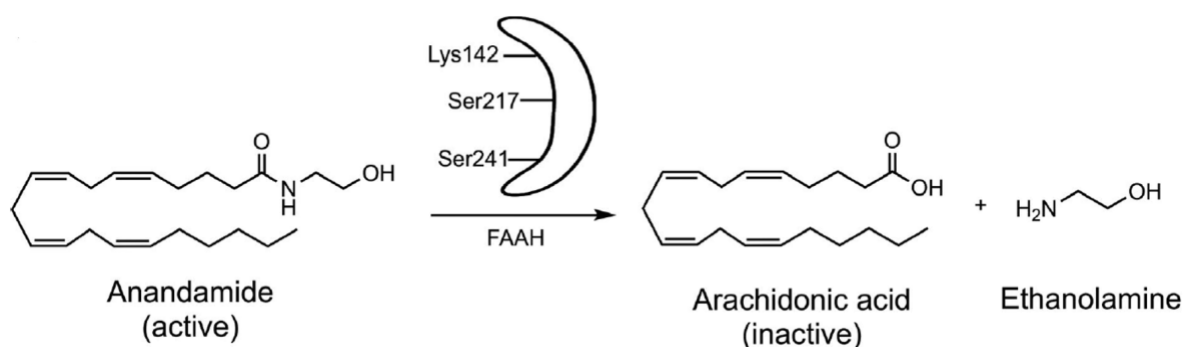


Figure 5. Hydrolysis of AEA by FAAH forms metabolites AA and ethanolamine.

X-ray crystallography of rat enzyme shows that FAAH possesses a catalytic triad (Figure 6) of serine-serine-lysine (**S241–S217–K142**) which is hypothesized to perform the catalytic cleavage of the amide bond in AEA. Further investigation discovered that **K142** acts as a base and is protonated by **S217**, then a proton is transferred from **S241** to **S217**. **S241**, as a nucleophile attacks the carbonyl of the amide bond in AEA. **S217** is now able to act as an acid and donate a proton to the nitrogen atom of the amide substrate, resulting in a partial charge which makes it a good leaving group. **S241** and the carbonyl product forms an acyl-enzyme as an intermediate, as **K142** and **S217** share a proton. AA is released as a free fatty acid product when a water molecule interacts. Finally, the residues in the triad will return to their initial protonation states (Ahn et al., 2009).

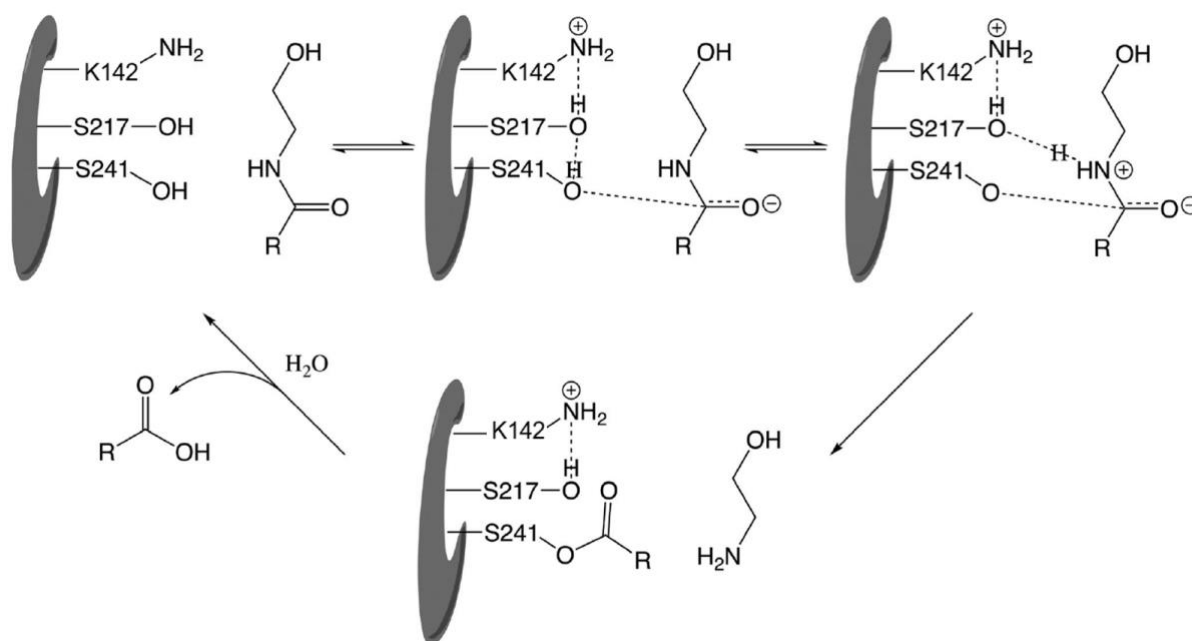


Figure 6. Catalytic triad and mechanism for the hydrolytic cleavage of AEA. Wilt et al., 2020.

Targeting CB1 receptors has shown an association with fibrosis. A common research strategy is to use mice as a model by inducing pulmonary fibrosis via bleomycin (BL-PF) (Liu et al., 2017; Mouratis & Aidinis, 2011). Bronchoalveolar lavage fluid (BALF), IPF patient lung tissue, and BL-PF mice were examined and found to have overactivity in the endocannabinoid system (Bozkurt, 2019; Cinar et al., 2017). It is possible that inhibiting parts of the endocannabinoid system may provide relief to IPF suffers. FAAH inhibitors have been previously developed in various ways. Substrate-derived

inhibitors such as trifluoromethyl ketones, see Figure 7a, are shown to inhibit AEA hydrolysis and can prevent membrane degradation but often have issues due to being highly hydrophobic and/or having low selectivity (Ahn et al., 2009; Boger et al., 1999). Electrophilic ketone inhibitors such as OL-135, see Figure 7b, form stable hemiketals between the active site and adjacent carbonyls to inhibit the enzyme with 60-fold higher selectivity than trifluoromethyl ketone; however they have solubility drawbacks, OL-135 specifically performed poorly *in vivo* (Ahn et al., 2009; Boger et al., 2005; Lichtman et al., 2004). Another type, carbamates (**URB597**), see Figure 7c, are based on known inhibitors that underwent structural changes to inhibit FAAH through carbamylation to make covalent changes to the active site. These inhibitors are irreversible, highly potent, but are not as selective as other inhibitors (Ahn et al., 2009; Mor et al., 2004). PF-3845, which is a potent urea based inhibitor (Figure 7d), has time-dependent activity and also performs covalent modification of the active site (Ahn et al., 2009). Boronic acid inhibitors, see Figure 7e, show promise by forming reversible covalent complexes in the active site of FAAH but also work on serine proteases which could cause selectivity issues (Ahn et al., 2009). Lastly,azole, benzothiazole, and 4-phenylthiazole based inhibitors have shown to be potent binders in rat FAAH (S. R. Wilt et al., 2020).

Pulmonary fibrosis also contributes to pulmonary hypertension which is seen in those with pulmonary disease and fibrosis. In a study where FAAH knockout mice were used, there was a decrease in hypoxic pulmonary vasoconstriction and a notable increase of AA in wild-type mice with lung hypoxia (Wenzel et al., 2013).

The inhibition of CB1 receptors helps to improve bleomycin-induced fibrosis when FAAH is also inhibited; however, inhibition of CB2 showed modest profibrotic activity, indicating that treatment of CB1 and FAAH in tandem may be necessary but this is not the case for CB2 (Palumbo-Zerr et al., 2012). In mouse models, it was found that FAAH acts specifically with CB1 which may negate any off-target profibrotic effects from CB2 (McKinney & Cravatt, 2005). URB937 is a known inhibitor of FAAH and showed protecting effects in mouse models where the mice had received irradiation to trigger

radiation-induced lung injury. Lung fluid analysis showed a decrease in inflammatory cytokines and histopathology determined a decrease in pro-inflammatory and pro-fibrotic cytokines (Li et al., 2017).

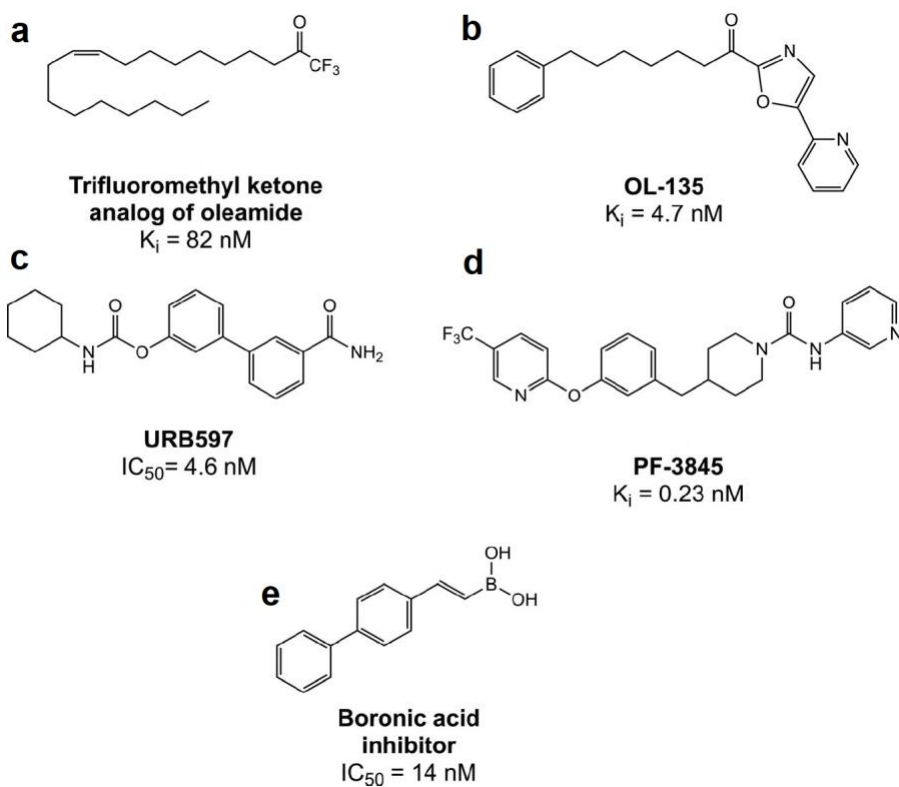


Figure 7. Various known types of inhibitors for FAAH.

### Arachidonic Acid and Cytochrome P450

AA is a polyunsaturated fatty acid and is the starting material for a pathway that is associated with pain and inflammation while AEA is used to bind cannabinoid receptors and relieve pain (Clayton et al., 2002; McKinney & Cravatt, 2005). AA can be released during inflammation from the plasma membrane by phospholipase A2 (PLA2) as well as being a product of FAAH activity. Cyclooxygenase (COX) is one enzyme that is involved in the AA metabolism as well as lipoxygenase (LOX) and cytochrome p450 (CYP450). The COX pathway is the target for pain medication such as nonsteroidal anti-inflammatory drugs (NSAIDs) to inhibit the pro-inflammatory products (prostaglandins and prostacyclins) while the LOX pathway is best known for its role in asthma which can be treated with LOX inhibitors like Zileuton (Malkowski et al., 2000; Rossi et al., 2010). CYP450 catalyzes the oxidation of AA to epoxyeicosatrienoic acids (EETs). EETs are highly biologically active and are

known for their ability to help mediate different conditions within the body. They are considered to be anti-inflammatory, analgesic, anti-fibrotic, and antihypertensive which make them sought-after parts of drug discovery (Inceoglu et al., 2007; H. S. Kim et al., 2021). Hydrolysis of EETs by soluble epoxide hydrolase (sEH) forms dihydroxyeicosatrienoic acids (DHETs) which are pro-inflammatory (Figure 8) (Spector et al., 2004). Utilizing sEH inhibitors has been found to stabilize EET levels and showed a decrease in inflammation as a result (Node et al., 1999).

### **Soluble Epoxide Hydrolase**

sEH, a part of the aforementioned arachidonic cascade, see Figure 8, is an enzyme that hydrolyses the epoxide within EETs to their corresponding diols. sEH's mechanism was studied in rats and it was found that it possesses a catalytic triad responsible for hydrolysis. The enzyme catalyzes the addition of water to the epoxides of EETs and it hydrolyzes EETs to diols (DHETs). The sEH triad is composed of **D333**, **Y381**, and **Y465**. The two tyrosine residues in the active site appear to provide the correct orientation needed for substrate binding and stabilization while **D333** acts as a reactive nucleophile in the enzyme to attack one of the carbons in the epoxide, leading to the epoxide opening, and a formation of covalent-enzyme substrate intermediate is. Neighboring **H523** residue, which is paired to **D495**, acts as a base to activate water which then attacks the ester bond on the **D333**-substrate complex. Finally, the resulting tetrahedral bond dissociates, and the diol product is released (Arand et al., 1996; Hopmann & Himo, 2006). These pro-inflammatory diols are more polar than the epoxide and are able to move in and out of cells more readily (Wagner et al., 2017). Not only is this hydrolysis a problem because it limits the amount of EETs that are present (and therefore their beneficial effects) but also because the metabolic products of this hydrolysis are DHETs which can cause increased inflammation (Imig & Hammock, 2009). EETs, while useful and very biologically active, are not found in high levels even in the presence of known sEH inhibitors, which is useful when considering any off-target effects that may happen from sEH inhibition with regards to over-abundance of EETs (Morisseau & Hammock, 2013).

sEH inhibitors have been developed over the years to prevent the formation of DHETs. The originally designed inhibitors were competitive inhibitors using chalcone oxides, see Figure 9a, and glycidols, see Figure 9b. Chalcone oxides inhibit by stabilizing the covalent enzyme-inhibitor intermediate with the most potent being 4-phenylchalcone oxide ( $IC_{50} = 64$  nM). These compounds are poor substrates making their effects brief and the molecules themselves are unstable. Glycidols are less useful as even the most potent, ((2S,3S)-3-(4-nitrophenyl)glycidol, having an  $IC_{50}$  of 1.6  $\mu$ M), inhibits more poorly than the chalcone oxide (Imig & Hammock, 2009; Spector et al., 2004).

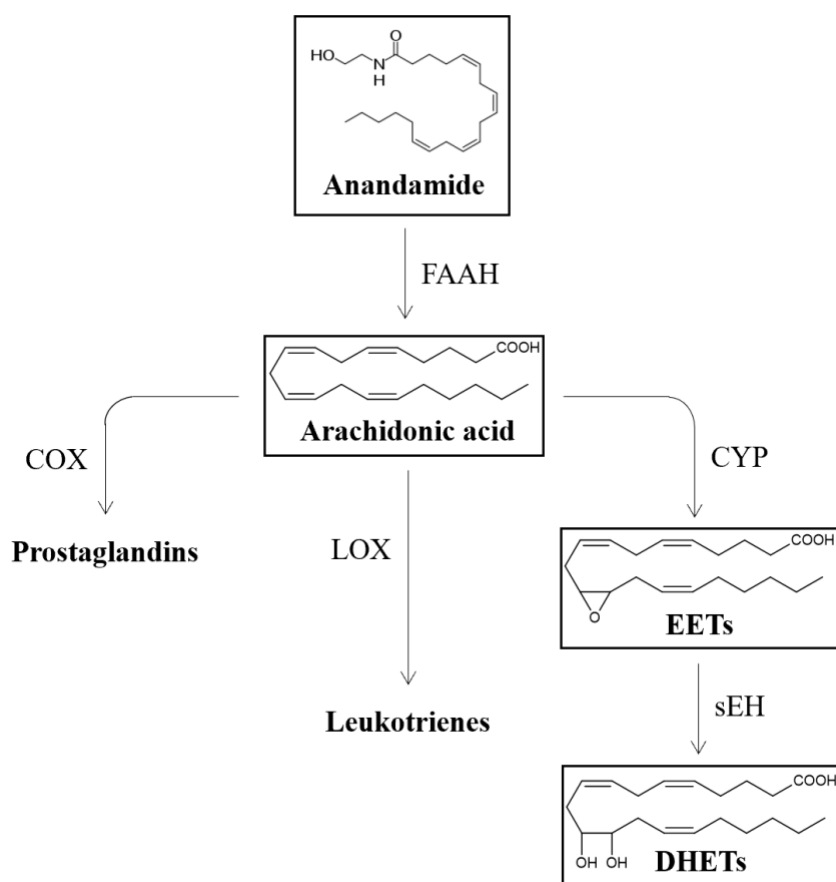


Figure 8. Anandamide is hydrolyzed by FAAH before moving into the arachidonic cascade.



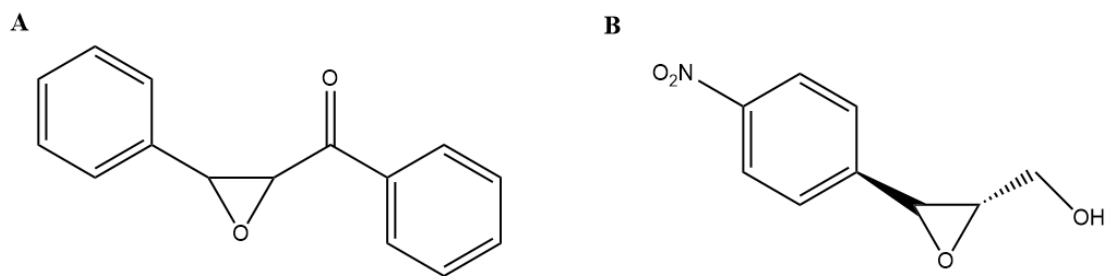


Figure 9. Original sEH inhibitors containing chalcone oxides (a) and glycidols (b)

Dicyclohexylurea (DCU), see Figure 10a, and 12-(3-adamantane-1-ylureido)dodecanoic acid (AUDA), see Figure 10b, were also formerly popular sEH inhibitors, that are potent *in vitro*, and are known for their antihypertensive and antiinflammatory effects. DCU is a selective sEH inhibitor with  $IC_{50}$  of 90 nM (mouse sEH) and is soluble in both water and organic solvents which can pose formulation problems. AUDA was formed after the incorporation of polar functional groups, it is easy to use as it can be orally administered and has an  $IC_{50}$  of 18 nM (mouse); however, it has issues with bioavailability, as lipophilic compounds are not present for *in vivo* studies. These sEH inhibitors while potent *in vitro* lack needed *in vivo* activity. N-[1-(1-oxopropyl)-4-piperidinyl]-N'-[4-(trifluoromethoxy)phenyl]-urea (TPPU), see Figure 10c, was created as a second-generation sEH inhibitor and is a potent *in vivo* inhibitor. It is often used in animal models to determine potential effectiveness against disease. It is a potent inhibitor with a  $K_i$  of  $0.9 \pm 0.1$  nM and an  $IC_{50}$  of 2.8 nM (mouse sEH) (Imig & Hammock, 2009; Morisseau & Hammock, 2008; Wan et al., 2019).

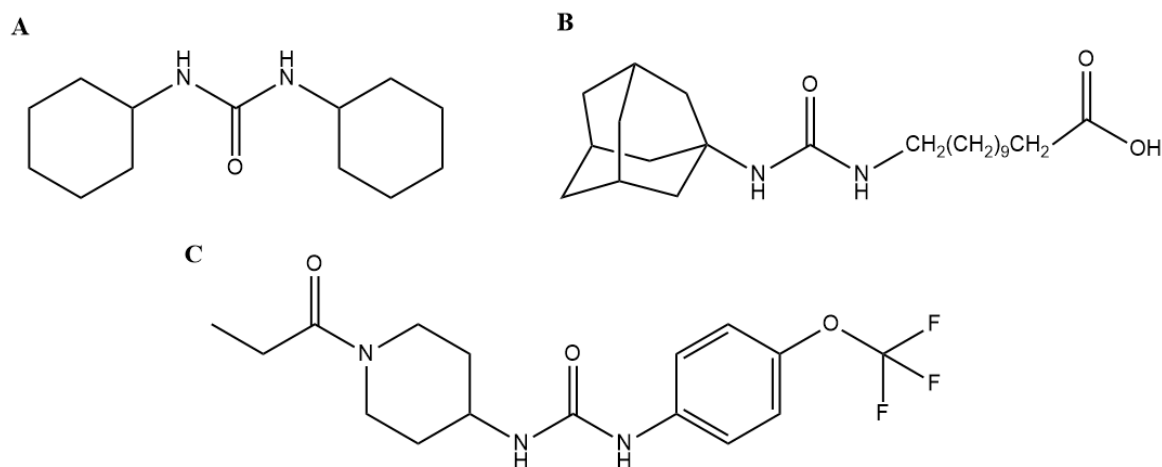


Figure 10. Second generation urea-based sEH inhibitors containing : (a) cyclohexyl (DCU); (b) adamantyl-dodecanoic acid (AUDA); and (c) piperidine moiety (TPPU).

In a study by Deng et al. (2011), *in vivo* studies were done by deleting genes that encode for the production of sEH enzymes. This resulted in an increase of EETs and lowered inflammation levels. While sEH is widely distributed throughout the body these effects were found to have some organ specificity for the lungs. It is thought that EETs are regulating NF- $\kappa$   $\beta$  which is a transcriptional activator involved in inflammation (Deng et al., 2011). In another study by Zhou et al., (2017), TPPU was given to bleomycin-treated rats and was able to increase the bodyweight of the mice (weight loss is a common side effect of PF), decrease fibrotic tissue, and improve survivability, see Figure 11a, 11b. This showed that sEH inhibition was able to lower mortality and lowered associated pro-fibrotic genes, which increase EETs that are anti-inflammatory, analgesic, and stimulate fibrinolysis (the breakdown of fibrotic tissue), see Figure 11c (Zhou et al., 2016).

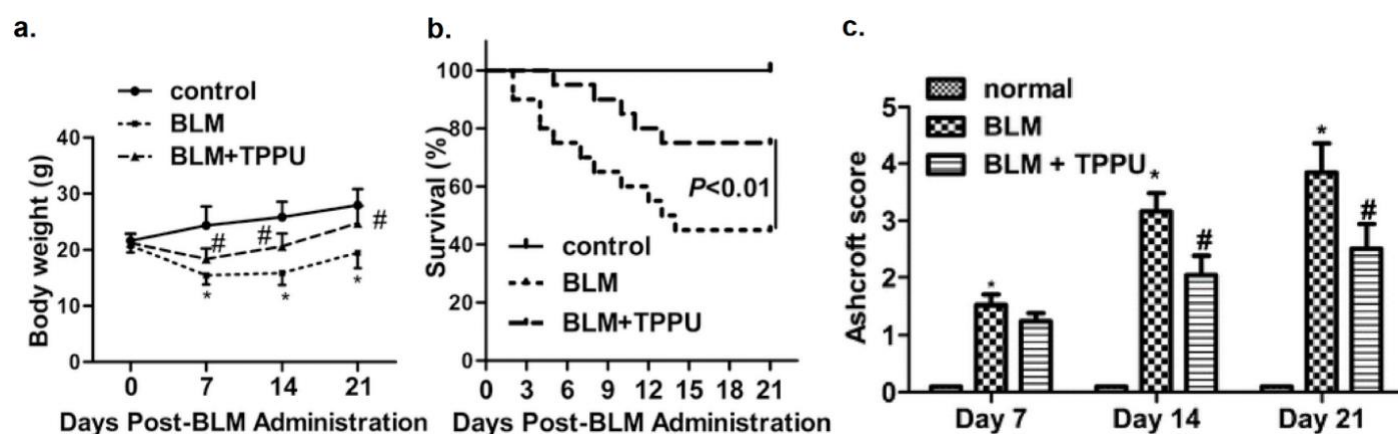


Figure 11. Control group mice compared to mice treated with bleomycin and bleomycin plus the inhibitor TPPU. A) Reduction in body weight loss (a common IPF side effect) using TPPU vs. bleomycin only. B) Decreased rates of mortality with TPPU treatment when compared to those with no treatment C) Ashcroft scoring of tissues taken from mice to view collagen deposition. Figure Zhou et al., 2016.

### Designed Multiple Ligands – A Polypharmacology Approach

As previously discussed, there are two targets, sEH and FAAH that can be used to treat pain, inflammation, and fibrosis. As such, it is beneficial to design single therapeutics which could target both of these enzymes simultaneously, which is also known as designed multiple ligands (DMLs). Producing DMLs is an innovative drug design approach, commonly referred to as polypharmacology, wherein multifunctional compounds are used for multifactorial diseases like IPF. DMLs improve the

efficacy of a treatment by impacting multiple pathways at once. This is not only good for patient outcomes, but fixed-dose combination medications (or DMLs) are more likely to be approved by the U.S. Food and Drug Administration (FDA) compared to multiple single-dose treatments, see Figure 12 (Brown & Wobst, 2021; Gattrell et al., 2013; Geldenhuys et al., 2011; Morphy et al., 2004).

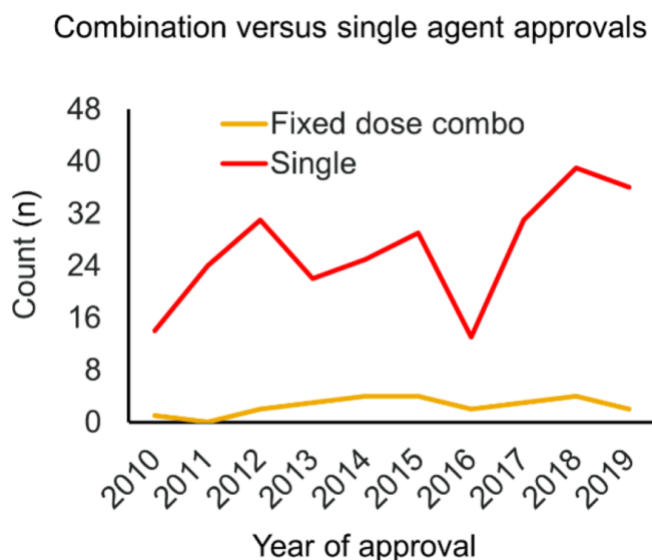
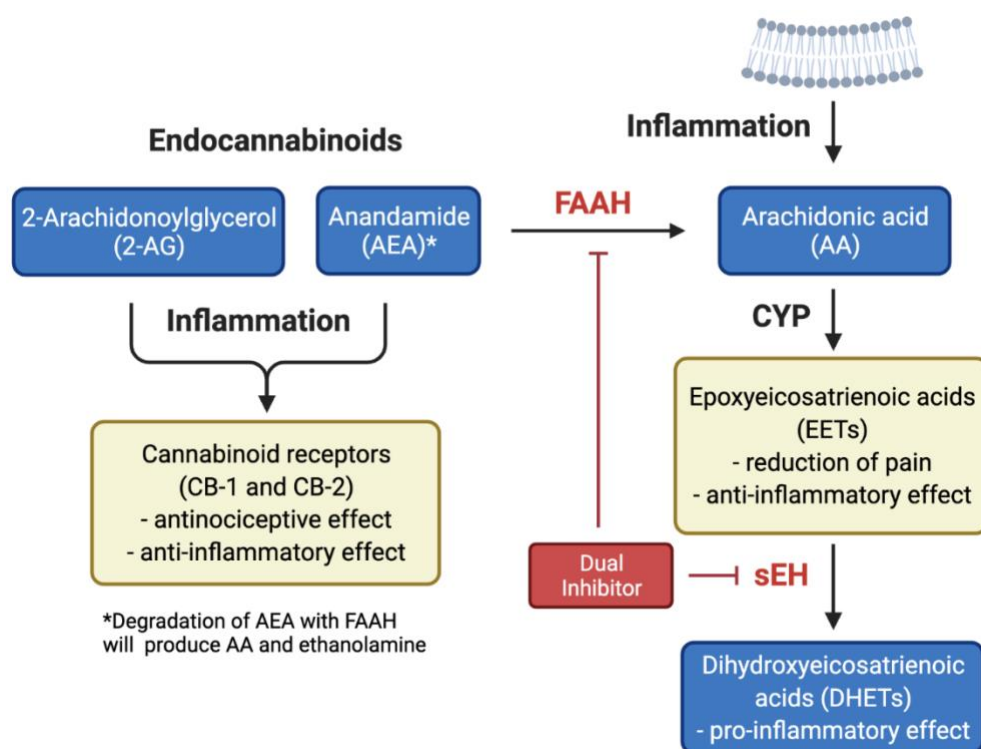


Figure 12. Comparison of the fixed and single dose combination therapies the FDA has approved from 2010 to 2019. Figure Brown & Wobst, 2021.

There are many advantages to developing DMLs, including potential for higher efficacy and fewer side effects compared to cocktail drugs (Proschak et al., 2019). First, potential drug-drug interactions will be avoided; namely two drugs that are safe when given independently of each other cannot be assumed to be safe in combination. In addition, two drugs used together could produce highly unpredictable pharmacokinetic/pharmacodynamic (PK/PD) relationships, which could, in turn, increase the cost of both, preclinical and clinical studies. Next, the polypharmacology approach will decrease the time to determine the dosing for *in vivo* studies. Finally, the DMLs could provide potential synergism and a more robust effect since both inhibited enzymes are involved in inflammation pathways (Connor et al., 2004; Peters, 2013; Proschak et al., 2019; Verma et al., 2018).

To develop new DML therapeutics, one needs to look at the common overlap of the two targets. A scaffold, or core of a chemical structure, can be used for this purpose. If an enzyme has a characterized active site, it is possible to identify which structures will fit within the active site to

design a scaffold (Wills & Lipkus, 2020). The list of structures may also identify the pharmacophore which is the area that is responsible for the biological activity and should not be changed. Proschak et al. (2019)(Proschak et al., 2019) classified three types of DMLs according to their pharmacophoric structures: linked, fused, and merged pharmacophores. Linker DMLs are designed by simple connecting (anchoring) two individual pharmacophores via a linking group. Fused DMLs are similar, the pharmacophores are connected directly, without a linker group. Both, linked and fused types of multitarget compounds usually have molecular weights above 500 and increased lipophilicity, which is important in drug design and could lead to poor solubility and poor permeability according to Lipinski Rule of Five (C. A. Lipinski, 2000). However, these two types of conjugated pharmacophores are a valuable tool in the early structure-activity relationship studies and the discovery of multitarget activity. Merged pharmacophores, see Figure 14, are of the greatest interest in multitarget drug discovery. Here, the key pharmacophoric elements required to interact with each target of interest are combined (merged) into one single pharmacophore (Morphy & Rankovic, 2005; Proschak et al., 2019).



*Figure 13.* AEA and 2-AG are ligands for cannabinoid receptors that provide relief from pain and inflammation; however, AEA is hydrolyzed by FAAH resulting in AA which is further processed through the CYP450 pathway forming EETs and eventually pro-inflammatory DHETs (via sEH).

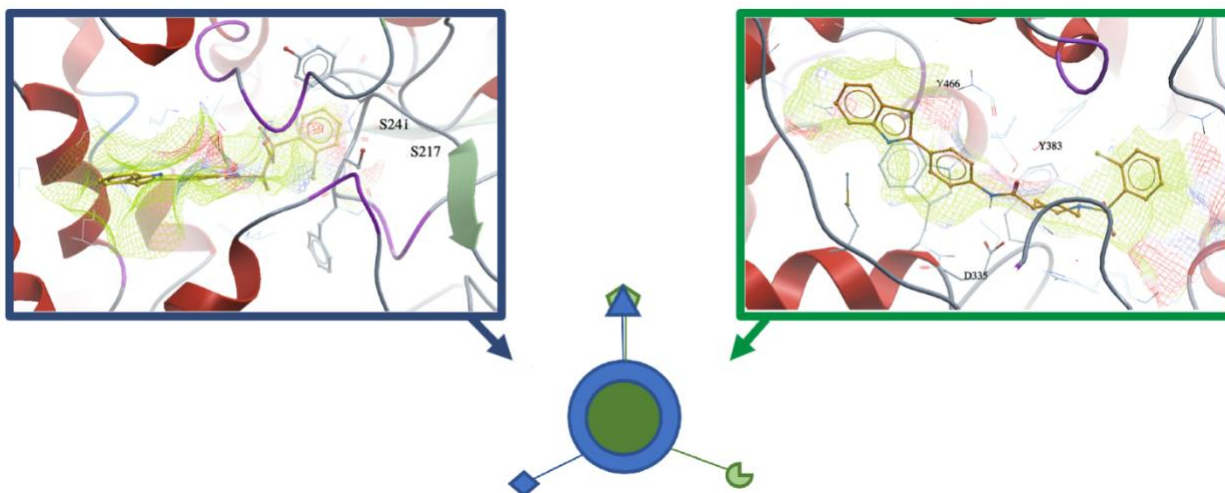


*Figure 14.* The two target enzymes with known inhibitors with the goal of finding similarities to develop a merged ligand as a multitarget drug.

### Proposed Research and Design

In a study by Sasso et al. (2015), it was determined that there is a synergistic effect to treating sEH and FAAH together. A known inhibitor of sEH, TPPU, and FAAH inhibitor, N-cyclohexyl-carbamic acid, 3'-(aminocarbonyl)-6-hydroxy[1,1'-biphenyl]-3-yl ester or URB937, were used independently and then again, in tandem, to compare the varying effects. When used independently both molecules worked inhibited their targets, as expected, to lower the reaction time to both heat and mechanical stimuli in animal models. Next these compounds were used together to observe if they were able to give antihyperalgesic synergism. Using an isobologram, Figure 15, the Sasso group found that the ED<sub>50</sub>, the ability to have a pharmaceutical effect in 50% of the test subjects, was less than half of the expected ED<sub>50</sub>. Specifically, this mouse model showed a depression in both edema (inflammation) as well as acute pain (Kenny & McPhee, 2021; O. Sasso et al., 2015). This study is promising and leads to the theory that a DML for these enzymes is possible and that pain and inflammation can be treated synergistically using this proposed pathway.

We have high confidence in the DML approach because it has been successfully utilized in several medicinal chemistry programs (Gattrell et al., 2012; Morphy et al., 2004; O'Boyle & Meegan, 2011). For example, Portoghese et al. have successfully designed and synthesized bivalent m agonist/d antagonists by linking m agonists and d antagonists fragments (Aceto et al., 2012;

Portoghese et al., 1986). This strategy proposed here to obtain dual-acting sEH/FAAH compounds has however never been carried out before.

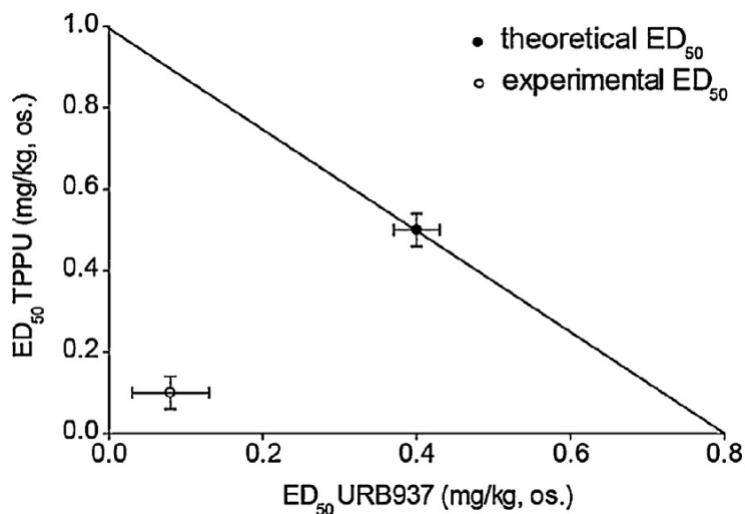


Figure 15. Isobologram for the withdrawal latency of mice after a painful stimulus comparing expected values versus experimental. Figure Sasso et al., 2015.

Previous work by Wang et al., (2009) on FAAH inhibitors development showed that the binding pocket of rat FAAH benefited from piperidine-based molecules. Furthermore, adding large groups to the left side and keeping the right side small gave favorable interactions within the FAAH binding pocket. SAR studies determined that a piperidine ring with a sulfonyl group on the right-hand side were key contributors to activity and that benzothiazole moiety gave better inhibition than 4-phenylthiazoles with their accompanying group choices, see Figure 16. Further exploration, using computer modeling, showed the benzothiazole's potency comes from the group providing the hydrophobic interactions (from pocket residues **F381**, **I491**, **Y335**, and **F432**) needed. Hydrogen bonding occurred on the catalytic residues **S217** and **S241**, (X. Wang et al., 2009).

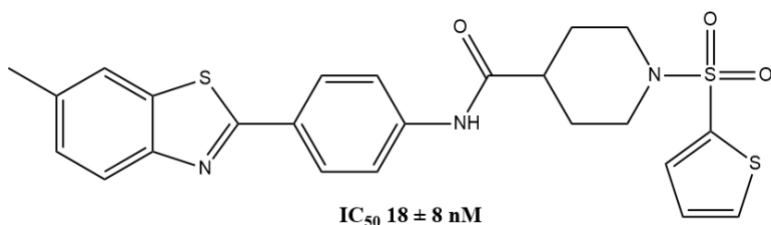
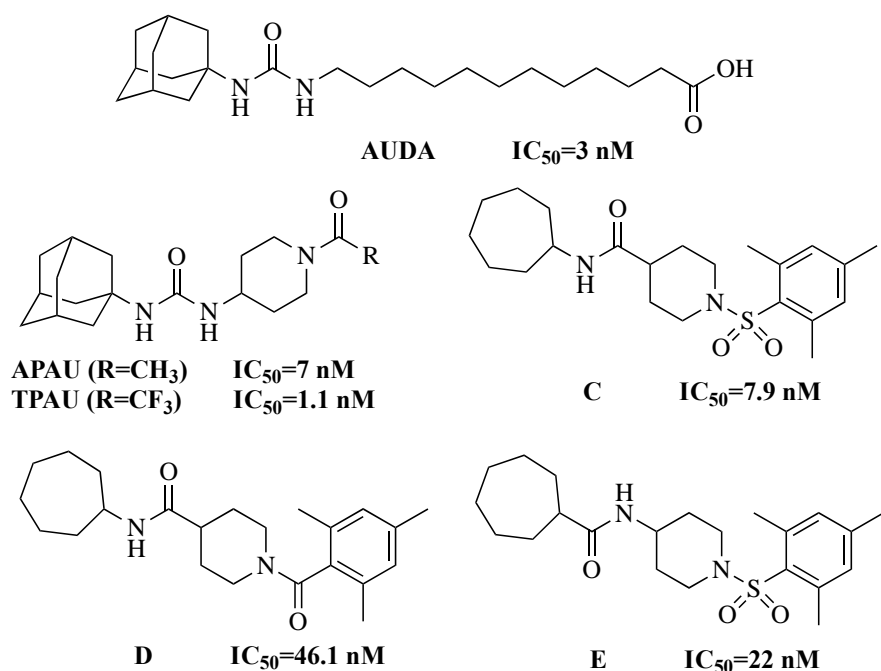


Figure 16. An  $IC_{50}$  of  $18 \pm 8 \text{ nM}$  was obtained for rat FAAH with a benzothiazole molecule containing piperidine and sulfonyl groups.

Earlier sEH inhibitors utilized the urea moiety in their structures and while this yielded many inhibitors with low  $IC_{50}$ 's, these compounds have poor water solubility. Further SAR optimization of these first-generation sEH inhibitors led to the discovery of inhibitors such as 12-(3-adamantan-1-ylureido) dodecanoic acid (AUDA), see Figure 17a, which provided better solubility but was readily metabolized *in vivo* (Kim et al., 2004; Morisseau et al., 1999; Morisseau et al., 2002). Success has been found using piperidines, see Figure 17b, giving optimal  $IC_{50}$ 's, and pharmacokinetic properties (Jones et al., 2006; Shen et al., 2009). SAR exploration determined that urea should be present in the pharmacophore for hydrogen bonding with **Y381**, **Y465**, and a **D333** residue in the catalytic pocket of human sEH (Gomez et al., 2006). The use of an amide, see Figure 17d, in lieu of sulfonamide, see Figure 17c, resulted in an inhibitor that was six times less effective ( $IC_{50} = 46.1$  nM), while reversing the amide group, Figure 17e, led to a decrease in activity indicating the proton placement of the hydrogen in NH is important for sEH inhibition. SAR comparisons from this study suggest a sulfonyl group being present on the right-hand side is beneficial for inhibition (Pecic et al., 2012).



**Figure 17.** Known sEH inhibitors and previous SAR studies: a) AUDA (first-generation urea-based sEH inhibitor) b) APAU and TPAU - urea-piperidine based sEH inhibitors (second-generation sEH inhibitors) c) Amide-piperidine-sulfonamide inhibitor (non-urea sEH inhibitor) d) Amide-piperidine-amide analog, and e) reverse amide analog.

Here, we will employ a DML strategy wherein pharmacophoric fragments from selective sEH inhibitors and selective FAAH inhibitors will be chemically joined to obtain dual sEH/FAAH inhibitors. We will utilize the information gathered from *Wang et al., 2009* and *Pecic et al., 2012* to create dual inhibitors using an amide, piperidine, and a sulfonamide as our scaffold and then modulating with bulky groups on each end. First, we will start with a series of FAAH inhibitors using 4-phenylthiazole on the left and test different modulations on the right-hand side of our scaffold. Next, we will synthesize dual FAAH and sEH inhibitors by adding various side groups to the right of the scaffold but with benzothiazole on the left. Finally, using the lead right-hand modulation and our scaffold, we will synthesize additional 4-phenylthiazoles. This will be done to compare them to our benzothiazoles, to deduce which group is the most effective on the left of our scaffold to inhibit both enzymes in tandem. Inhibition will be verified using biological assays and molecular modeling, ADME-Tox properties will be examined, and characterization will also be done. These studies will give us which bulky side groups will give the best inhibition of both enzymes when paired with our scaffold.



## CHAPTER 2

## RESULTS &amp; DISCUSSION

## FAAH Inhibitors: 2-naphthyl and 4-phenylthiazoles

## Design, Synthesis, and SAR

In previous studies, see Figure 18, Wang et al. (2009) examined various benzothiazole and 4-phenylthiazole piperidine moieties as FAAH inhibitors identified from high-throughput screening and follow-up structure–activity relationship (SAR) studies. This study mostly focused on the benzothiazole–piperidine analogs and reported only three analogs with various 4-phenylthiazole groups on the left side of the piperidine series of analogs. Mor et al. (2008) reported two potent 2-naphthyl containing FAAH inhibitors. We hypothesized that the FAAH inhibitory activity may be achieved by introducing the 2-naphthyl ring into piperidine series of analogs. Our design started with introducing 2-naphthyl ring on the left side of the piperidine moiety and linking the small thiophene, phenyl or 2-fluorophenyl rings on the right side of the central piperidine moiety via sulfonamide bond.

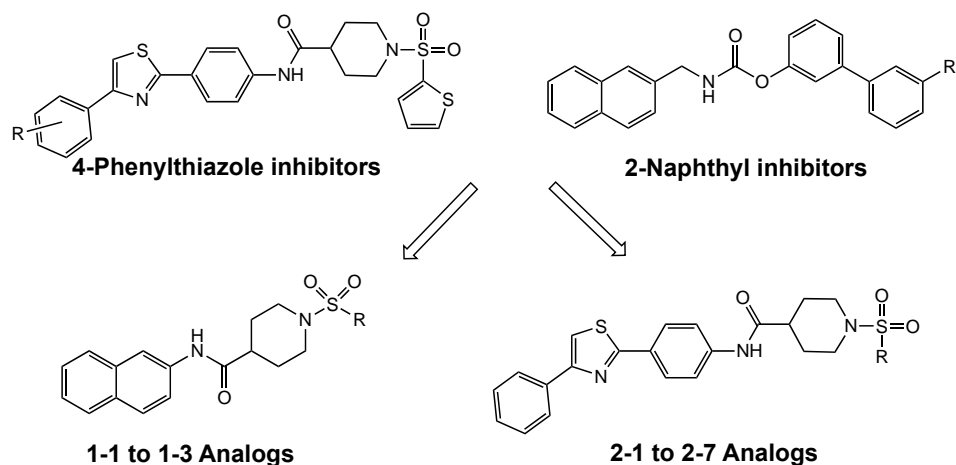


Figure 18. Design of new series of fatty acid amide hydrolase inhibitors.

Our docking experiments, Table 4, suggested that this series of bulky, hydrophobic naphthyl analogs fits well in the binding pocket of the human FAAH, according to the obtained low ICM docking scores. The first tested 2-naphthyl-piperidine analog **1-1** showed only weak submicromolar potency with IC<sub>50</sub> of 1,700 nM. Replacing the thiophene ring with other small rings, such as phenyl **1-2**, or 2-fluorophenyl **1-3**, did not improve the inhibitory activity of this series of analogs, as shown in Table 4,

with IC<sub>50</sub>s of 4,500 nM and 1,200 nM, respectively, indicating that 4-phenylthiazole moiety is the important structural feature on the piperidine series of FAAH inhibitors. We decided to turn our attention to the 4-phenylthiazole analogs, as this moiety showed improved potency and was not well-explored in previous studies, namely only three analogs were synthesized and evaluated in rat FAAH inhibition assay, see Figure 18. In addition, 4-phenylthiazole without any substitution on the phenyl ring was never tested, and our docking experiments suggested that this moiety will occupy the same hydrophobic pocket as the other bulky, hydrophobic groups previously reported.

In order to explore the structural requirements for this series of analogs, we prepared several compounds containing 4-phenylthiazole moiety without any substituents on the phenyl ring on the left side of the piperidine ring, and fluorine and chlorine atoms at various positions on the aromatic ring on the right side of the molecule and evaluated these analogs for inhibition against human FAAH enzyme. Biological evaluation of the first 4-phenylthiazole analog (**2-1**), containing a thiophene ring on the right side of the piperidine moiety, showed very good inhibitory potency against human FAAH enzyme with IC<sub>50</sub> of 23.4 nM. We continued our SAR exploration of the 4-phenylthiazole analogs with probing the 2-fluorophenyl (**2-2**), 2-chlorophenyl (**2-3**), 4-fluorophenyl (**2-4**), 4-chlorophenyl (**2-5**), 2,4-difluorophenyl (**2-6**), and 2,4-dichlorophenyl (**2-7**) groups on the right side of the 4-phenylthiazole piperidine moiety. All analogs showed improved potencies, having IC<sub>50</sub>s in the low-to-medium nanomolar range, and also suggesting that *ortho*- and *para*-substituted and *ortho-para* disubstituted fluorine atoms are better tolerated than the chlorines at the same positions on the ring. In addition, the improved potencies in the binding pocket of the human FAAH are suggesting potential favorable interactions within the enzyme binding pocket, which were confirmed by our docking experiments.

### Homology Model

In order to better explore the possible binding modes and interactions for the 4-phenylthiazole analogs, we have conducted molecular modeling studies. As the crystal structure of the human FAAH enzyme has not been reported, we decided to build a homology model. As a template for building the human FAAH enzyme homology model, we selected the crystal structure of the rat FAAH (PDB code:

3QK5) as its crystal structure is solved at the highest resolution (2.20 Å) that we found deposited (Gustin et al., 2011). The sequence alignment of the human FAAH enzyme shows very good sequence identity with rat (and many other species) FAAH enzyme sequence template, with 80% sequence similarity, see Figures 19 and 20. We also noticed that the alignment of rat and human FAAH sequences contains many conserved residues (shown by green), especially located in the proximity of the catalytic site of the FAAH enzyme, that are essential for proper enzyme function.

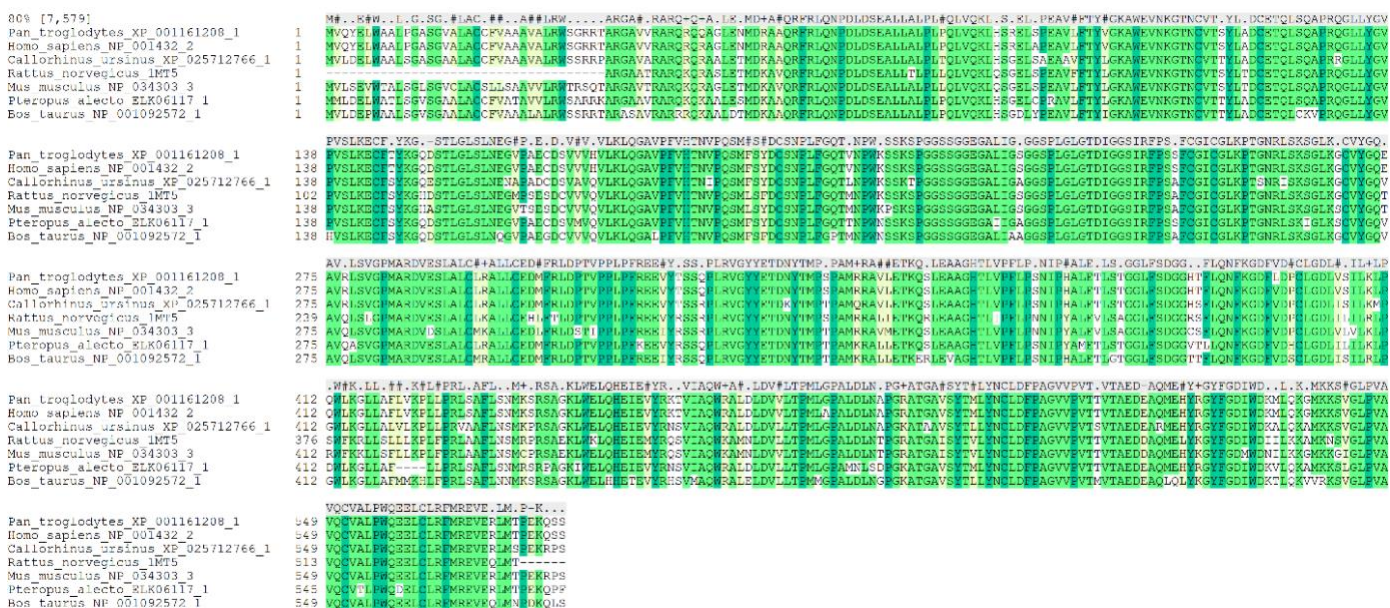


Figure 19. Multiple sequence alignment of FAAH enzymes

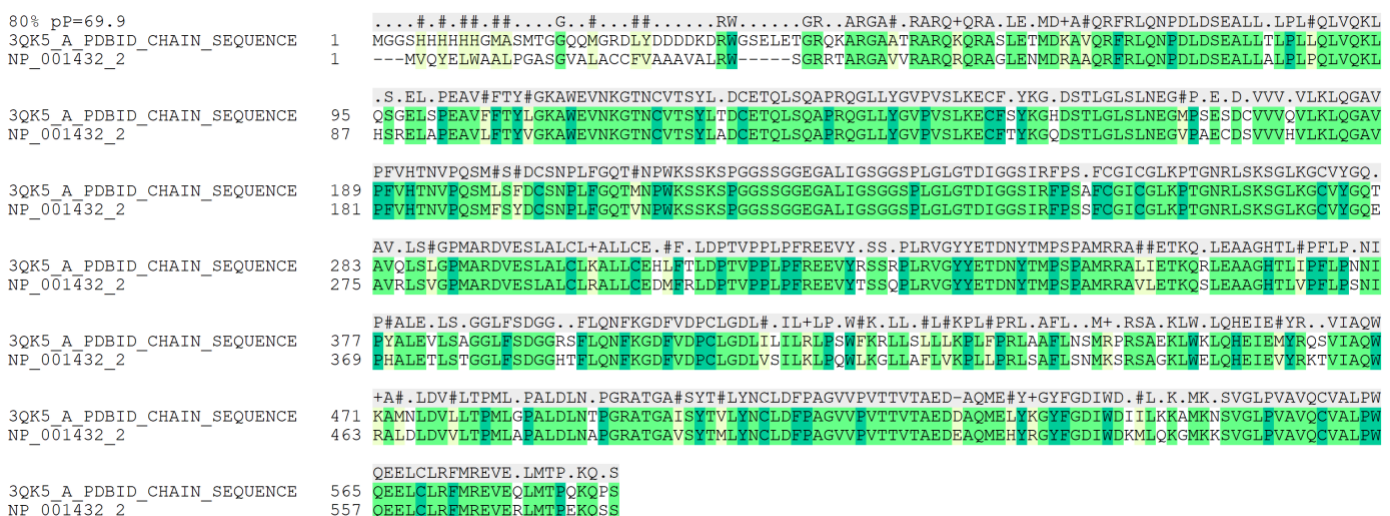
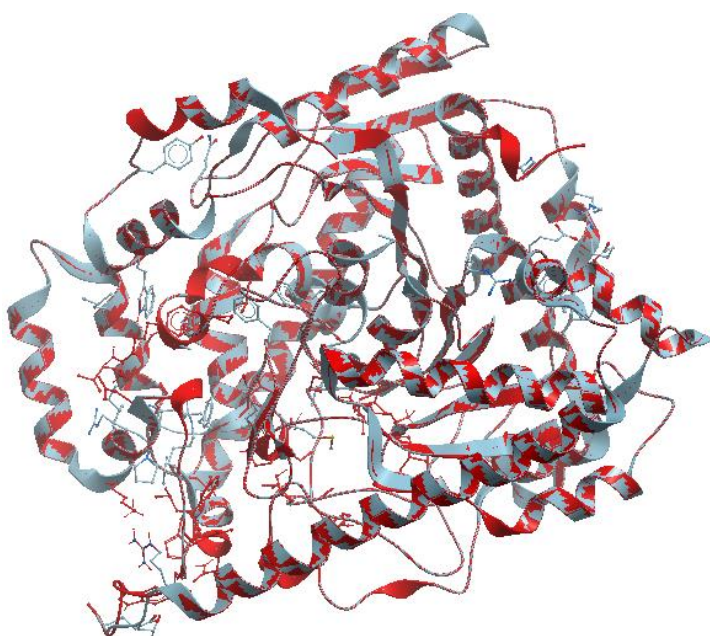


Figure 20. Sequence alignment of rat and human FAAH

We first built and energy minimized the homology model using ICM Pro program, and then, we assessed validity of the model. In order to evaluate the constructed human FAAH enzyme homology model for the docking studies, we used several different programs for evaluation that are available via the server of the UCLA DOE Institute for Genomics and Proteomics. Evaluation methods verify whether a model satisfies standard and geometric criteria and assesses the overall quality of the model. We used PROCHECK, ERRAT, VERIFY-3D, WHAT-IF, and PROVE and assessed the quality of the human FAAH enzyme model we constructed (Colovos & Yeates, 1993; Eisenberg et al., 1997; Gustin et al., 2011; Laskowski et al., 1996; Pontius et al., 1996; Vriend & Sander, 1993). We first determined the root-mean-square deviation (RMSD) between the backbone atoms of the template and the homology model, getting RMSD value of 0.238 Å, indicating a close homology, see Figure 21. Therefore, we decided to proceed with the next evaluation steps.



*Figure 21.* Superimposed Homology model of human FAAH with the template rat FAAH (PDB: 3QK5)

We then evaluated our homology model using the program Procheck. The aim of this program is to assess the detailed residue-by-residue stereochemical quality of the enzyme structure. Ramachandran plots for the human FAAH homology model are shown in Figure 22. A simple measure of quality that can be used from the plot is the percentage of residues in core region and

allowed regions should be very high (>90% residues). Another important factor in structural assessment is Goodness factor or G-Factor which shows the quality of dihedral, covalent, and overall bond angles. These scores should be above  $-0.5$  for a reliable model. From observing the Ramachandran plot, it can be seen that 89.1% of the residues are in the most favorable region. In addition, 10.5% of the residues were found in the additionally allowed region. To add on, the model was found to have a G factor of 0.2, meaning the quality of the bond angles indicates the high quality of our homology model.

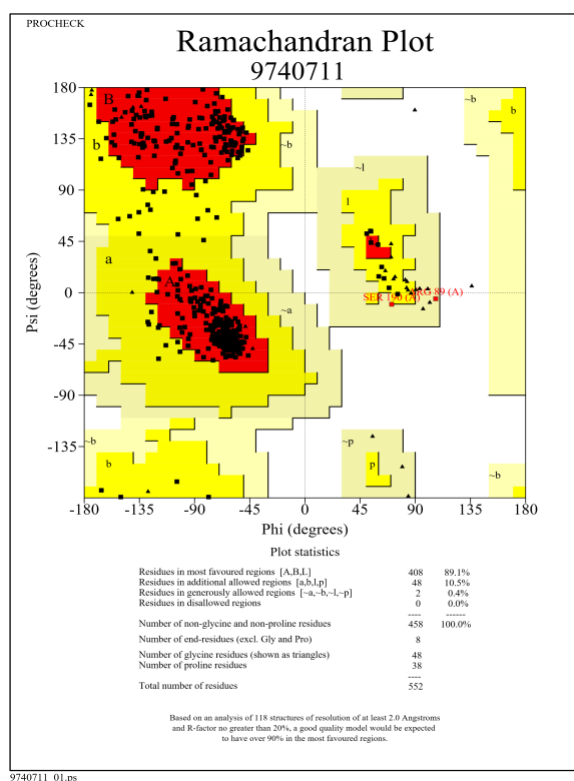


Figure 22. Ramachandran plot of human FAAH homology model

The results obtained from Errat are shown in Figure 23. This program evaluates an overall quality factor of nonbonded atomic interactions. The normally accepted range is above 50% for a high-quality model. The template structure of rat FAAH enzyme, PDB:3QK5, has an Errat value of 85.294. From running an Errat on the FAAH homology model, it was found to have an overall quality factor of 93.585, suggesting the backbone conformation and nonbonded interactions of the homology model are all within a normal range. Verify3D evaluates energetic and empirical methods to produce

averaged data points for each residue in order to evaluate the quality of protein structures. Verify3D results shown in Figure 24 represent the Verify3D average data score of the homology model generated in comparison with template. Using this scoring function, if more than 80% of the residue has scored above 0.2, then the structure is considered high quality. From the data collected in the table, it was observed that 92.65% of the residues had averaged a 3D score above 0.2.

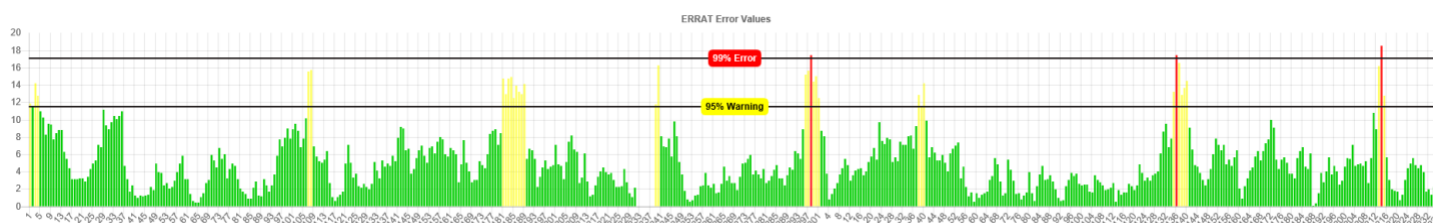


Figure 23. Errat analysis of human FAAH homology model

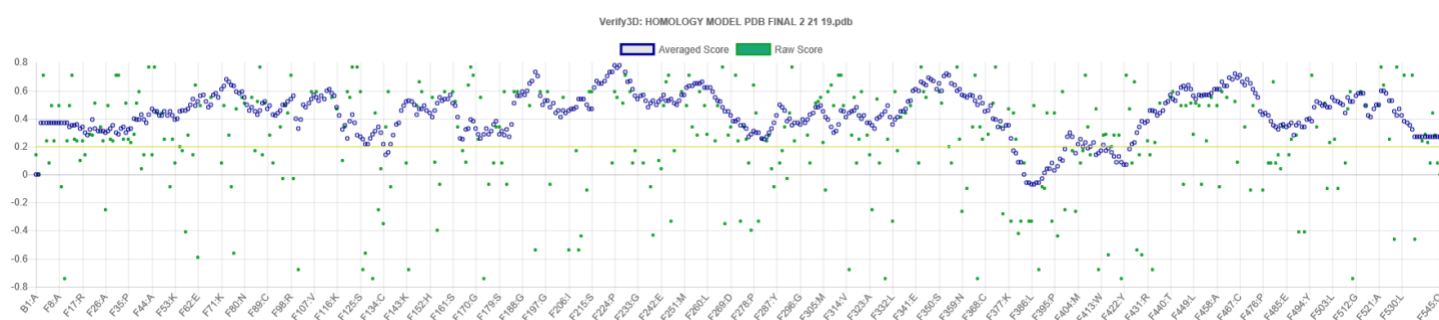


Figure 24. Verify 3D analysis of human FAAH homology model

WHAT-IF is used to check the normality of the local environment of amino acids. The program evaluates the following: bond lengths, bond angles, omega angle restraints, side-chain planarity, improper dihedral distribution, and inside/outside distribution. It does extensive checking of many stereochemical parameters of the residues in the model and it gives an overall summary of the quality of the structure as compared with current reliable structures. For a reliable structure, the WHAT-IF packing scores should be above  $-5.0$ . In the case of our homology model Table 3, the packing score is  $-0.794$ ; therefore, the WHAT-IF evaluation also indicates that the homology model structure is very reasonable. The Prove results for the human FAAH homology model are shown in Figure 25. Prove provides an average volume Z-score of all the atoms. High scores have been found to be associated

with uncertainty in the structure. Structures with poor resolution generally have a Z-score RMS >1.2; while for well-resolved structures, the Z-score RMS is around 1.0 (Pontius et al., 1996). Our model showed that the average Z-score for the model for all resolutions hovered slightly above 0 but below 0.1 with the exception of one outlier at about 0.8. The Prove score shows that the model is valid, but it contains an unusual number of buried atoms within it. The buried atoms are most likely hydrophobic residues within the enzyme.

Table 3. What check results for human FAAH homology model

Overall Summary Report: <span style="color: green;">Pass</span>	
1st generation packing quality	-0.794
Ramachandran plot appearance	-0.805
Chi-1/Chi-2 rotamer normality	-1.119
Backbone conformation	-32.479
Bond lengths	0.404
Bond angles	0.66
Omega angle restraints	0.909
Side chain planarity	0.262
B-factor distribution	0.33

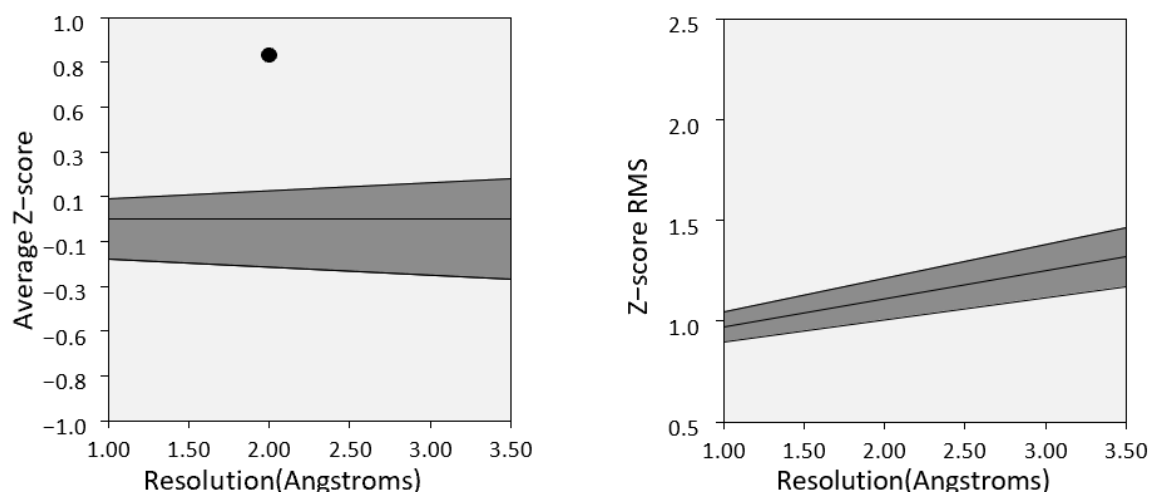


Figure 25. Z-score results from Prove test of homology model

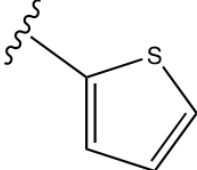
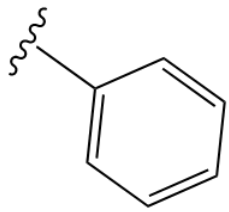
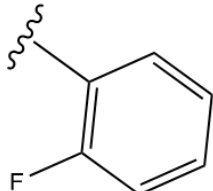
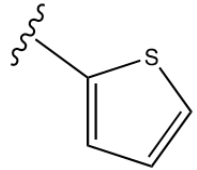
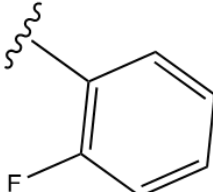
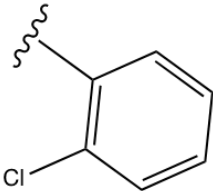
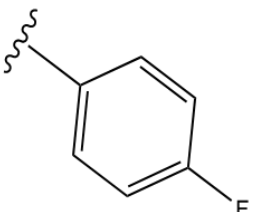
In summary, the geometric quality of the backbone conformation, the residue interaction, the residue contacts, and the energy profile of the human FAAH homology model are all well within the limits established for reliable structure and we proceeded with the docking experiments.

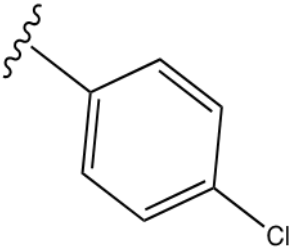
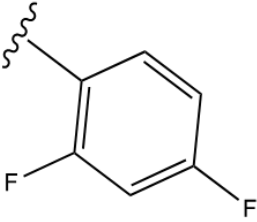
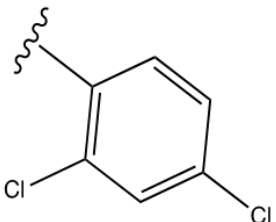
### Docking Experiments

In order to better understand the binding modes and interactions of these inhibitors within the catalytic site of the human FAAH enzyme, we performed docking studies. The ICM docking score represents unitless approximations of the binding free energy between the inhibitor and the enzyme where a lower docking score suggests a higher chance the inhibitor is bound to the enzyme (Schapira et al., 1999). Scoring functions from this docking experiment are reported in Table 4, favorable docking scores should be near -30 or lower. The known irreversible FAAH inhibitor URB-597 was also docked for comparison. Although the docking scores for the naphthyl analogs **1-1** to **1-3** had reasonable ICM scores, we were not able to correlate these values with the obtained IC<sub>50</sub> values. On the other hand, the docking scores for **URB-597** and for the potent 4-phenylthiazole analogs **2-1** to **2-7** were in the agreement with our *in vitro* data, suggesting that our homology model could be an important tool in the future design for the 4-phenylthiazole series of FAAH inhibitors. After visual inspections of binding modes of these inhibitors, we observed that several inhibitors formed a complex with the FAAH enzyme through H-bonding with different amino acid residues. All other non-covalent interactions (listed in Table 5) were also located in the proximity of the catalytic triad of the human FAAH enzyme, suggesting that the low nanomolar potency of these compounds is probably due to these interactions.



Table 4. FAAH inhibitory activity and docking scores of analogs 1-1 to 1-3 and 2-1 to 2-7.

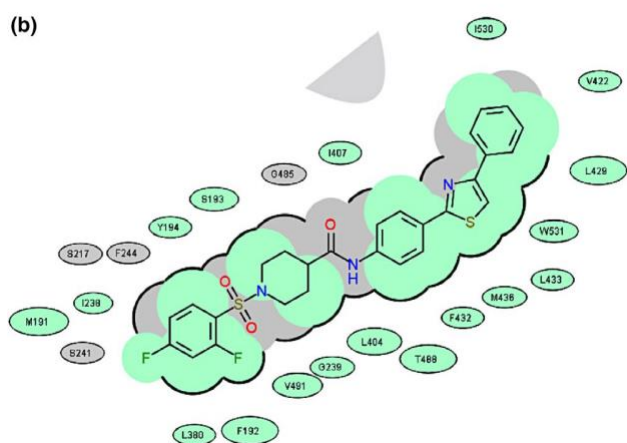
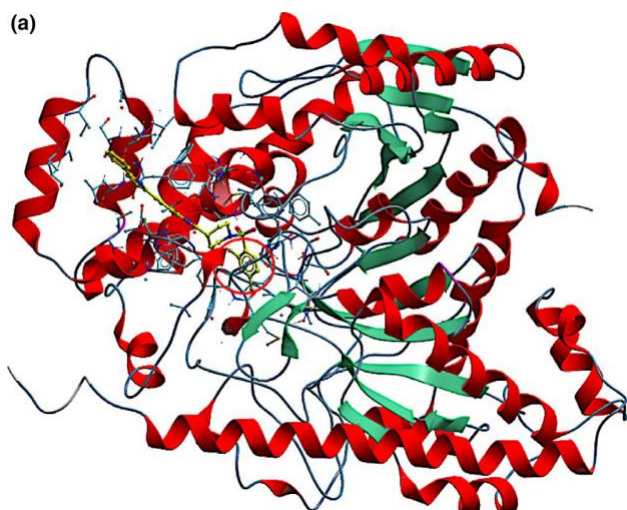
Compound	R	FAAH IC <sub>50</sub> (nM)	Docking Score
URB-597	—	38	-21.45
1-1	 2-thiophenyl	1700	-32.73
1-2	 phenyl	4500	-29.11
1-3	 2-fluorobenzene	1200	-29.9
2-1	 2-thiophenyl	23.4	-25.87
2-2	 2-fluorophenyl	19.5	-22.34
2-3	 2-chlorophenyl	30.8	-23.16
2-4	 4-fluorophenyl	9.6	-27.78

Compound	R	FAAH IC <sub>50</sub> (nM)	Docking Score	
2-5		4-chlorophenyl	54	-21.46
2-6		2,4-difluorophenyl	8.4	-31.75
2-7		2,4-dichlorophenyl	11.9	-25.01

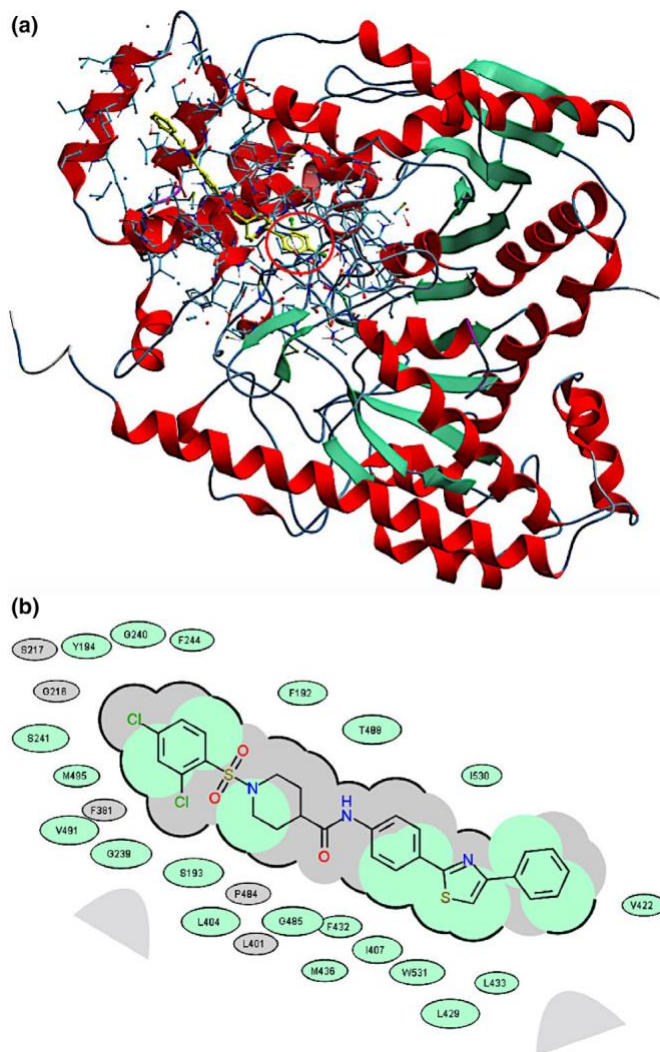
In addition, we also observed that the 4-phenylthiazole moiety was orientated toward the enzyme surface and that the right side of analogs **2-2**, **2-3**, **2-5**, **2-6**, and **2-7** is deeply buried within the catalytic site. Figures 26 and 27 show the observed orientation for the most potent fluoro- and chloro-analogs **2-6** and **2-7**, respectively. This could also rationalize the differences in the observed IC<sub>50</sub> values of this series of inhibitors (see Figures 28-32). According to the list of the non-covalent interactions (Table 5), all synthesized 4-phenylthiazole analogs are located in the proximity of the catalytic triad residues **S217** and **S241**. We believe that 4-phenylthiazole analogs probably form a non-covalent complex with **S241** and **S217**, similar to the intermediate formed by FAAH and AEA (Figure 6) during the mechanism of hydrolysis. We also observed potential  $\pi$ - $\pi$  interactions between **F192** and the phenyl aromatic ring of the analogs **2-4**, **2-6**, and **2-7** which could rationalize the improved potencies of these analogs.

Table 5. The list of non-covalent interactions of 4-phenylthiazole series of analogs.

Compound	H-bonds	Hydrophobic interactions	Other non-covalent interactions
2-1	L401, G485	F192, S193, Y194, I238, G239, G240, S241, F244, F381, L404, I407, V422, L429, L433, M436, T488, V491, W531	M191, G402, D403, F432
2-2	0	F192, S193, Y194, G239, G240, S241, F244, F381, D403, L404, I407, V422, L429, L433, G485, T488, V491, I530, W531	M191, G216, S217, L380, L401, M495
2-3	0	F192, S193, Y194, I238, G239, G240, S241, F244, D403, L404, I407, V422, L429, L433, M436, T488, V491, I530, W531	M191, G216, S217, L380, L401, G485, M495
2-4	0	F192, S193, Y194, S217, G239, S241, F244, L380, F381, L404, I407, L429, F432, L433, M436, T488, V491, I530, W531	M191, G216, G240
2-5	T488	M191, F192, S193, Y194, I238, G239, D403, L404, I407, V422, L429, L433, M436, I530, W531	S241, F244, L401, G485, V491
2-6	G485, S241	M191, F192, S193, Y194, I238, G239, L380, L404, I407, V422, L429, F432, L433, M436, T488, V491, I530, W531	S217, F244
2-7	0	F192, S193, Y194, G239, G240, S241, F244, L404, I407, V422, L429, F432, L433, M436, G485, T488, V491, M495, I530, W531	G216, S217, F381, L401, P484
URB-597	G272, C269	F192, I238, K263, L266, G268, Y271, E274, R277, L278	L154, S190, M191, K267, C269, V270, Q273



*Figure 26.* (a) A docking pose of the inhibitor **2-6** in the catalytic site of the human fatty acid amide hydrolase (FAAH) enzyme, suggesting that 2,4-difluorophenyl part (circled in red) of the inhibitor is orientated within the binding pocket. (b) 2D representation for the lowest energy conformation of inhibitor **2-6** in the binding pocket of human FAAH. Green shading represents hydrophobic region; gray paraboloids represent accessible surface for large areas; broken thick line around ligand shape indicates accessible surface; size of residue ellipse represents the strength of the contact



*Figure 27.* (a) A docking pose of the inhibitor **2-7** in the catalytic site of the human fatty acid amide hydrolase (FAAH) enzyme, showing that 2,4-dichlorophenyl moiety (circled in red) is located deeply in the binding pocket of the human FAAH enzyme. (b) 2D representation for the lowest energy conformation of inhibitor **2-7** in the binding pocket of human FAAH. Green shading represents hydrophobic region; gray parabolas represent accessible surface for large areas; broken thick line around ligand shape indicates accessible surface; size of residue ellipse represents the strength of the contact

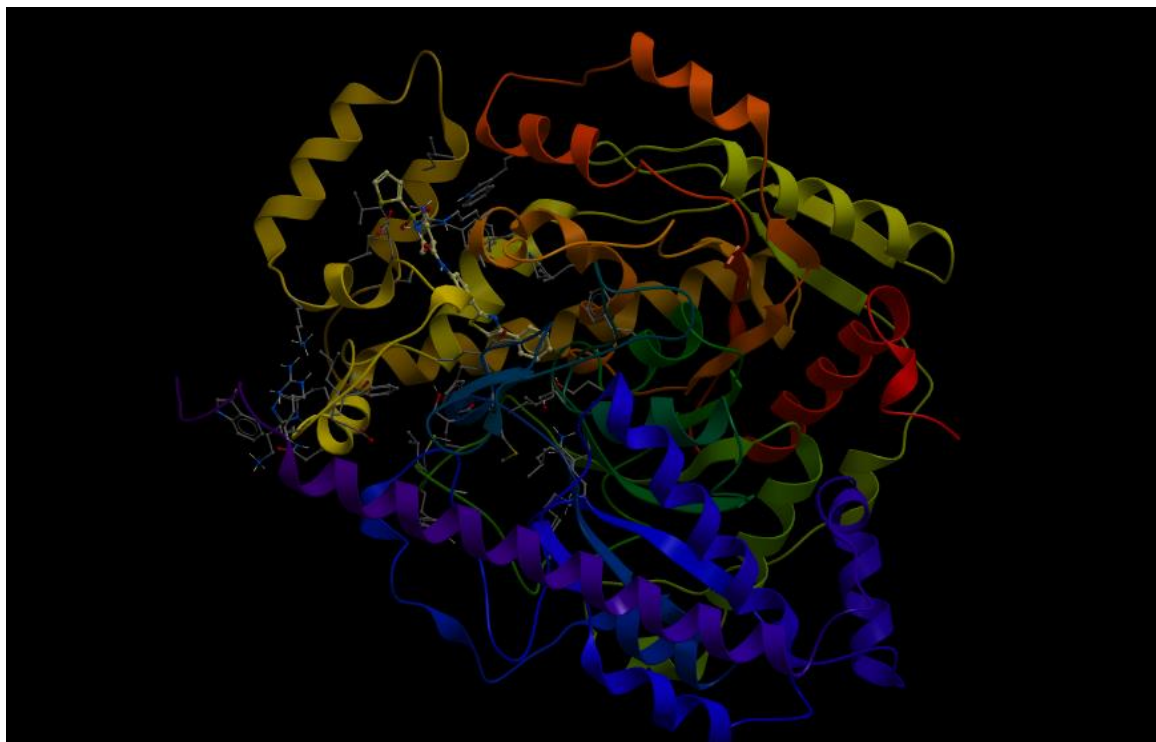


*Figure 28.* A docking pose of the inhibitor **2-1** in the catalytic site of the human FAAH enzyme

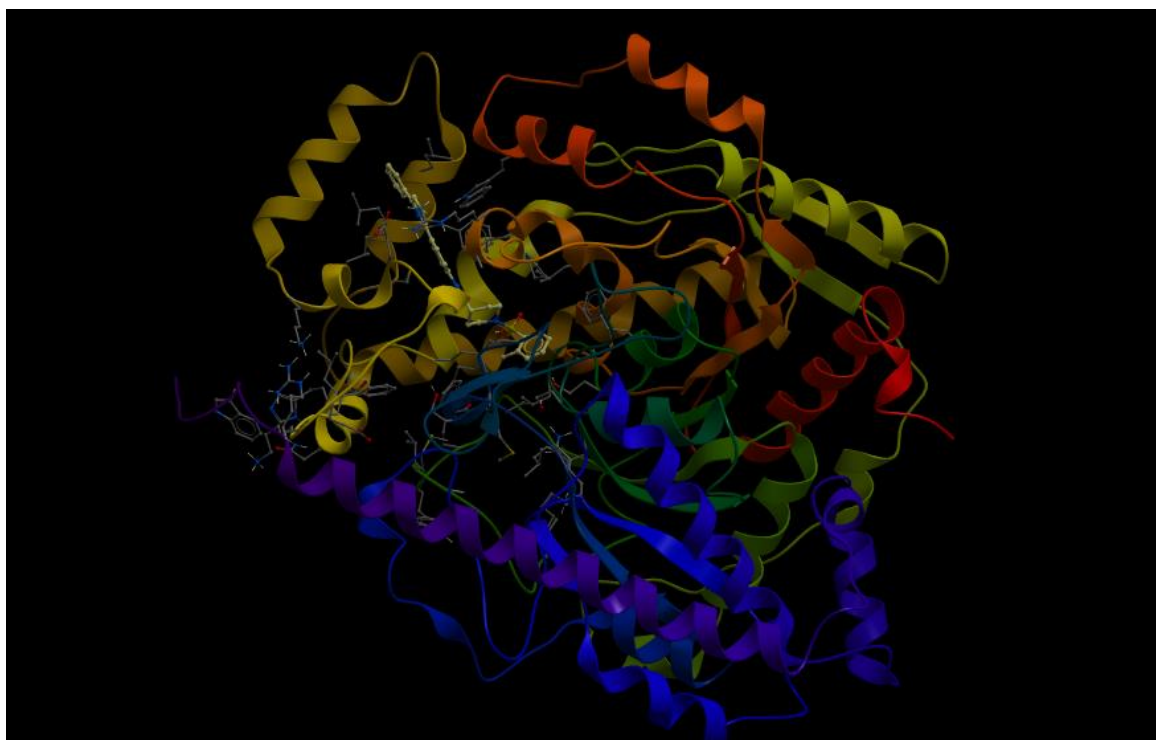


*Figure 29.* A docking pose of the inhibitor **2-2** in the catalytic site of the human FAAH enzyme

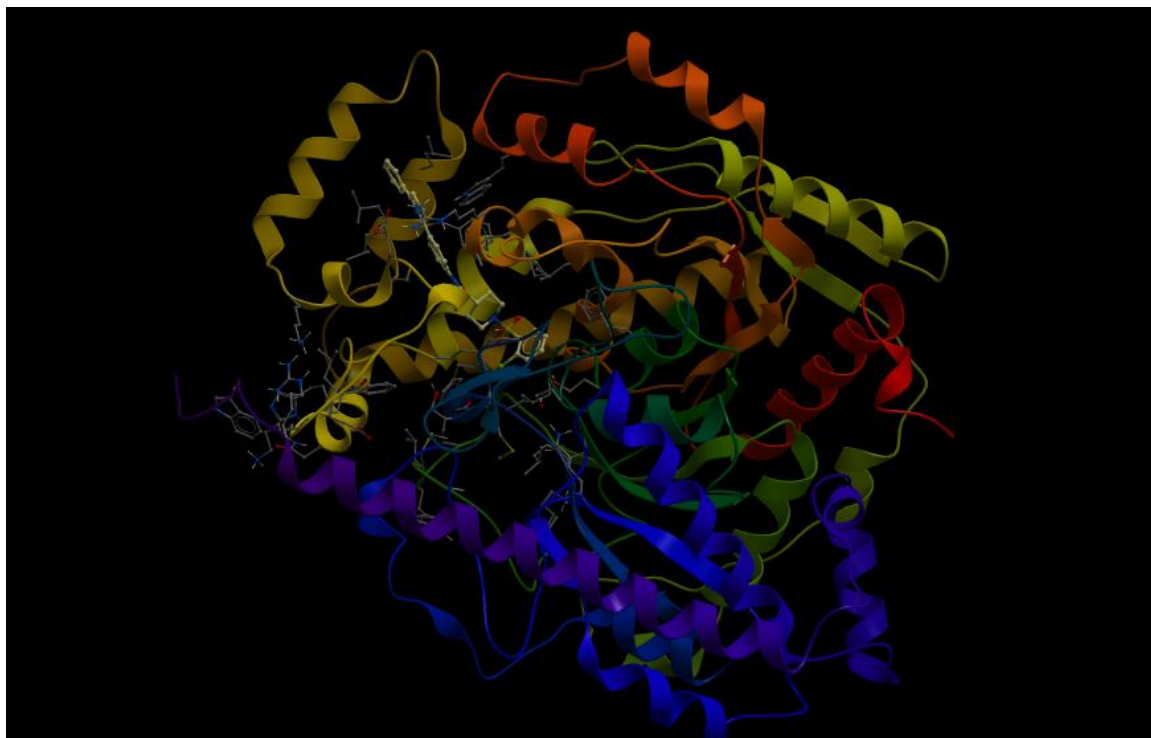


*Figure 30.* A docking pose of the inhibitor **2-3** in the catalytic site of the human FAAH enzyme

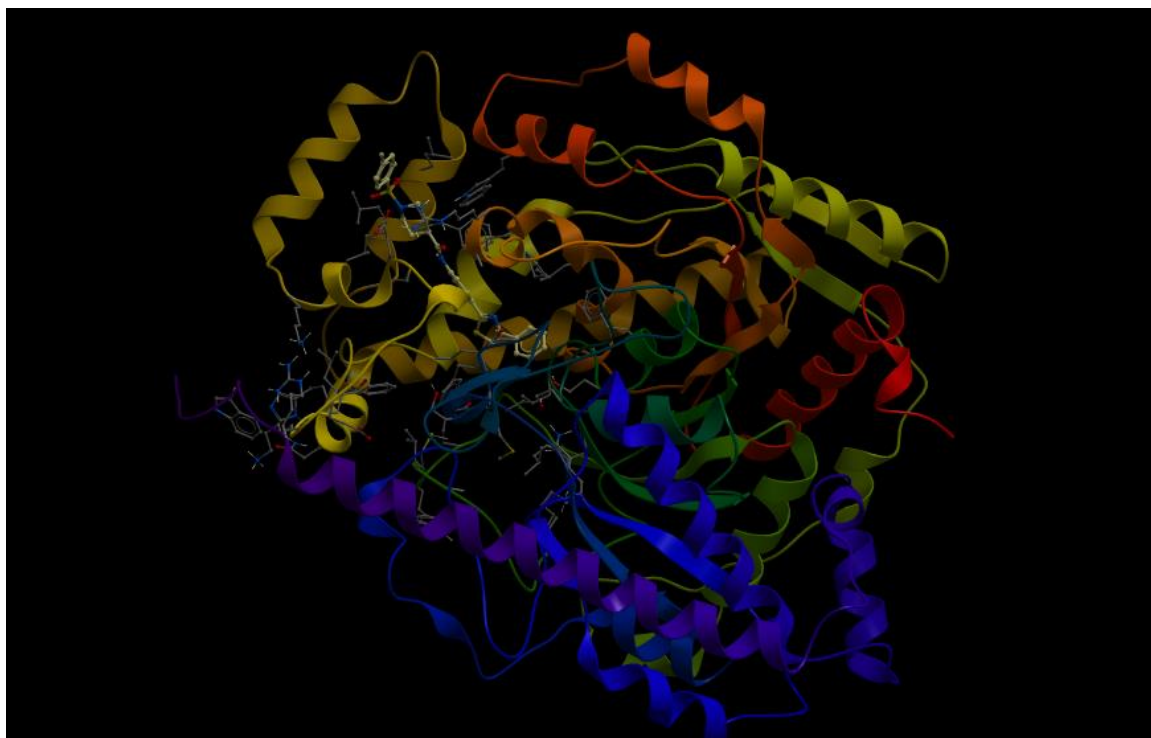


*Figure 31.* A docking pose of the inhibitor **2-4** in the catalytic site of the human FAAH enzyme

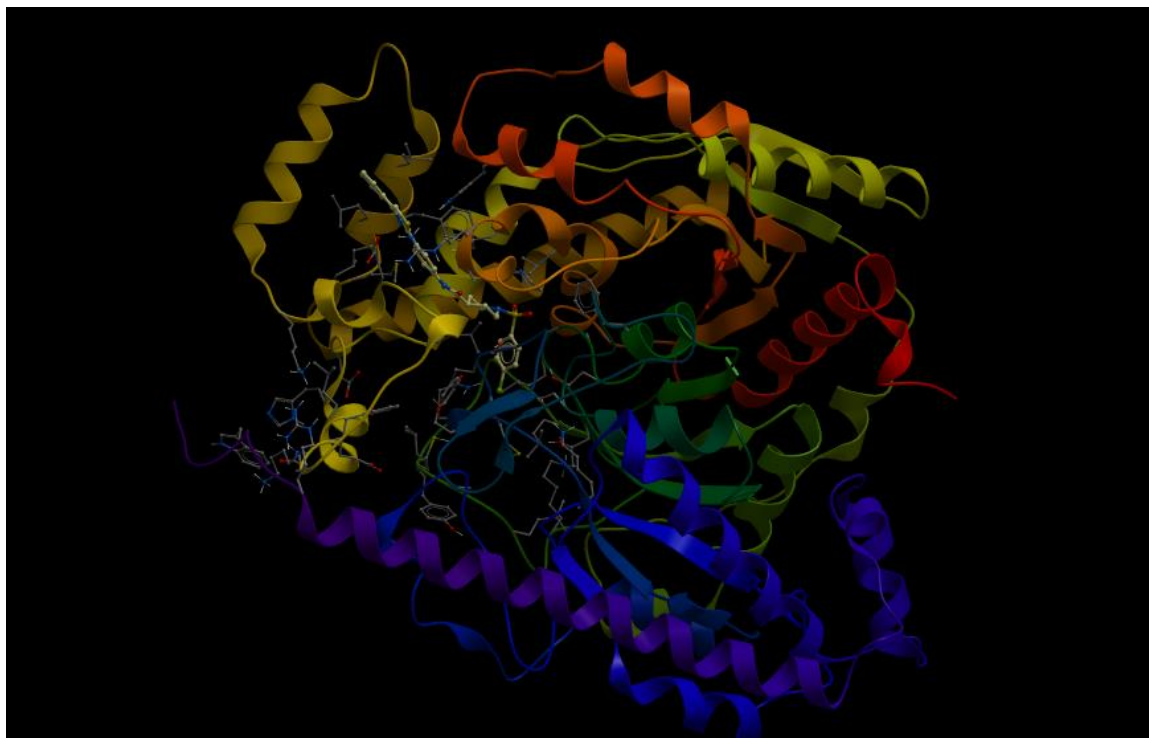


Figure 32. A docking pose of the inhibitor **2-5** in the catalytic site of the human FAAH enzyme

### Predicting ADME-Tox Properties

Finally, we calculated and performed prediction of the several pharmacokinetic parameters important for the drug development process, Table 6. Unfavorable absorption, distribution, metabolism, excretion, and toxicology (ADMET) properties have been identified as a major cause of drug candidate failure in the pharmaceutical industry (Dowden & Munro, 2019; Takebe et al., 2018). *In silico* ADMET prediction represents the use of computer modeling software to understand structure–property relationships and predicts the *in vivo* behavior of potential drug candidates in the human body (Lombardo et al., 2017).



Table 6. Predicted ADME-Tox properties of synthesized analogs.

Compound	Mol. Wt.	cLogP	cLogS	Drug Like-ness	Bad Groups	# of Rot Bonds	# of H-B Accept.	# of H-B Donors	CACO2	HalfLife (hrs)	hERG Inhib.	Tox Score
URB-597	338.163	4.022	-6.168	1.008	0	6	5	3	-4.985	0.85	0.714	2
1-1	400.092	4.355	-5.95	-0.033	0	5	7	1	-5.156	1.531	0.149	1.242
1-2	394.135	4.424	-6.359	-0.081	0	5	7	1	-5.053	2.264	0.342	1.242
1-3	412.126	4.573	-6.836	0.015	0	5	7	1	-5.148	3.264	0.255	1.242
2-1	509.09	5.785	-8.176	0.714	0	7	8	1	-5.135	1.083	0.149	0
2-2	521.124	6.003	-9.062	0.666	0	7	8	1	-5.177	2.048	0.31	0
2-3	537.095	6.448	-9.159	0.807	0	7	8	1	-5.163	2.048	0.182	0
2-4	521.124	6.123	-9.103	1.123	0	7	8	1	-5.207	1.839	0.31	0
2-5	537.095	6.568	-9.543	1.223	0	7	8	1	-5.168	1.839	0.182	0
2-6	539.115	6.273	-9.268	0.707	0	7	8	1	-5.263	3.732	0.371	0
2-7	571.056	7.163	10.085	0.802	0	7	8	1	-5.257	3.732	0.209	0

High logP values usually mean poor absorption/barrier penetration and is also an integral part of the well-known Lipinski Rule of 5 prediction (Lipinski et al., 1997). The Lipinski Rule of Five states that a drug candidate is more likely to exhibit poor absorption if two or more of the following criteria are fulfilled: more than 5 H-bond donors (HBD), more than 10 H-bond acceptors (HBA), the molecular weight is greater than 500 g/mol, and the calculated Log P (CLogP) is greater than 5. All final compounds showed predicted octanol/water partition coefficient (clogP) in the relatively acceptable range (2.0–6.5 is considered a good logP), moderate predicted aqueous solubility (acceptable range for logS is between –6.5 and –0.5 moles/liter) and no unwanted or reactive chemical functionalities (referred as “bad groups” in the table). Other predicted values that we examined were all within optimum ranges: hydrogen bond donors, hydrogen bond acceptors, and overall drug likeness, which should be within –1 and 1 range. Veber’s Rule, states that drug candidates will have good oral bioavailability if the number of rotatable bonds present in a molecule is less than 10 (Veber et al., 2002). Our compounds had 5 and 7 rotatable bonds, in line with this rule. However, there are several exceptions to Lipinski’s Rule and specifically how it applies to drugs that are being transported into cells by transport proteins located in the cell membrane (Benet et al., 2016). On the other hand, Veber’s rule does not consider a molecular weight cutoff at 500 as a significant factor for absorption and suggests that the good oral bioavailability can be predicted by observing the number of rotatable bonds (N of Rot Bonds) and polar surface area (PSA).

The ICM-Chemist-Pro Caco-2 prediction scores higher than –5 suggest a highly permeable drug candidate, while scores of below –6 represent a poorly permeable compound. As part of our Tox studies, we analyzed several important toxicology descriptors, LD<sub>50</sub>, hERG inhibition, and the Tox score. Prediction of the hERG inhibition is performed because pharmacological blockade of the hERG channel results in a severe life-threatening cardiac side effect possibly causing sudden death, leading to the withdrawal of many drugs from the development process (Jing et al., 2015; Lee et al., 2019). The ICM Chemist- Pro tool predicts that scores above or equal to 0.5 will probably exhibit some hERG inhibition at 100 μM or less, while compounds with predicted values below 0.5 will likely not be

hERG inhibitors. The human colon epithelial cancer cell (Caco-2) line model<sup>59</sup> is an established model for prediction of permeability of orally administered drugs and, in turn, the absorption of potential drug candidates. Predicted Caco2 permeability for these compounds indicates high permeability and this series of analogs had excellent predicted values for hERG inhibition. All final compounds (except standard URB-597) had values below 0.5. Our further prediction of plasma half-life showed that these compounds have a moderate predicted half-life of 1.05–3.75 hr (12-48 hours considered ideal). As part of the toxicity study predictions, we calculated the Tox score for each compound synthesized. This value represents the identification of potentially toxic parts/bi-products (during metabolism) of the molecule. All newly synthesized 4-phenylthiazole analogs had no unfavorable substructure/substituents, shown as a tox score of 0. Finally, the drug likeness score was considered. This is a purely empirical value and is based on several factors calculated above. The scores are on a scale of –1 to 1 and should not exceed 1, of which only **2-4** and **2-5** exceeded. These compounds were not the highest performing inhibitors and may not be further considered.

### Dual FAAH and sEH Inhibitors: Benzothiazoles

#### Design and Synthesis

Previously in our lab, we identified potent non-urea sEH inhibitors using high throughput screening (HTS) in combination with structure–activity relationship (SAR) studies. These molecules were derivatives of isonipecotic acid (e.g., inhibitor **a** show in Figure 33). Our SAR studies showed that the pharmacophore for the sEH inhibitors should include a central sulfonamide moiety connected next to the piperidine ring. We also observed that the bulky, hydrophobic groups on the left-hand side of the molecules are positively correlated with inhibitory potency (Pecic et al., 2012; Xie et al., 2009). In addition, we were able to successfully co-crystallize one of the non-urea inhibitors with human sEH (Pecic et al., 2013). Our docking experiments revealed that an amide functional group binds in the proximity of key amino acid residues needed for catalytic activity, two tyrosine residues (**Y383** and **Y466**), and one aspartic acid (**D335**) (Pecic et al., 2018).

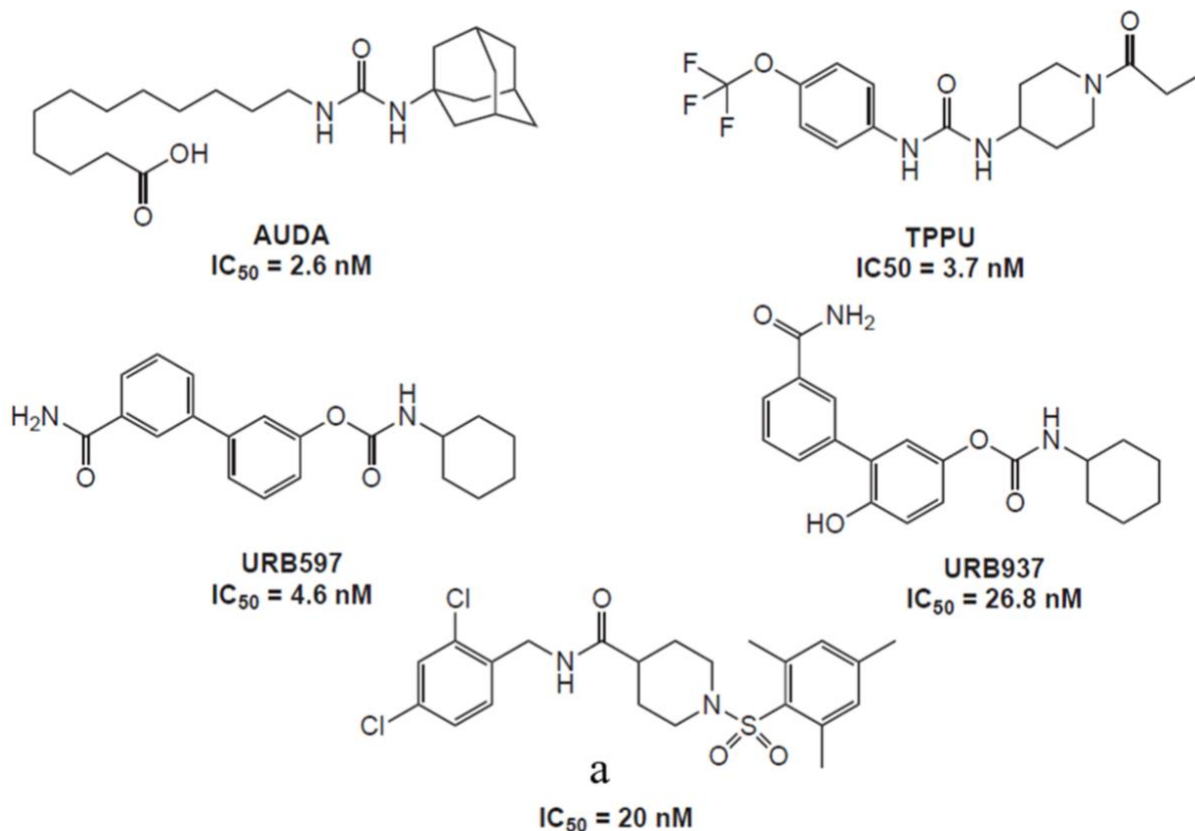


Figure 33. Known FAAH and sEH inhibitors.

The orientation of this amide moiety is similar to the orientation of the urea groups on urea sEH inhibitors (e.g., AUDA, Figure 33); thus, the amide group likely satisfies the same hydrogen bonding interactions with tyrosine and aspartic acid residues that contribute to highly potent urea inhibitors. Using information obtained from SAR studies in combination with molecular modeling and crystallography data, we were able to determine a particular pharmacophore for this series of sEH inhibitors (e.g., inhibitor **b**, shown in red, Figure 34) required to inhibit the sEH enzyme. Wang et al. (2010) performed an HTS and identified the benzothiazole inhibitor **c**, see Figure 34, as a potent rat FAAH inhibitor having an  $IC_{50}$  of 18 nM (Wang et al., 2009).

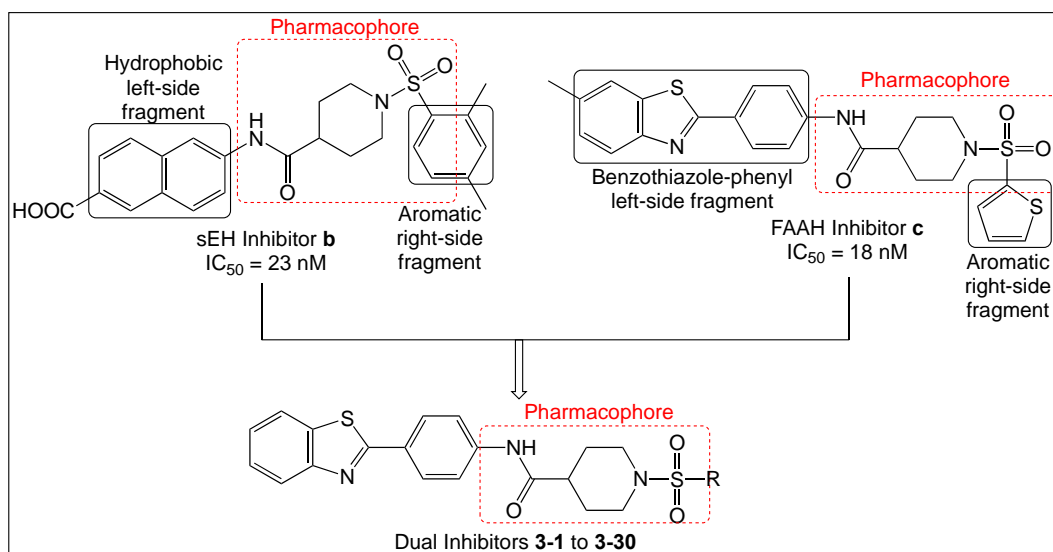


Figure 34. Design strategy for synthesis of dual sEH/FAAH inhibitors.

Their SAR studies indicated that the sulfonamide group, the piperidine ring, and benzothiazole on the left-hand side of the molecule were key components to their activity. The sulfonamide group likely forms hydrogen bonding interactions with the catalytic serine group, similar to the hydrogen-bonded network between the FAAH enzyme and the pyridyl nitrogen and oxazolyl oxygen of the  $\alpha$ -keto-oxazole FAAH inhibitors (Boger et al., 2005). In addition, the modeling study performed by Wang et al. (2010) also indicated that the benzothiazole ring satisfies hydrophobic interactions within the hydrophobic binding pocket of the rat FAAH enzyme that confers extraordinary potency (Wang et al., 2009). We also identified several potent 4-phenylthiazole FAAH inhibitors that possess the piperidine moiety connected to the phenyl ring via a sulfonamide bond (Wilt et al., 2020). These studies have shown that all three components, sulfonamide bond, piperidine ring and benzothiazole/4-phenylthiazole moieties, are important for the FAAH inhibition, but more work has to be done in order to access the particular relationship of each of these moieties with the inhibition potencies. Overall, these extensive SAR studies indicate that modifications to the aromatic ring on the left- and right-hand sides of the pharmacophore (shown in red in Figure 34) should allow for improved sEH and FAAH inhibition. This data guided our design for the preparation of the dual inhibitors wherein modifications to the right side of the aromatic ring were carried out. Since inhibition of each enzyme showed analgesic effect individually, and co-administration of sEH and FAAH inhibitors resulted in a

significant synergistic reduction in pain behavior in animal models of pain, we hypothesized that dual inhibitors will treat pain at a lower dose, and consequently with fewer side-effects (Sasso, 2014; Sasso et al., 2015; Wagner et al., 2011). We decided to employ a DML strategy wherein inhibitors used the core pharmacophore (a phenyl ring connected to a piperidine moiety, which is connected to the sulfonamide bond) common to the sEH inhibitor **b**, as seen in Figure 34, and the FAAH inhibitor **c**, shown in Figure 34, with modifications on the aromatic rings on either side. Figure 34 shows representative structures with the key pharmacophoric regions boxed (Gattrell et al., 2012; Morphy & Rankovic, 2005). Given that the benzothiazole ring contributes to high FAAH inhibitory potency and bulky hydrophobic groups are well-tolerated in that position for sEH inhibitory potency, we kept this structure constant (general structure 4) while modifying aromatic groups bound to the sulfonamide group (Pecic et al., 2012; Pecic et al., 2013). Following the established synthetic procedure shown in experimental section, we started from the readily available 2-(4-aminophenyl) benzothiazole and Boc-isonipepic acid. EDC coupling yielded the amide **d**, which was subjected to Boc-deprotection with trifluoroacetic acid (TFA) which provided the key amine intermediate **e**, (Pecic et al., 2018). Coupling with different R-sulfonyl chlorides furnished final compounds **3-1** to **3-30** in moderate yields (16–84%).

### Biological Evaluation and SAR

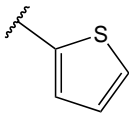
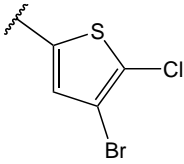
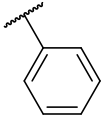
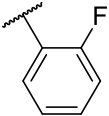
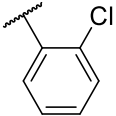
All synthesized analogs **3-1** to **3-30** were tested *in vitro* in both human sEH and human FAAH inhibition assays. The inhibition potencies of analyzed analogs against both enzymes are summarized in Table 7. Our initial SAR investigation started with the synthesis of the thiophene-2-yl analog, **3-1**. This analog showed inhibition potency in the low nanomolar range for human FAAH enzyme ( $IC_{50} = 16$  nM), but only moderate inhibition potency at the human sEH enzyme ( $IC_{50} = 420$  nM). The introduction of bromine and chlorine atoms on the thiophene ring (analog **3-2**) led to significantly diminished inhibition potencies at both enzymes. We decided to replace the thiophene ring with a phenyl ring, which allowed us to access many sterically and electronically diverse chemical groups, which could in turn improve inhibition profiles for both enzymes. The phenyl analog **3-3**,

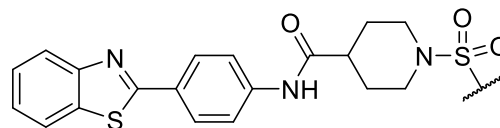
showed excellent inhibition potency with the human FAAH enzyme, having an  $IC_{50}$  of 8.6 nM, but only low micromolar inhibition for human sEH enzyme ( $IC_{50}$  = 1100 nM). Fluoro-, chloro-, bromo- and methyl- groups placed at the *ortho* position (**3-4**, **3-5**, **3-6**, and **3-7**, respectively) were all well tolerated in the human FAAH binding pocket and led to low nanomolar inhibition potency on human FAAH enzyme. The bulkier, electron-donating methoxy- group (**3-8**) was less potent for human FAAH ( $IC_{50}$  = 80 nM). Placement of chloro-, bromo-, or methyl- groups in the *ortho* position improved potency at the sEH enzyme relative to the unsubstituted inhibitor (**3-3**). This led to the best dual sEH/FAAH inhibitor of the series (**3-5**) with equally high potency for sEH ( $IC_{50}$  = 9.6 nM) and FAAH ( $IC_{50}$  = 7 nM). Next, we introduced the same replacements into the *meta*-position on the phenyl ring. We noticed that adding fluoro-, chloro-, bromo-, methyl- or methoxy groups at the *meta* position (**3-9**, **3-10**, **3-11**, **3-12** and **3-13**, respectively) had comparable potencies relative to the unsubstituted inhibitor (**3-3**). These inhibitors retain low nanomolar inhibition potencies for human FAAH enzyme with low potency at the human sEH enzyme ( $IC_{50}$ s ranged from 620 to 2400 nM). Modification of the *para* position with fluoro-, chloro, bromo-, methyl- and methoxy- substitutions (**3-14**, **3-15**, **3-16**, **3-17** and **3-18**, respectively) led to a loss of potency towards FAAH relative to the unsubstituted inhibitor (**3-3**). Surprisingly, the introduction of the 2,4-disubstitutions for fluoro-, chloro-, bromo and methoxy- groups (**3-19**, **3-20**, **3-21**, **3-22** and **3-23**, respectively) led to inhibitors with potency at both enzymes comparable to the same single *ortho*- substitutions and improved potency relative to *para*- substitutions. Thus, the benefit from *ortho*- substitutions is greater than the loss from *para*- substitutions. The fluoro- and methyl- 3,5-disubstitutions (**3-24** and **3-25**) had low potency at both enzymes ( $IC_{50}$ s > 10,000 nM on FAAH and 1,000 nM on sEH). Additionally, the fluoro-, chloro-, methyl- and isopropyl- tri-substitutions (**3-26**, **3-27**, **3-28** and **3-29**, respectively) and the pentafluoro- substitution (**3-30**) had lower potency than the 2,4-disubstituted molecules. This suggests compounds that are more substituted are not favored in the active sites of FAAH and sEH.

## Molecular Modeling Studies

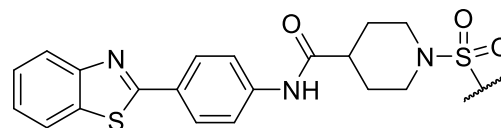
Our design and evaluation of synthesized analogs were complemented with *in silico* experiments. Since the crystal structure of the human FAAH enzyme has not been reported, we built and evaluated a homology model for the human FAAH enzyme (Wilt et al., 2020). We docked all synthesized analogs, **3-1** to **3-30**, in both the human FAAH enzyme homology model and the human sEH enzyme crystal structure derived from PDB: 4HAI. Docking scores obtained in these experiments are shown in Table 7 and all non-covalent interactions are shown in Table 8A and Table 8B for FAAH and sEH enzymes, respectively.

Table 7. Fatty acid amide hydrolase (FAAH) and soluble epoxide hydrolase (sEH) inhibitory activities and docking scores of analogs 3-1 to 3-30.

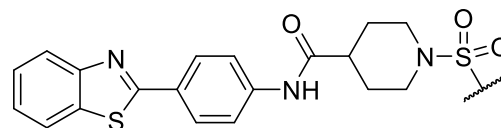
Compound	R	FAAH IC <sub>50</sub> (nM)	sEH IC <sub>50</sub> (nM)	Docking Score FAAH	Docking Score sEH
URB 597	-	38	-	-31.45	-22.16
AUDA	-	-	2.6	-22.18	-25.83
2-thiophenyl 3-1		16	420	-21.04	-22.35
2-(4-bromo-5-chlorophenyl) 3-2		2700	5900	-12.3	-21.02
phenyl 3-3		8.6	1100	-23.77	-30.32
2-fluorophenyl 3-4		1.3	150	-28.05	-32.42
2-chlorophenyl 3-5		7	9.6	-28.93	-33.03



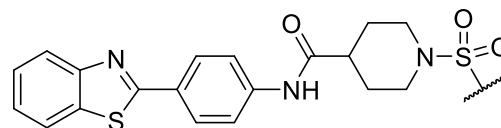




Compound	R	FAAH IC <sub>50</sub> (nM)	sEH IC <sub>50</sub> (nM)	Docking Score FAAH	Docking Score sEH
2-bromophenyl 3-6		6.1	24	-26.88	-30.93
2-methylphenyl 3-7		9.6	35	-34.41	-32.44
2-methoxyphenyl 3-8		80	26	-29.93	-32.98
3-fluorophenyl 3-9		13.4	1700	-35.20	-34.19
3-chlorophenyl 3-10		7.2	2400	-32.98	-29.41
3-bromophenyl 3-11		51.6	1100	-32.17	-29.25
3-methylphenyl 3-12		7	940	-36.5	-30.08
3-methoxyphenyl 3-13		14.6	620	-26.88	-32.16
4-fluorophenyl 3-14		77	1300	-19.99	-28.91
4-chlorophenyl 3-15		260	710	-22.49	-27.61



Compound	R	FAAH IC <sub>50</sub> (nM)	sEH IC <sub>50</sub> (nM)	Docking Score FAAH	Docking Score sEH
4-bromophenyl 3-16		185	580	-23.64	-31.23
4-methylphenyl 3-17		>10000	370	-29.02	-32.60
4-methoxyphenyl 3-18		>10000	84	-18.66	-31.59
2,4-difluorophenyl 3-19		11.4	195	-27.22	-33.84
2,4-dichlorophenyl 3-20		31.3	13.1	-23.64	-34.11
2,4-dibromophenyl 3-21		10	36	-37.38	-34.20
2,4-dimethylphenyl 3-22		5.5	29.2	-33.14	-32.08
2,4-dimethoxyphenyl 3-23		36.2	180	-33.22	-34.47



Compound	R	FAAH IC <sub>50</sub> (nM)	sEH IC <sub>50</sub> (nM)	Docking Score FAAH	Docking Score sEH
3,5-difluorophenyl 3-24		>10000	1100	-36.69	-32.39
3,5-dimethylphenyl 3-25		>10000	3600	-41.62	-33.18
2,4,6-trifluorophenyl 3-26		250	6600	-26.88	-30.58
2,4,6-trichlorophenyl 3-27		270	1300	-33.37	-29.05
2,4,6-trimethylphenyl 3-28		84	790	-28.97	-31.33
2,4,6-triisopropylphenyl 3-29		2233	840	-18.61	-24.48
2,3,4,5,6-pentafluorophenyl 3-30		>10000	2670	-37.58	-27.90

Table 8a. The list of hydrogen bonds, hydrophobic interactions and other non-covalent interactions of analogs docked in human FAAH enzyme.

Compound	H-bonds	Hydrophobic interactions	Other non-covalent interactions
URB-597	G485	F192, S193, Y194, G239, F244, L401, L404, I407, M436, T488, V491, W531	M191, G240, S241, F381, D403, R486, I530
AUDA	G272	M191, F192, S193, Y194, I238, G239, F244, V270, Q273, L278, V491	S190, S217, S241, C269, Y271, E274
2-tiophenyl 3-1	N/A	F192, S193, Y194, G239, G240, S241, F244, F381, L404, I407, V422, L429, F432, L433, M436, T488, V491, I530, W531	M191, G216, S217, L380, L401, G485
2-(4-bromo-5-chlorophenyl) 3-2	G485	F192, S193, Y194, I238, G239, G240, S241, F244, L404, I407, V422, L429, L433, T488, V491, I530, W531	M191, G216, S217, F381, L401, P484
phenyl 3-3	N/A	F192, S193, Y194, G239, S241, F244, L380, F381, L404, I407, V422, L429, F432, L433, M436, T488, V491, I530, W531	G216, S217, M191, I238, G240
2-fluorophenyl 3-4	N/A	F192, S193, Y194, I238, G239, G240, S241, F244, F381, L404, I407, V422, L429, F432, L433, M436, T488, V491, I530, W531	M191, G216, S217, L380, L401, G485, M495
2-chlorophenyl 3-5	N/A	F192, S193, Y194, I238, G239, G240, S241, F244, F381, L404, I407, V422, L429, F432, L433, M436, T488, V491, I530, W531	M191, G216, S217, L380, G485, M495
2-bromophenyl 3-6	N/A	F192, S193, Y194, I238, G239, L380, L404, I407, V422, L429, L433, M436, T488, V491, M495, I530, W531	M191, S241, F244, F381, G485
2-methylphenyl 3-7	N/A	F192, S193, Y194, I238, G239, G240, S241, F244, F381, L404, I407, V422, L429, F432, L433, M436, T488, V491, I530, W531	M191, G216, S217, L380, L401, G485, M495
2-methoxyphenyl 3-8	N/A	F192, S193, Y194, I238, G239, G240, S241, F244, F381, L404, I407, V422, L429, F432, L433, M436, T488, V491, I530, W531	M191, G216, S217, L380, G485, M495
3-fluorophenyl 3-9	N/A	F192, S193, Y194, I238, G239, G240, S241, F244, F381, L404, I407, V422, L429, F432, L433, M436, T488, V491, I530, W531	M191, G216, S217, L380, L401, G485

Compound	H-bonds	Hydrophobic interactions	Other non-covalent interactions
3-chlorophenyl 3-10	N/A	F192, S193, Y194, I238, G239, G240, S241, F244, F381, L404, I407, V422, L429, F432, L433, M436, T488, V491, I530, W531	M191, G216, S217, L380, L401, G485
3-bromophenyl 3-11	G485	F192, S193, Y194, I238, G239, G240, S241, F244, L404, I407, V422, L429, L433, T488, V491, I530, W531	M191, G216, F381, L401, P484
3-methylphenyl 3-12	G485	F192, S193, Y194, L380, F381, L404, I407, V422, L429, F432, L433, T488, V491, M495, I530, W531	M191, T377, L401, D403, P484
3-methoxyphenyl 3-13	G485	F192, S193, Y194, I238, G239, S241, F244, L404, I407, V422, L429, L433, T488, V491, I530, W531	M191, S217, F381, L401, D403, P484
4-fluorophenyl 3-14	N/A	F192, S193, Y194, G239, G240, S241, F244, F381, L404, I407, V422, L429, F432, L433, M436, T488, V491, I530, W531	M191 G216, S217, L380
4-chlorophenyl 3-15	N/A	M191, F192, S193, Y194, I238, G239, F381, L404, I407, V422, L429, F432, L433, M436, T488, V491, I530, W531	S241, F244, M495
4-bromophenyl 3-16	N/A	M191, F192, S193, G239, L404, I407, V422, L429, F432, L433, M436, T488, I530, W531	Y194, S217, S241, F244, G485, V491
4-methylphenyl 3-17	N/A	M191, F192, S193, I238, G239, L404, I407, V422, L429, F432, L433, M436, T488, I530, W531	Y194, S217, S241, F244, G485, V491
4-methoxyphenyl 3-18	N/A	M191, F192, S193, I238, G239, L380, F381, L404, I407, V422, L429, F432, L433, M436, T488, I530, W531	Y194, S241, F244, V491
2,4-difluorophenyl 3-19	N/A	M191, F192, S193, I238, G239, L380, F381, L404, I407, V422, L429, F432, L433, M436, T488, V491, I530, W531	Y194, S241, F244, M495
2,4-dichlorophenyl 3-20	N/A	M191, F192, S193, Y194, I238, G239, L404, I407, V422, L429, L433, M436, T488, I530, W531	G216, S217, S241, F244, L401, G485, V491
2,4-dibromophenyl 3-21	N/A	M191, F192, S193, Y194, I238, G239, L380, L404, I407, L429, L433, M436, T488, V491, I530, W531	G216, S241, F244, G485
2,4-dimethylphenyl 3-22	G485	F192, S193, Y194, G239, G240, S241, F244, L404, I407, V422, L429, L433, T488, V491, M495, I530, W531	M191, G216, F381, P484

Compound	H-bonds	Hydrophobic interactions	Other non-covalent interactions
2,4-dimethoxyphenyl 3-23	N/A	M191, F192, S193, Y194, I238, G239, L380, F381, L404, I407, L429, L433, T488, V491, I530, W531	S217, S241, F244, L401, P484, G485
3,5-difluorophenyl 3-24	G485	Y194, G239, F381, F432, L404, I407, V422, L429, F432, L433, T488, V491, M495, I530, W531	F192, T377, L401, D403, P484
3,5-dimethylphenyl 3-25	G485	F192, S193, Y194, L380, F381, L404, I407, V422, L429, F432, L433, T488, V491, M495, I530, W531	M191, T377, L401, D403, P484
2,4,6-trifluorophenyl 3-26	N/A	M191, F192, S193, Y194, I238, G239, L380, L404, I407, V422, L429, F432, L433, M436, T488, I530, W531	G216, S217, S241, F244, G485, V491, M495
2,4,6-trichlorophenyl 3-27	N/A	M191, F192, S193, Y194, I238, G239, L266, G268, Y271, T377, F381, L404, F432, M436, T488, V491, M495	S190, S217, T236, G240, S241, K267, V270
2,4,6-trimethylphenyl 3-28	N/A	M191, F192, S193, Y194, I238, G239, L380, L404, I407, V422, L429, L433, M436	G216, S217, S241, F244, P484, G485
2,4,6-triisopropylphenyl 3-29	I238	M191, F192, S193, Y194, G239, F244, L266, G268, Y271, L278, T377, L380, F381, L404, F432, M436, T488, V491, M495	S190, S217, T236, D237, G240, S241, K267, C269, V270, L401, P484
2,3,4,5,6-pentafluorophenyl 3-30	G485	S193, Y194, G239, S376, T377, L380, F381, D403, L404, I407, V422, F432, L433, T488, V491, M495, I530, W531	F192, L401, P484

Table 8b. The list of hydrogen bonds, hydrophobic interactions and other non-covalent interactions of analogs docked in human sEH enzyme.

Compound	H-bonds	Hydrophobic interactions	Other non-covalent interactions
URB-597	L417, Y466	F267, D335, W336, T360, Y383, M419, V498, L499, H524, W525	Q384, L408, S415
AUDA	Y466, H524, W525	D335, W336, M339, T360, F381, Y383, S412, M419, F497, V498, L499	F267, Q384, L408, R410, A411, K495, G523
2-tiophenyl 3-1	D335	F267, W336, M339, P371, I375, F381, Y383, L408, L417, M419, L428, M469, N472, V498, L499, H524	Q384, Y466, W525
2-(4-bromo-5-chlorophenyl) 3-2	Y466	F267, W336, M339, P371, I375, F381, Y383, L408, L417, M419, L428, M469, N472, V498, L499, H524, W525	P268, D335, Q384, F387, S418
Phenyl 3-3	D335	F267, W336, M339, P371, I375, F381, Y383, L408, L417, M419, L428, M469, N472, V498, L499, H524	Q384, Y466, W525
2-fluorophenyl 3-4	Y466	D335, W336, M339, T360, P361, I363, F381, Y383, L407, R410, S415, L417, M419, V498, L499, M503, H524, W525	Q384, S407, A411, M469, D496
2-chlorophenyl 3-5	D335	F267, W336, M339, P371, I375, F381, Y383, F387, L408, L417, M419, L428, M469, N472, V498, L499, H524	P268, Q384, Y466, W525
2-bromophenyl 3-6	D335	F267, W336, M339, P371, I375, F381, Y383, F387, L408, L417, M419, L428, M469, N472, V498, L499, H524	P268, Q384, Y466, W525
2-methylphenyl 3-7	N/A	D335, W336, M339, T360, P361, I363, F381, Y383, L408, R410, S415, L417, M419, Y466, V498, L499, M503, H524, W525	F267, Q384, S407, A411, M469

Compound	H-bonds	Hydrophobic interactions	Other non-covalent interactions
2-methoxyphenyl 3-8	Y466	W336, M339, T360, P361, I363, I375, F381, Y383, L408, R410, S415, L417, M419, V498, L499, M503, H524, W525	D335, Q384, S407, A411, M469, D496
3-fluorophenyl 3-9	Y466	F267, W336, M339, P371, I375, F381, Y383, L408, L417, M419, L428, M469, V498, L499, H524	D335, Q384, F387
3-chlorophenyl 3-10	D335	W336, M339, P361, I363, F381, Y383, L408, R410, S415, L417, M419, Y466, V498, L499, M503	P268, Q384, Y466, W525
3-bromophenyl 3-11	Y466	W336, M339, T360, P361, I363, F381, Y383, L408, R410, S415, L417, M419, V498, L499, M503, H524, W525	D335, Q384, S407, A411, M469, D496
3-methylphenyl 3-12	Y466	F267, D335, W336, M339, P371, I375, F381, Y383, Q384, L408, L417, M419, L428, Y466, M469, V498, L499, H524	D335, Q384, F387
3-methoxyphenyl 3-13	N/A	D335, W336, M339, T360, P361, I363, F381, Y383, L408, R410, S415, L417, M419, Y466, V498, L499, M503, H524, W525	F267, Q384, S407, A411, M469
4-fluorophenyl 3-14		F267, W336, M339, P371, I375, F381, Y383, L408, L417, M419, L428, M469, N472, V498, L499, H524	P268, D335, Q384, S418, Y466, W525
4-chlorophenyl 3-15	N/A	F267, W336, M339, P371, I375, F381, Y383, L408, L417, M419, L428, Y466, M469, N472, V498, L499, H524	P268, D335, Q384, S418, W525
4-bromophenyl 3-16	Y466	F267, D335, W336, M339, P371, I375, F381, Y383, L408, L417, M419, M469, V498, L499, H524, W525	D335, Q384, F387, S415, L428



Compound	H-bonds	Hydrophobic interactions	Other non-covalent interactions
4-methylphenyl 3-17	N/A	F267, W336, M339, P371, I375, F381, Y383, L408, L417, M419, L428, Y466, M469, N472, V498, L499, H524	P268, D335, Q384, W473, W525
4-methoxyphenyl 3-18	Y466	W336, M339, I363, I375, F381, Y383, L408, R410, S415, L417, M419, V498, L499, M503, H524, W525	F267, D335, T360, Q384, S407, A411, D496
2,4-difluorophenyl 3-19	D335	F267, W336, M339, P371, I375, F381, F387, Y383, L408, L417, M419, L428, M469, N472, L499, V498, H524	P268, Q384, S418, Y466, W525
2,4-dichlorophenyl 3-20	N/A	F267, W336, M339, P371, I375, F381, Y383, F387, L408, L417, M419, L428, M469, N472, V498, L499, H524	P268, D335, Q384, S418, Y466, W525
2,4-dibromophenyl 3-21	Y466	F267, W336, M339, P371, I375, F381, Y383, L408, L417, M419, L428, M469, N472, V498, L499, H524, W525	D335, Q384, F387, S415
2,4-dimethylphenyl 3-22		F267, W336, M339, P371, I375, F381, Y383, F387, L408, L417, M419, L428, M469, N472, V498, L499, H524	P268, D335, Q384, Y466, W473, W525
2,4-dimethoxyphenyl 3-23	Y466	W336, M339, P361, I363, I375, F381, Y383, L408, R410, S415, L417, M419, V498, L499, M503, H524, W525	F267, D335, T360, Q384, S407, A411, D496
3,5-difluorophenyl 3-24	Y466	W336, M339, I375, F381, Y383, L408, R410, S415, L417, M419, M469, L499, V498, H524, W525	D335, T360, Q384, S407, A411, N472, D496
3,5-dimethylphenyl 3-25		W336, M339, I375, F381, Y383, L408, R410, S415, L417, M419, Y466, M469, V498, L499, H524, W525	F267, D335, T360, Q384, S407, A411, D496

Compound	H-bonds	Hydrophobic interactions	Other non-covalent interactions
2,4,6-trifluorophenyl 3-26	Y466	W336, M339, T360, P361, I363, F381, Y383, L408, R410, S415, L417, M419, M469, V498, L499, M503, H524, W525	F267, D335, Q384, S407, A411, D496
2,4,6-trichlorophenyl 3-27	N/A	F267, W336, M339, P371, I375, F381, Y383, F387, L408, L417, M419, L428, M469, N472, V498, L499, H524, W525	P268, D335, Q384, S418, Y466
2,4,6-trimethylphenyl 3-28	D335	F267, W336, M339, P371, I375, F381, Y383, F387, L408, L417, M419, L428, M469, N472, V498, L499, H524	P268, Q384, S418, Y466
2,4,6-triisopropylphenyl 3-29	Y466	W336, M339, T360, P361, I363, P371, I375, F381, Y383, L408, R410, L417, M419, Y466, M469, V498, L499, M503, H524, W525	D335, S374, Q384, S407, D496
2,3,4,5,6- pentafluorophenyl 3-30	Y466	W336, M339, T360, P361, I363, I375, F381, Y383, L408, R410, S415, L417, M419, M469, V498, L499, M503, H524, W525	F267, D335, Q384, S407, A411, D496

There are many factors that affect the reliability of pose predictions and scoring, and some molecular modeling software appear to better perform on hydrophobic vs. hydrophilic pockets, some are better with small molecules vs. peptides, etc. (Li et al., 2018). For the human FAAH enzyme, the low values for the potential energy (docking scores) were obtained for all the analogs that also show *in vitro* low nanomolar inhibition potencies (e.g., **3-7**, **3-11**, **3-12**, **3-21**, **3-23**, etc.). Analysis of these values show that most of the obtained docking energies are correlated with inhibitory potency ( $R^2 = 0.3255$ ,  $p = 0.0023$ ) with the exception of compounds with very poor potency on FAAH ( $IC_{50} > 10,000$ ) (Figure 35).

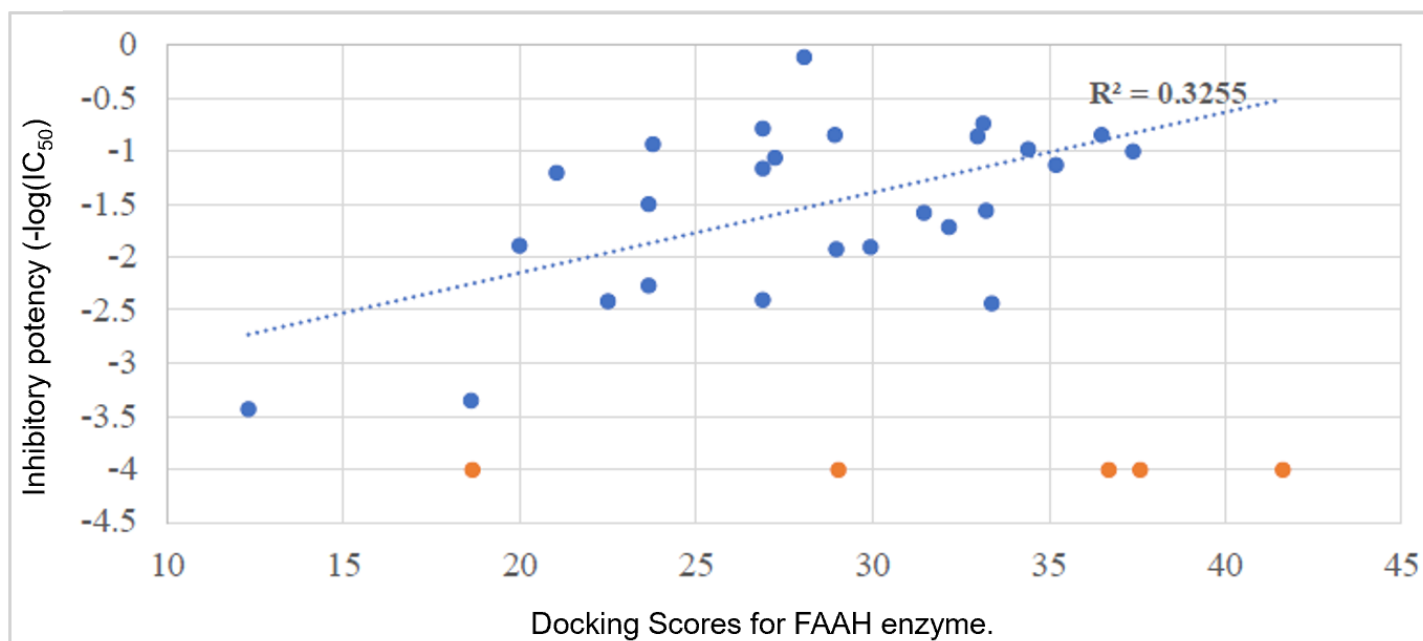


Figure 35. Correlation of inhibitory potency ( $-\log(\text{IC}_{50})$ ) vs Docking Scores for FAAH enzyme.

This suggests that the potency of these inhibitors is primarily based on Van der Waals interactions between the enzyme active site and inhibitors. After visual inspection of the top binding modes of the most active inhibitors, we noticed that all docked compounds are located in the proximity of **S241** and **S217**, both residues of the catalytic triad, **S241-S217-K142**, which is responsible for the hydrolytic cleavage of the amide bond of the substrate anandamide by the FAAH enzyme (Ahn, Johnson, & Cravatt, 2009). We were able to define the most important residues within the binding pocket of the FAAH enzyme and tried to explain the increased *in vitro* inhibition potencies by observing and analyzing the type of contacts of the most active FAAH inhibitor identified in this study, **3-4**, with the inhibitory potency of 1.3 nM, and other analogs with low nanomolar inhibition potencies, e.g., **3-5**, **3-6**, **3-10** and **3-22**. The aromatic part of the inhibitor **3-4** is found to be embedded between several hydrophobic amino acid residues (**F192**, **S193**, **Y194**, **I238**, **G239**, **G240**, **S241**, **F244**, **F381**, **L404**, **I407**, **V422**, **L429**, **F432**, **L433**, **M436**, **T488**, **V491**, **I530**, **W531**) and forms other important non-covalent interactions (**M191**, **G216**, **S217**, **L380**, **L401**, **G485**, **M495**), which we believe all contribute to high inhibitory potency of this analog (Table 8A). The best dual inhibitor identified herein, **3-5** has a very similar defined binding pocket, showing the importance of selected

hydrophobic and other non-covalent interactions for the low nanomolar inhibition potency, see Figure 36 and 37, Table 8A.

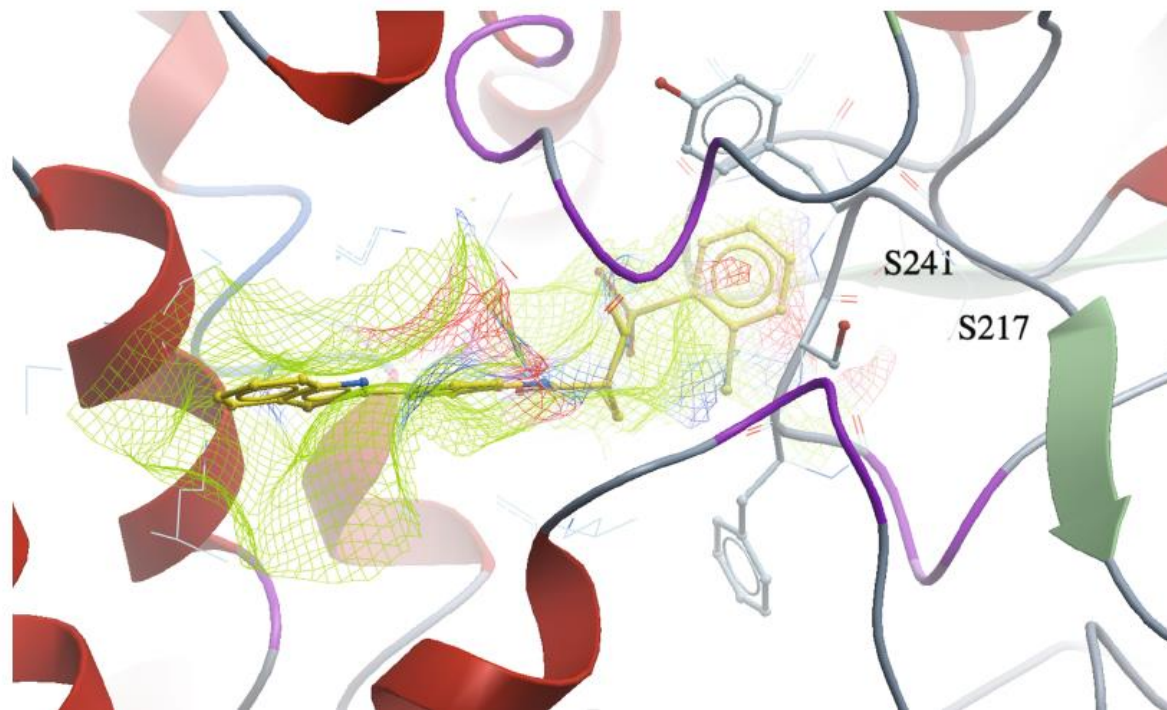


Figure 36. 3d docking pose of the inhibitor **3-5** in the catalytic site of the human FAAH enzyme.

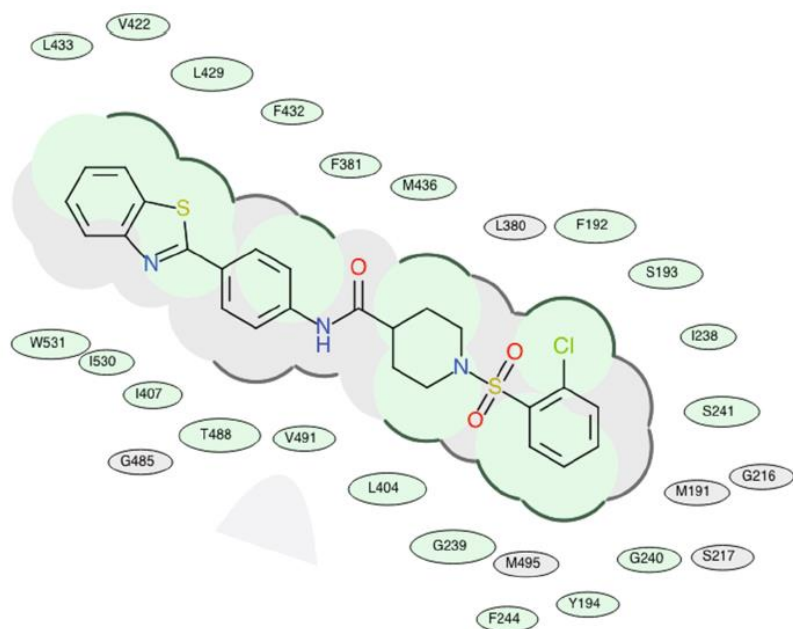


Figure 37. 2D representation for the lowest energy conformation of inhibitor **3-5** in the binding pocket of human FAAH. Green shading represents hydrophobic region; gray parabolas represent accessible surface for large areas; broken thick line around ligand shape indicates accessible surface; size of residue ellipse represents the strength of the contact

The poor correlation of docking energies with *in vitro* experiments were observed with only three analogs, **3–24**, **3–25** and **3–30**, but visual inspection of these compounds within the binding pocket of the human FAAH homology model reveals the absence of several important contacts with residues, **S241** and **S217**, that are present with the biologically active analogs, which could explain the lower inhibition potencies of these three analogs, Table 8A. The docking experiments of all synthesized inhibitors in the human sEH enzyme model revealed that most of the analogs are located in the proximity of key amino acids within the catalytic pocket that are involved in the hydrolysis of EETs. Compared with docking scores for the FAAH enzyme, the docking scores of sEH poorly correlated with sEH potency, Figure 38.

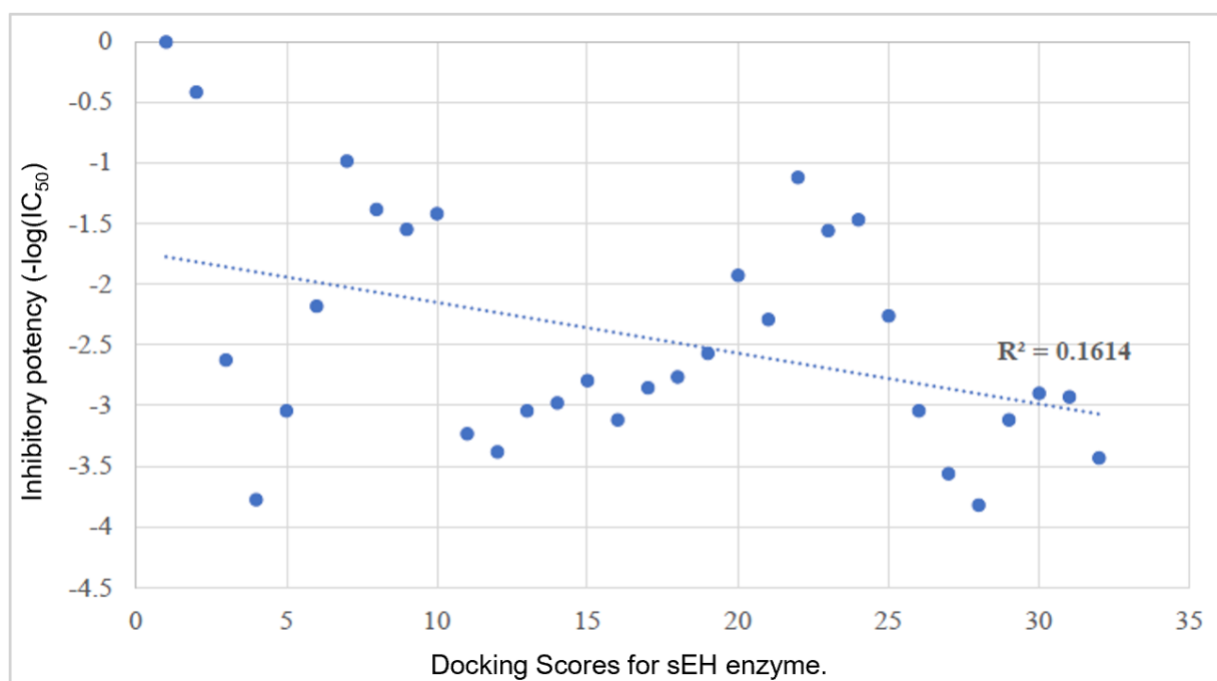
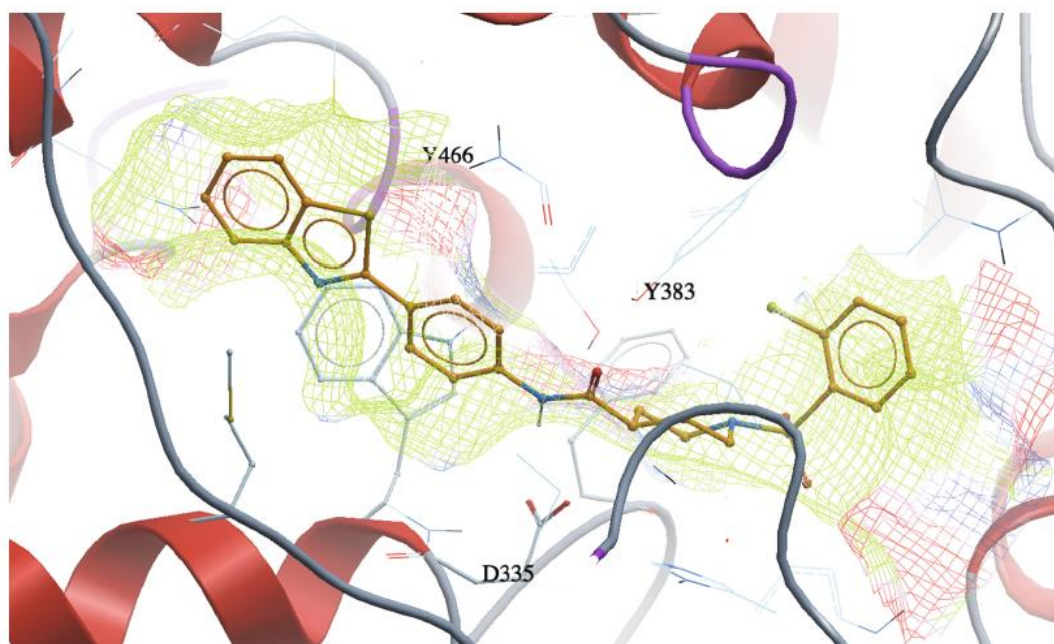


Figure 38. Correlation of inhibitory potency ( $-\log(\text{IC}_{50})$ ) vs. Docking Scores for sEH enzyme.

All potent sEH inhibitors (e.g. **3–5**, **3–6**, **3–7**, **3–8**, **3–20**, **3–21** and **3–22**) have good docking scores, Table 7, however, the analogs that were inactive in the *in vitro* inhibition assay, also have good docking scores in our docking experiments. This possibly indicates that sEH potency is primarily determined based on hydrogen bonding interactions with the catalytic residues rather than hydrophobic interactions with the binding pocket which probably is responsible for the good docking scores in this series of analogs. Our previous molecular modeling studies and X-ray crystallographic

structure showed that two tyrosine residues (**Y383** and **Y466**) and one aspartic acid residue (**D335**), located in the hydrolase catalytic pocket of sEH, are involved in hydrogen bonding with the inhibitors. One of the most potent sEH inhibitors identified in this study, and the best dual inhibitor, **3-5**, is in the close proximity of these three amino acid residues, see Figures 39 and 40, Table 8B.



*Figure 39.* 3D docking pose of the inhibitor **3-5** in the catalytic site of the human soluble epoxide hydrolase (sEH) enzyme.

This inhibitor forms a hydrogen bond with **D335** via amide bond, and has several important hydrophobic interactions (**F267**, **W336**, **M339**, **P371**, **I375**, **F381**, **Y383**, **F387**, **L408**, **L417**, **M419**, **L428**, **M469**, **N472**, **V498**, **L499**, **H524**), that, combined with other noncovalent interactions (**P268**, **Q384**, **Y466**, **W525**), contribute to the high inhibition potency of this compound. We also noticed that all low nanomolar sEH inhibitors identified in this study are docked in the proximity of the key amino acid residues, **Y383**, **Y466**, and **D335**, located in the catalytic site of the sEH enzyme, Table 8B, while inactive compounds lack this interaction. Finally, we looked at the binding poses of the potent dual inhibitors, **3-5**, **3-6**, **3-20**, **3-21**, and **3-22**, within both, human FAAH and sEH enzyme binding pockets. We observed that the benzothiazole moiety of all aforementioned ligands is located in the proximity of the two hydrophobic residues, **V422** and **L433** in the human FAAH binding pockets, while

this group probably interacts with one of the methionine residues (**M419** or **M469**) within human sEH binding pocket.

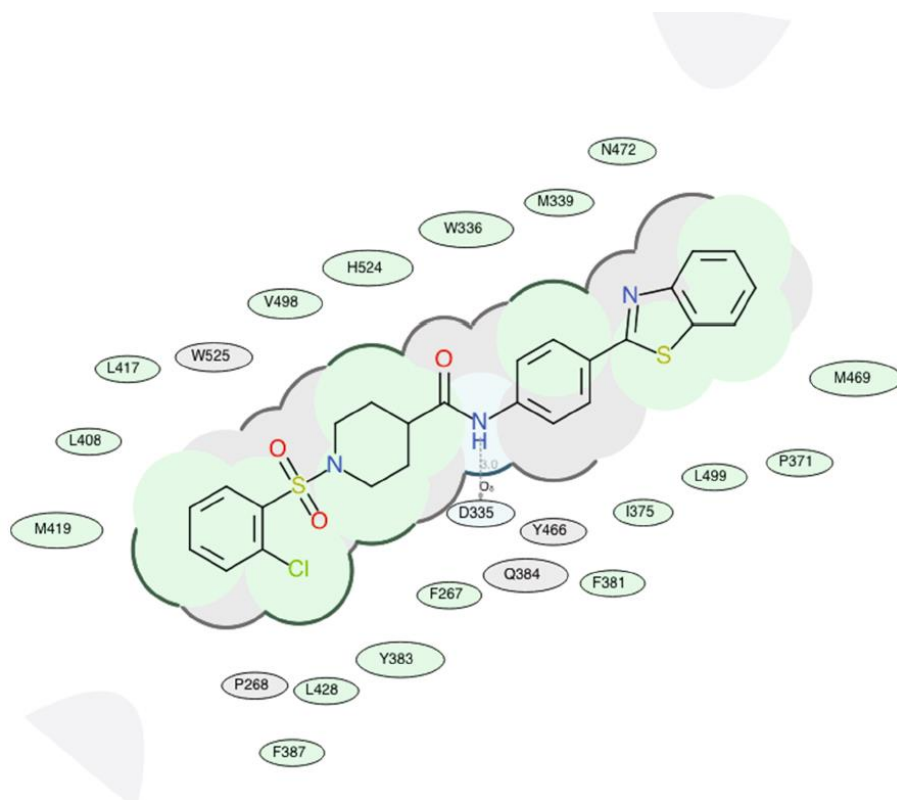


*Figure 40.* 2D representation for the lowest energy conformation of inhibitor **3–5** in the binding pocket of human sEH. Green shading represents hydrophobic region; gray parabolas represent accessible surface for large areas; broken thick line around ligand shape indicates accessible surface; size of residue ellipse represents the strength of the contact.

### Predicting ADME-Tox Properties

Based on the encouraging biological results described above, we performed some selected ADMET predictions to assess their drug-like properties. Using the ICM-Chemist-Pro tool, we started our investigations (see Table 9) by calculating simple physicochemical descriptors, such as cLogP and aqueous solubility (cLogS).

Table 9. Predicted ADMET properties of synthesized analogs.

Compound	Mol. Wt.	cLog P	cLog S	Drug Likeness	Bad Group	# of Rot Bonds	# of H-B Accept.	# of H-B Donors	Caco 2	Half-Life (h)	hERG Inhib.	Tox Score
URB-597	338.407	4.022	-6.168	1.008	0	6	5	3	-4.985	0.85	0.714	2
AUDA	392.584	6.107	-6.679	-0.016	0	15	5	3	-4.760	2.838	0.601	0.878
2- thiophen-yl 3-1	483.619	5.317	-6.918	0.584	0	6	8	1	-5.12	2.05	0.106	0
4-bromo-5-chloro thiophen-2-yl 3-2	596.957	6.757	-8.513	0.740	0	6	8	1	-5.348	1.213	0.106	0
phenyl 3-3	477.597	5.386	-7.327	0.553	0	6	8	1	-5.055	2.873	0.149	0
2-fluorophenyl 3-4	495.587	5.535	-7.804	0.541	0	6	8	1	-5.252	3.20	0.255	0
2-chlorophenyl 3-5	512.039	5.980	-7.900	0.644	0	6	8	1	-5.180	3.205	0.182	0
2-bromophenyl 3-6	556.493	6.117	-8.070	0.396	0	6	8	1	-5.276	3.21	0.106	0
2-methylphenyl 3-7	491.624	5.667	-7.664	0.428	0	6	8	1	-5.216	3.71	0.182	0
2-methoxyphenyl 3-8	507.623	5.356	-7.277	0.382	0	7	9	1	-5.217	4.47	0.182	0
3-fluorophenyl 3-9	495.587	5.655	-7.506	0.595	0	6	8	1	-5.289	7.20	0.255	0
3-chlorophenyl 3-10	512.039	6.100	-8.086	0.658	0	6	8	1	-5.231	7.44	0.182	0
3-bromophenyl 3-11	556.493	6.237	-8.273	0.409	0	6	8	1	-5.319	7.44	0.106	0
3-methylphenyl 3-12	491.624	5.787	-7.519	0.379	0	6	8	1	-5.289	7.26	0.182	0
3-methoxyphenyl 3-13	507.623	5.476	-7.339	0.625	0	7	9	1	-5.225	5.78	0.182	0
4-fluorophenyl 3-14	495.587	5.655	-7.844	0.911	0	6	8	1	-5.298	3.23	0.255	0
4-chlorophenyl 3-15	5112.039	6.100	-8.285	1.013	0	6	8	1	-5.141	3.23	0.182	0



Compound	Mol. Wt.	cLog P	cLog S	Drug Likeness	Bad Group	# of Rot Bonds	# of H-B Accept.	# of H-B Donors	Caco 2	Half-Life (h)	hERG Inhib.	Tox Score
4-bromophenyl 3-16	556.493	6.237	-8.476	0.722	0	6	8	1	-5.270	3.24	0.106	0
4-methylphenyl 3-17	491.624	5.787	-7.783	0.498	0	6	8	1	-5.237	3.46	0.182	0
4-methoxyphenyl 3-18	507.623	5.476	-7.587	0.817	0	7	9	1	-5.195	4.20	0.182	0
2,4-difluorophenyl 3-19	513.577	5.805	-8.010	0.511	0	6	8	1	-5.343	5.28	0.357	0
2,4-dichlorophenyl 3-20	546.481	6.695	-8.826	0.6212	0	6	8	1	-5.346	5.28	0.182	0
2,4-dibromophenyl 3-21	635.389	6.967	-9.177	0.362	0	6	8	1	-5.397	5.29	0.106	0
2,4-dimethylphenyl 3-22	505.651	6.068	-7.953	-0.018	0	6	8	1	-5.347	5.87	0.274	0
2,4-dimethoxyphenyl 3-23	537.649	5.447	-7.40	0.385	0	8	10	1	-5.262	6.69	0.371	0
3,5-difluorophenyl 3-24	513.577	5.925	-7.285	0.662	0	6	8	1	-5.370	5.56	0.357	0
3,5-dimethylphenyl 3-25	505.651	6.188	-7.451	0.719	0	6	8	1	-5.382	5.00	0.274	0
2,4,6-trifluorophenyl 3-26	531.568	5.954	-8.057	0.943	0	6	8	1	-5.391	10.10	0.310	0
2,4,6-trichlorophenyl 3-27	580.923	7.289	-9.402	0.9648	0	6	8	1	-5.426	10.10	0.310	0
2,4,6-trimethylphenyl 3-28	519.678	6.349	-7.788	0.772	0	6	8	1	-5.361	10.10	0.255	0
2,4,6-triisopropylphenyl 3-29	603.840	8.500	-10.319	1.060	0	9	8	1	-5.396	3.90	0.342	0
2,3,4,5,6-pentafluorophenyl 3-30	567.549	6.013	-9.372	0.738	0	6	8	1	-5.263	4.45	0.342	2.408

It has been shown previously that these parameters are good predictors for drug candidate permeability (Clark, 2003; Kelder et al., 1999). All synthesized analogs in this study, **3-1** to **3-30**, are in the agreement with Lipinski Rule of 5 in terms of cLogP, the number of hydrogen bond acceptors and the number of hydrogen bond donors. Several inhibitors have molecular weights that exceed 500 g/mol, but these numbers are very close to 500 Da and as the prediction rule states, potential orally active drugs should not violate more than one of the four criteria. Therefore, we believe that these inhibitors represent excellent candidates for future follow-up SAR studies and drug development. In addition, another important rule that predicts oral bioavailability. All compounds synthesized in this study have 6 to 9 rotatable bonds, satisfying Verber's Rule. In this study, all synthesized analogs showed values close to, but below,  $-6.5$  mol/L, suggesting a moderate aqueous solubility. Improving solubility of these potential drug candidates, if needed, can be addressed in the future guided design of follow-up inhibitors or in the drug formulation process. The next important parameter to consider for the drug design and development is permeability, and we assessed it using the Caco-2 prediction tool (van Breemen & Li, 2005). As shown in Table 9, all compounds synthesized in this study have predicted scores for Caco-2 between  $-5$  and  $-6$ , suggesting moderately permeable drug candidates. We also wanted to predict the plasma half-life of synthesized dual inhibitors. Our analysis showed that inhibitors **3-26**, **3-27** and **3-28** have the longest predicted half-life in hours (10.10 h) whereas the inactive compound **3-2** had the shortest predicted half-life of 1.2 h. The most potent inhibitors identified in this study, **3-5**, **3-6**, **3-20**, **3-21**, and **3-22** showed a moderate predicted half-life of 3.2 to 5.7 h. No compounds synthesized in this study exceeded a value of 0.5 making them unlikely to be hERG inhibitors. The only compound that showed a toxicity score was analog **3-30**. Finally, we calculated a "drug-like" properties for each synthesized compound. Only two compounds, **3-15** and **3-29**, slightly exceed a value of 1. In addition, these two analogs show moderate and low inhibition profiles against both enzymes, respectively, and will not be considered for future follow up studies.

## Dual FAAH and sEH Inhibitors: 4-phenylthiazoles

### Design and Synthesis

Our design of new dual inhibitors was guided by several rationales. Previously, Wang et al. (2009) explored the methylbenzothiazole ring on the left side of the pharmacophore (phenyl ring-amide-piperidine moiety- sulfonamide bond, shown in red in Figure 41).

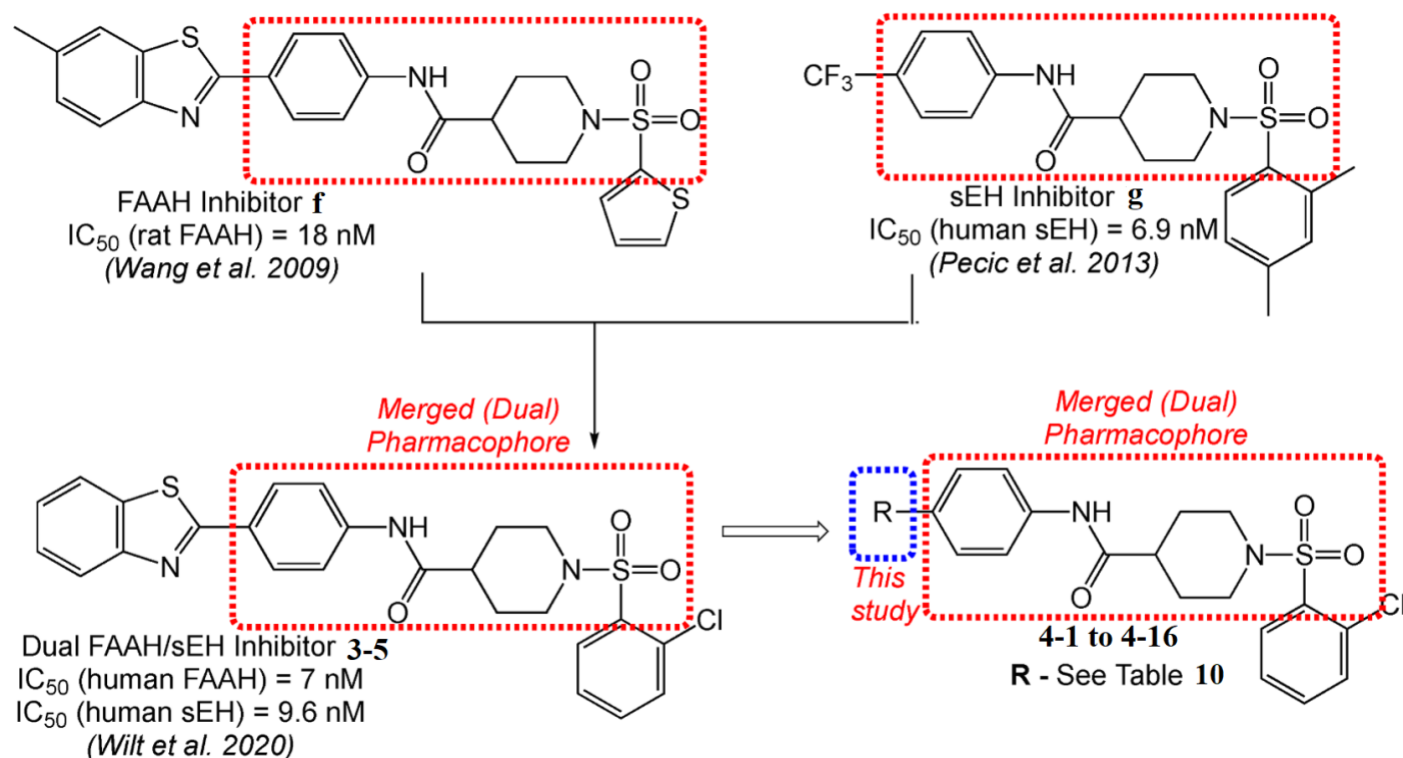


**Figure 41.** Design strategy used to optimize new dual FAAH/sEH inhibitors. Key pharmacophoric features required to interact with both targets are merged in one united pharmacophore (shown in red box). The site of interest where SAR is performed in this study is shown in blue box.

The most potent FAAH inhibitor in this study, **f**, demonstrated the importance of this bulky hydrophobic system for the potent inhibition at the active site of the rat FAAH enzyme. In separate studies, it was observed that the bulky, hydrophobic groups on the left-hand side of sEH inhibitors, represented with **g**, are important for modulating human sEH enzymes (Pecic et al., 2012; Pecic et al., 2013). We decided to keep the benzothiazole ring on the left side of the pharmacophore and investigated the SAR of the aromatic ring bound to the sulfonamide group (S. Wilt et al., 2020). In short, our SAR showed that halogens (fluoro-, chloro- and bromo-) and methyl-groups, placed at the *ortho* and at both *ortho/para* positions, are all well tolerated in the human FAAH and human sEH

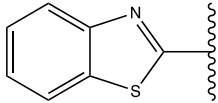
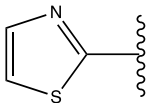
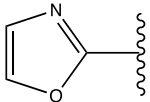
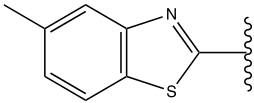
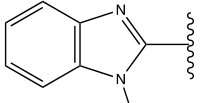
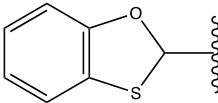
enzymes leading to low nanomolar inhibition potencies on both enzymes. The molecular docking experiments revealed that these dual inhibitors interact within catalytic sites of both enzymes. The most potent compound identified in this study, **3-15**, see Figure 41, had high potency for human FAAH ( $IC_{50} = 7$  nM) and human sEH ( $IC_{50} = 9.6$  nM). This potency is probably due to Van der Waals interactions in the substrate binding pockets and hydrogen bonding with either enzyme's catalytic triad, **S241-S217-K142** and **Y383-Y466-D335** in FAAH and sEH catalytic sites, respectively (see Molecular Modeling section). Although we were able to identify several highly potent dual inhibitors, these all possess very similar structural features and similar predicted pharmacokinetic and pharmacodynamic properties.

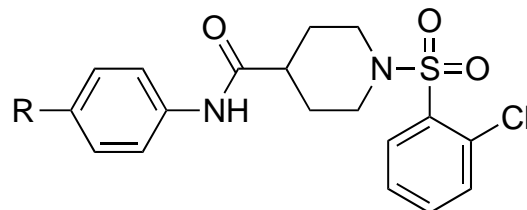
We decided to further explore the chemical space important for dual inhibition and discover new scaffolds that will in turn provide diverse ADMET properties. In addition, this new SAR knowledge will positively impact basic science knowledge in the drug discovery and drug design fields. In a separate study, we were able to utilize the 4-phenylthiazole moiety whose framework was previously examined by Wang et al. (2009) and were able to incorporate it in several potent FAAH inhibitor (Wang et al., 2009; Wilt et al., 2020). Using information obtained from these above mentioned SAR studies in combination with molecular modeling and crystallography data, we decided to explore whether modifying the benzothiazole moiety can affect inhibitory potency. To evaluate the effect of this group on the inhibitory capacity of the dual inhibitors, we kept the 2-chlorophenyl group connected to the sulfonamide bond of the pharmacophore and synthesized 16 analogs with various groups on the left side of the molecule, see Figure 41.

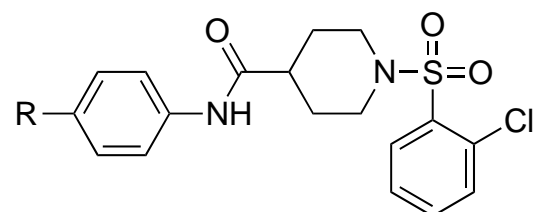
To explore the importance of the benzothiazole functionality on the activity, we prepared three different classes of analogs, Table 10. The first group consists of 7 compounds, **4-1** to **4-7**, that utilize a simplification strategy where the benzothiazole part was replaced with smaller groups. Next, the second group of analogs, **4-8** to **4-11**, was designed using bio-isostere and/or ring variations and varying alkyl substituents strategies. Finally, the third group represented with five analogs, **4-12** to **4-**

**16**, was designed to determine the importance of the 4-phenylthiazole moiety in the activity for both enzymes.

Table 10. Fatty acid amide hydrolase (FAAH) and soluble epoxide hydrolase (sEH) inhibitory activities and docking scores of analogs.

Compound	R	FAAH IC <sub>50</sub> (nM) <sup>a, b</sup>	sEH IC <sub>50</sub> (nM) <sup>a, b</sup>	Docking Score FAAH	Docking Score sEH
URB 597	-	32	-	-31.45	-22.16
AUDA	-	-	1.9	-22.18	-25.83
3-5		7	9.6	-28.93	-33.03
4-1	-H	510	>10000	-19.43	-24.71
4-2	-F	220	>10000	-20.90	-25.99
4-3	-Cl	160	>10000	-20.50	-27.11
4-4	-Br	130	>10000	-20.89	-27.85
4-5	-CH <sub>3</sub>	110	>10000	-22.50	-28.05
4-6		102	9.2	-28.02	-22.56
4-7		140	180	-21.14	-26.43
4-8		1.8	8.7	-31.42	-28.90
4-9		330	1400	-28.87	-23.19
4-10		142	22.7	-17.62	-25.98





Compound	R	FAAH IC <sub>50</sub> (nM) <sup>a, b</sup>	sEH IC <sub>50</sub> (nM) <sup>a, b</sup>	Docking Score FAAH	Docking Score sEH
4-11		>10000	170	-20.65	-24.72
4-12		30.8	3.1	-30.69	-33.58
4-13		18.2	2.4	-26.57	-33.19
4-14		25.1	9.6	-30.65	-33.39
4-15		9.8	2.5	-33.54	-31.14
4-16		11.1	2.3	-30.50	-30.60

As shown in the reaction scheme in the experimental section (Figure 59), using previously established procedures, starting from commercially available methyl isonipecotate and 2-chlorobenzenesulfonyl chloride, sulfonamide **i** was obtained in 74% yield via a coupling reaction with Hünig's base and microwave irradiation (Pecic et al., 2018). Saponification of the methyl ester with a 2 M aqueous solution of lithium hydroxide furnished the carboxylic acid **j** in 91% yield. Compound **j**

was subsequently coupled with different anilines under standard EDC peptide coupling conditions and microwave irradiation yielding compounds **4-1** to **4-11** in moderate yields. Five different 4-phenylthiazole anilines, **5-12** to **5-16** (inner box Figure 60), were also prepared by condensation of the commercially available 4-aminothiobenzamide and various 2-bromoacetophenones and subsequently coupling them with **j** yielding final compounds **4-12** to **4-16** in moderate yields.

### Biological Evaluation and SAR

The potency of the newly designed and synthesized analogs **4-1** to **4-16** were assessed against both human FAAH and human sEH, Table 10. The SAR study started with a first set of analogs, **4-1** to **4-7**, designed using simplification tactics to examine whether the benzothiazole ring is an essential part of the pharmacophore. The first analog, **4-1**, possessing no substituent on the phenyl ring of the pharmacophore, showed complete loss of inhibition potency at the human sEH enzyme, but led to moderate inhibition potency on the human FAAH enzyme with an  $IC_{50}$  of 510 nM. Placement of fluoro-, chloro-, bromo- and methyl groups (**4-2**, **4-3**, **4-4**, and **4-5**, respectively) at the *para* position of the phenyl group in the pharmacophore did not restore any potency against sEH, but improved the inhibition potencies against human FAAH with  $IC_{50}$ s in the 100–200 nM range. The introduction of the bulkier and more polar thiazole ring, **4-6**, led to a significant improvement in the inhibition potency of the human sEH enzyme ( $IC_{50} = 9.2$  nM), and comparable inhibitory potency on the human FAAH enzyme to the **4-2** to **4-5** analogs. Interestingly, the introduction of the oxazole rings, **4-7**, did not have much of an effect on the inhibitory potency on human FAAH ( $IC_{50} = 140$  nM) while reducing sEH inhibitory potency 20-fold ( $IC_{50} = 180$  nM) relative to the thiazole analog **4-6**. This result could be explained with the difference in the steric/electronic properties of the sulfur atom compared to the oxygen and implies that sulfur (more bulky and less electronegative) has greater surface area resulting in closer Van der Waals interactions.

The next set of analogs, **4-8** to **4-11**, were aimed to test whether the benzothiazole bioisosteres may have improved potency relative to the reference compound, **h**. First, a methyl group was introduced at position 6 of the benzothiazole ring. The methyl group did not affect the binding of

the benzothiazole moiety and **4-8** showed excellent inhibition potencies with both enzymes, human FAAH ( $IC_{50} = 1.8$  nM) and human sEH ( $IC_{50} = 8.7$  nM). The replacement of the benzothiazole ring with N-methylbenzimidazole, **4-9**, led to diminished inhibitory potency on both enzymes.

On the other hand, placement of the benzooxathiol moiety, **4-10**, was well tolerated in the human sEH ( $IC_{50} = 22.7$  nM) and has shown moderate inhibition potency on the human FAAH ( $IC_{50} = 142$  nM). With the design of analog **4-11**, we decided to extend the alkyl linker to the aromatic moiety and this strategy led to complete loss of inhibition potency on the human FAAH, while this change was well-tolerated by the human sEH enzyme ( $IC_{50} = 170$  nM). The third set of analogs, **4-12** to **4-16**, explored the potency of the 4-phenylthiazole moiety on both enzymes. All five analogs showed excellent inhibition potencies in the low nanomolar range with both enzymes. This suggests that analogs with this bulky moiety on the left side of the pharmacophore are favored in the active sites of both enzymes and are important for the potent dual inhibition.

Most compounds pursued as FAAH inhibitors have been irreversible covalent inhibitors (Otrubova et al., 2011). Indeed, in the last several years, the majority of the research has been focused on developing irreversible covalent FAAH inhibitors, largely because an irreversibly inhibited FAAH would not be affected by accumulations of its substrate, anandamide (Keith et al., 2020). In fact, the known FAAH inhibitor, URB 597, the same one we used as a reference compound in this study, operates via carbamylation of the catalytic serine residue (**S241**) in the active site of FAAH (Ahn et al., 2009). Inhibition through carbamylation mechanism is time-dependent because the inhibitory potency depends on the rate of this mechanism and thus decreases the  $IC_{50}$  with longer incubation times (Kodani et al., 2018). Using this principle, we decided to elucidate the type of inhibition for the previously discovered dual inhibitor **c** and one of 4-phenylthiazole analogs, **4-15**. We noticed that the potencies of both **3-5** and **4-15** do not change with time, Table 11, while the control URB 597 showed significant increase in potency over the same period. These findings suggest that **3-5** and **4-15** (and most likely other 4-phenylthiazole analogs identified in this study) are probably inhibiting FAAH in a reversible manner (i.e., are not forming a covalent bond with **S241**). However,



to fully investigate the mode of noncovalent inhibition (competitive or mixed) of this set of inhibitors, we will need to perform more kinetic analyses which will be addressed in our future follow-up studies.

Table 11. Effects of 60 minutes preincubation of URB 597, 3-5 and 4-15 on FAAH potency

Compound	IC50 <sup>a</sup>	IC50 <sup>b</sup>
URB 597	38.0	4.0
3-5	7.0	8.1
4-15	9.8	9.0

a) Values obtained after a 5 min preincubation with the FAAH enzyme;

b) Values obtained after a 60 min preincubation with the FAAH enzyme

### Molecular Modeling Studies

Molecular docking experiments were performed to better understand the binding modes of dual inhibitors. We previously reported the preparation and validation of the homology model of the human FAAH enzyme (Wilt et al., 2020) since the X-Ray crystallographic structure is not available. The crystal structure of human sEH complexed with the piperidine-amide inhibitor is available at RCSB Protein Data Bank (**PDB: 4HAI**). Using ICM Pro software, all compounds were docked in both the human FAAH homology model and human sEH model. The ICM Pro docking scores, Table 10, represent unitless approximations of the binding free energy between the ligand (inhibitor) and the enzyme where lower docking scores (especially below -30) suggest a higher chance that the inhibitor is bound to the enzyme. Our main goal is to determine whether docking scores obtained in these docking experiments could be correlated with *in vitro* results. Further, if scoring is reliable, we could use Virtual Ligand Screening in the future design of dual inhibitors. There was not complete correlation between the *in vitro* results and docking scores (Figures 42 and 43); however, all potent dual inhibitors with the 4-phenylthiazole moiety, **4-12** to **4-16**, have docking scores below -30. The poor correlation between predicted affinities and experimentally determined affinities is quite common in molecular modeling experiments (Xu et al., 2015).

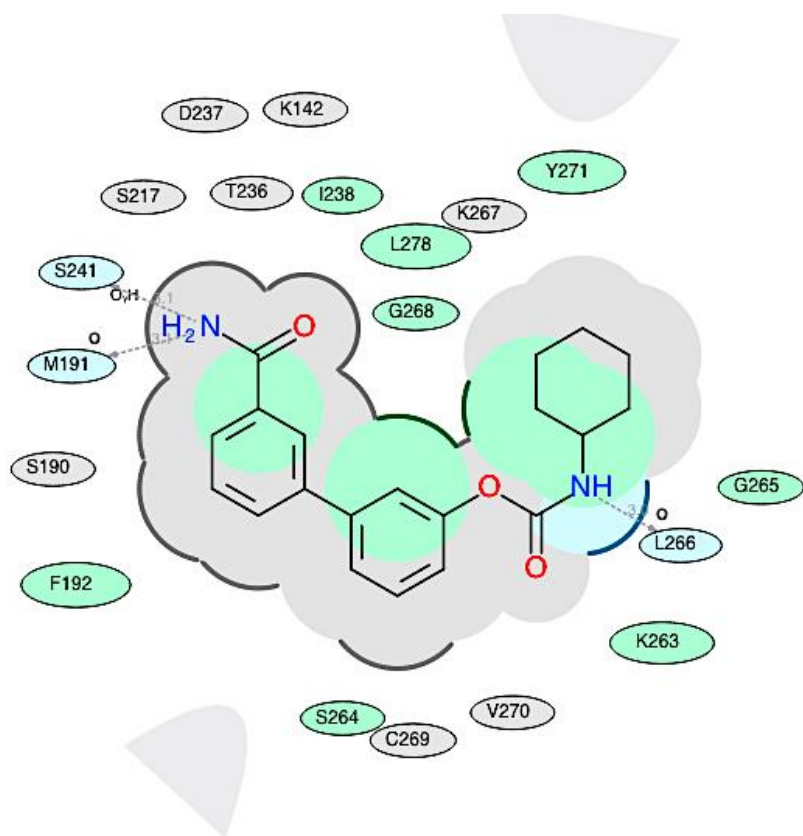


Figure 42. A 2D docking pose of the inhibitor URB 597 in the catalytic site of the human FAAH enzyme.

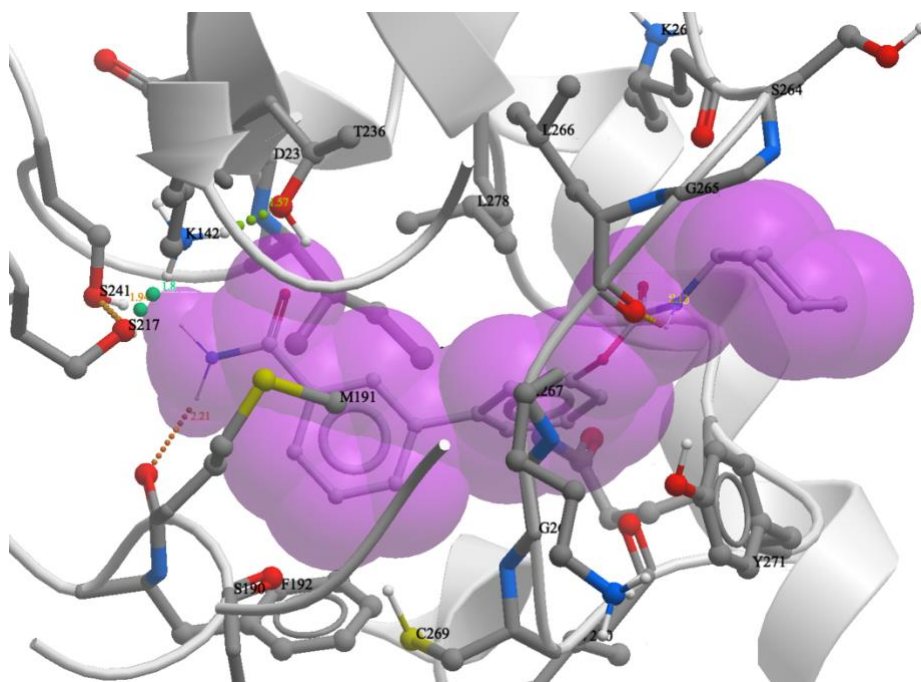


Figure 43. A 3D docking pose of the inhibitor URB 597 in the catalytic site of the human FAAH enzyme

Since we noticed an agreement in scoring with *in vitro* results for 4-phenylthiazole analogs, we will still be able to use docking scores in the future design of at least this set of dual inhibitors. This will be tested in our follow-up experiments. For obtaining the docking poses of ligands in the enzyme binding pockets, ICM Molsoft software is using several different interaction potentials, such as van der Waals potentials, optimized electrostatic term, hydrophobic term and lone-pair-based potential (which is involved in hydrogen bonding). Conformational sampling is based on the biased probability Monte Carlo (BPMC) procedure (Abagyan & Totrov, 1994). This approach has been validated in many medicinal chemistry settings (Lam et al., 2018, 2019; Scarpino et al., 2018). We started our docking experiments by first docking the known FAAH and sEH inhibitors, URB-597 and AUDA, respectively, Figures 42-45. All important interactions of these inhibitors with the residues within active sites are present in our model and are in agreement with the previously reported models (Imig & Hammock, 2009; Mileni et al., 2010) .

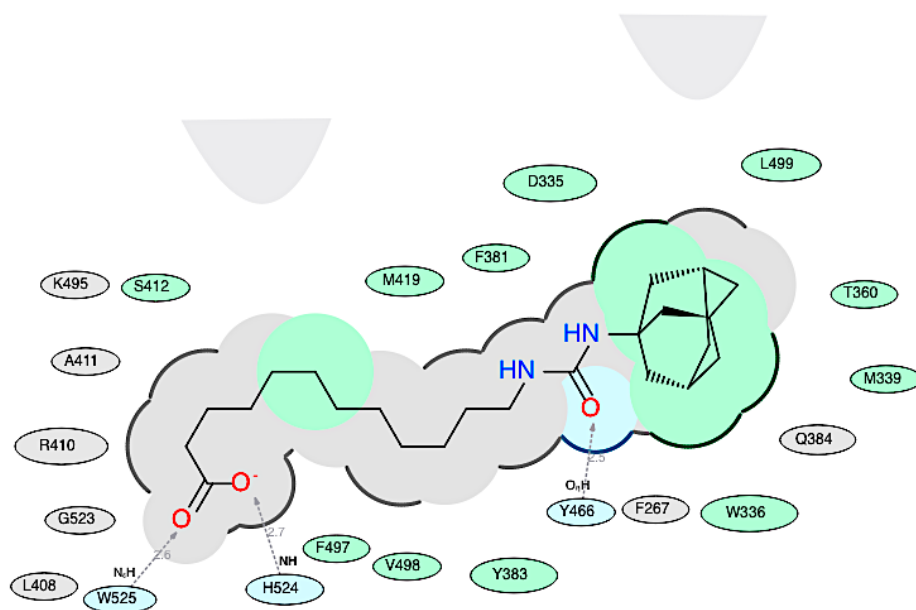
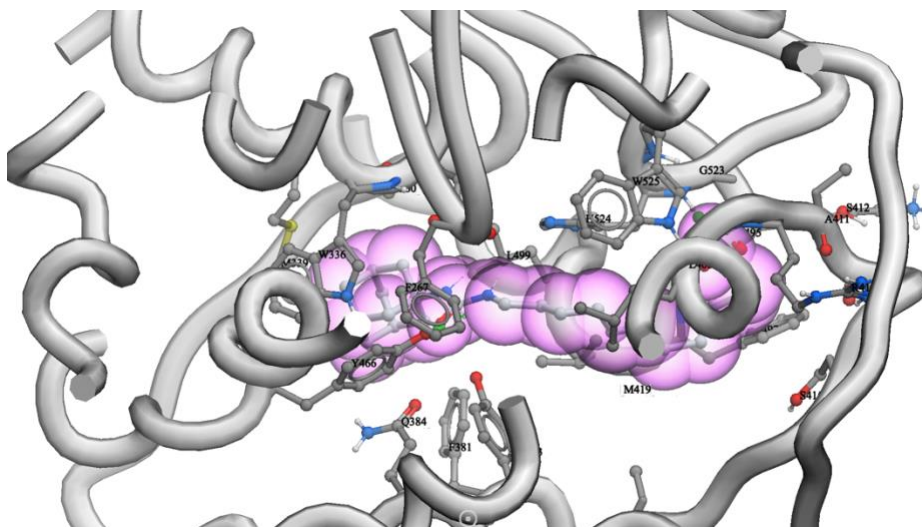
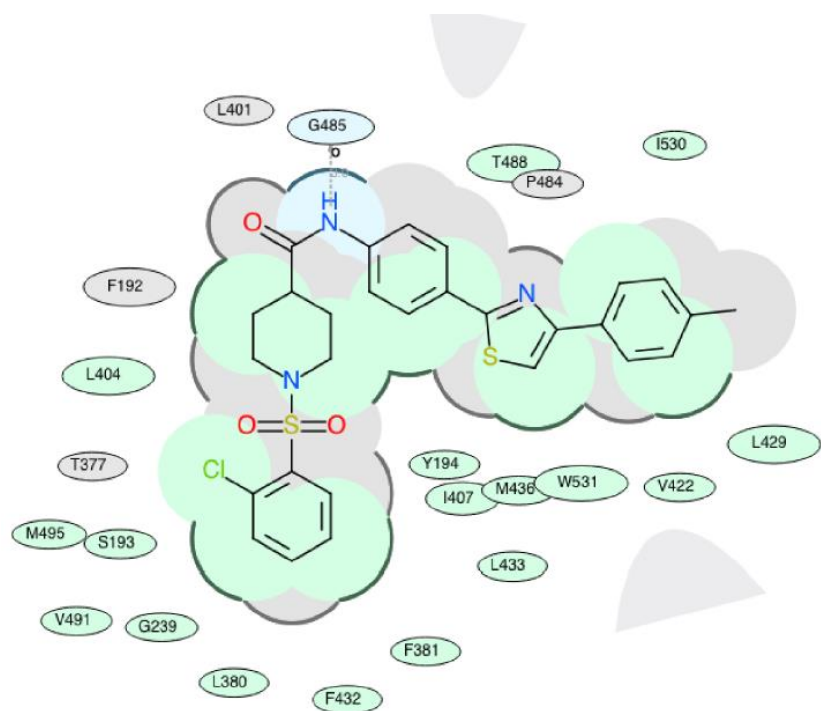


Figure 44. A 2D docking pose of the inhibitor AUDA in the catalytic site of the human sEH enzyme

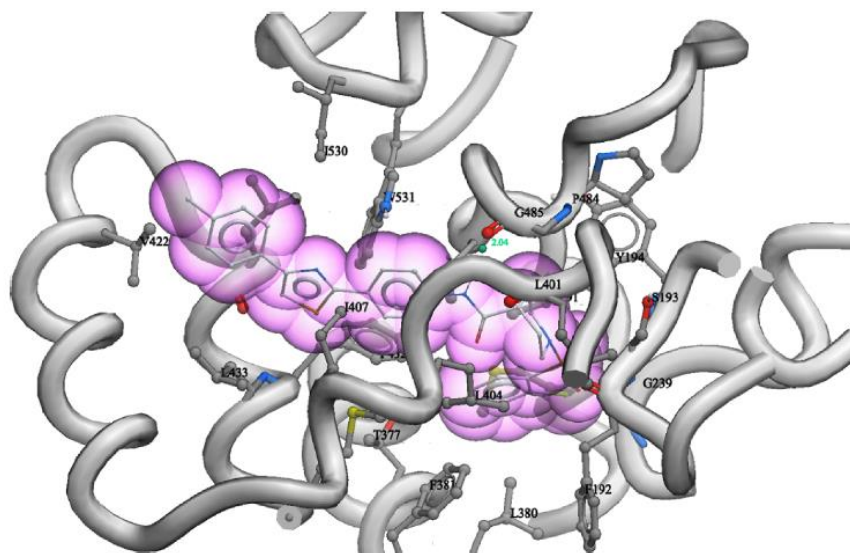


*Figure 45.* A 3D docking pose of the inhibitor AUDA in the catalytic site of the human sEH enzyme

Next, we focused our attention on to visual inspection of the binding poses of the 4-phenylthiazole set of analogs within both sEH and FAAH active sites. We selected dual inhibitor **4-15** as a representative compound from this series to analyze binding modes in more details and to try to define the pharmacophore needed for dual binding. As shown in Figures 46 and 47, the inhibitory potency of **4-15** within the human FAAH binding site is based on several intermolecular interactions: a possible hydrogen bonding between **G485** and –NH– (as a hydrogen bond donor) and many non-polar and hydrophobic interactions, Table 12. The 2-chlorophenyl ring of the inhibitor **4-15** is found to be embedded between several hydrophobic and aromatic amino acid residues (**Y194**, **I238**, **L380**, **F381**, **L433**, **V491** and **F432**). The piperidine part interacts with **F192** and **L404**, while the aromatic 4-phenylthiazole moiety forms several important non-covalent interactions with **Y194**, **L429**, **V422**, **I530** and **W531**, which we believe all contribute to high inhibitory potency of this analog. We noticed that the 4-phenylthiazole moiety is directed towards the large deep pocket (broken thick line around 4-methylphenyl ring in Figure 46 represents the accessible surface) that opens toward the solvent and probably will allow access to many more structural modifications. These will be further explored in our follow-up studies.



*Figure 46.* Binding of **4-15** in human FAAH active site (2D representation): green shading represents hydrophobic regions; gray parabolas represent accessible surfaces for large areas; gray dotted lines represent hydrogen bonds; broken thick line around **4-15** shape indicates accessible surfaces; size of residue ellipse represents the strength of the contact.



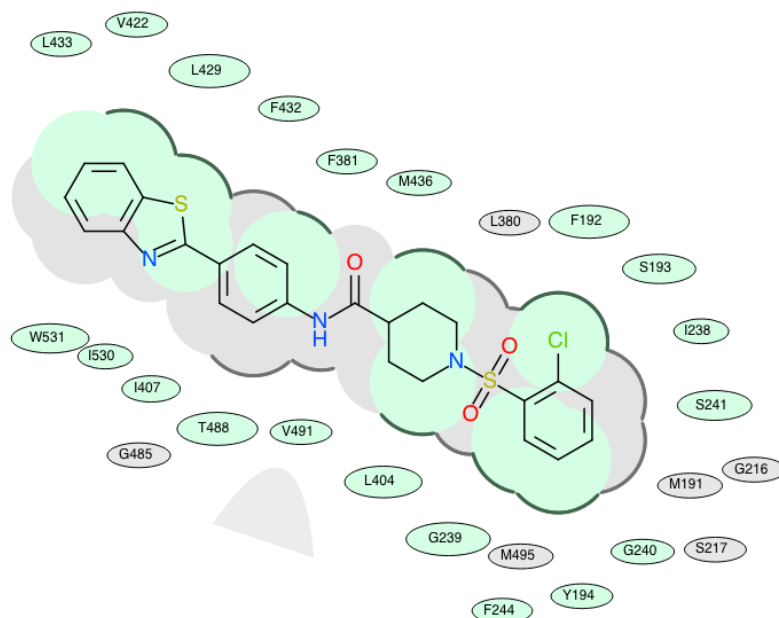
*Figure 47.* Binding of **4-15** in human FAAH active site (3D representation): Important amino acid residues in the proximity of **4-15** are shown and labeled. Hydrogen bond with **G485** is shown in green with the distance in Å.

Table 12. The list of hydrogen bonds and hydrophobic interactions of **3-5** and **4-15** docked in human FAAH enzyme.

3-5 in FAAH active site			4-15 in FAAH active site		
Residue	Type of bond	Distance (Å)	Residue	Type of bond	Distance (Å)
F192	Hydrophobic	3.39	F381	Hydrophobic	3.87
F244	Hydrophobic	3.63	F432	Hydrophobic	3.95
F381	Hydrophobic	3.93	G239	Hydrophobic	3.44
F432	Hydrophobic	4.32	G485	H-bond	3.02
G239	Hydrophobic	3.52	I407	Hydrophobic	3.48
G240	Hydrophobic	4.18	I530	Hydrophobic	3.85
I238	Hydrophobic	4.22	L380	Hydrophobic	3.55
I407	Hydrophobic	3.61	L404	Hydrophobic	3.80
I530	Hydrophobic	3.82	L429	Hydrophobic	3.87
L404	Hydrophobic	3.78	L433	Hydrophobic	3.89
L429	Hydrophobic	3.60	M436	Hydrophobic	4.34
L433	Hydrophobic	4.08	M495	Hydrophobic	3.85
M436	Hydrophobic	3.70	S193	Hydrophobic	4.00
S193	Hydrophobic	4.29	T488	Hydrophobic	4.06
S241	Hydrophobic	4.02	V422	Hydrophobic	3.47
T488	Hydrophobic	3.74	V491	Hydrophobic	4.36
V422	Hydrophobic	4.39	W531	Hydrophobic	3.78
V491	Hydrophobic	3.95	Y194	Hydrophobic	4.38
W531	Hydrophobic	3.66			
Y194	Hydrophobic	3.82			

The dual inhibitor **3-5** (identified previously) was used to compare its binding pose with the newly identified **4-15** from the 4-phenylthiazole series. The visual inspection of the dual inhibitor **3-5** in the active site of FAAH, Figures 48 and 49, revealed that this analog shares many same non-polar and hydrophobic interactions similar to **4-15**, e.g. **S193** in the proximity of the chlorine atom, **L404** interacting with the piperidine ring and **W531** probably forming  $\pi$ - $\pi$  interactions with the aromatic rings of benzothiazole moiety in Table 12. Next, we noticed the absence of the hydrogen bond with the **G485**. However, this dual inhibitor is interacting with both **S217** and **S241**, the two residues that

are part of the FAAH catalytic triad (**K142-S217-S241**), which probably accounts for the high FAAH potency of this inhibitor (Ahn et al., 2009).



*Figure. 48.* A 2D docking pose of the inhibitor **3-5** in the catalytic site of the human FAAH enzyme

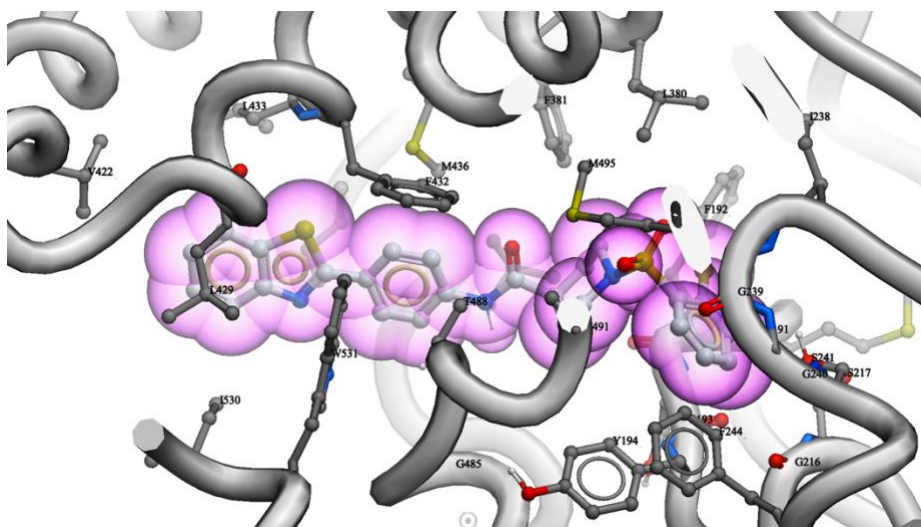


*Figure 49.* A 3D docking pose of the inhibitor **3-5** in the catalytic site of the human FAAH enzyme

The visual inspection of **4-15** docked into the human sEH reveals that the potency of this inhibitor is based on Van der Waals interactions and H bonding interactions within the active site, Figures 50 and 51. The amide bond of **4-15** is in close proximity to two tyrosine residues (**Y383** and **Y466**) and one aspartic acid residue (**D335**). These three residues are involved in the hydrolysis of

the substrate EET in the catalytic pocket of the sEH enzyme (Pecic et al., 2013). In addition, the dual inhibitor **4-15** forms many hydrophobic interactions that probably contribute to the high inhibition potency of this compound in Table 13. The 2-chlorophenyl moiety is surrounded with several aromatic and hydrophobic residues: **F387**, **L408**, **L417** and **W525**. The piperidine ring is interacting with **Y383**, **L428** and **V498**, while the 4-phenyl thiazole is embedded with several hydrophobic residues: **W336**, **Y343**, **I375**, **F381**, **W473** and **A476**. This suggests that the potency of this inhibitor is primarily based on van der Waals and  $\pi$ - $\pi$  interactions between the enzyme active site and **4-15**.

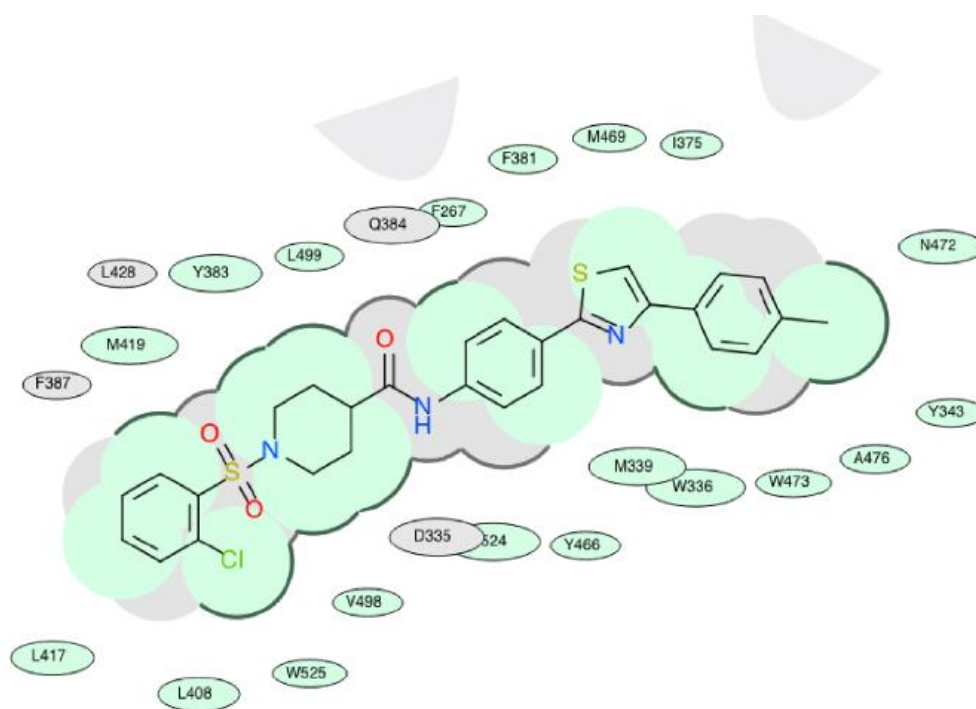


*Figure 50.* Binding of **4-15** in human sEH active site (2D representation): green shading represents hydrophobic regions; gray paraboloids represent accessible surfaces for large areas; gray dotted lines represent hydrogen bonds; broken thick line around **4-15** shape indicates accessible surfaces; size of residue ellipse represents the strength of the contact.



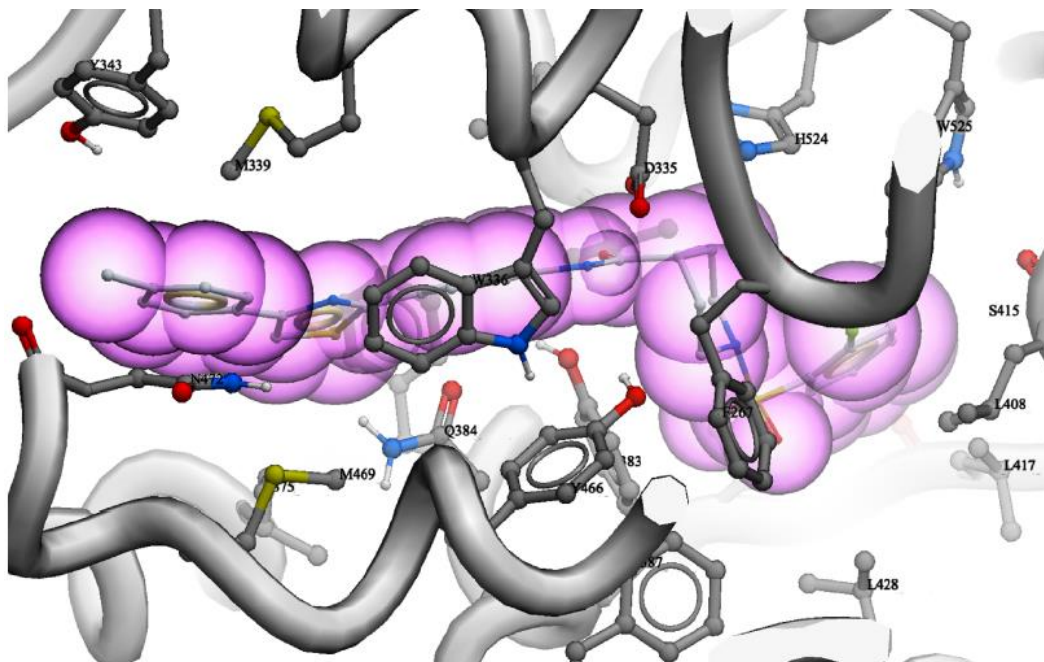


*Figure 51.* Binding of **4-15** in human sEH active site (3D representation): Important amino acid residues in the proximity of **4-15** are shown and labeled.

The 4-phenylthiazole moiety is also opened towards the large hydrophobic pocket, suggesting that various additional groups should probably fit there, permitting to expand our SAR knowledge at-large. We also compared the binding modes of the previously identified dual inhibitor **3-5** within sEH active site (Figures 52 and 53 and Table 13) with the binding modes of the **4-15**. First, we noticed that the nitrogen atom of the amide bond is in the proximity of **D335** and is forming hydrogen bond with this residue. Next, we observed the same interactions of the 2-chlorophenyl moiety as in **4-15**: **F387**, **L428**, **L417** and **W525**, plus the additional **L408** interaction. Similarly, piperidine ring possesses same interactions with **Y383** and **V498**, and additional **F267** and **H524**. Finally, the benzothiazole is interacting with **W336** and **I375**, and several additional amino acid residues: **M339**, **P371**, **M469** and **L499**. Very similar binding poses, and several shared interactions of both dual inhibitors within binding pockets probably explain the similar high potency of these two inhibitors for both, sEH and FAAH enzymes *in vitro*.

Table 13. The list of hydrogen bonds and hydrophobic interactions of **3-5** and **4-15** docked in human sEH enzyme.

h in sEH active site			4-15 in sEH active site		
Residue	Type of bond	Distance (Å)	Residue	Type of bond	Distance (Å)
D335	H-bond	3.00	A476	Hydrophobic	3.82
F267	Hydrophobic	4.27	F267	Hydrophobic	4.02
F381	Hydrophobic	4.11	F381	Hydrophobic	3.69
F387	Hydrophobic	4.19	H524	Hydrophobic	3.20
H524	Hydrophobic	3.65	I375	Hydrophobic	4.09
I375	Hydrophobic	4.22	L408	Hydrophobic	3.34
L408	Hydrophobic	4.42	L417	Hydrophobic	3.55
L417	Hydrophobic	4.10	L499	Hydrophobic	3.99
L428	Hydrophobic	3.73	M339	Hydrophobic	3.31
L499	Hydrophobic	4.38	M419	Hydrophobic	3.11
M339	Hydrophobic	3.67	M469	Hydrophobic	4.32
M419	Hydrophobic	3.29	N472	Hydrophobic	3.55
M469	Hydrophobic	3.51	V498	Hydrophobic	3.72
N472	Hydrophobic	3.65	W336	Hydrophobic	3.42
P371	Hydrophobic	4.21	W473	Hydrophobic	4.33
V498	Hydrophobic	3.46	W525	Hydrophobic	3.15
W336	Hydrophobic	3.31	Y343	Hydrophobic	4.06
Y383	hydrophobic	2.94	Y383	Hydrophobic	3.37
			Y466	Hydrophobic	4.12

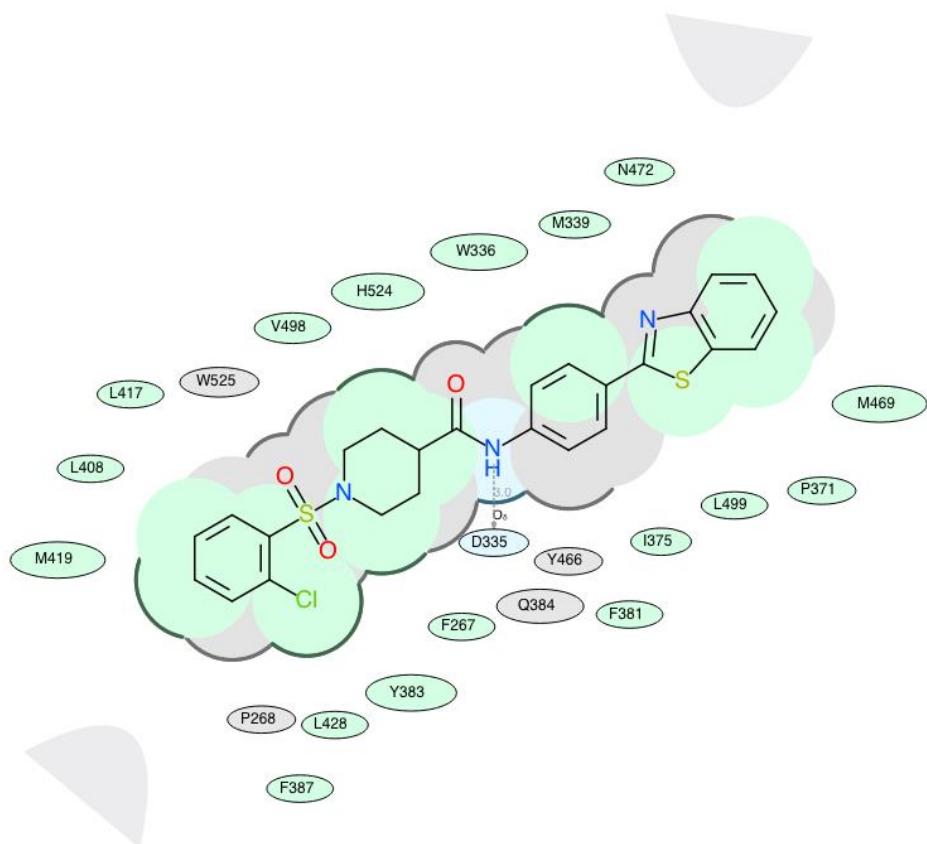


Figure 52. A 2D docking pose of the inhibitor **3-5** in the catalytic site of the human sEH enzyme

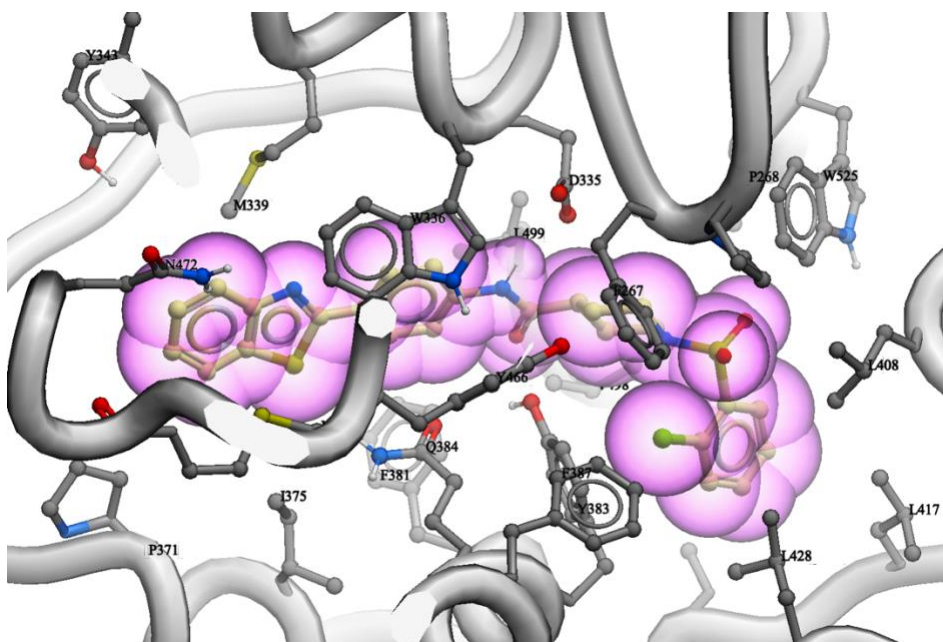
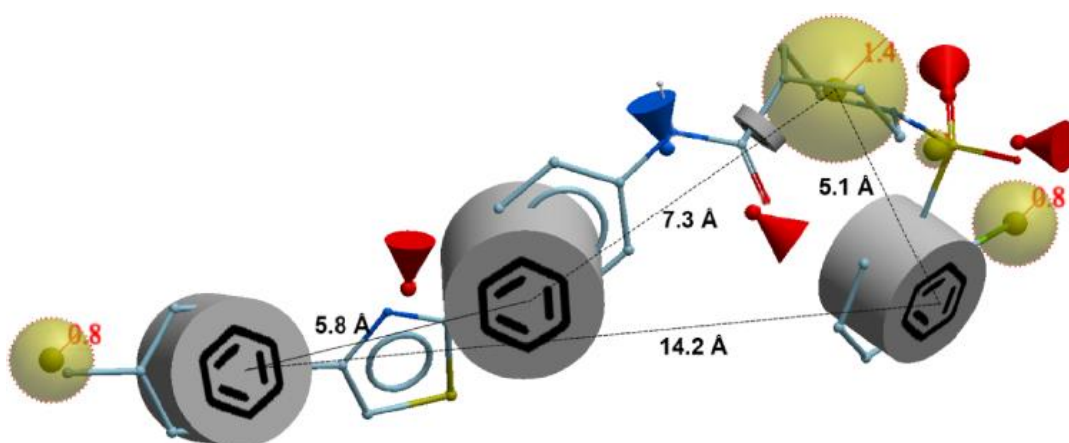


Figure 53. A 3D docking pose of the inhibitor **3-5** in the catalytic site of the human sEH enzyme

Finally, the chemical space for this set of dual inhibitors is summarized in Figure 54. To be potent, a dual inhibitor should possess one hydrogen bond donor (shown in blue), four hydrogen

bond acceptors (shown in red), the three lipophilic parts- with two located at both ends of the molecule (yellow sphere), and three aromatic parts (shown as grey barrels). The model suggests placement of particular isostere groups within the distances between the pharmacophore and within these pharmacophoric regions should produce potent dual inhibitors, and our follow-up SAR studies will be guided by the discoveries described here.



*Figure 54.* Proposed pharmacophore for dual inhibitors based on the binding of **4-15** in both FAAH and sEH enzymes. Potential hydrogen bond donors are represented with blue cone, hydrogen bond acceptors with red cones, the lipophilic part of the molecule are shown as yellow spheres and aromatic parts are shown as grey barrels. The distances between major pharmacophoric parts are represented with dotted lines.

## Predicting ADME-Tox Properties

Before performing *in vivo* preclinical experiments, several pharmacokinetic and pharmacodynamic properties were predicted *in silico* for the most potent dual inhibitors **4-8** and **4-12** to **4-16**, using the ICM-Pro-Chemist tool in Table 14. We were particularly interested in the Lipinski Rule of Five and Veber's Rule. According to the Veber's rule, a compound having less than 10 rotatable bonds and a PSA equal to or less than 140 Å is considered a good drug candidate in terms of absorption. All six dual inhibitors **4-8** and **4-12** to **4-16** have molecular weights slightly above the 500 g/mol cutoff and calculated LogP values are above **3-5** in Table 14. Nevertheless, these inhibitors have less than 10 HBA, less than 5 HBD, and are not violating either of the two Veber's rule. In addition, the higher molecular weight of the dual inhibitors makes them less likely to cross the blood brain barrier and cause CNS side effects.

Table 14. Predicted ADMET properties for selected dual sEH/FAAH inhibitors

	Mol Weight	cLogP	N of HBA	N of HBD	PSA	N of Rot Bonds	Caco-2	Half Life (h)	hERG	LD50	Tox Score	Drug Likeness
4-8	526.066	5.39	8	1	64.5	6	-5.32	1.95	0.25	399.22	0	0.33
4-12	538.0770	5.68	8	1	64.5	7	-5.19	1.91	0.18	435.06	0	0.81
4-13	556.0674	5.86	8	1	64.5	7	-5.26	2.26	0.29	439.39	0	0.96
4-14	572.5190	6.39	8	1	64.5	7	-5.25	2.26	0.21	444.02	0	0.98
4-15	552.1040	6.24	8	1	64.5	7	-5.21	2.26	0.25	449.33	0	0.70
4-16	568.1030	5.75	9	1	72.04	8	-5.13	3.04	0.39	440.99	0	0.94

Next, we ran Caco-2 prediction experiments. All tested dual inhibitors **4-8** and **4-12** to **4-16** have predicted Caco-2 scores between -5 and -6, suggesting they are moderately permeable drug candidates. Therefore, this set of newly discovered dual inhibitors should have good oral bioavailability and the information in Table 14 should be used for formulation in *in vivo* experiments. To access some metabolic parameters, the half-lives of the dual inhibitors **4-8** and **4-12** to **4-16** were predicted. The analysis showed that **4-12** has the shortest half-life of 1.91 hrs while **4-16** has the longest predicted half-life of around 3h. As a part of the pharmacodynamic analysis, several factors important for the possible toxic effects of the drug candidates were then predicted.

The predicted results show that none of the new dual inhibitors will likely exhibit unwanted hERG inhibition since the predicted hERG score is less than the cutoff value of 0.5 for all tested compounds. To predict the toxic doses of these dual inhibitors, half lethal dose values (LD<sub>50</sub> values in mg/kg body weight) were predicted in Table 14. According to the globally harmonized system of classification of labelling of chemicals, there are 6 toxicity classes defined with Class I (LD<sub>50</sub> values ≤ 5 mg/kg) as the most toxic and Class VI (LD<sub>50</sub> values ≤ 5000 mg/kg) as relatively non-toxic compounds.<sup>62</sup> Dual inhibitors **4-8** and **4-12** to **4-16** belong to Class IV with values within this class range (300 < LD<sub>50</sub> ≤ 2000 mg/kg). Furthermore, the calculated Tox score of 0 predicts that none of the analyzed analogs in this group have potentially toxic functional groups and/or by-products during metabolism. Finally, a “drug-likeness” was calculated for compounds **4-8** and **4-12** to **4-16**. Scores

between -1 and 1 suggest that the tested compound is a good candidate. According to Table 14, all newly described dual inhibitors fall into this range.

### ***In vivo* Analysis of Antinociception**

The most potent dual sEH/FAAH inhibitor identified in our previous study, **h**, was used to demonstrate antinociception following intraperitoneal administration in a rat model of acute inflammatory pain. The Formalin Test (Dubuisson & Dennis, 1977) is commonly used to evaluate the ability of an analgesic drug to provide relief against acute inflammatory pain. The test involves subcutaneous injection of dilute formalin into the plantar surface of the rat's hind paw to elicit pain behaviors such as licking and guarding of the injected hind paw. The time spent licking and guarding is quantified in two distinct phases. The first phase lasts 10 min after injection and involves direct activation of nociceptors (Hunskar & Hole, 1987). The second phase begins approximately 20 min after injection and is mediated via inflammatory processes, as common nonsteroidal anti-inflammatory drugs block the second, but not the first, phase (Hunskar & Hole, 1987). Figure 55A shows pain-related behaviors following injection of **3-5** and an effective dose of ketoprofen, a traditional nonsteroidal anti-inflammatory drug (NSAID), in the first phase of the Formalin Test. A one-way ANOVA revealed that administration of either a dose of **3-5** or ketoprofen was ineffective at inhibiting licking and guarding behaviors compared to rats treated with vehicle [ $F(3, 20) = 0.187$ ,  $p = 0.90$ ]. Figure 55B shows pain-related behaviors following administration of formalin, **3-5**, and ketoprofen in the second phase of the Formalin Test. A one-way ANOVA revealed that intraperitoneal administration of **3-5** and ketoprofen attenuated pain behaviors induced by the intraplantar injection of formalin [ $F(3, 20) = 6.834$ ,  $p = 0.002$ ]. A Tukey post-hoc test revealed that licking and guarding behaviors were significantly attenuated following administration of the high dose of **3-5** (1 mg/kg) and ketoprofen (Tukey: Vehicle vs. 1 mg/kg,  $p < 0.05$ ; Vehicle vs. ketoprofen,  $p < 0.05$ ). Administration of the low dose of **3-5** (0.1 mg/kg) did not attenuate licking and guarding behaviors (Tukey: Vehicle vs. 0.1 mg/kg,  $p > 0.05$ ). Lastly, there was no difference in the magnitude of pain relief produced by 1 mg/kg **3-5** and 30 mg/kg of ketoprofen (Tukey: 1 mg/kg vs. ketoprofen,  $p > 0.05$ ).

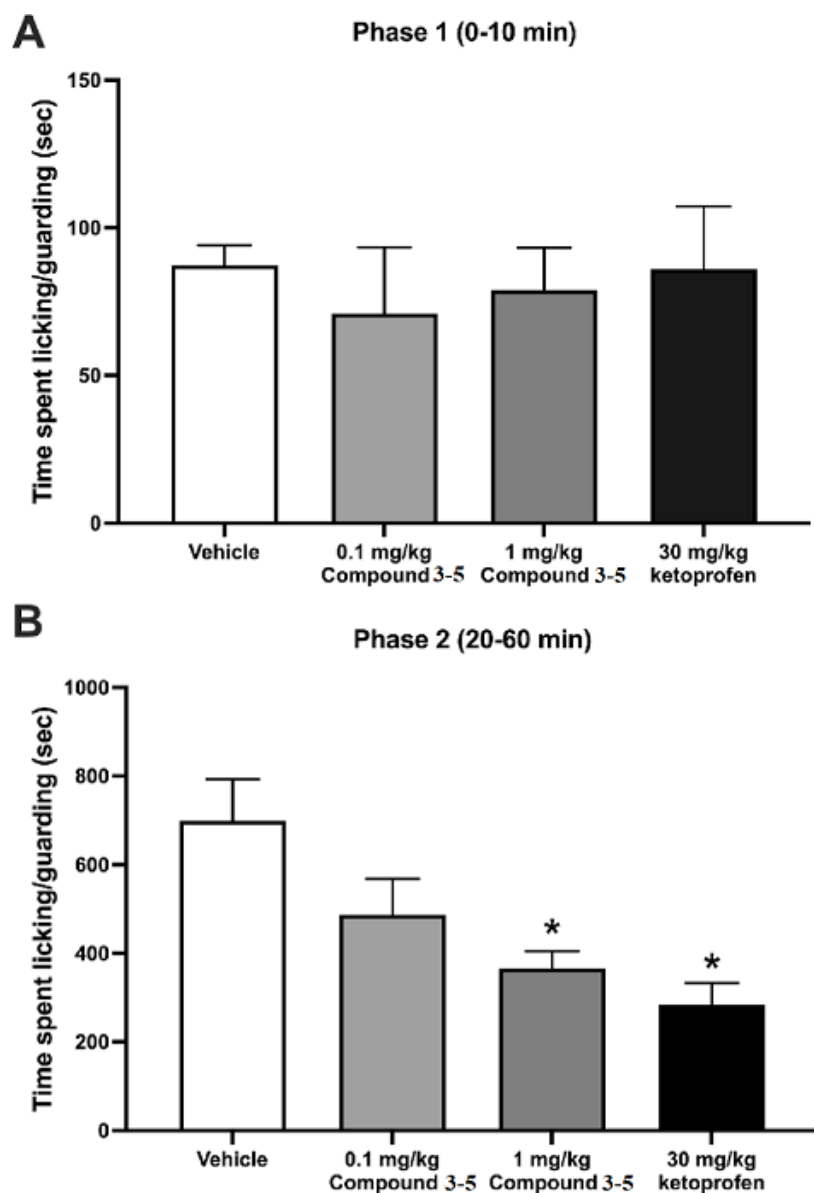


*Figure 55.* Antinociceptive effects of **3-5** against formalin-induced inflammatory pain. (A) Pain-related behaviors (licking and guarding of the injected hind paw) in the first phase of the Formalin Test. (B) Pain-related behaviors in the second phase of the Formalin Test.  $n = 6/\text{group}$ . \* indicates  $p < 0.05$  from vehicle treated rats.

These data provide the first evidence of antinociception following administration of a dual sEH/FAAH inhibitor. Intraperitoneal administration of the higher dose of **3-5** attenuates licking and guarding behaviors induced by an intraplantar injection of formalin. The lower dose of **3-5** was ineffective suggesting a dose-dependent relationship in antinociception. The magnitude of antinociception produced by 1 mg/kg of **3-5** is comparable to antinociception produced by a high dose of ketoprofen (30 mg/kg). The results with ketoprofen are consistent with other studies demonstrating that 30 mg/kg is an effective dose against formalin-induced pain (Jourdan et al., 1997). The

differences observed between Phase 1 and Phase 2 of the Formalin Test indicate that **3-5** produces pain relief in a manner consistent with drugs that prevent pro-inflammatory states such as NSAIDs. NSAIDs such as indomethacin and naproxen also inhibit pain-related behaviors in the second phase of the formalin test, but not the first phase (Hunskar & Hole, 1987). In contrast, stronger analgesics such as opioids block pain behaviors in both phases, in part, because they directly inhibit nociceptors which generate pain in Phase 1 and Phase 2 (Hunskar & Hole, 1987). Given that the second phase is largely mediated by inflammatory processes, the antinociceptive effect observed in Figure 55B is presumably due to the drug's ability to block pro-inflammatory mechanisms via sEH inhibition such as the conversion of EETs to DHETs as opposed to directly inhibiting nociceptors (Wang et al., 2021). Another contributor to the antinociceptive effects seen in Figure 53B is the inhibition of FAAH. FAAH inhibition has been shown to inhibit pain on the Formalin Test (Finn et al., 2021; Guindon & Hohmann, 2009), and pharmacological inhibitors of FAAH such as URB937 have also attenuated pain on the Formalin Test (Clapper et al., 2010). Similarly, the pain relief produced by FAAH inhibition is present in Phase 2 of the Formalin Test (Clapper et al., 2010). The role of inhibiting FAAH in the antinociceptive effects of **3-5** needs to be further explored as intraplantar injection of formalin increases the expression of AEA in the periaqueductal gray, an important brain region for pain processing (Walker et al., 1999). Since **3-5** is our lead compound, these studies provide initial proof-of-concept data to suggest that dual sEH/FAAH inhibition can produce pain relief. Further analysis of the contribution of sEH inhibition and FAAH inhibition and *in vivo* potency and efficacy compared to existing analgesics and other novel dual inhibitors is needed.



## CHAPTER 3

### CONCLUSIONS

We successfully synthesized 61 compounds using microwave irradiation, evaluated them in sEH and FAAH inhibition assays, performed molecular modeling and calculated their ADME-Tox properties in ICM-Pro. We also evaluated *in vivo* the benzothiazole inhibitor, **3-5**, using a rat model of acute inflammatory pain. Dual inhibitors possessing the 4-phenylthiazol moiety were identified and benzothiazole inhibitors were further explored. Several important SAR observations were established which will further guide our follow-up design and synthesis. Molecular modeling studies of these compounds revealed important residues within the catalytic sites of both enzymes that are responsible for the low nanomolar potencies of these inhibitors. Our calculation of predicted ADME-Tox properties suggests that several of these inhibitors have the potential to be further developed as new lead candidates and therapeutics in pain management. Evaluation of **3-5** in rat models revealed that the antinociception produced by **3-5** is comparable to ketoprofen, a traditional NSAID. Information obtained here will be helpful during the drug formulation and planning of future *in vivo* experiments, and it will help toward our long-term goal to develop novel non-opioid therapeutics for pain management and fibrosis treatment.

## CHAPTER 4

### EXPERIMENTAL

#### Materials and Methods

All solvents and reagents were obtained from Sigma–Aldrich, Matrix Scientific, TCI, and Acrōs Organic and used without further purification. Analytical thin-layer chromatography (TLC) was performed on aluminum plates precoated with silica gel, also obtained from Sigma–Aldrich. Column chromatography was carried out on Merck 938S silica gel. Proton and carbon NMR spectra were recorded with a Bruker 400 MHz NMR spectrometer. Spectra were referenced to the residual solvent peak: proton chemical shifts are reported relative to the residual solvent peak (chloroform = 7.26 ppm or dimethyl sulfoxide = 2.50 ppm) as follows: chemical shift ( $\delta$ ), proton ID, multiplicity (s = singlet, bs = broad singlet, d = doublet, bd = broad doublet, dd = doublet of doublets, t = triplet, q = quartet, m = multiplet, integration, coupling constant(s) in Hz). Carbon chemical shifts are reported relative to the residual deuterated solvent signals (chloroform = 77.2 ppm, or dimethyl sulfoxide = 39.5 ppm). All compounds described were of > 95% purity. Purity was confirmed by high-resolution liquid chromatography mass spectrometer (ThermoFisher Scientific system). Elution was isocratic with water (30%, +0.1% formic acid) and acetonitrile (70%, +0.1% formic acid) at a flow rate of 0.4 mL/min. Melting points were measured with a MEL-TEMP II melting point apparatus and are reported uncorrected. Human recombinant FAAH enzyme (Item No. 100101183, Batch No. 0523867) and human recombinant sEH enzyme (Item No. 10011669) were obtained from Cayman Chemical. Molecular modeling studies and docking experiments were performed using ICM Pro Molsoft software.

#### Synthesis, Assay, and Modeling of 2-naphthyl and 4-phenylthiazoles Analogs

The synthesis of 2-naphthyl analogs **1-1** to **1-3** and 4-phenylthiazole analogs **2-1** to **2-6** are illustrated in Figure 56 and 57, respectively. In short, 2-naphthylamine **I**, and 1-Boc-piperidine-4-carboxylic acid **m**, were coupled under standard EDC-amide coupling conditions to get the amide **n** in 57% yield. The Boc protecting group was subsequently removed using trifluoroacetic acid (TFA). The

obtained amine was sulfonated with 2-thiophenylsulfonyl chloride, benzenesulfonyl chloride and 2-fluorobenzenesulfonyl chloride to afford analogs **1-1** to **1-3**, respectively. The synthesis of analogs **2-1** to **2-6** started with condensation of commercially available 2-bromoacetophenone **q**, and 4-aminothiobenzamide **r**. The obtained 4-phenylthiazole aniline **s**, was coupled to 1-Boc-piperidine-4-carboxylic **m**, using EDC as coupling reagent and microwave irradiation. The Boc group of the resulting amide **t** was removed with TFA to afford the amine **u**, which was reacted with various different sulfonyl chlorides to yield the target analogs **2-1** to **2-6** in moderate yields.

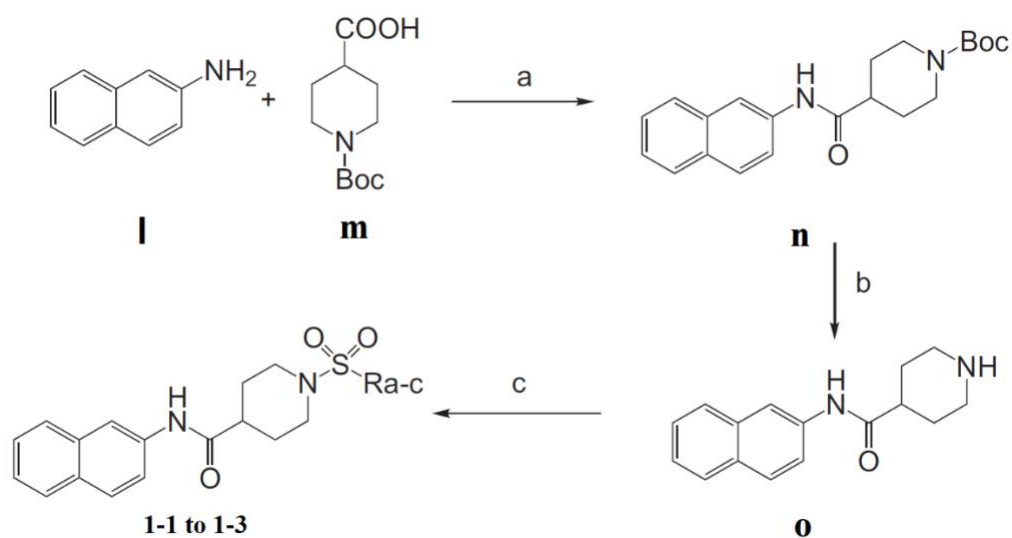


*Figure 56.* Reagents and conditions: (a) EDC, CH<sub>2</sub>Cl<sub>2</sub>, rt, 48 hr, 57%; (b) TFA, CH<sub>2</sub>Cl<sub>2</sub>, rt, 24 hr, 62%; (c) R-sulfonyl chloride, DiPEA, CH<sub>2</sub>Cl<sub>2</sub>, rt, 24 hr, 38%–86%. **1-1**: -thiophene-2-yl; **1-2**: -phenyl; **1-3**: -2-fluorophenyl.

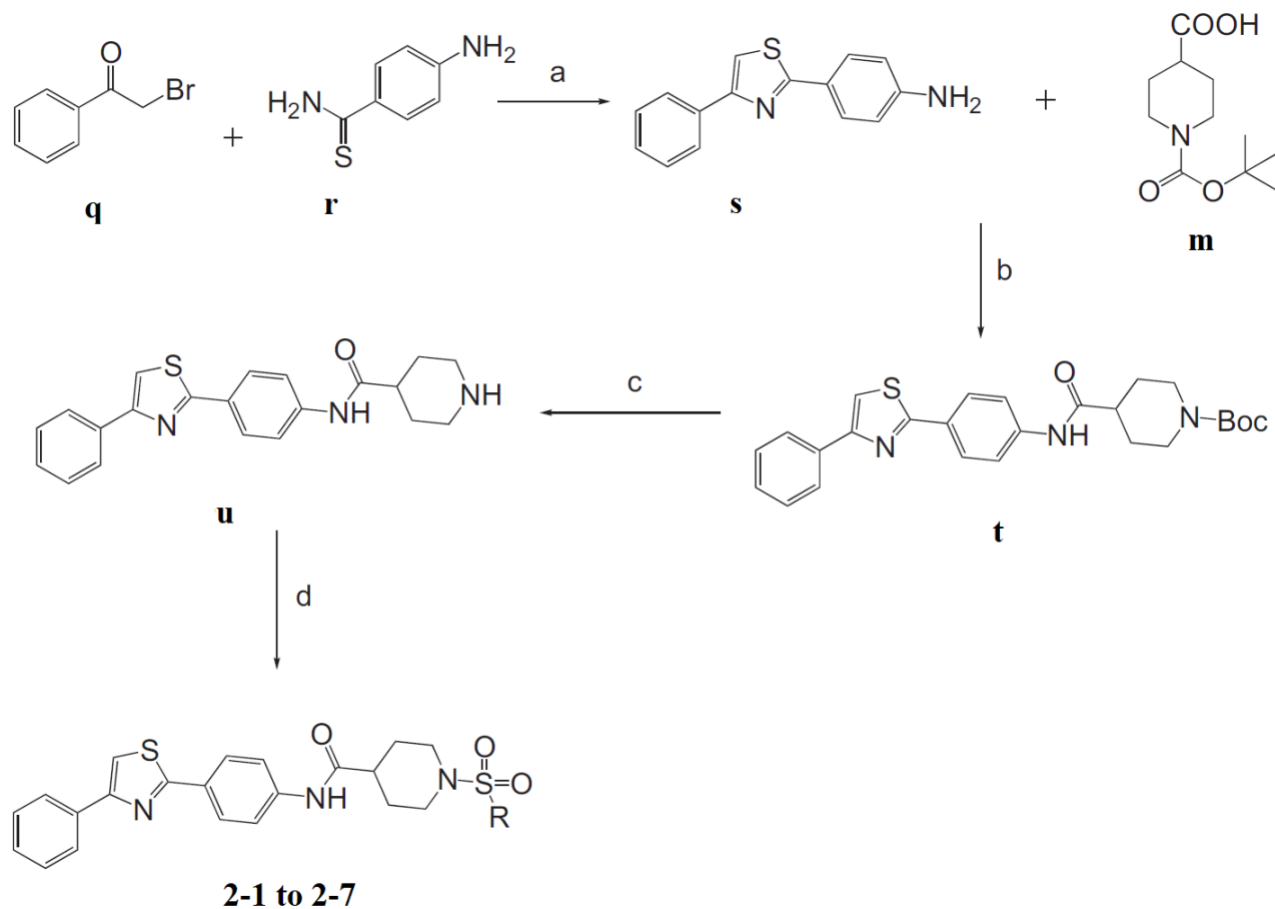


**Figure 57.** Reagents and conditions: (a) *i*PrOH, 60°C, 2 hr, 90%; (b) EDC, DMAP, CH<sub>2</sub>Cl<sub>2</sub>, MW irradiation 15 min, 80°C, 53%; (c) TFA, CH<sub>2</sub>Cl<sub>2</sub>, rt, 24 hr, 94%; (d) Triethylamine, CH<sub>2</sub>Cl<sub>2</sub>, R-sulfonyl chloride, MW irradiation 20 min, 40%–72%. **2-1**: 2-thiophenyl; **2-2**: 2-chlorophenyl; **2-3**: 2-fluorophenyl; **2-4**: 4-chlorophenyl; **2-5**: 4-fluorophenyl; **2-6**: 2,4-difluorophenyl; **2-7**: 2,4-dichlorophenyl.

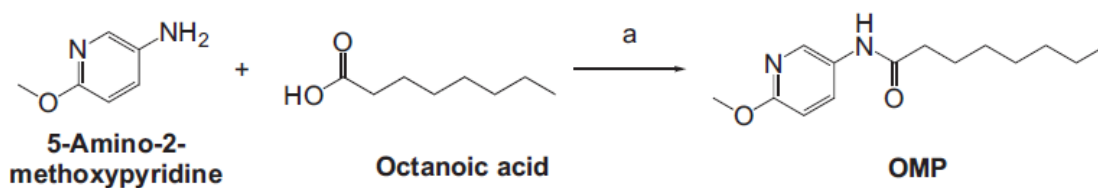


**Figure 58.** Reagents and conditions: (a) EDC, CH<sub>2</sub>Cl<sub>2</sub>, rt, 24 hr, 49%

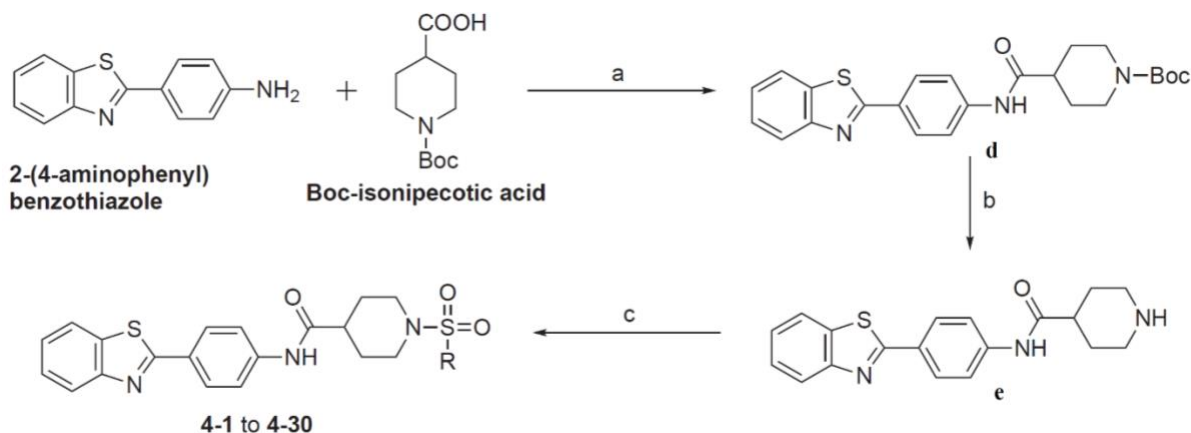


Figure 59. Reagents and conditions (a) EDC, DCM, rt, 24 h, 48%; (b) TFA, DCM, rt, 24 h, 87%; (c) R-sulfonyl chloride, Et<sub>3</sub>N, DCM, rt, 24 h, 16-84%.

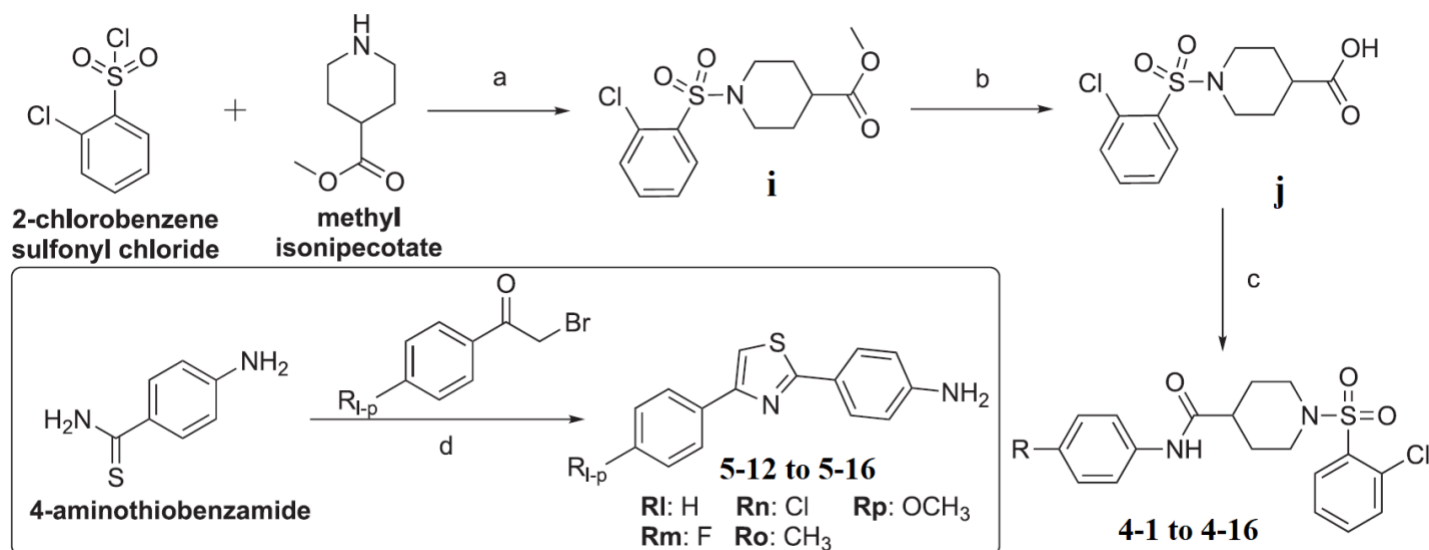


Figure 60. Reagents and conditions: (a) DIPEA, DCM, 20 min, 80 °C, microwave irradiation, 74%; (b) LiOH/H<sub>2</sub>O, 16 h, rt, DCM, rt, 24 h, 91%; (c) **5-12 to 5-16** (see the inner box) or R-aniline (see **Table 10** for R), EDC, DMAP, DCM, 20 min, 80 °C, microwave irradiation, 24–91%; (d) iPrOH, 2.5 h, 60 °C, 57–95%.

### General Procedure (Figure 56) for the Preparation of Naphthyl Analogs 1-1 to 1-3

*tert*-butyl 4-(naphthalen-2-ylcarbonyl)piperidine-1-carboxylate (**n**): The mixture of *N*-Boc-piperidinecarboxylic acid **m** (1.01 g, 4.4 mmol) and EDC (1.27 g, 6.6 mmol) was dissolved in anhydrous dichloromethane (45 mL) and was stirred at room temperature. 2-Naphthylamine **l** (756 mg, 5.28 mmol) was slowly added to the reaction mixture and stirred for 48 hours at room temperature under argon atmosphere. The reaction mixture was transferred to the separatory funnel

and organic layer was washed with 2N HCl (100 mL), aqueous solution of saturated NaHCO<sub>3</sub> (2x100 mL), and was then dried over anhydrous sodium sulfate. The product was recrystallized with hexane and collected upon filtration. The product **n** was obtained as an off-white solid, 891 mg, 57% yield. <sup>1</sup>H NMR (400 MHz, CDCl<sub>3</sub>) δ 8.24 (s, 1H), 7.77 (t, *J* = 8.4 Hz, 4H), 7.47 - 7.40 (m, 3H), 4.2 (bs, 1H), 2.78 (bs, 2H), 2.45 - 2.41 (m, 1H), 1.91 (d, *J* = 14.8 Hz, 2H) 1.81 - 1.77 (m, 2H), 1.49 (s, 9H). <sup>13</sup>C NMR (100 MHz, CDCl<sub>3</sub>): δ 173.0, 154.7, 135.2, 133.8, 130.6, 128.7, 127.6, 127.5, 126.5, 125.0, 119.8, 116.8, 79.8, 44.2, 28.4 ppm.

*N*-(naphthalen-2-yl)piperidine-4-carboxamide (**o**): The amide **n** (800 mg, 2.25 mmol) was dissolved in anhydrous dichloromethane (25 mL) and was then cooled down to 0°C. TFA (4.32 mL, 56.5 mmol) was slowly added and the reaction mixture was stirred at 0°C for additional 30 minutes. Reaction mixture was stirred at room temperature for 48 hours under argon atmosphere. Next, the reaction mixture was concentrated. The crude product was dissolved in ethyl acetate (25 mL), and 10% aqueous solution of NaOH (25 mL) was added slowly and vigorously stirred for 15 minutes. The mixture was transferred to the separatory funnel, organic layer was collected, dried over anhydrous sodium sulfate, filtered and concentrated. The product **o** was collected as an off-white solid, 351 mg, 62% yield. <sup>1</sup>H NMR (400 MHz, DMSO-*d*<sub>6</sub>) δ 10.21 (s, 1H), 8.32 (s, 1H), 7.86 – 7.78 (m, 3H), 7.60 (dd, *J* = 2, 6.8 Hz, 1H), 7.46 (t, *J* = 6.8 Hz, 1H), 7.39 (t, *J* = 8 Hz, 1H), 3.92 (bs, 1H), 3.23 (d, *J* = 12.4 Hz, 2H), 2.80 (t, *J* = 10 Hz, 2H), 2.66 – 2.59 (m, 1H), 1.89 (d, *J* = 12 Hz, 2H), 1.78 – 1.70 (m, 2H). <sup>13</sup>C NMR (100 MHz, DMSO-*d*<sub>6</sub>): δ 173.4, 137.2, 133.8, 130.1, 128.7, 127.8, 127.6, 126.8, 124.9, 120.4, 115.6, 44.0, 41.7, 27.2 ppm.

The amine **o** (50 mg, 0.19 mmol) was dissolved in anhydrous dichloromethane (20 mL), the reaction mixture was brought to 0°C and *N,N*-diisopropylethylamine (97 μL, 0.59 mmol) was added. The reaction mixture was stirred for 30 minutes, followed by the addition of corresponding benzene- (or 2-thiophene-) sulfonyl chloride (0.30 mmol). The reaction mixture was then stirred at room temperature under argon atmosphere for 48 hours. Next, the reaction was transferred to the separatory funnel where the organic layer was washed with aqueous solution of saturated

NaHCO<sub>3</sub> (50 mL), then dried over anhydrous sodium sulfate, filtered and concentrated. The crude product was purified by column chromatography (ethyl acetate/hexane 1:1).

*N*-(naphthalen-2-yl)-1-(thiophen-2-ylsulfonyl)piperidine-4-carboxamide (**1-1**): was obtained as an off-white solid in the amount of 30 mg (38% yield): <sup>1</sup>H NMR (400 MHz, DMSO-*d*<sub>6</sub>) δ 8.28 (s, 1H), 8.07 (dd, *J* = 1.2, 4 Hz, 1H), 7.84 – 7.78 (m, 3H), 7.68 (dd, *J* = 1.2, 2.4 Hz, 1H), 7.55 (dd, *J* = 2, 6.8 Hz, 1H), 7.45 (t, *J* = 7.6 Hz, 1H), 7.38 (t, *J* = 7.4 Hz, 1H), 7.324 – 7.30 (m, 1H), 3.68 (d, *J* = 12 Hz, 2H), 2.46 – 2.42 (m, 2H), 1.96 (dd, *J* = 2.8, 10.4 Hz, 2H), 1.78 – 1.68 (m, 2H). <sup>13</sup>C NMR (100 MHz, DMSO-*d*<sub>6</sub>): δ 173.2, 137.1, 135.9, 134.1, 133.8, 133.3, 130.1, 128.7, 127.8, 127.7, 126.8, 124.9, 120.4, 115.6, 45.8, 41.7, 28.0 ppm. HRMS-ESI+: calculated for C<sub>20</sub>H<sub>20</sub>N<sub>2</sub>O<sub>3</sub>S<sub>2</sub> + H: 401.0988; Found: 401.0980.

*N*-(naphthalen-2-yl)-1-(phenylsulfonyl)piperidine-4-carboxamide (**1-2**): was obtained as an off-white solid in the amount of 39 mg (50% yield). <sup>1</sup>H NMR (400 MHz, DMSO-*d*<sub>6</sub>) δ 10.02 (s, 1H), 8.27 (s, 1H), 7.84 – 7.72 (m, 6H), 7.67 (t, *J* = 8 Hz, 2H), 7.54 (d, *J* = 6.8 Hz, 1H), 7.45 (t, *J* = 8 Hz, 1H), 7.38 (t, *J* = 8.4 Hz, 1H), 3.69 (d, *J* = 12 Hz, 2H), 2.39 – 2.33 (m, 3H), 1.93 – 1.89 (m, 2H), 1.72 – 1.64 (m, 2H). <sup>13</sup>C NMR (100 MHz, DMSO-*d*<sub>6</sub>): δ 173.2, 137.1, 136.0, 133.8, 133.6, 130.1, 129.8, 128.7, 127.8, 127.7, 126.8, 124.9, 120.4, 115.6, 45.8, 41.8, 28.1 ppm. HRMS-ESI+: calculated for C<sub>22</sub>H<sub>22</sub>N<sub>2</sub>O<sub>3</sub>S + H: 395.1424; Found: 395.1416.

1-((2-fluorophenyl)sulfonyl)-*N*-(naphthalen-2-yl)piperidine-4-carboxamide (**1-3**): was obtained as a white solid in the amount of 70 mg (86% yield). <sup>1</sup>H NMR (400 MHz, DMSO-*d*<sub>6</sub>) δ 10.08 (s, 1H), 8.29 (s, 1H), 7.84 – 7.78 (m, 5H), 7.57 – 7.52 (m, 2H), 7.47 (t, *J* = 10.6 Hz, 2H), 7.38 (t, *J* = 6.8 Hz, 1H), 3.76 (d, *J* = 12 Hz, 2H), 2.66 (t, *J* = 11.6 Hz, 2H), 1.92 (d, *J* = 10.4 Hz, 2H), 1.71 – 1.61 (m, 2H). <sup>13</sup>C NMR (100 MHz, DMSO-*d*<sub>6</sub>): δ 173.2, 159.9, 157.4, 137.1, 136.4, 136.3, 133.8, 131.2, 130.1, 128.7, 127.8, 127.7, 126.8, 125.6, 125.3, 125.1, 124.9, 120.4, 118.1, 117.9, 115.7, 45.3, 41.9, 28.2 ppm. HRMS-ESI+: calculated for C<sub>22</sub>H<sub>21</sub>FN<sub>2</sub>O<sub>3</sub>S + H: 413.1330; Found: 413.1322.

**General Procedure (Figure 57) for the Preparation of 4-phenylthiazole Analogs 2-1 to 2-7**

The mixture of 2-bromoacetophenone (1.2 g, 6.02 mmol) and 4-aminothiobenzamide (918 mg, 6.02 mmol) were dissolved in isopropanol (25 mL). The reaction was stirred at 60 °C for 2 hours. The reaction mixture was cooled to 0 °C, the crude product was filtered and washed with additional 2 mL cold isopropanol. The crude product, **s** was used for the next step without further purification. **s** was obtained as a dark green solid in the amount of 1.370 g (90% yield). <sup>1</sup>H NMR (400 MHz, DMSO-d<sub>6</sub>) δ 8.12 (s, 1H), 8.04 – 7.98 (m, 4H), 7.47 (t, J = 7.6 Hz, 2H), 7.37 (d, J = 7.2 Hz, 1H), 7.21 (d, J = 8.8 Hz, 2H), 4.44 (bs, 1H). <sup>13</sup>C NMR (100 MHz, DMSO-d<sub>6</sub>): δ 166.5, 154.9, 133.9, 128.8, 128.2, 127.6, 126.1, 120.3, 114.0 ppm.

*N*-*boc*-piperidinecarboxylic acid **m** (750 mg, 3.27 mmol), 1-ethyl-3-(3-dimethylaminopropyl) carbodiimide (EDC) (753 mg, 3.92 mmol), amine **s** (825 mg, 3.27 mmol) and catalytic amount of 4-dimethylaminopyridine (DMAP) were dissolved in 20 mL anhydrous dichloromethane. The reaction mixture was subjected to microwave irradiation at 80 °C for 15 min. The mixture was transferred to a separatory funnel and the organic layer was washed with aqueous solution of 1M HCl (20 mL), aqueous solution of saturated NaHCO<sub>3</sub> (20 mL) and brine (20 mL). The organic layer was then dried over anhydrous sodium sulfate, filtered and concentrated. The crude product was purified by column chromatography (ethyl acetate/hexane 1:1) and 815 mg, 53% of **t** was obtained as a white solid. <sup>1</sup>H NMR (400 MHz, CDCl<sub>3</sub>) δ 7.99-7.96 (m, 3H), 7.62 (d, J = 8.8 Hz, 2H), 7.43 (t, J = 8 Hz, 3H), 7.36-7.32 (m, 1H), 4.18 (bs, 1H), 4.00 (bs, 1H), 2.88 - 2.75 (m, 2H), 2.51 – 2.36 (m, 2H), 1.90 (d, J = 12 Hz, 2H), 1.80 - 1.61 (m, 2H), 1.47 (s, 9H). <sup>13</sup>C NMR (100 MHz, CDCl<sub>3</sub>): δ 179.0, 172.9, 167.3, 156.3, 154.8, 154.8, 139.5, 134.5, 129.9, 128.8, 128.3, 127.5, 126.5, 119.9, 80.0, 44.4, 40.8, 28.5, 27.9 ppm.

The amide **t** (792 mg, 1.71 mmol) was dissolved in anhydrous dichloromethane (20 mL), and reaction mixture was cooled down to 0 °C. Trifluoroacetic acid (TFA) (2.62 mL, 34.2 mmol) was added slowly and the reaction mixture was stirred at room temperature for 24 hours under argon atmosphere. Solvents were evaporated, and the crude product was recrystallized from diethyl ether,



and 685 mg (94% yield) was obtained as a TFA salt. A small amount of product was freebased and used for  $^1\text{H}$  and  $^{13}\text{C}$  NMR analysis.  $^1\text{H}$  NMR (400 MHz,  $\text{DMSO-}d_6$ )  $\delta$  10.13 (s, 1H), 8.10 (s, 1H), 8.05 (d,  $J = 7.2$  Hz, 2H), 7.97 (d,  $J = 8.8$  Hz, 2H), 7.78 (d,  $J = 8.8$  Hz, 2H), 7.47 (t,  $J = 7.2$  Hz, 2H), 7.37 (t,  $J = 7.6$  Hz, 1H), 3.01 (d,  $J = 11.6$  Hz, 2H), 2.55 – 2.53 (m, 1H), 1.72 (d,  $J = 10.8$  Hz, 2H), 1.60 – 1.50 (m, 2H).  $^{13}\text{C}$  NMR (100 MHz,  $\text{DMSO-}d_6$ ):  $\delta$  173.9, 166.8, 154.9, 141.3, 134.0, 128.7, 128.1, 127.6, 126.8, 126.1, 119.2, 113.8, 45.3, 43.4, 29.0 ppm.

The amine **u** (100 mg, 0.209 mmol) was dissolved in 20 mL of anhydrous dichloromethane and triethylamine (0.2 mL, 1.045 mmol) was added, followed by addition of corresponding benzene- (or 2-thiophene-) sulfonyl chloride (0.314 mmol) and was subjected to microwave irradiation at 80 °C for 15 min. Reaction mixture was then transferred to the separatory funnel, organic layer was washed with 30 mL of aqueous solution of saturated sodium bicarbonate, dried over anhydrous sodium sulfate and then concentrated. The final 4-phenylthiazole analogs were purified by column chromatography (ethyl acetate/hexane 1:4).

*N*-(4-(4-phenylthiazol-2-yl)phenyl)-1-(thiophen-2-ylsulfonyl)piperidine-4-carboxamide (**2-1**): was obtained as a white solid in the amount of 54 mg (50% yield):  $^1\text{H}$  NMR (400 MHz,  $\text{DMSO-}d_6$ )  $\delta$  10.12 (s, 1H), 8.11 (s, 1H), 8.07 – 8.03 (m, 3H), 7.96 (d,  $J = 8.8$  Hz, 2H), 7.74 (d,  $J = 8.8$  Hz, 2H), 7.68 – 7.67 (m, 1H), 7.47 (t,  $J = 7.6$  Hz, 2H), 7.35 (d,  $J = 12.8$  Hz, 1H), 7.30 (t,  $J = 3.6$  Hz, 1H), 3.68 (d,  $J = 12$  Hz, 2H), 2.47 – 2.40 (m, 3H), 1.92 (d,  $J = 13.6$  Hz, 2H), 1.75 – 1.65 (m, 2H).  $^{13}\text{C}$  NMR (100 MHz,  $\text{DMSO-}d_6$ ):  $\delta$  173.0, 166.9, 155.1, 141.2, 135.6, 134.2, 133.9, 133.1, 128.9, 128.5, 128.3, 128.0, 127.0, 126.3, 119.5, 114.0, 45.5, 41.5, 27.6 ppm. HRMS-ESI+: calculated for  $\text{C}_{25}\text{H}_{23}\text{N}_3\text{O}_3\text{S}_3 + \text{H}$ : 510.0974; Found: 510.0962.

1-((2-fluorophenyl)sulfonyl)-*N*-(4-(4-phenylthiazol-2-yl)phenyl)piperidine-4-carboxamide (**2-2**): was obtained as a white solid in the amount of 44 mg (40% yield).  $^1\text{H}$  NMR (400 MHz,  $\text{DMSO-}d_6$ )  $\delta$  10.14 (s, 1H), 8.10 (s, 1H), 8.03 (d,  $J = 7.2$  Hz, 2H), 7.96 (d,  $J = 8$  Hz, 2H), 7.83 – 7.73 (m, 4H), 7.54 – 7.43 (m, 2H), 7.36 (t,  $J = 7.2$  Hz, 1H), 3.75 (d,  $J = 12.4$  Hz, 2H), 2.65 (t,  $J = 11.6$  Hz, 2H), 1.91 (d,  $J = 10.4$  Hz, 2H), 1.68 – 1.60 (m, 2H).  $^{13}\text{C}$  NMR (100 MHz,  $\text{DMSO-}d_6$ ): 173.0, 166.9, 155.1, 141.2,

136.1, 136.0, 134.2, 131.0, 128.9, 128.3, 128.0, 127.0, 126.2, 125.4, 125.3, 125.0, 119.5, 117.8, 117.6, 114.0, 45.0, 41.6, 27.9  $\delta$  ppm. HRMS-ESI+: calculated for  $C_{27}H_{24}FN_3O_3S_2 + H$ : 522.1316; Found: 522.1302.

1-((2-chlorophenyl)sulfonyl)-*N*-(4-(4-phenylthiazol-2-yl)phenyl)piperidine-4-carboxamide (**2-3**): was obtained as an off-white solid in the amount of 62.1 mg (55% yield).  $^1H$  NMR (400 MHz, DMSO- $d_6$ )  $\delta$  10.19 (s, 1H), 8.10 (s, 1H), 8.05 – 7.95 (m, 5H), 7.76 – 7.67 (m, 4H), 7.58 (t,  $J = 8$  Hz, 1H), 7.47 (t,  $J = 7.6$  Hz, 2H), 7.37 (t,  $J = 7.6$  Hz, 1H), 3.78 (d,  $J = 12.8$  Hz, 2H), 2.84 (t,  $J = 12.4$  Hz, 2H), 2.55 – 2.51 (m, 1H), 1.89 (d,  $J = 10.8$  Hz, 2H), 1.62 (dd,  $J = 11.6, 9.2$  Hz, 2H).  $^{13}C$  NMR (100 MHz, DMSO- $d_6$ ):  $\delta$  172.9, 166.7, 154.9, 141.0, 135.8, 134.4, 134.0, 132.2, 131.5, 130.8, 128.8, 128.7, 128.1, 127.8, 126.8, 126.0, 119.3, 113.8, 44.7, 41.7, 28.0 ppm. HRMS-ESI+: calculated for  $C_{27}H_{24}ClN_3O_3S_2 + H$ : 538.1020; Found: 538.1007.

1-((4-fluorophenyl)sulfonyl)-*N*-(4-(4-phenylthiazol-2-yl)phenyl)piperidine-4-carboxamide (**2-4**): was obtained as white solid in the amount of 79 mg (72% yield).  $^1H$  NMR (400 MHz, DMSO- $d_6$ )  $\delta$  10.09 (s, 1H), 8.09 (s, 1H), 8.03 (d,  $J = 7.2$  Hz, 2H), 7.96 (d,  $J = 8.8$  Hz, 2H), 7.87 – 7.83 (m, 2H), 7.73 (d,  $J = 8.8$  Hz, 2H), 7.52 – 7.44 (m, 4H), 7.36 (t,  $J = 7.6$  Hz, 1H), 3.68 (d,  $J = 12$  Hz, 2H), 2.36 (t,  $J = 11.6$  Hz, 3H), 1.89 (d,  $J = 10.4$  Hz, 2H), 1.70-1.62 (m, 2H).  $^{13}C$  NMR (100 MHz, DMSO- $d_6$ ):  $\delta$  172.8, 166.7, 154.9, 141.0, 134.0, 132.1, 132.0, 130.5, 130.4, 128.7, 128.1, 127.8, 126.8, 126.0, 119.3, 116.7, 116.4, 113.8, 45.2, 41.4, 27.5 ppm. HRMS-ESI+: calculated for  $C_{27}H_{24}FN_3O_3S_2 + H$ : 522.1316; Found: 522.1302.

1-((4-chlorophenyl)sulfonyl)-*N*-(4-(4-phenylthiazol-2-yl)phenyl)piperidine-4-carboxamide (**2-5**): was obtained as a white solid, 59 mg (53% yield).  $^1H$  NMR (400 MHz, DMSO- $d_6$ )  $\delta$  10.12 (s, 1H), 8.09 (s, 1H), 8.03 (d,  $J = 7.2$  Hz, 2H), 7.95 (d,  $J = 8.8$  Hz, 2H), 7.80-7.77 (m, 2H), 7.73 (d,  $J = 8.8$  Hz, 4H), 7.46 (t,  $J = 7.2$  Hz, 2H), 7.36 (d,  $J = 7.2$  Hz, 1H), 3.68 (d,  $J = 12$  Hz, 2H), 2.42 – 2.35 (m, 3H), 1.89 (d,  $J = 10.8$  Hz, 2H), 1.71 – 1.61 (m, 2H).  $^{13}C$  NMR (100 MHz, DMSO- $d_6$ ):  $\delta$  172.8, 166.7, 154.9, 141.0, 138.1, 134.6, 134.0, 129.5, 129.3, 128.7, 128.1, 127.8, 126.8, 126.1, 119.3, 113.8, 45.2, 41.3, 28.0, 27.5 ppm. HRMS-ESI+: calculated for  $C_{27}H_{24}ClN_3O_3S_2 + H$ : 538.1020; Found: 538.1006.

1-((2,4-difluorophenyl)sulfonyl)-*N*-(4-(4-phenylthiazol-2-yl)phenyl)piperidine-4-carboxamide (**2-6**): was obtained as off-white solid, 46 mg (41% yield). <sup>1</sup>H NMR (400 MHz, DMSO-*d*<sub>6</sub>) δ 10.15 (s, 1H), 8.10 (s, 1H), 8.04 (d, *J* = 7.2 Hz, 2H), 7.96 (d, *J* = 8.8 Hz, 2H), 7.92 – 7.86 (m, 1H), 7.74 (d, *J* = 9.2 Hz, 2H), 7.66 – 7.61 (m, 1H), 7.47 (t, *J* = 7.2 Hz, 2H), 7.38 – 7.32 (m, 2H), 3.73 (d, *J* = 12.4 Hz, 2H), 2.66 (t, *J* = 11.6 Hz, 2H), 1.91 (d, *J* = 10.4 Hz, 2H), 1.69 – 1.59 (m, 2H). <sup>13</sup>C NMR (100 MHz, DMSO-*d*<sub>6</sub>): δ 173.0, 166.9, 155.1, 141.2, 134.2, 133.1, 128.9, 128.3, 128.0, 127.0, 126.2, 119.5, 114.0, 112.8, 106.5, 44.9, 41.6, 27.9 ppm. HRMS-ESI+: calculated for C<sub>27</sub>H<sub>23</sub>F<sub>2</sub>N<sub>3</sub>O<sub>3</sub>S<sub>2</sub> + H: 540.1222; Found: 540.1205.

1-((2,4-dichlorophenyl)sulfonyl)-*N*-(4-(4-phenylthiazol-2-yl)phenyl)piperidine-4-carboxamide (**2-7**): was obtained as an pale yellow solid in the amount of 93 mg (68 % yield). <sup>1</sup>H NMR (400 MHz, DMSO-*d*<sub>6</sub>) δ 10.19 (s, 1H), 8.10 (s, 1H), 8.05 – 7.94 (m, 6H), 7.75 (d, *J* = 8.8 Hz, 2H), 7.67 (d, *J* = 10.8 Hz, 1H), 7.47 (t, *J* = 7.6 Hz, 2H), 7.37 (t, *J* = 7.6 Hz, 1H), 3.77 (d, *J* = 12.8 Hz, 2H), 2.86 (t, *J* = 12 Hz, 2H), 2.55 – 2.51 (m, 1H), 1.89 (d, *J* = 10.8 Hz, 2H), 1.62 (dd, *J* = 12, 8.8 Hz, 2H). <sup>13</sup>C NMR (100 MHz, DMSO-*d*<sub>6</sub>): δ 172.8, 166.7, 154.9, 141.0, 138.4, 134.9, 134.0, 132.8, 132.2, 131.7, 128.7, 128.1, 127.9, 127.8, 126.8, 126.0, 119.3, 113.8, 44.7, 41.6, 28.0 ppm. HRMS-ESI+: calculated for C<sub>27</sub>H<sub>23</sub>Cl<sub>2</sub>N<sub>3</sub>O<sub>3</sub>S<sub>2</sub> + H: 572.3428; Found: 572.0631.

### OMP Synthesis (Figure 58)

A mixture of octanoic acid (350 mg, 2.43 mmol), 5-Amino-2-methoxypyridine (302 mg, 2.43 mmol) and EDC (700 mg, 3.65 mmol) was dissolved in anhydrous DCM (20 mL) and stirred overnight. The mixture was transferred to separatory funnel, washed with aqueous solution of 1M HCl (200 mL), followed by aqueous solution of saturated sodium bicarbonate, organic layer was dried over anhydrous sodium sulfate, filtered and concentrated. The crude OMP was purified by column chromatography (ethyl acetate/hexane 1:4).

*N*-(6-methoxypyridin-3-yl) octanamide (**OMP**): <sup>1</sup>H NMR (400 MHz, CDCl<sub>3</sub>) δ 8.14 (s, 1H), 7.90 (dd, *J* = 2.8, 6.4 Hz, 1H), 7.51 (s, 1H), 6.71 (d, *J* = 8.8 Hz, 1H), 3.91 (s, 3H), 2.35 (t, *J* = 7.2 Hz, 2H), 1.71 (t, *J* = 6.8 Hz, 2H), 1.29 - 1.28 (m, 8H), 0.88 (t, *J* = 6.8 Hz, 3H). <sup>13</sup>C NMR (100 MHz,

CDCl<sub>3</sub>):  $\delta$  171.9, 160.9, 138.6, 132.4, 128.6, 110.5, 53.5, 37.3, 31.6, 29.2, 29.0, 25.6, 22.5, 14.0 ppm.

HRMS-ESI+: calculated for C<sub>14</sub>H<sub>23</sub>N<sub>2</sub>O<sub>2</sub> + H: 251.1760; Found: 251.1749.

## Synthesis, Assay, and Modeling of Benzothiazole-phenyl Analogs

### General Procedure for the Preparation of Benzothiazole-phenyl Analogs

The mixture of *N*-Boc-4-piperidinecarboxylic acid (250 mg, 1.09 mmol), 1-ethyl-3-(3-dimethylaminopropyl)carbodiimide, EDC (252 mg, 1.31 mmol) and a catalytic amount of 4-dimethylaminopyridin, DMAP were dissolved in anhydrous tetrahydrofuran, THF (40 mL). The reaction mixture was stirred at room temperature for 1.5 hours under an argon atmosphere. Then, 2-(4-aminophenyl) benzothiazole (197 mg, 0.87 mmol) was added to the stirring solution. The reaction mixture was stirred at room temperature for 48 hours under an argon atmosphere. After removal of the solvent under reduced pressure, the residue was dissolved in ethyl acetate (40 mL). The mixture was transferred to a separatory funnel and the organic layer was washed with an aqueous solution of 1 M hydrochloric acid, HCl (3x25 mL), followed by an aqueous solution of saturated sodium bicarbonate, NaHCO<sub>3</sub> (25 mL), dried over anhydrous sodium sulfate, Na<sub>2</sub>SO<sub>4</sub>, filtered and concentrated. The crude product **d** was purified by flash chromatography (1:4 ethyl acetate/hexane solvent system) and recrystallized from diethyl ether: *tert*-butyl 4-((4-(benzo[d]thiazol-2-yl)phenyl)carbonyl)piperidine-1-carboxylate, **d** white solid, yield 70% (0.87 mmol, 267 mg), mp: 238-240 °C. <sup>1</sup>H NMR (400 MHz, CDCl<sub>3</sub>)  $\delta$  ppm 8.05 – 8.02 (m, 3H), 7.88 (d, *J* = 7.2 Hz, 1H), 7.67 (d, *J* = 8.4 Hz, 2H), 7.62 (s, 1H), 7.47 (t, *J* = 7.2 Hz, 1H), 7.36 (t, *J* = 6.8 Hz, 1H), 4.17 (bs, 1H), 2.77 (t, *J* = 11.2 Hz, 2H), 2.43 – 2.37 (m, 1H), 1.89 (d, *J* = 10.8 Hz, 2H), 1.79 – 1.70 (m, 3H), 1.47 (s, 9H). <sup>13</sup>C NMR (100 MHz, CDCl<sub>3</sub>)  $\delta$  172.9, 167.5, 154.8, 154.2, 140.4, 135.0, 129.6, 128.5, 126.4, 125.2, 123.1, 121.7, 119.9, 79.9, 44.5, 28.7, 28.5 ppm.

The amide **d** (250 mg, 0.57 mmol) was dissolved in anhydrous dichloromethane, DCM (10 mL), and stirred in an ice bath at 0°C. Trifluoroacetic acid, TFA (1 mL, 11.4 mmol) was added dropwise into the solution and the reaction mixture was stirred at room temperature for 24 hours under an argon atmosphere. Following concentration *in vacuo*, the crude product was triturated with

diethyl ether and filtered. The product **e** was obtained as a TFA salt and used for next step without further purification. A small amount was free-based and used for NMR analysis: *N*-(4-(benzo[*d*]thiazol-2-yl)phenyl)piperidine-4-carboxamide, **6** pale green solid, yield 91% (0.57 mmol, 234 mg), mp: 242-244 °C. <sup>1</sup>H NMR (400 MHz, DMSO-*d*<sub>6</sub>) δ ppm 10.31 (s, 1H), 8.11 (d, *J* = 8 Hz, 1H), 8.02 (t, *J* = 9.2 Hz, 3H), 7.81 (d, *J* = 8.8 Hz, 2H), 7.52 (t, *J* = 8.4 Hz, 1H), 7.43 (t, *J* = 8 Hz, 1H), 4.23 (bs, 1H), 3.14 (d, *J* = 12.4 Hz, 2H), 2.68 (t, *J* = 12.4 Hz, 2H), 2.59 – 2.55 (m, 1H), 1.82 (d, *J* = 11.6 Hz, 2H), 1.65 (q, *J* = 12, 11.6 Hz, 2H). <sup>13</sup>C NMR (100 MHz, DMSO-*d*<sub>6</sub>) δ 173.5, 166.9, 153.6, 142.1, 134.2, 127.9, 127.4, 126.5, 125.2, 122.5, 122.2, 119.3, 44.1, 42.1, 27.5 ppm.

The amine **e**, as a TFA salt (100 mg, 0.22 mmol), was dissolved in anhydrous DCM (20 mL), and stirred in an ice bath at 0°C. Triethylamine (0.19 mL, 1.33 mmol) was added and the reaction mixture was warmed to room temperature. Corresponding benzenesulfonyl chloride (0.33 mmol) was added to the reaction mixture and the reaction mixture was stirred for 48 hours at room temperature under an argon atmosphere. Next, the mixture was transferred to a separatory funnel where the organic layer was washed with an aqueous solution of saturated NaHCO<sub>3</sub> (30 mL). The organic layer was dried over anhydrous sodium sulfate, filtered and concentrated. The crude product was purified by flash chromatography (1:4 ethyl acetate/hexane solvent system) and recrystallized from diethyl ether.

*N*-(4-(benzo[*d*]thiazol-2-yl)phenyl)-1-(thiophen-2-ylsulfonyl)piperidine-4-carboxamide, **3-1** was obtained as an off-white solid in the amount of 18 mg (17% yield): <sup>1</sup>H NMR (400 MHz, DMSO-*d*<sub>6</sub>) δ 10.19 (s, 1H), 8.12 (d, *J* = 7.6 Hz, 1H), 8.07-8.00 (m, 4H), 7.78 (d, *J* = 8.8 Hz, 2H), 7.67 (d, *J* = 2.4 Hz, 1H), 7.52 (t, *J* = 8 Hz, 1H), 7.44 (t, *J* = 12 Hz, 1H), 7.31 (t, *J* = 5.2 Hz, 1H), 3.68 (d, *J* = 12 Hz, 2H), 2.47-2.38 (m, 3H), 1.95 (d, *J* = 14 Hz, 2H), 1.70 (q, *J* = 16, 8.8 Hz, 2H). <sup>13</sup>C NMR (100 MHz, DMSO-*d*<sub>6</sub>): δ 173.0, 167.0, 153.7, 142.0, 135.5, 134.3, 133.8, 133.0, 128.4, 128.0, 127.6, 126.6, 125.5, 122.6, 122.3, 119.4, 45.4, 41.4, 27.5 ppm. HRMS-ESI+: calculated for C<sub>23</sub>H<sub>21</sub>N<sub>3</sub>O<sub>3</sub>S<sub>3</sub> + H: 484.0823; Found: 484.0818.

*N*-(4-(benzo[*d*]thiazol-2-yl)phenyl)-1-((4-bromo-5-chlorothiophen-2-yl)sulfonyl)piperidine-4-carboxamide, **3-2** was obtained as an off-white solid in the amount of 55 mg (42% yield): <sup>1</sup>H NMR (400 MHz, DMSO-*d*<sub>6</sub>) δ 10.20 (s, 1H), 8.12 (d, *J* = 7.2 Hz, 1H), 8.03 (t, *J* = 8.8 Hz, 3H), 7.80 (t, *J* = 22.4 Hz, 2H), 7.53 (t, *J* = 7.2 Hz, 1H), 7.44 (t, *J* = 6.8 Hz, 1H), 3.69 (d, *J* = 12 Hz, 2H), 2.62 (t, *J* = 12 Hz, 2H), 1.97 (d, *J* = 10.4 Hz, 2H), 1.74 (q, *J* = 11.6, 9.6 Hz, 2H). <sup>13</sup>C NMR (100 MHz, DMSO-*d*<sub>6</sub>): δ 173.0, 167.0, 153.6, 141.6, 134.9, 133.9, 133.5, 132.2, 127.9, 127.1, 126.6, 125.3, 122.6, 122.2, 119.4, 112.1, 45.3, 41.4, 27.5 ppm. HRMS-ESI+: calculated for C<sub>23</sub>H<sub>19</sub>BrClN<sub>3</sub>O<sub>3</sub>S<sub>3</sub> + H: 595.9539; Found: 595.9529.

*N*-(4-(benzo[*d*]thiazol-2-yl)phenyl)-1-(phenylsulfonyl)piperidine-4-carboxamide, **3-3** was obtained as an off-white solid in the amount of 40 mg (38% yield): <sup>1</sup>H NMR (400 MHz, DMSO-*d*<sub>6</sub>) δ 10.15 (s, 1H), 8.11 (d, *J* = 7.2 Hz, 1H), 8.01 (t, *J* = 9.2 Hz, 3H), 7.79-7.65 (m, 5H), 7.52 (t, *J* = 6.8 Hz, 1H), 7.43 (t, *J* = 8 Hz, 1H), 3.69 (d, *J* = 12 Hz, 2H), 2.36 (t, *J* = 9.6 Hz, 3H), 1.87 (d, *J* = 10.4 Hz, 2H), 1.69 (q, *J* = 11.6, 9.2 Hz, 2H). <sup>13</sup>C NMR (100 MHz, DMSO-*d*<sub>6</sub>): δ 173.0, 167.0, 153.7, 142.0, 135.7, 134.3, 133.3, 129.5, 128.1, 127.5, 126.7, 125.3, 122.7, 122.3, 119.4, 45.4, 41.6, 27.4 ppm. HRMS-ESI+: calculated for C<sub>25</sub>H<sub>23</sub>N<sub>3</sub>O<sub>3</sub>S<sub>2</sub> + H: 478.1259; Found: 478.1252.

*N*-(4-(benzo[*d*]thiazol-2-yl)phenyl)-1-((2-fluorophenyl)sulfonyl)piperidine-4-carboxamide, **3-4** was obtained as an off-white solid in the amount of 51 mg (46% yield): <sup>1</sup>H NMR (400 MHz, DMSO-*d*<sub>6</sub>) δ 10.22 (s, 1H), 8.11 (d, *J* = 7.2 Hz, 1H), 8.02 (t, *J* = 8.8 Hz, 3H), 7.84-7.77 (m, 4H), 7.53, (t, *J* = 8.4 Hz, 2H), 7.44 (q, *J* = 9.2, 7.2 Hz, 2H), 3.75 (d, *J* = 12.8 Hz, 2H), 2.66 (t, *J* = 11.6 Hz, 2H), 2.48-2.45 (m, 1H), 1.92 (d, *J* = 10.4 Hz, 2H), 1.65 (q, *J* = 11.6, 8.8 Hz, 2H). <sup>13</sup>C NMR (100 MHz, DMSO-*d*<sub>6</sub>): δ 172.9, 166.9, 159.3, 156.9, 153.6, 141.9, 135.9, 135.8, 134.2, 130.8, 127.9, 127.5, 126.5, 125.2, 124.8, 122.5, 122.2, 119.3, 117.6, 117.4, 54.8, 44.8, 41.4, 27.7 ppm. HRMS-ESI+: calculated for C<sub>25</sub>H<sub>22</sub>FN<sub>3</sub>O<sub>3</sub>S<sub>2</sub> + H: 496.1165; Found: 496.1154.

*N*-(4-(benzo[*d*]thiazol-2-yl)phenyl)-1-((2-chlorophenyl)sulfonyl)piperidine-4-carboxamide, **3-5** was obtained as an off-white solid in the amount of 93 mg (83% yield): <sup>1</sup>H NMR (400 MHz, DMSO-*d*<sub>6</sub>) δ 10.25 (s, 1H), 8.11 (d, *J* = 7.2 Hz, 1H), 8.02 (t, *J* = 8.8 Hz, 4H), 7.79 (d, *J* = 8.8 Hz, 2H), 7.73 (q,

$J = 8, 10$  Hz, 2H), 7.59-7.50 (m, 2H), 7.43 (t,  $J = 8$  Hz, 1H), 3.78 (d,  $J = 12.8$  Hz, 2H), 2.84 (t,  $J = 12.4$  Hz, 2H), 2.57-2.52 (m, 1H), 1.89 (d,  $J = 13.2$  Hz, 2H), 1.65 (q,  $J = 15.6, 12$  Hz, 2H).  $^{13}\text{C}$  NMR (100 MHz, DMSO- $d_6$ ):  $\delta$  178.8, 173.0, 166.9, 153.6, 141.9, 135.9, 134.5, 134.2, 132.3, 131.5, 130.9, 127.9, 127.8, 127.5, 126.6, 125.2, 122.5, 122.2, 119.4, 99.5, 44.6, 41.7, 27.9 ppm. HRMS-ESI+: calculated for  $\text{C}_{25}\text{H}_{22}\text{ClN}_3\text{O}_3\text{S}_2 + \text{H}$ : 512.0869; Found: 512.0858.

*N*-(4-(benzo[*d*]thiazol-2-yl)phenyl)-1-((2-bromophenyl)sulfonyl)piperidine-4-carboxamide, **3-6** was obtained as an off-white solid in the amount of 96 mg (78% yield):  $^1\text{H}$  NMR (400 MHz, DMSO- $d_6$ )  $\delta$  10.26 (s, 1H), 8.11 (t,  $J = 6.8$  Hz, 1H), 8.02 (t,  $J = 10.4$  Hz, 4H), 7.91-7.89 (m, 1H), 7.79 (d,  $J = 7.6$  Hz, 2H), 7.64-7.49 (m, 3H), 7.45-7.40 (m, 1H), 3.76 (d,  $J = 12.8$  Hz, 2H), 2.86 (t,  $J = 12.0$  Hz, 2H), 2.55 (d,  $J = 11.6$  Hz, 1H), 1.89 (d,  $J = 12.0$  Hz, 2H), 1.63 (q,  $J = 11.2, 11.2$  Hz, 2H).  $^{13}\text{C}$  NMR (100 MHz, DMSO- $d_6$ ):  $\delta$  173.0, 166.9, 153.6, 142.0, 137.5, 135.8, 134.4, 134.2, 131.6, 128.2, 127.9, 127.4, 126.5, 125.2, 122.5, 122.2, 119.5, 119.3, 44.6, 41.7, 27.9 ppm. HRMS-ESI+: calculated for  $\text{C}_{25}\text{H}_{22}\text{BrN}_3\text{O}_3\text{S}_2 + \text{H}$ : 556.0364; Found: 556.0356.

*N*-(4-(benzo[*d*]thiazol-2-yl)phenyl)-1-(*o*-tolylsulfonyl)piperidine-4-carboxamide, **3-7** was obtained as an off-white solid in the amount of 91 mg (84% yield):  $^1\text{H}$  NMR (400 MHz, DMSO- $d_6$ )  $\delta$  10.24 (s, 1H), 8.11 (d,  $J = 7.6$  Hz, 1H), 8.02 (t,  $J = 8.8$  Hz, 3H), 7.83 (d,  $J = 8$  Hz, 1H), 7.79, (d,  $J = 8.8$  Hz, 2H), 7.60-7.50 (m, 2H), 7.48-7.41 (m, 3H), 7.78 (d,  $J = 8.8$  Hz, 2H), 7.67 (d,  $J = 2.4$  Hz, 1H), 7.52 (t,  $J = 8$  Hz, 1H), 3.66 (d,  $J = 12.4$  Hz, 2H), 2.70 (t,  $J = 12$  Hz, 2H), 2.58 (s, 3H), 1.90 (d,  $J = 10.4$  Hz, 2H), 1.68-1.59 (m, 2H).  $^{13}\text{C}$  NMR (100 MHz, DMSO- $d_6$ ):  $\delta$  177.0, 173.1, 167.0, 153.7, 142.1, 137.3, 135.9, 134.3, 133.1, 133.0, 132.9, 129.6, 128.0, 128.0, 127.6, 126.6, 126.5, 126.4, 126.4, 125.3, 125.2, 122.6, 122.3, 119.4, 114.7, 110.1, 44.4, 41.9, 27.9, 20.2 ppm. HRMS-ESI+: calculated for  $\text{C}_{26}\text{H}_{25}\text{N}_3\text{O}_3\text{S}_2 + \text{H}$ : 492.1416; Found: 492.1407.

*N*-(4-(benzo[*d*]thiazol-2-yl)phenyl)-1-((2-methoxyphenyl)sulfonyl)piperidine-4-carboxamide, **3-8** was obtained as a white solid in the amount of 61 mg (54% yield):  $^1\text{H}$  NMR (400 MHz, DMSO- $d_6$ )  $\delta$  10.23 (s, 1H), 8.11 (d,  $J = 7.6$  Hz, 1H), 8.02 (t,  $J = 8.4$  Hz, 3H), 7.78 (t,  $J = 8.8$  Hz, 3H), 7.65 (t,  $J = 7.6$  Hz, 1H), 7.53 (t,  $J = 7.2$  Hz, 1H), 7.43 (t,  $J = 7.2$  Hz, 1H), 7.27 (d,  $J = 7.6$  Hz, 1H), 7.11 (t,  $J = 7.6$  Hz,

1H), 3.91 (s, 3H), 3.74 (d,  $J = 10.4$  Hz, 2H), 2.68 (t,  $J = 12$  Hz, 2H), 1.87 (d,  $J = 13.6$  Hz, 2H), 1.61 (t,  $J = 12.4$  Hz, 2H).  $^{13}\text{C}$  NMR (100 MHz, DMSO- $d_6$ ):  $\delta$  173.1, 166.9, 156.6, 153.6, 142.0, 134.8, 134.2, 130.6, 127.9, 126.5, 126.0, 124.8, 123.4, 122.5, 122.2, 120.2, 119.3, 113.1, 55.9, 44.9, 41.9, 28.1 ppm. HRMS-ESI+: calculated for  $\text{C}_{26}\text{H}_{25}\text{N}_3\text{O}_4\text{S}_2 + \text{H}$ : 508.1365; Found: 508.1354.

*N*-(4-(benzo[*d*]thiazol-2-yl)phenyl)-1-((3-fluorophenyl)sulfonyl)piperidine-4-carboxamide, **3-9** was obtained as an off-white solid in the amount of 79 mg (72% yield):  $^1\text{H}$  NMR (400 MHz, DMSO- $d_6$ )  $\delta$  10.17 (s, 1H), 8.12 (d,  $J = 7.6$  Hz, 1H), 8.02 (t,  $J = 8.8$  Hz, 3H), 7.79-7.71 (m, 3H), 7.65-7.62 (m, 3H), 7.53 (t,  $J = 6.8$  Hz, 1H), 7.44 (t,  $J = 8.0$  Hz, 1H), 3.72 (d,  $J = 12$  Hz, 2H), 2.42 (q,  $J = 12.0, 9.6$  Hz, 3H), 1.91 (d,  $J = 10.8$  Hz, 2H), 1.66 (q,  $J = 11.6, 9.2$  Hz, 2H).  $^{13}\text{C}$  NMR (100 MHz, DMSO- $d_6$ ):  $\delta$  173.0, 167.0, 160.6, 153.6, 142.0, 137.5, 134.3, 131.9, 128.0, 127.5, 126.6, 125.3, 123.7, 122.6, 122.3, 120.5, 119.4, 114.3, 45.3, 41.4, 27.6 ppm. HRMS-ESI+: calculated for  $\text{C}_{25}\text{H}_{22}\text{FN}_3\text{O}_3\text{S}_2 + \text{H}$ : 496.1165; Found: 496.1154.

*N*-(4-(benzo[*d*]thiazol-2-yl)phenyl)-1-((3-chlorophenyl)sulfonyl)piperidine-4-carboxamide, **3-10** was obtained as an off-white solid in the amount of 81 mg (72% yield):  $^1\text{H}$  NMR (400 MHz, DMSO- $d_6$ )  $\delta$  10.61 (s, 1H), 8.11 (d,  $J = 7.2$  Hz, 1H), 8.04 (q,  $J = 2.4, 8.8$  Hz, 2H), 7.84-7.69 (m, 4H), 7.52 (t,  $J = 7.2$  Hz, 1H), 7.43 (t,  $J = 8$  Hz, 1H), 3.71 (d,  $J = 12$  Hz, 2H), 2.46-2.38 (m, 3H), 1.91 (d,  $J = 10.8$  Hz, 2H), 1.70-1.61 (m, 2H).  $^{13}\text{C}$  NMR (100 MHz, DMSO- $d_6$ ):  $\delta$  172.9, 166.9, 153.6, 141.9, 137.8, 134.2, 134.1, 133.1, 131.5, 127.9, 127.5, 126.8, 126.5, 126.1, 125.2, 122.5, 122.2, 119.4, 99.5, 45.3, 41.4, 27.5 ppm. HRMS-ESI+: calculated for  $\text{C}_{25}\text{H}_{22}\text{ClN}_3\text{O}_3\text{S}_2 + \text{H}$ : 512.0869; Found: 512.0858.

*N*-(4-(benzo[*d*]thiazol-2-yl)phenyl)-1-((3-bromophenyl)sulfonyl)piperidine-4-carboxamide, **3-11** was obtained as an off-white solid in the amount of 75 mg (61% yield):  $^1\text{H}$  NMR (400 MHz, DMSO- $d_6$ )  $\delta$  10.16 (s, 1H), 8.11 (d,  $J = 7.2$  Hz, 1H), 8.04-7.95 (m, 5H), 7.91 (s, 1H), 7.78 (t,  $J = 10.0$  Hz, 3H), 7.64 (t,  $J = 8$  Hz, 1H), 7.53 (t,  $J = 8$  Hz, 1H), 7.44 (t,  $J = 8$  Hz, 1H), 3.71 (d,  $J = 11.6$  Hz, 2H), 2.44 (t,  $J = 11.6$  Hz, 3H), 1.91 (d,  $J = 11.6$  Hz, 2H), 1.67 (t,  $J = 7.6$  Hz, 2H).  $^{13}\text{C}$  NMR (100 MHz, DMSO- $d_6$ ):  $\delta$  172.9, 166.9, 153.6, 136.0, 134.2, 131.6, 129.5, 127.9, 126.5, 122.5, 122.4, 122.2, 119.3, 45.2, 41.3, 27.5 ppm. HRMS-ESI+: calculated for  $\text{C}_{25}\text{H}_{22}\text{BrN}_3\text{OS}_2 + \text{H}$ : 556.0364; Found: 556.0356.



*N*-(4-(benzo[*d*]thiazol-2-yl)phenyl)-1-(*m*-tolylsulfonyl)piperidine-4-carboxamide, **3-12** was obtained as an off-white solid in the amount of 53 mg (49% yield): <sup>1</sup>H NMR (400 MHz, DMSO-*d*<sub>6</sub>) δ 10.14 (s, 1H), 8.11 (d, *J* = 7.2 Hz, 1H), 8.01 (t, *J* = 8.8 Hz, 3H), 7.76 (d, *J* = 8.8 Hz, 2H), 7.58 (s, 1H), 7.57-7.50 (m, 4H), 7.43 (t, *J* = 8 Hz, 1H), 3.67 (d, *J* = 12 Hz, 2H), 2.43 (s, 3H), 2.38 – 2.31 (m, 3H) 1.90 (d, *J* = 10.4 Hz, 2H) 1.70 – 1.62 (m, 2H). <sup>13</sup>C NMR (100 MHz, DMSO-*d*<sub>6</sub>): δ 174.5, 172.9, 166.9, 159.0, 153.6, 152.5, 150.8, 150.6, 145.0, 143.3, 141.9, 139.1, 135.4, 134.2, 133.7, 129.1, 127.9, 127.5, 127.4, 126.5, 126.0, 125.2, 124.5, 122.5, 122.2, 119.3, 116.7, 115.2, 110.4 ppm. HRMS-ESI+: calculated for C<sub>26</sub>H<sub>25</sub>N<sub>3</sub>O<sub>3</sub>S<sub>2</sub> + H: 492.1416; Found: 492.1407.

*N*-(4-(benzo[*d*]thiazol-2-yl)phenyl)-1-((3-methoxyphenyl)sulfonyl)piperidine-4-carboxamide, **3-13** was obtained as a white solid in the amount of 59 mg (47% yield): <sup>1</sup>H NMR (400 MHz, DMSO-*d*<sub>6</sub>) δ 10.14 (s, 1H), 8.11 (d, *J* = 8 Hz, 1H), 8.01 (t, *J* = 8.8 Hz, 3H), 7.76 (d, *J* = 8.8 Hz, 2H), 7.58 (t, *J* = 8.4 Hz, 1H), 7.52 (t, *J* = 7.2 Hz, 1H), 7.429 (t, *J* = 7.2 Hz, 1H), 7.31 (q, *J* = 8 Hz, 6.8 Hz, 2H), 7.22 (s, 1H), 3.85 (s, 3H), 3.69 (d, *J* = 12 Hz, 2H), 2.38 (t, *J* = 11.6 Hz, 3H), 1.90 (d, *J* = 11.6 Hz, 2H), 1.66 (q, *J* = 11.6 Hz, 9.6 Hz, 2H). <sup>13</sup>C NMR (100 MHz, DMSO-*d*<sub>6</sub>): δ 172.6, 166.7, 159.9, 153.1, 142.5, 136.9, 134.1, 130.6, 127.9, 127.6, 126.1, 125.7, 122.5, 122.2, 119.3, 188.9, 112.2 55.6, 45.3, 41.4, 27.5 ppm. HRMS-ESI+: calculated for C<sub>26</sub>H<sub>25</sub>N<sub>3</sub>O<sub>4</sub>S<sub>2</sub> + H: 508.1365; Found: 508.1354.

*N*-(4-(benzo[*d*]thiazol-2-yl)phenyl)-1-((4-fluorophenyl)sulfonyl)piperidine-4-carboxamide, **3-14** was obtained as an off-white solid in the amount of 67 mg (61% yield): <sup>1</sup>H NMR (400 MHz, DMSO-*d*<sub>6</sub>) δ 10.17 (s, 1H), 8.12 (d, *J* = 7.2 Hz, 1H), 8.02 (t, *J* = 8.8 Hz, 3H), 7.86 (q, *J* = 5.2, 4.0 Hz, 2H), 7.77 (d, *J* = 8.8 Hz, 2H), 7.51-7.49 (m, 3H), 7.44 (t, *J* = 8.0 Hz, 1H), 3.69 (d, *J* = 11.6 Hz, 2H), 2.39 (t, *J* = 9.6 Hz, 3H), 1.91 (d, *J* = 10.8 Hz, 2H), 1.67 (q, *J* = 11.6, 9.2 Hz, 2H). <sup>13</sup>C NMR (100 MHz, DMSO-*d*<sub>6</sub>): δ 172.9, 166.9, 163.2, 153.6, 141.9, 134.2, 132.0, 130.5, 130.4, 127.9, 127.5, 126.5, 125.2, 122.5, 122.2, 119.3, 116.7, 116.4, 45.2, 41.4, 27.5 ppm. HRMS-ESI+: calculated for C<sub>25</sub>H<sub>22</sub>FN<sub>3</sub>O<sub>3</sub>S<sub>2</sub> + H: 496.1165; Found: 496.1154.

*N*-(4-(benzo[*d*]thiazol-2-yl)phenyl)-1-((4-chlorophenyl)sulfonyl)piperidine-4-carboxamide, **3-15** was obtained as an off-white solid in the amount of 84 mg (75% yield): <sup>1</sup>H NMR (400 MHz, DMSO-*d*<sub>6</sub>)

$\delta$  10.19 (s, 1H), 8.12 (d,  $J = 7.6$  Hz, 1H), 8.02 (t,  $J = 8.8$  Hz, 3H), 7.79 (q,  $J = 9.2, 12$ , Hz, 6H), 7.53 (t,  $J = 7.2$  Hz, 1H), 7.43 (t,  $J = 8$  Hz, 2H), 3.68 (d,  $J = 12$  Hz, 2H), 2.42 (q,  $J = 12, 9.2$  Hz, 3H), 1.91 (d,  $J = 11.2$  Hz, 2H), 1.69 (q,  $J = 11.6, 9.2$  Hz, 2H).  $^{13}\text{C}$  NMR (100 MHz, DMSO- $d_6$ ):  $\delta$  173.3, 167.5, 138.5, 133.9, 129.6, 129.3, 127.9, 122.6, 122.3, 119.4, 45.2, 41.8, 27.5 ppm. HRMS-ESI+: calculated for  $\text{C}_{25}\text{H}_{22}\text{ClN}_3\text{O}_3\text{S}_2 + \text{H}$ : 512.0869; Found: 512.0858.

*N*-(4-(benzo[*d*]thiazol-2-yl)phenyl)-1-((4-bromophenyl)sulfonyl)piperidine-4-carboxamide, **3-16** was obtained as an off-white solid in the amount of 38 mg (31% yield):  $^1\text{H}$  NMR (400 MHz, DMSO- $d_6$ )  $\delta$  10.17 (s, 1H), 8.11 (d,  $J = 7.6$  Hz, 1H), 8.01 (t,  $J = 8.8$  Hz, 3H), 7.88 (d,  $J = 8.8$  Hz, 2H), 7.77 (d,  $J = 8.8$  Hz, 2H), 7.71 (d,  $J = 8.8$  Hz, 2H), 7.52 (t,  $J = 8.4$  Hz, 1H), 7.43 (t,  $J = 8.0$  Hz, 1H), 3.67 (d,  $J = 12.0$  Hz, 2H), 2.43-2.36 (m, 3H), 1.90 (d,  $J = 13.6$  Hz, 2H), 1.66 (q,  $J = 15.2, 9.2$  Hz, 2H).  $^{13}\text{C}$  NMR (100 MHz, DMSO- $d_6$ ):  $\delta$  172.9, 166.9, 153.6, 141.9, 135.0, 134.2, 132.4, 129.3, 127.9, 127.5, 127.1, 126.5, 122.5, 122.2, 119.3, 45.1, 41.3, 27.5 ppm. HRMS-ESI+: calculated for  $\text{C}_{25}\text{H}_{22}\text{BrN}_3\text{OS}_2 + \text{H}$ : 556.0364; Found: 556.0355.

*N*-(4-(benzo[*d*]thiazol-2-yl)phenyl)-1-tosylpiperidine-4-carboxamide, **3-17** was obtained as an off-white solid in the amount of 73 mg (68% yield):  $^1\text{H}$  NMR (400 MHz, DMSO- $d_6$ )  $\delta$  10.14 (s, 1H), 8.11 (d,  $J = 8$  Hz, 1H), 8.01 (t,  $J = 8.8$  Hz, 3H), 7.76 (d,  $J = 9.2$  Hz, 2H), 7.65 (d,  $J = 8$  Hz, 2H), 7.52 (t,  $J = 6.8$  Hz, 1H), 7.44 (q,  $J = 8.2$  Hz, 3H), 3.65 (d,  $J = 12$  Hz, 2H), 2.42 (s, 3H), 2.31 (q,  $J = 11.6, 9.6$  Hz, 3H), 1.89 (d,  $J = 10.4$  Hz, 2H), 1.66 (q,  $J = 11.2, 9.6$  Hz, 2H).  $^{13}\text{C}$  NMR (100 MHz, DMSO- $d_6$ ):  $\delta$  173.0, 166.9, 153.6, 143.4, 141.9, 134.2, 132.6, 129.8, 127.9, 127.4, 127.4, 126.5, 125.2, 122.2, 119.3 ppm. HRMS-ESI+: calculated for  $\text{C}_{26}\text{H}_{25}\text{N}_3\text{O}_3\text{S}_2 + \text{H}$ : 492.1416; Found: 492.1409.

*N*-(4-(benzo[*d*]thiazol-2-yl)phenyl)-1-((4-methoxyphenyl)sulfonyl)piperidine-4-carboxamide, **3-18** was obtained as a white solid in the amount of 54 mg (48% yield):  $^1\text{H}$  NMR (400 MHz, DMSO- $d_6$ )  $\delta$  10.17 (s, 1H), 8.11 (d,  $J = 8$  Hz, 1H), 8.01 (t,  $J = 8.8$  Hz, 3H), 7.7 (d,  $J = 8.8$  Hz, 2H), 7.70 (d,  $J = 8.8$  Hz, 2H), 7.52 (t,  $J = 7.2$  Hz, 1H), 7.43 (t,  $J = 7.2$  Hz, 1H), 7.17 (d,  $J = 8.8$  Hz, 2H), 3.86 (s, 3H), 3.64 (d,  $J = 12$  Hz, 2H), 2.38-2.28 (m, 3H), 1.89 (d,  $J = 10.8$  Hz, 2H), 1.66 (q,  $J = 11.2$  Hz, 9.6 Hz, 2H).  $^{13}\text{C}$  NMR (100 MHz, DMSO- $d_6$ ):  $\delta$  173.0, 166.9, 162.6, 153.6, 141.9, 134.2, 129.6, 127.9, 122.5, 122.2,

119.3, 114.5, 55.7, 45.2, 41.4, 27.5 ppm. HRMS-ESI+: calculated for  $C_{26}H_{25}N_3O_4S_2 + H$ : 508.1365;

Found: 508.1356.

*N*-(4-(benzo[*d*]thiazol-2-yl)phenyl)-1-((2,4-difluorophenyl)sulfonyl)piperidine-4-carboxamide, **3-19** was obtained as an off-white solid in the amount of 28 mg (25% yield):  $^1H$  NMR (400 MHz, DMSO- $d_6$ )  $\delta$  10.22 (s, 1H), 8.12 (d,  $J = 7.6$  Hz, 1H), 8.03 (t,  $J = 8.8$  Hz, 3H), 7.90 (q,  $J = 8.4, 6.4$  Hz, 1H), 7.79 (d,  $J = 8.8$  Hz, 2H), 7.64 (t,  $J = 10.8$  Hz, 1H), 7.53 (t,  $J = 7.2$  Hz, 1H), 7.44 (t,  $J = 8.0$  Hz, 1H), 7.36 (t,  $J = 8.0$  Hz, 1H), 3.74 (d,  $J = 12.0$  Hz, 2H), 2.68 (t,  $J = 12.0$  Hz, 2H), 1.92 (d,  $J = 10.8$  Hz, 2H), 1.65 (q,  $J = 11.6, 8.8$  Hz, 2H).  $^{13}C$  NMR (100 MHz, DMSO- $d_6$ ):  $\delta$  172.9, 166.9, 153.6, 141.9, 134.2, 126.5, 125.2, 122.5, 122.2, 119.3, 54.8, 44.7, 41.5, 27.7 ppm. HRMS-ESI+: calculated for  $C_{25}H_{21}F_2N_3O_3S_2 + H$ : 514.1071; Found: 514.1065.

*N*-(4-(benzo[*d*]thiazol-2-yl)phenyl)-1-((2,4-dichlorophenyl)sulfonyl)piperidine-4-carboxamide, **3-20** was obtained as an off-white solid in the amount of 58 mg (48% yield):  $^1H$  NMR (400 MHz, DMSO- $d_6$ )  $\delta$  10.27 (s, 1H), 8.11 (d,  $J = 7.2$  Hz, 1H), 8.05-7.94 (m, 4H), 7.81 (s, 1H), 7.79 (d,  $J = 9.2$  Hz, 2H), 7.67 (d,  $J = 10.8$  Hz, 1H), 7.52 (t,  $J = 7.2$  Hz, 1H), 7.43 (t,  $J = 8$  Hz, 1H), 3.77 (d,  $J = 12.8$  Hz, 2H), 2.86 (t,  $J = 12.6$  Hz, 2H), 2.54 (t,  $J = 11.6$  Hz, 1H), 1.89 (d,  $J = 10.8$  Hz, 2H), 1.65 (q,  $J = 12, 8.8$  Hz, 2H).  $^{13}C$  NMR (100 MHz, DMSO- $d_6$ ):  $\delta$  173.0, 166.9, 153.6, 141.9, 138.4, 134.2, 132.9, 132.2, 131.7, 127.9, 127.5, 126.6, 125.2, 122.6, 122.2, 119.4, 44.7, 41.6, 27.9 ppm. HRMS-ESI+: calculated for  $C_{25}H_{21}Cl_2N_3O_3S_2 + H$ : 546.0480; Found: 546.0476.

*N*-(4-(benzo[*d*]thiazol-2-yl)phenyl)-1-((2,4-dibromophenyl)sulfonyl)piperidine-4-carboxamide, **3-21** was obtained as an off-white solid in the amount of 39 mg (28% yield):  $^1H$  NMR (400 MHz, DMSO- $d_6$ )  $\delta$  10.26 (s, 1H), 8.19 (s, 1H), 8.12 (d,  $J = 7.6$  Hz, 1H), 8.04 (d,  $J = 7.6$  Hz, 3H), 7.95 (d,  $J = 8.4$  Hz, 1H), 7.85-7.79 (m, 3H), 7.53 (t,  $J = 7.2$  Hz, 1H), 7.43 (t,  $J = 7.6$  Hz, 1H), 3.75 (d,  $J = 11.2$  Hz, 2H), 2.88 (t,  $J = 12.0$  Hz, 2H), 2.58-2.55 (m, 1H), 1.89 (d,  $J = 13.2$  Hz, 2H), 1.64 (q,  $J = 10.8, 12.0$  Hz, 2H).  $^{13}C$  NMR (100 MHz, DMSO- $d_6$ ):  $\delta$  173.0, 166.9, 153.6, 141.8, 137.6, 137.0, 134.2, 133.0, 131.3, 127.9, 127.1, 126.5, 125.0, 122.5, 122.2, 120.7, 119.3, 44.6, 41.6, 27.9 ppm. HRMS-ESI+: calculated for  $C_{25}H_{21}Br_2N_3O_3S_2 + H$ : 633.9469; Found: 633.9461.

*N*-(4-(benzo[*d*]thiazol-2-yl)phenyl)-1-((2,4-dimethylphenyl)sulfonyl)piperidine-4-carboxamide, **3-22** was obtained as an off-white solid in the amount of 83 mg (75% yield): <sup>1</sup>H NMR (400 MHz, DMSO-*d*<sub>6</sub>) δ 10.22 (s, 1H), 8.11 (d, *J* = 7.2 Hz, 1H), 8.02 (t, *J* = 8.8 Hz, 3H), 7.78 (d, *J* = 8.8 Hz, 2H), 7.71 (d, *J* = 8 Hz, 1H), 7.52 (t, *J* = 6.8 Hz, 1H) 7.43 (t, *J* = 8 Hz, 1H), 7.24 (t, *J* = 11.2 Hz, 1H), 3.63 (d, *J* = 12.4 Hz, 2H), 2.66 (t, *J* = 12 Hz, 2H), 2.53 (s, 3H), 2.35 (s, 3H), 1.89 (d, *J* = 10.4 Hz, 2H), 1.62 (q, *J* = 12, 9.2 Hz, 2H). <sup>13</sup>C NMR (100 MHz, DMSO-*d*<sub>6</sub>): δ 173.0, 166.9, 153.6, 143.3, 141.9, 137.0, 134.2, 133.4, 132.7, 129.8, 127.9, 127.4, 126.8, 126.5, 125.2, 122.5, 122.2, 119.3, 44.2, 41.8, 27.8, 20.7, 20.0 ppm. HRMS-ESI+: calculated for C<sub>27</sub>H<sub>27</sub>N<sub>3</sub>O<sub>3</sub>S<sub>2</sub> + H: 506.1572; Found: 506.1566.

*N*-(4-(benzo[*d*]thiazol-2-yl)phenyl)-1-((2,4-dimethoxyphenyl)sulfonyl)piperidine-4-carboxamide, **3-23** was obtained as an off-white solid in the amount of 73 mg (62% yield): <sup>1</sup>H NMR (400 MHz, DMSO-*d*<sub>6</sub>) δ 10.22 (s, 1H), 8.11 (d, *J* = 8 Hz, 1H), 8.02 (t, *J* = 8.8 Hz, 3H), 7.79 (d, *J* = 8.8 Hz, 2H), 7.67, (d, *J* = 8.4 Hz, 1H), 7.52 (t, *J* = 8 Hz, 1H), 7.43 (t, *J* = 8 Hz, 1H), 6.75 (s, 1H), 6.66 (d, *J* = 8.8 Hz, 1H), 3.87 (d, *J* = 11.6 Hz, 3H), 3.69 (d, *J* = 10 Hz, 2H), 2.62 (t, *J* = 10.4, 2H), 2.44 (d, *J* = 11.2, 1H), 1.86 (d, *J* = 10.8, 2H), 1.60 (q, *J* = 11.6 Hz, 9.2 Hz, 2H). <sup>13</sup>C NMR (100 MHz, DMSO-*d*<sub>6</sub>): δ 173.4, 167.1, 164.5, 158.4, 153.8, 142.2, 134.4, 132.7, 128.1, 127.6, 126.7, 122.7, 122.4, 119.5, 118.2, 105.2, 99.7, 56.2, 55.9, 45.1, 42.2, 28.3 ppm. HRMS-ESI+: calculated for C<sub>27</sub>H<sub>27</sub>N<sub>3</sub>O<sub>5</sub>S<sub>2</sub> + H: 538.1470; Found: 538.1462.

*N*-(4-(benzo[*d*]thiazol-2-yl)phenyl)-1-((3,5-difluorophenyl)sulfonyl)piperidine-4-carboxamide, **3-24** was obtained as an off-white solid in the amount of 60 mg (53% yield): <sup>1</sup>H NMR (400 MHz, DMSO-*d*<sub>6</sub>) δ 10.19 (s, 1H), 8.12 (d, *J* = 7.2 Hz, 1H), 8.03 (t, *J* = 8.8 Hz, 3H), 7.80-7.71 (m, 3H), 7.57-7.52 (m, 3H), 7.44 (t, *J* = 8.0 Hz, 1H), 3.75 (d, *J* = 12.4 Hz, 2H), 2.55-2.41 (m, 4H), 1.92 (d, *J* = 10.4 Hz, 2H), 1.67 (q, *J* = 11.6, 9.2 Hz, 2H). <sup>13</sup>C NMR (100 MHz, DMSO-*d*<sub>6</sub>): δ 172.9, 166.9, 153.6, 141.9, 134.2, 127.9, 127.5, 126.5, 125.2, 122.5, 122.2, 119.3, 111.3, 111.0, 45.2, 41.3, 27.5 ppm. HRMS-ESI+: calculated for C<sub>25</sub>H<sub>21</sub>F<sub>2</sub>N<sub>3</sub>O<sub>3</sub>S<sub>2</sub> + H: 514.1071; Found: 514.1064.

*N*-(4-(benzo[*d*]thiazol-2-yl)phenyl)-1-((3,5-dimethylphenyl)sulfonyl)piperidine-4-carboxamide, **3-25** was obtained as an off-white solid in the amount of 70 mg (63% yield): <sup>1</sup>H NMR (400 MHz, DMSO-

$d_6$ )  $\delta$  10.13 (s, 1H), 8.12 (d,  $J = 7.2$  Hz, 1H), 8.01 (t,  $J = 8.8$  Hz, 3H), 7.76 (d,  $J = 9.2$  Hz, 2H), 7.52 (t,  $J = 7.2$  Hz, 1H), 7.43 (t,  $J = 8$  Hz, 1H), 7.36 (d,  $J = 6$  Hz, 3H), 3.66 (d,  $J = 11.6$  Hz, 2H), 2.38 (s, 6H), 2.33 (t,  $J = 10$  Hz, 3H), 1.90 (d,  $J = 10.8$  Hz, 2H), 1.66 (q,  $J = 15.6, 9.2$  Hz, 2H).  $^{13}\text{C}$  NMR (100 MHz, DMSO- $d_6$ ):  $\delta$  173.0, 166.9, 153.6, 141.9, 138.9, 135.2, 134.4, 134.2, 127.9, 127.4, 126.5, 125.2, 124.8, 122.5, 122.2, 119.3, 45.3, 41.5, 27.5, 20.7 ppm. HRMS-ESI+: calculated for  $\text{C}_{27}\text{H}_{27}\text{N}_3\text{O}_5\text{S}_2 + \text{H}$ : 538.1470; Found: 538.1462.

*N*-(4-(benzo[*d*]thiazol-2-yl)phenyl)-1-((2,4,6-trifluorophenyl)sulfonyl)piperidine-4-carboxamide, **3-26** was obtained as an off-white solid in the amount of 19 mg (16% yield):  $^1\text{H}$  NMR (400 MHz, DMSO- $d_6$ )  $\delta$  10.24 (s, 1H), 8.12 (d,  $J = 7.2$  Hz, 1H), 8.03 (t,  $J = 8.8$  Hz, 3H), 7.79 (d,  $J = 8.8$  Hz, 2H), 7.54-7.50 (m, 3H), 7.43 (t,  $J = 8.0$  Hz, 1H), 3.77 (d,  $J = 12.4$  Hz, 2H), 2.77 (t,  $J = 11.2$  Hz, 2H), 1.95 (d,  $J = 10.4$  Hz, 2H), 1.67 (q,  $J = 11.6, 9.2$  Hz, 2H).  $^{13}\text{C}$  NMR (100 MHz, DMSO- $d_6$ ):  $\delta$  172.9, 166.9, 153.6, 141.9, 134.2, 127.9, 127.5, 126.5, 125.2, 122.5, 122.2, 119.4, 44.5, 41.3, 27.6 ppm. HRMS-ESI+: calculated for  $\text{C}_{25}\text{H}_{22}\text{F}_3\text{N}_3\text{O}_3\text{S}_2 + \text{H}$ : 532.0976; Found: 532.0968.

*N*-(4-(benzo[*d*]thiazol-2-yl)phenyl)-1-((2,4,6-trichlorophenyl)sulfonyl)piperidine-4-carboxamide, **3-27** was obtained as an off-white solid in the amount of 65 mg (51% yield):  $^1\text{H}$  NMR (400 MHz, DMSO- $d_6$ )  $\delta$  10.28 (s, 1H), 8.11 (d,  $J = 8$  Hz, 1H), 8.03 (t,  $J = 8.8$  Hz, 3H), 7.93 (s, 2H), 7.79 (d,  $J = 8.8$  Hz, 2H), 7.52 (t,  $J = 8.8$  Hz, 1H), 7.45 (t,  $J = 8$  Hz, 1H), 3.84 (d,  $J = 13.2$  Hz, 2H), 2.98 (t,  $J = 12$  Hz, 2H), 2.58 (t,  $J = 11.2$  Hz, 1H), 1.91 (d,  $J = 11.2$  Hz, 2H), 1.61 (t,  $J = 9.2$  Hz, 2H).  $^{13}\text{C}$  NMR (100 MHz, DMSO- $d_6$ ):  $\delta$  172.9, 166.9, 153.6, 141.9, 135.4, 134.1, 131.5, 129.6, 126.6, 122.5, 122.2, 119.4, 45.8, 44.6, 41.7, 27.9 ppm. HRMS-ESI+: calculated for  $\text{C}_{25}\text{H}_{20}\text{Cl}_3\text{N}_3\text{O}_3\text{S}_2 + \text{H}$ : 580.0090; Found: 580.0081.

*N*-(4-(benzo[*d*]thiazol-2-yl)phenyl)-1-(mesitylsulfonyl)piperidine-4-carboxamide, **3-28** was obtained as an off-white solid in the amount of 72 mg (63% yield):  $^1\text{H}$  NMR (400 MHz, DMSO- $d_6$ )  $\delta$  10.29 (s, 1H), 8.11 (d,  $J = 7.2$  Hz, 1H), 8.02 (t,  $J = 8.8$  Hz, 3H), 7.79 (d,  $J = 8.8$  Hz, 2H), 7.52 (t,  $J = 6.8$  Hz, 1H), 7.43 (t,  $J = 8.4$  Hz, 1H), 7.09 (s, 2H), 3.52 (d,  $J = 12.8$  Hz, 2H), 2.77 (t,  $J = 12.4$  Hz, 2H), 2.56 (s, 6H), 2.28 (s, 3H), 1.88 (d,  $J = 10.8$  Hz, 2H), 1.58 (q,  $J = 16, 9.2$  Hz, 2H).  $^{13}\text{C}$  NMR

(100 MHz, DMSO- $d_6$ ):  $\delta$  173.3, 167.1, 153.8, 142.6, 142.2, 139.8, 136.0, 134.4, 132.0, 131.8, 130.0, 128.1, 127.7, 126.7, 125.4, 122.7, 122.4, 119.5, 43.4, 42.3, 27.8, 22.9, 22.5, 20.6 ppm. HRMS-ESI+: calculated for  $C_{28}H_{29}N_3O_3S_2 + H$ : 520.1729; Found: 520.1721.

*N*-(4-(benzo[*d*]thiazol-2-yl)phenyl)-1-((2,4,6-triisopropylphenyl)sulfonyl)piperidine-4-carboxamide, **3-29** was obtained as an off-white solid in the amount of 92 mg (69% yield):  $^1H$  NMR (400 MHz, DMSO- $d_6$ )  $\delta$  10.30 (s, 1H), 8.11 (d,  $J = 7.6$  Hz, 1H), 8.02 (t,  $J = 8.8$  Hz, 2H), 7.79 (d,  $J = 8.8$  Hz, 2H), 7.52 (t,  $J = 6.8$  Hz, 1H) 7.43 (t,  $J = 7.2$  Hz, 1H), 7.29 (s, 2H), 4.14-4.07 (m, 2H), 3.53 (d,  $J = 12$  Hz, 2H), 2.97-2.90 (m, 1H), 2.79 (t,  $J = 10.4$  Hz, 2H) 2.56 (t,  $J = 10.8$  Hz, 1H), 1.93 (d,  $J = 10.8$  Hz, 2H), 1.60 (q,  $J = 11.6, 9.6$  Hz, 2H), 1.21 (d,  $J = 6.8$  Hz, 18H).  $^{13}C$  NMR (100 MHz, DMSO- $d_6$ ):  $^{13}C$  NMR (100 MHz, DMSO- $d_6$ ):  $\delta$  173.0, 166.9, 154.1, 153.0, 151.0, 142.0, 134.2, 129.8, 127.9, 127.4, 126.5, 125.0, 123.8, 122.5, 122.2, 119.3, 43.1, 41.9, 33.3, 28.7, 27.6, 24.5, 23.3 ppm. HRMS-ESI+: calculated for  $C_{34}H_{41}N_3O_3S_2 + H$ : 604.2668; Found: 604.2658.

*N*-(4-(benzo[*d*]thiazol-2-yl)phenyl)-1-((perfluorophenyl)sulfonyl)piperidine-4-carboxamide, **3-30** was obtained as an off-white solid in the amount of 95 mg (76% yield):  $^1H$  NMR (400 MHz, DMSO- $d_6$ )  $\delta$  10.26 (s, 1H), 8.12 (d,  $J = 7.6$  Hz, 1H), 8.03 (t,  $J = 8.8$  Hz, 3H), 7.80 (d,  $J = 8.8$  Hz, 2H), 7.53 (t,  $J = 6.8$  Hz, 1H), 7.44 (t,  $J = 6.8$  Hz, 1H), 3.78 (d,  $J = 11.6$  Hz, 2H), 2.85 (t,  $J = 11.2$  Hz, 2H), 1.99 (d,  $J = 10.8$  Hz, 2H), 1.71 (q,  $J = 12.0, 8.8$  Hz, 2H).  $^{13}C$  NMR (100 MHz, DMSO- $d_6$ ):  $\delta$  172.8, 166.9, 153.6, 141.9, 134.2, 127.9, 127.5, 126.5, 122.5, 122.2, 119.4, 44.5, 41.2, 27.6 ppm. HRMS-ESI+: calculated for  $C_{25}H_{18}F_5N_3O_3S_2 + H$ : 568.0788; Found: 568.0780.

### **sEH and FAAH IC<sub>50</sub> Assay Conditions Human FAAH Enzyme Inhibition Assay**

Measurement of sEH potency was performed using cyano(2-methoxynaphthalen-6-yl)methyl trans-(3-phenyloxyran-2-yl) methyl carbonate (CMNPC) as the fluorescent substrate (Jones et al., 2005). Human sEH (1 nM) was incubated with the inhibitor for 5 min in pH 7.0 Bis-Tris/HCl buffer (25 mM) containing 0.1 mg/mL of bovine serum albumin (BSA) at 30 °C prior to substrate introduction ([S] = 5  $\mu$ M). Activity was determined by monitoring the appearance of 6-methoxy-2-naphthaldehyde over 10 min by fluorescence detection with an excitation wavelength of 330 nm and an emission

wavelength of 465 nm. Reported IC<sub>50</sub> values are the average of the three replicates with at least two data points above and at least two below the IC<sub>50</sub>. Measurement of FAAH potency was performed using the substrate *N*-(6-methoxypyridin-3-yl) octanamide (OMP) ([S]<sub>final</sub> = 50 μM) in sodium phosphate buffer (0.1 M, pH = 8, 0.1 mg/mL BSA). Progress of the reaction was measured by fluorescence detection of 6-methoxypyridin-3-amine at an excitation wavelength of 303 nm and an emission wavelength of 394 nm at 37 °C by the use of microplate reader (Molecular Devices., CA, USA). All experiments were run in triplicate, and values reported as average +/- SD. The substrate OMP was synthesized following a previously reported synthetic procedure and reaction conditions (Stephanie R. Wilt et al., 2020).

### **Synthesis, Assay, and Modeling Studies of Additional 4-phenylthiazole Analogs**

#### **General Procedure for the Preparation of 4-1 to 4-16**

2-chlorobenzenesulfonyl chloride (9.5 mmol), methyl isonipecotate (14.25 mmol) and N,N-diisopropylethylamine (28.5 mmol) were dissolved in anhydrous dichloromethane (20 mL) and were subjected to microwave irradiation at 80 °C for 20 min. After removal of the solvent under reduced pressure, the residue was re-dissolved in ethyl acetate (25 mL), the organic layer was washed twice with 1 N HCl (25 mL), then aqueous solution of saturated sodium bicarbonate (25 mL), brine (25 mL), and was then dried over anhydrous sodium sulfate, filtered and concentrated. The crude product, a yellowish oil, was purified by flash chromatography (1:4 ethyl acetate/hexane solvent system) and the final product **i** was obtained as a yellow oil. Saponification of this methyl ester was achieved via the following procedure: a stirred solution of **i** (2.2 g, 6.92 mmol) in tetrahydrofuran (25 mL) was treated with a 2 M aqueous solution of lithium hydroxide (2 mL) and the reaction was stirred overnight at room temperature. Following concentration in vacuo, water (15 mL) and ethyl acetate were added (50 mL). The mixture was then cooled to 0 °C and 1 N HCl was added dropwise, while stirring, until the reaction became acidic. The organic layer was separated, dried over anhydrous sodium sulfate, filtered, and concentrated. The crude product was recrystallized in diethyl ether, and **j** was obtained as a white solid (1.93 g, 91% yield). Next, 0.23 mmol of a carboxylic acid **j**, 0.575 mmol of 1-ethyl-3-

(3-dimethylaminopropyl) carbodiimide (EDC), 0.46 mmol of corresponding aniline and a catalytic amount of 4-dimethylaminopyridine (DMAP) were dissolved in 20 mL anhydrous dichloromethane and subjected to microwave irradiation at 80 °C for 20 min. The solvent was removed under reduced pressure and the residue was dissolved in ethyl acetate (20 mL), washed twice with 1 N HCl (2x25 mL) and aqueous solution of saturated sodium bicarbonate (25 mL). The organic layer was separated, dried over anhydrous sodium sulfate, filtered, and concentrated. The crude product was purified by flash chromatography using 1:1 ethyl acetate/hexane solvent system and final compounds were obtained.

Methyl 1-((2-chlorophenyl)sulfonyl)piperidine-4-carboxylate (**i**) was obtained as a yellowish thick oil in the amount of 2.25 g (74% yield). <sup>1</sup>H NMR (400 MHz, CDCl<sub>3</sub>) δ 8.01-7.98 (m, 1H), 7.49-7.42 (m, 2H), 7.37-7.33 (m, 1H), 3.73-3.68 (m, 2H), 3.62 (s, 3H), 2.89-2.82 (m, 2H), 2.41-2.34 (m, 1H), 1.94-1.88 (m, 2H), 1.77-1.67 (m, 2H). <sup>13</sup>C NMR (100 MHz, CDCl<sub>3</sub>): δ 174.4, 136.5, 133.7, 132.3, 132.0, 127.0, 60.4, 51.9, 45.0, 40.2, 27.9, 21.1, 14.3 ppm.

1-((2-chlorophenyl)sulfonyl)piperidine-4-carboxylic acid (**j**) was obtained as a white solid in the amount of 1.93 g (91% yield). <sup>1</sup>H NMR (400 MHz, CDCl<sub>3</sub>) δ 8.05 (d, *J* = 1.2 Hz, 1H), 7.53-7.46 (m, 4H), 7.41-7.37 (m, 3H), 3.79-3.74 (m, 2H), 2.95-2.89 (m, 2H), 2.49-2.41 (m, 1H), 2.01-1.95 (m, 2H), 1.83-1.73 (m, 2H). <sup>13</sup>C NMR (100 MHz, CDCl<sub>3</sub>): δ 180.4, 136.5, 133.7, 132.3, 132.3, 132.1, 127.0, 77.4, 44.9, 40.1, 27.6 ppm.

1-((2-chlorophenyl)sulfonyl)-*N*-phenylpiperidine-4-carboxamide (**4-1**) was obtained as a white solid in the amount of 37 mg (43% yield): mp 126-128 °C. <sup>1</sup>H NMR (400 MHz, DMSO-*d*<sub>6</sub>) δ 9.88 (s, 1H), 8.01-7.99 (m, 1H), 7.73-7.55 (m, 5H), 7.27 (q, *J* = 7.6 Hz, 2H), 7.01 (t, *J* = 7.6, 1H), 3.76 (d, *J* = 12.8 Hz, 2H), 2.85-2.78 (m, 2H), 2.48-2.43 (m, 1H), 1.85 (d, *J* = 13.2 Hz, 2H), 1.64-1.54 (m, 2H). <sup>13</sup>C NMR (100 MHz, DMSO-*d*<sub>6</sub>): δ 172.5, 139.1, 135.8, 134.4, 132.2, 131.5, 130.8, 128.6, 127.8, 123.1, 119.1, 44.7, 41.6, 28.0 ppm. HRMS-ESI+: calculated for C<sub>18</sub>H<sub>19</sub>N<sub>2</sub>O<sub>3</sub>SCI + H: 379.0883; Found: 379.0874.



1-((2-chlorophenyl)sulfonyl)-*N*-(4-fluorophenyl)piperidine-4-carboxamide (**4-2**) was obtained as a white solid in the amount of 65 mg (72% yield): mp 172-174 °C. <sup>1</sup>H NMR (400 MHz, DMSO-*d*<sub>6</sub>) δ 9.95 (s, 1H), 8.00 (d, *J* = 7.6 Hz, 1H), 7.69 (q, *J* = 8.4 Hz, 2H), 7.58 (d, *J* = 4.8 Hz, 3H), 7.11 (t, *J* = 8.4 Hz, 2H), 3.75 (d, *J* = 12 Hz, 2H), 2.82 (t, *J* = 12.4 Hz, 2H), 2.47-2.42 (m, 1H), 1.85 (d, *J* = 12.8 Hz, 2H), 1.59 (q, *J* = 12.4 Hz, 2H). <sup>13</sup>C NMR (100 MHz, DMSO-*d*<sub>6</sub>): δ 172.4, 159.0, 156.6, 135.8, 135.5, 135.5, 134.4, 132.2, 131.5, 130.8, 127.8, 120.9, 120.8, 115.2, 115.0, 44.7, 41.5, 28.0 ppm. HRMS-ESI+: calculated for C<sub>18</sub>H<sub>18</sub>N<sub>2</sub>O<sub>3</sub>SClF+ H: 397.0789; Found: 397.0780.

*N*-(4-chlorophenyl)-1-((2-chlorophenyl)sulfonyl)piperidine-4-carboxamide (**4-3**) was obtained as a white solid in the amount of 52 mg (55% yield): mp 177-180 °C. <sup>1</sup>H NMR (400 MHz, DMSO-*d*<sub>6</sub>) δ 10.03 (s, 1H), 8.00 (d, *J* = 8.0 Hz, 1H), 7.73-7.55 (m, 5H), 7.32 (d, *J* = 9.2 Hz, 2H), 3.75 (d, *J* = 12.8 Hz, 2H), 2.81 (t, *J* = 12.4 Hz, 2H), 2.49-2.43 (m, 1H), 1.84 (d, *J* = 10.8 Hz, 2H), 1.63-1.53 (m, 2H). <sup>13</sup>C NMR (100 MHz, DMSO-*d*<sub>6</sub>): δ 172.7, 138.0, 135.8, 134.4, 132.2, 131.8, 130.8, 128.5, 127.8, 126.6, 120.6, 44.6, 41.4, 27.9 ppm. HRMS-ESI+: calculated for C<sub>18</sub>H<sub>18</sub>N<sub>2</sub>O<sub>3</sub>SCl<sub>2</sub>+ H: 413.0493; Found: 413.0482.

*N*-(4-bromophenyl)-1-((2-chlorophenyl)sulfonyl)piperidine-4-carboxamide (**4-4**) was obtained as a white solid in the amount of 81 mg (77% yield): mp 184-186 °C. <sup>1</sup>H NMR (400 MHz, DMSO-*d*<sub>6</sub>) δ 10.03 (s, 1H), 8.00-7.98 (m, 1H), 7.72-7.43 (m, 7H), 3.74 (d, *J* = 12.8 Hz, 2H), 2.81 (d, *J* = 12.8 Hz, 2H), 2.48-2.43 (m, 1H), 1.84 (d, *J* = 10.4 Hz, 2H), 1.62-1.54 (m, 2H). <sup>13</sup>C NMR (100 MHz, DMSO-*d*<sub>6</sub>): δ 172.5, 138.2, 135.6, 134.2, 132.0, 131.3, 131.2, 130.6, 127.6, 120.8, 114.4, 44.4, 41.4, 27.7 ppm. HRMS-ESI+: calculated for C<sub>18</sub>H<sub>18</sub>N<sub>2</sub>O<sub>3</sub>SClBr+ H: 456.9988; Found: 456.9979.

1-((2-chlorophenyl)sulfonyl)-*N*-(*p*-tolyl)piperidine-4-carboxamide (**4-5**) was obtained as a white solid in the amount of 51 mg (57% yield): mp 151-154 °C. <sup>1</sup>H NMR (400 MHz, DMSO-*d*<sub>6</sub>) δ 9.95 (s, 1H), 8.00 (d, *J* = 8.4 Hz, 1H), 7.69 (q, *J* = 8.4 Hz, 2H), 7.58 (d, *J* = 4.8 Hz, 3H), 7.11 (t, *J* = 8.4 Hz, 2H), 3.75 (d, *J* = 12.0 Hz, 2H), 2.82 (t, *J* = 12.4 Hz, 2H), 2.47-2.40 (m, 1H), 2.23 (s, 3H), 1.84 (d, *J* = 12.8 Hz, 2H), 1.59 (q, *J* = 12.4 Hz, 2H). <sup>13</sup>C NMR (100 MHz, DMSO-*d*<sub>6</sub>): δ 172.3, 136.6, 135.8,

134.4, 132.2, 131.9, 131.5, 130.8, 128.9, 127.8, 119.1, 44.7, 41.5, 28.0, 20.4 ppm. HRMS-ESI+: calculated for  $C_{19}H_{21}N_2O_3SCl+ H$ : 393.1040; Found: 393.1029.

1-((2-chlorophenyl)sulfonyl)-*N*-(4-(thiazol-2-yl)phenyl)piperidine-4-carboxamide (**4-6**) was obtained as a light gray solid in the amount of 78 mg (74% yield): mp 204-205 °C.  $^1H$  NMR (400 MHz, DMSO- $d_6$ )  $\delta$  10.15 (s, 1H), 8.00 (t,  $J = 1.6$  Hz, 1H), 7.89-7.86 (m, 3H), 7.73-7.66 (m, 5H), 3.76 (d,  $J = 12.8$  Hz, 2H), 2.86-2.80 (m, 2H), 2.54-2.48 (m, 1H), 1.87 (t,  $J = 2.8$  Hz, 2H), 1.66-1.55 (m, 2H).  $^{13}C$  NMR (100 MHz, DMSO- $d_6$ ):  $\delta$  172.8, 166.8, 143.6, 140.8, 135.8, 134.4, 132.2, 131.5, 130.8, 127.9, 127.8, 126.7, 119.6, 119.3, 44.7, 41.6, 28.0 ppm. HRMS-ESI+: calculated for  $C_{21}H_{20}N_3O_3S_2Cl+ H$ : 462.0713; Found: 462.0701.

1-((2-chlorophenyl)sulfonyl)-*N*-(4-(oxazol-2-yl)phenyl)piperidine-4-carboxamide (**4-7**) was obtained as a dark yellow solid in the amount of 93 mg (91% yield): mp 229-231 °C.  $^1H$  NMR (400 MHz, DMSO- $d_6$ )  $\delta$  10.18 (s, 1H), 8.15-7.57 (m, 10H), 7.32 (s, 1H), 3.76 (d,  $J = 12.4$  Hz, 2H), 2.83 (t,  $J = 12.0$  Hz, 2H), 2.55-2.50 (m, 1H), 1.87 (d,  $J = 10.8$  Hz, 2H), 1.65-1.55 (m, 2H).  $^{13}C$  NMR (100 MHz, DMSO- $d_6$ ):  $\delta$  172.9, 160.7, 141.1, 139.6, 135.8, 134.4, 132.3, 131.5, 130.8, 128.3, 127.8, 126.6, 121.7, 119.2, 44.7, 41.6, 28.0 ppm. HRMS-ESI+: calculated for  $C_{21}H_{20}N_3O_4SCl+ H$ : 446.0941; Found: 446.0941.

1-((2-chlorophenyl)sulfonyl)-*N*-(4-(5-methylbenzo[*d*]thiazol-2-yl)phenyl)piperidine-4-carboxamide (**4-8**) was obtained as a white solid in the amount of 63 mg (52% yield): mp >250 °C.  $^1H$  NMR (400 MHz, DMSO- $d_6$ )  $\delta$  10.29 (s, 1H), 8.07-8.03 (m, 3H), 7.94 (d,  $J = 8.0$  Hz, 2H), 7.83-7.72 (m, 4H), 7.65-7.61 (m, 1H), 7.40-7.37 (m, 1H), 3.83 (d,  $J = 12.8$  Hz, 2H), 2.89 (t,  $J = 12.4$  Hz, 2H), 2.55-2.51 (m, 1H), 2.44 (s, 3H), 1.94 (d,  $J = 10.8$  Hz, 2H), 1.72-1.62 (m, 2H).  $^{13}C$  NMR (100 MHz, DMSO- $d_6$ ):  $\delta$  173.0, 165.8, 151.7, 141.8, 135.8, 135.0, 134.4, 134.4, 132.3, 131.5, 131.0, 128.0, 127.8, 127.8, 127.6, 122.1, 121.7, 119.3, 44.7, 41.7, 28.0, 21.0 ppm. HRMS-ESI+: calculated for  $C_{26}H_{24}N_3O_3S_2Cl+ H$ : 526.1026; Found: 526.1014.

1-((2-chlorophenyl)sulfonyl)-*N*-(4-(1-methyl-1*H*-benzo[*d*]imidazol-2-yl)phenyl)piperidine-4-carboxamide (**4-9**) was obtained as a light gray solid in the amount of 80 mg (68% yield): mp 195-198

°C.  $^1\text{H}$  NMR (400 MHz,  $\text{DMSO-}d_6$ )  $\delta$  10.18 (s, 1H), 8.01 (d,  $J = 6.4$  Hz, 1H), 7.78-7.55 (m, 9H), 7.28-7.20 (m, 2H), 3.79 (dd,  $J = 28.0, 12.0$  Hz, 5H), 2.84 (t,  $J = 12.4$  Hz, 2H), 2.57-2.53 (m, 1H), 1.89 (d,  $J = 10.4$  Hz, 2H), 1.66-1.58 (m, 2H).  $^{13}\text{C}$  NMR (100 MHz,  $\text{DMSO-}d_6$ ):  $\delta$  172.9, 152.8, 142.4, 140.3, 136.5, 135.8, 134.4, 132.3, 131.5, 130.9, 129.8, 127.8, 124.6, 122.1, 121.8, 118.8, 118.7, 110.4, 44.7, 41.7, 31.6, 28.0 ppm. HRMS-ESI+: calculated for  $\text{C}_{26}\text{H}_{25}\text{N}_4\text{O}_3\text{SCl}^+ \text{H}$ : 509.1414; Found: 509.1400.

*N*-(4-(benzo[*d*][1,3]oxathiol-2-yl)phenyl)-1-((2-chlorophenyl)sulfonyl)piperidine-4-carboxamide (**4-10**) was obtained as a gray solid in the amount of 28 mg (24% yield): mp 221-224 °C.  $^1\text{H}$  NMR (400 MHz,  $\text{DMSO-}d_6$ )  $\delta$  10.30 (s, 1H), 8.13 (d,  $J = 8.8$  Hz, 2H), 8.01 (d,  $J = 8.0$  Hz, 1H), 7.83-7.69 (m, 6H), 7.60-7.55 (m, 1H), 7.41-7.36 (m, 2H), 3.77 (d,  $J = 12.8$  Hz, 2H) 2.84 (t,  $J = 12.0$  Hz, 2H), 2.58-2.52 (m, 1H), 1.89 (d,  $J = 10.4$  Hz, 2H), 1.67-1.56 (m, 2H).  $^{13}\text{C}$  NMR (100 MHz,  $\text{DMSO-}d_6$ ):  $\delta$  172.9, 161.9, 149.8, 142.2, 141.4, 135.6, 134.2, 132.0, 131.3, 130.6, 127.9, 127.6, 124.9, 124.5, 120.5, 119.3, 119.0, 110.5, 44.4, 41.5, 27.7 ppm. HRMS-ESI+: calculated for  $\text{C}_{25}\text{H}_{23}\text{N}_2\text{O}_4\text{S}_2\text{Cl}^+ \text{H}$ : 515.0866; Found: 515.0860.

*N*-(4-(4-chlorobenzyl)phenyl)-1-((2-chlorophenyl)sulfonyl)piperidine-4-carboxamide (**4-11**) was obtained as a white solid in the amount of 69 mg (70% yield): mp 135-136 °C.  $^1\text{H}$  NMR (400 MHz,  $\text{DMSO-}d_6$ )  $\delta$  8.37 (t,  $J = 6.0$  Hz, 1H), 7.98 (d,  $J = 7.6$  Hz, 1H), 7.71-7.65 (m, 2H), 7.58-7.54 (m, 1H), 7.36-7.21 (m, 4H), 4.21 (d,  $J = 6.0$  Hz, 2H), 3.69 (d,  $J = 12.4$  Hz, 2H), 2.81-2.74 (m, 2H), 2.35-2.72 (m, 1H), 1.77 (q,  $J = 3.2$  Hz, 2H), 1.58-1.48 (m, 2H).  $^{13}\text{C}$  NMR (100 MHz,  $\text{DMSO-}d_6$ ):  $\delta$  173.5, 138.6, 135.8, 134.4, 132.2, 131.4, 131.2, 130.8, 128.9, 128.1, 127.8, 44.7, 41.2, 40.6, 28.14 ppm. HRMS-ESI+: calculated for  $\text{C}_{25}\text{H}_{24}\text{N}_2\text{O}_3\text{SCl}_2^+ \text{H}$ : 503.0963; Found: 503.0954.

1-((2-chlorophenyl)sulfonyl)-*N*-(4-(4-phenylthiazol-2-yl)phenyl)piperidine-4-carboxamide (**4-12**) was obtained as an off-white solid in the amount of 55 mg (44% yield): mp 172-174 °C.  $^1\text{H}$  NMR (400 MHz,  $\text{DMSO-}d_6$ )  $\delta$  10.19 (s, 1H), 8.10 (s, 1H), 8.05-7.95 (m, 5H), 7.76-7.67 (m, 4H), 7.58 (t,  $J = 8$  Hz, 1H), 7.47 (t,  $J = 7.6$  Hz, 2H), 7.37 (t,  $J = 7.6$  Hz, 1H), 3.78 (d,  $J = 12.8$  Hz, 2H), 2.84 (t,  $J = 12.4$  Hz, 2H), 2.55-2.51 (m, 1H), 1.89 (d,  $J = 10.8$  Hz, 2H), 1.62 (dd,  $J = 11.6, 9.2$  Hz, 2H).  $^{13}\text{C}$  NMR (100

MHz, DMSO-*d*<sub>6</sub>): δ 172.9, 166.7, 154.9, 141.0, 135.8, 134.4, 134.0, 132.2, 131.5, 130.8, 128.8, 128.7, 128.1, 127.8, 126.8, 126.0, 119.3, 113.8, 44.7, 41.7, 28.0 ppm. HRMS-ESI<sup>+</sup>: calculated for C<sub>27</sub>H<sub>24</sub>ClN<sub>3</sub>O<sub>3</sub>S<sub>2</sub>+ H: 538.1020; Found: 538.1007.

1-((2-chlorophenyl)sulfonyl)-N-(4-(4-(4-fluorophenyl)thiazol-2-yl)phenyl)piperidine-4-carboxamide (**4-13**) was obtained as a pale yellow solid in the amount 57 mg (45%): mp 182-185 °C. <sup>1</sup>H NMR (400 MHz, DMSO-*d*<sub>6</sub>) δ 10.18 (s, 1H), 8.10–8.06 (m, 3H), 8.20–8.00 (m, 1H), 7.97–7.94 (m, 2H), 7.76–7.67 (m, 4H), 7.60–7.56 (m, 1H), 7.30 (t, *J* = 9.2, 8.8 Hz, 2H), 3.77 (d, *J* = 12.4 Hz, 2H), 2.87–2.81 (m, 2H), 2.50 (s, 1H), 1.91–1.86 (m, 2H), 1.66–1.56 (m, 2H). <sup>13</sup>C NMR (100 MHz, DMSO-*d*<sub>6</sub>): δ 173.3, 167.3, 154.3, 141.5, 136.3, 134.9, 132.7, 132.0, 131.3, 128.6, 128.5, 128.3, 128.2, 127.3, 119.8, 116.2, 116.0, 114.1, 45.1, 42.1, 28.4 ppm. HRMS-ESI<sup>+</sup>: calculated for C<sub>27</sub>H<sub>23</sub>ClFN<sub>3</sub>O<sub>3</sub>S<sub>2</sub>+ H: 556.0932; Found 556.0919.

1-((2-chlorophenyl)sulfonyl)-N-(4-(4-(4-chlorophenyl)thiazol-2-yl)phenyl)piperidine-4-carboxamide (**4-14**) was obtained as an off-white solid in the amount of 61 mg (46% yield): mp 188-190 °C. <sup>1</sup>H NMR (400 MHz, DMSO-*d*<sub>6</sub>) δ 10.19 (s, 1H), 8.16 (s, 1H), 8.07–7.94 (m, 5H), 7.75–7.67 (m, 4H), 7.59–7.51 (m, 3H), 3.77 (d, *J* = 11.6 Hz, 2H), 2.84 (t, *J* = 12.0, 12.4 Hz, 2H), 2.50 (s, 1H), 1.88 (d, *J* = 13.6 Hz, 2H), 1.61 (q, *J* = 10.8, 11.2, 12.8 Hz, 2H). <sup>13</sup>C NMR (100 MHz, DMSO-*d*<sub>6</sub>): δ 173.3, 167.4, 154.1, 141.6, 136.3, 134.9, 133.3, 133.0, 132.7, 132.0, 131.3, 129.2, 128.2, 128.1, 127.3, 119.8, 115.0, 45.1, 42.1, 28.4 ppm. HRMS-ESI<sup>+</sup>: calculated for C<sub>27</sub>H<sub>23</sub>Cl<sub>2</sub>N<sub>3</sub>O<sub>3</sub>S<sub>2</sub>+ H: 572.0636; Found 572.0626.

1-((2-chlorophenyl)sulfonyl)-N-(4-(4-(*p*-tolyl)thiazol-2-yl)phenyl)piperidine-4-carboxamide (**4-15**) was obtained as a white solid in the amount of 65 mg (52% yield): mp 230-233 °C. <sup>1</sup>H NMR (400 MHz, DMSO-*d*<sub>6</sub>) δ 10.17 (s, 1H), 8.02 (s, 1H), 8.00 (dd, *J* = 0.4, 0.4 Hz, 1H), 7.97–7.91 (m, 4H), 7.76–7.67 (m, 4H), 7.60–7.56 (m, 1H), 7.27 (d, *J* = 7.6 Hz, 2H), 3.78 (d, *J* = 10.0 Hz, 2H), 2.87–2.81 (m, 2H), 2.50 (s, 1H), 2.34 (s, 3H), 1.91–1.87 (m, 2H), 1.67–1.56 (m, 2H). <sup>13</sup>C NMR (100 MHz, DMSO-*d*<sub>6</sub>): δ 173.3, 167.0, 155.5, 141.4, 137.9, 136.3, 134.9, 132.7, 131.9, 131.8, 131.3, 129.8, 128.3, 128.2,

127.2, 126.4, 119.8, 113.4, 45.1, 42.1, 28.4, 21.3 ppm. HRMS-ESI+: calculated for  $C_{28}H_{26}ClN_3O_3S_2+$  H: 552.1182; Found: 552.1170.

1-((2-chlorophenyl)sulfonyl)-N-(4-(4-(4-methoxyphenyl)thiazol-2-yl)phenyl)piperidine-4-carboxamide (**4-16**) was obtained as an off-white solid in the amount of 68 mg (52% yield): mp 207–209 °C.  $^1H$  NMR (400 MHz, DMSO- $d_6$ )  $\delta$  10.17 (s, 1H), 8.02–7.93 (m, 6H), 7.75–7.67 (m, 4H), 7.60–7.56 (m, 1H), 3.80 (s, 3H), 3.79–3.761 (m, 2H), 2.50 (s, 1H), 1.91–1.70 (m, 2H), 1.67–1.56 (m, 2H).  $^{13}C$  NMR (100 MHz, DMSO- $d_6$ ):  $\delta$  173.3, 166.9, 159.7, 155.3, 141.4, 136.3, 134.9, 132.7, 132.0, 131.3, 128.4, 128.2, 127.9, 127.3, 127.2, 119.8, 114.6, 112.2, 55.6, 45.1, 42.1, 28.4 ppm. HRMS-ESI+: calculated for  $C_{28}H_{26}ClN_3O_4S_2+$  H: 568.1132; Found 568.1119.

### **General Procedure for the Preparation of Anilines 5-12 to 5-16**

The mixture of 4-aminothiobenzamide (6.02 mmol) and corresponding 2-bromoacetophenone (6.02 mmol) were dissolved in isopropanol (25 ml; see Figure 60- inner box). The reaction was stirred at 60 °C for 2.5 hr. The reaction mixture was cooled to 0 °C, and the crude product was filtered and washed with an additional 2 ml cold isopropanol. The crude product (aniline) was used for the next step without further purification.

4-(4-phenylthiazol-2-yl)aniline (**5-12**) was obtained as a dark green solid in the amount of 1.370 g (90% yield).  $^1H$  NMR (400 MHz, DMSO- $d_6$ )  $\delta$  8.12 (s, 1H), 8.04–7.98 (m, 4H), 7.47 (t,  $J = 7.6$  Hz, 2H), 7.37 (d,  $J = 7.2$  Hz, 1H), 7.21 (d,  $J = 8.8$  Hz, 2H), 4.44 (bs, 1H).  $^{13}C$  NMR (100 MHz, DMSO- $d_6$ ):  $\delta$  166.5, 154.9, 133.9, 128.8, 128.2, 127.6, 126.1, 120.3, 114.0 ppm.

4-(4-(4-fluorophenyl)thiazol-2-yl)aniline (**5-13**) was obtained as a gray solid in the amount of 0.768 g (47% yield).  $^1H$  NMR (400 MHz, DMSO- $d_6$ )  $\delta$  8.14 (s, 1H), 8.10–8.02 (m, 4H), 7.35–7.27 (m, 4H).  $^{13}C$  NMR (100 MHz, DMSO- $d_6$ ):  $\delta$  166.3, 163.3, 160.8, 154.0, 137.6, 130.5, 129.7, 128.2, 128.1, 127.6, 121.6, 115.8, 115.5, 114.2 ppm.

4-(4-(4-chlorophenyl)thiazol-2-yl)aniline (**5-14**) was obtained as a gray solid in the amount of 1.007 g (58% yield).  $^1H$  NMR (400 MHz, DMSO- $d_6$ )  $\delta$  8.20 (s, 1H), 8.04 (t,  $J = 8.8, 9.2$  Hz, 4H), 7.52

(d,  $J = 8.0$  Hz, 2H), 7.31 (d,  $J = 8.0$  Hz, 2H).  $^{13}\text{C}$  NMR (100 MHz,  $\text{DMSO-}d_6$ ):  $\delta$  166.9, 154.2, 138.5, 133.2, 133.1, 129.8, 129.2, 128.2, 128.0, 121.8, 115.5. ppm.

4-(4-(*p*-tolyl)thiazol-2-yl)aniline (**5-15**) was obtained as a white shiny solid in the amount of 1.52 g (95% yield).  $^1\text{H}$  NMR (400 MHz,  $\text{DMSO-}d_6$ )  $\delta$  8.06 (s, 1H), 8.02 (d,  $J = 8.8$  Hz, 2H), 7.92 (d,  $J = 8.0$  Hz, 2H), 7.30-7.26 (m, 4H), 2.34 (s, 3H).  $^{13}\text{C}$  NMR (100 MHz,  $\text{DMSO-}d_6$ ):  $\delta$  166.1, 155.1, 137.6, 131.2, 129.3, 127.5, 126.0, 121.2, 113.4, 20.8 ppm.

4-(4-(4-methoxyphenyl)thiazol-2-yl)aniline (**5-16**) was obtained as a gray solid in the amount of 0.982 g (57% yield).  $^1\text{H}$  NMR (400 MHz,  $\text{DMSO-}d_6$ )  $\delta$  8.05-8.02 (m, 2H), 7.99-7.95 (m, 3H), 7.33 (d,  $J = 8.8$  Hz, 2H), 7.02 (d,  $J = 8.8\text{Hz}$ , 2H), 3.80 (s, 3H).  $^{13}\text{C}$  NMR (100 MHz,  $\text{DMSO-}d_6$ ):  $\delta$  165.9, 159.3, 154.9, 137.4, 129.9, 127.5, 127.5, 126.7, 121.7, 114.1, 112.4, 55.2 ppm.

## Biological Evaluation

Experimental details for the quantification of inhibitor potencies have been previously published for both FAAH and sEH enzymes. In brief, fluorescence generated by hydrolysis was quantified every 30s for 10 min and the linear portion of the curve was used to generate the reaction velocity (v<sub>inhibitor</sub>). Values were subtracted from wells containing no enzyme. Next, the IC<sub>50</sub> values were quantified by simple linear regression of the log [I] vs. % remaining activity (v<sub>inhibitor</sub>/v<sub>DMSO</sub>) and determining x when y = 0.50. All measurements were the average of triplicates. For all assays, the final DMSO concentration was 2%. sEH Assay. The substrate cyano(6-methoxynaphthalen-2-yl)methyl ((3-phenyloxiran-2-yl)methyl)carbonate (CMNPC) ([S]<sub>final</sub> = 5  $\mu\text{M}$ ) was added to wells containing human sEH in sodium phosphate buffer [0.1 M, pH = 7.4 and 0.1 mg/mL bovine serum albumin (BSA)], and formation of the fluorescent 6-methoxynaphthaldehyde ( $\lambda_{\text{excitation}} = 330$  nm,  $\lambda_{\text{emission}} = 465$  nm, 30 °C) was measured by the use of a microplate reader (Molecular Devices., CA, USA). Measurement of human FAAH potency was performed using the substrate N-(6-methoxypyridin-3-yl) octanamide (OMP ([S]<sub>final</sub> = 50  $\mu\text{M}$ ) in sodium phosphate buffer (0.1 M, pH = 8, 0.1 mg/ mL BSA). Progress of the reaction was measured by fluorescence detection of 6-

methoxypyridin-3-amine at an excitation wavelength of 303 nm and an emission wavelength of 394 nm at 37 °C by the use of a microplate reader (Molecular Devices., CA, USA). The substrate, OMP, was synthesized following a previously reported synthetic procedure and reaction conditions, shown in Figure 58.

### **Molecular Modeling**

Amino acid sequence of human FAAH enzyme was retrieved from NCBI protein database. Sequence alignment was carried out with the ICM Pro (based on ZEGA sequence alignment - Needleman and Wunsch algorithm with zero gap and penalties). To make the homology model, we used a homology algorithm from ICM Pro. Between several crystal structures available in PDB database, we selected as a template a crystal structure of rat FAAH enzyme (PDB code: **3QK5**). The sequence alignment and the rat FAAH PDB template were converted to the ICM homology model. Conversion included optimization of hydrogens, several amino acids (H, P, N, C and Q) and assignment of the secondary structure. In order to validate the model, programs Procheck, Verify3D, Errat, What check and Prove from SAVES metaserver were used. The small molecule docking experiments were performed following steps according to the ICM Pro program guidelines. ICM scores were obtained after this procedure. ADME properties for all synthesized target analogs were calculated using ICM Chemist program.

For the docking studies of the dual sEH/FAAH inhibitors, a crystal structure of human soluble epoxide hydrolase complexed with Ncycloheptyl- 1-(mesitylsulfonyl)piperidine-4-carboxamide (PDBfile: 4HAI)<sup>33</sup> and a homology model of human FAAH enzyme<sup>37</sup> were used. The PDB file 4HAI was first converted to an ICM file and the inhibitor, Ncycloheptyl- 1-(mesitylsulfonyl) piperidine-4-carboxamide, was removed. Docking experiments were performed following the program guidelines. ICM scores were obtained after this procedure. ADMET properties for all synthesized target analogs were calculated using the ICM Chemist Pro program. To generate a Consensus Pharmacophore based on the Atomic Property Fields<sup>71</sup> the following steps were executed according to the program guidelines: (i) dual inhibitors **4-12** to **4-16** were first converted into an ICM objects; (ii) using APF

fields, the dual inhibitors **4-12** to **4-16** were superimposed based on substructures; (iii) the ligands were selected and Choose the Consensus Ph4 menu option was applied; (iv) the threshold was selected as 0.90 (the pharmacophore will be displayed if the property is found in 90% or more of the ligands). The consensus is displayed as meshes in Fig. 54.

### **Formalin Test**

**Subjects:** Data were collected from male Sprague-Dawley rats purchased from Charles River (Hollister, CA, USA) and housed at California State University, East Bay (Hayward, CA, USA). All rats were at least 50 days old at the start of the study and randomly assigned to treatment groups. Experimenters were blinded to treatment groups. Procedures were approved by the Institutional Animal Care and Use Committee of California State University, East Bay.

**Drugs:** **3-5** was dissolved in DMSO to a stock concentration of 10 mM. The 10 mM stock was further diluted into injectable doses (0.1 and 1 mg/kg) using a vehicle solution comprising 10% ethanol, 10% cremophor, and 80% saline. Ketoprofen (Sigma-Aldrich, St. Louis, MO, USA) was dissolved in the same vehicle. Drugs were injected intraperitoneally in a volume of 1 mL/kg. All drugs were administered 30 min before hindpaw injection of formalin.

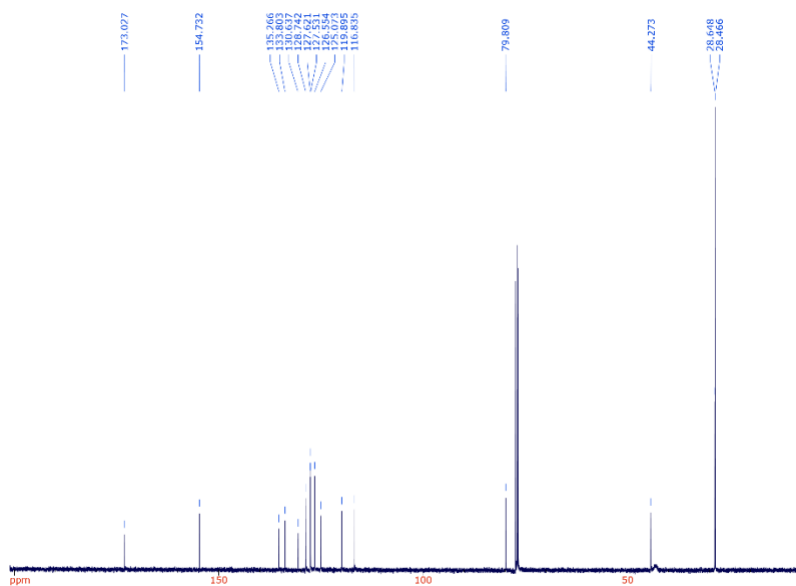
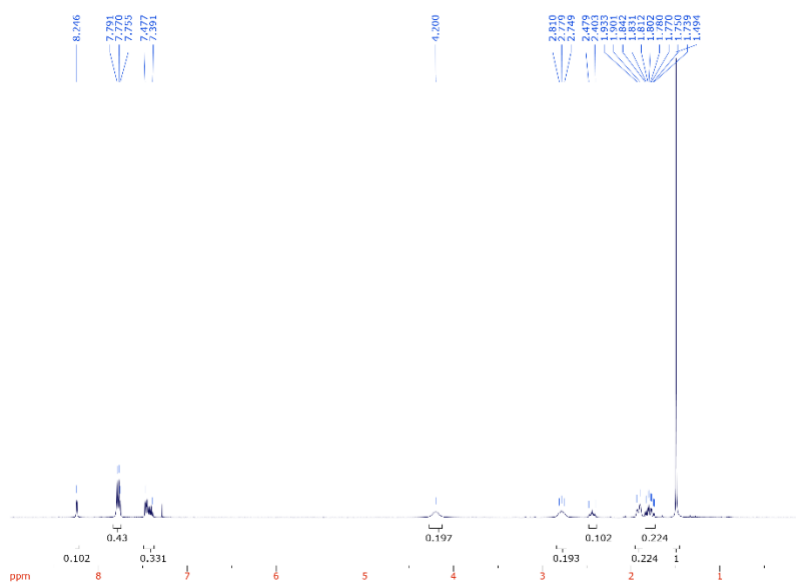
**Formalin Test:** The Formalin Test is a common test of acute inflammatory pain. Rats were removed from their home cages and briefly anesthetized with isoflurane. A dilute formalin solution (5%, 50  $\mu$ L) was then injected into the plantar surface of the right hindpaw. Rats were placed on an elevated mesh rack for observation. The amount of time spent licking or guarding the injected hindpaw was measured in seconds in 5 min blocks for one hour following hindpaw injection.

**Statistical Analysis:** All data are expressed as mean  $\pm$  SEM. A one-way analysis of variance (ANOVA) followed by a Tukey post-hoc test was used to evaluate differences between groups. Statistical significance was defined as a probability of  $<0.05$ .

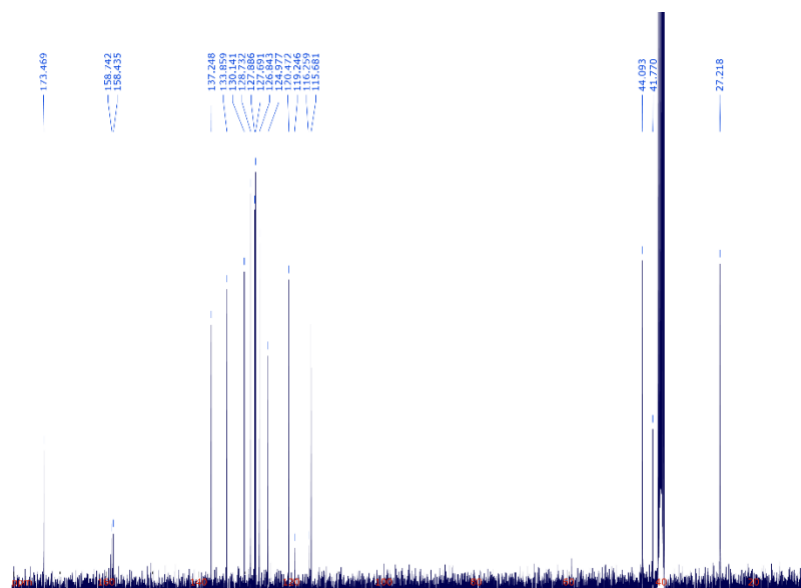
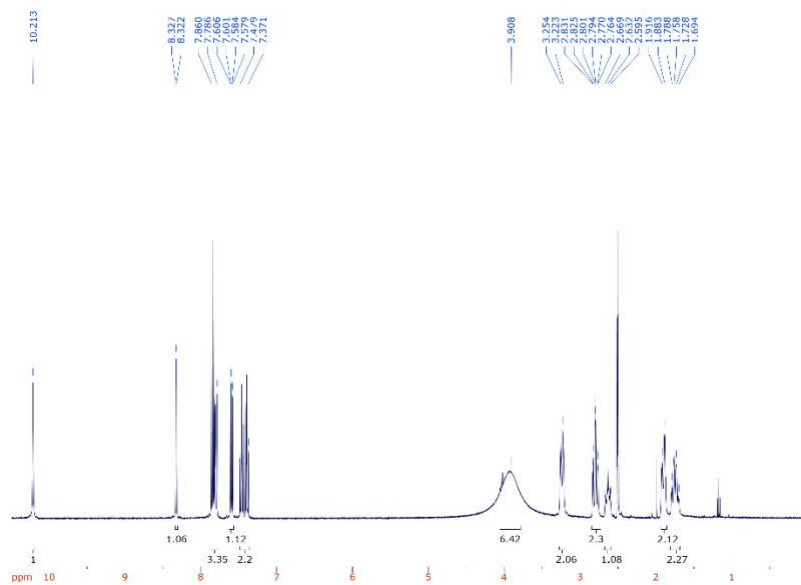


## APPENDIX

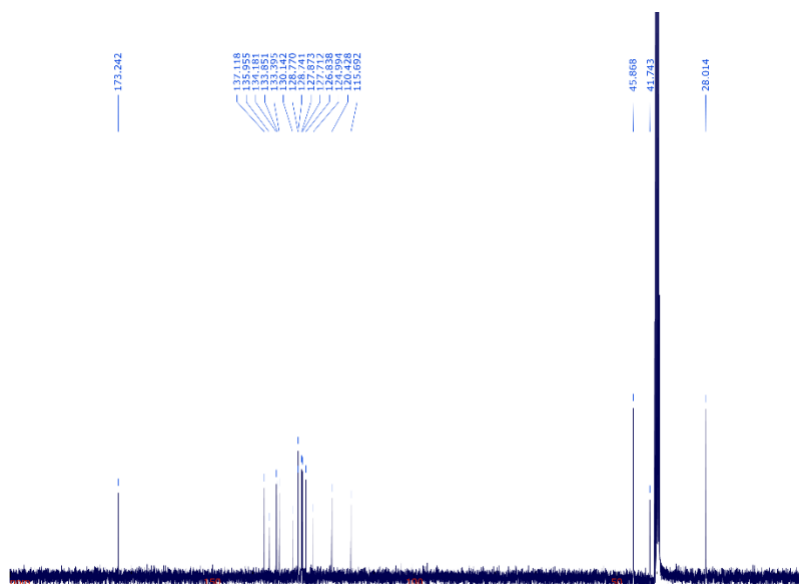
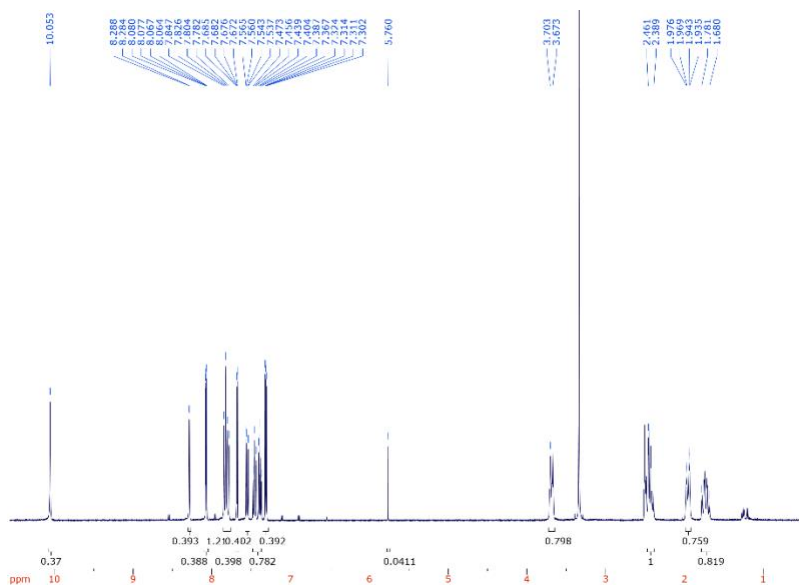
## NUCLEAR MAGNETIC RESONANCE DATA



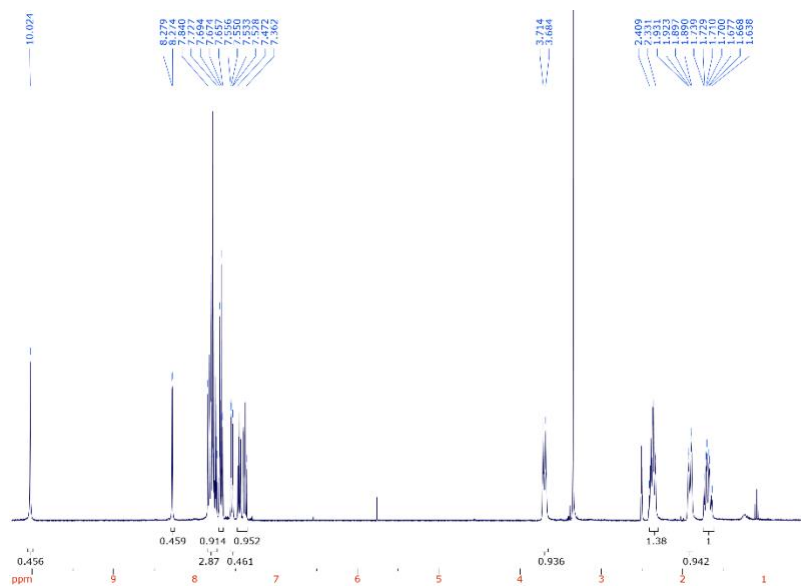
*tert*-butyl 4-(naphthalen-2-ylcarbamoyl)piperidine-1-carboxylate (n)

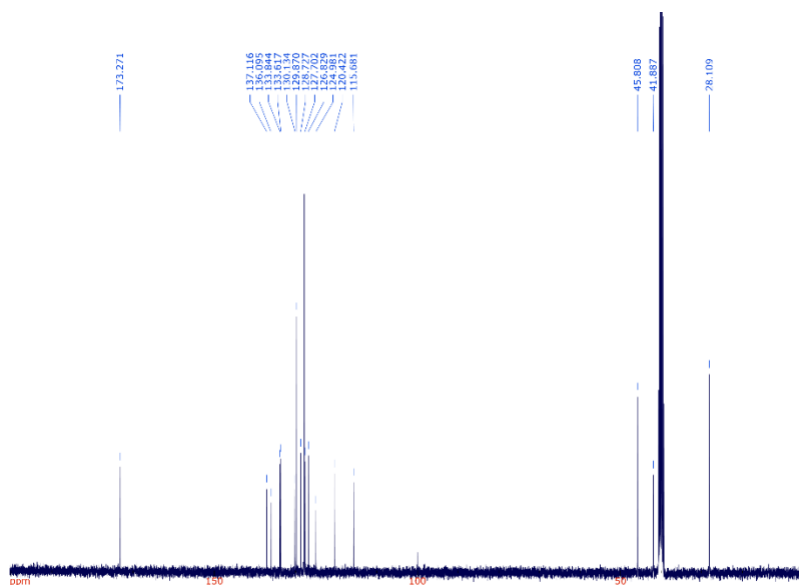


*N*-(naphthalen-2-yl)piperidine-4-carboxamide (o)

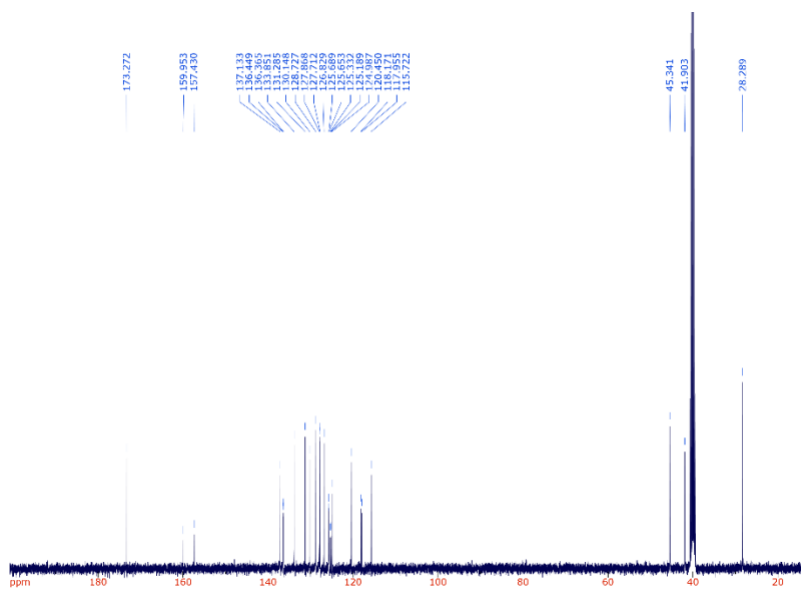
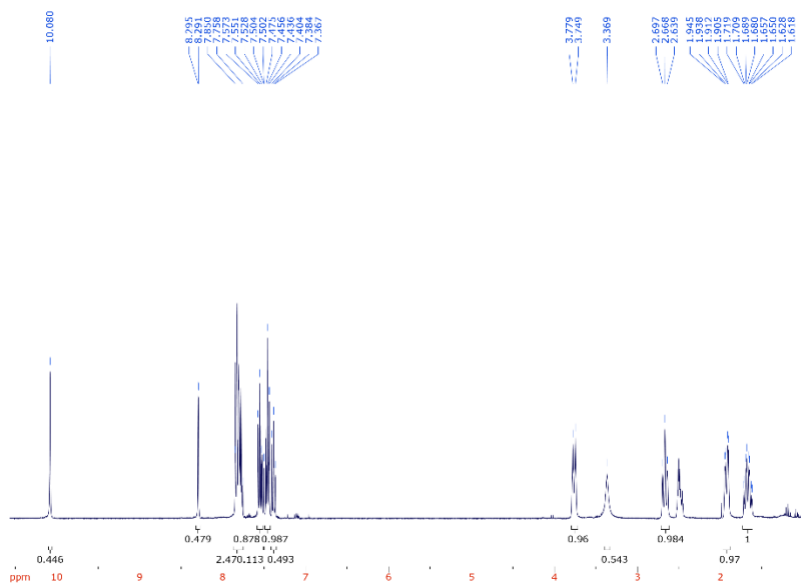


*N*-(naphthalen-2-yl)-1-(thiophen-2-ylsulfonyl)piperidine-4-carboxamide (**1-1**)

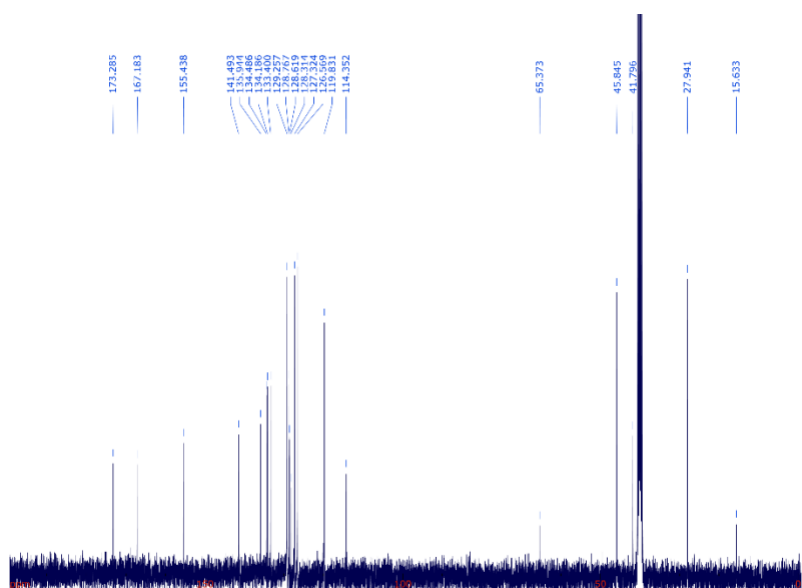
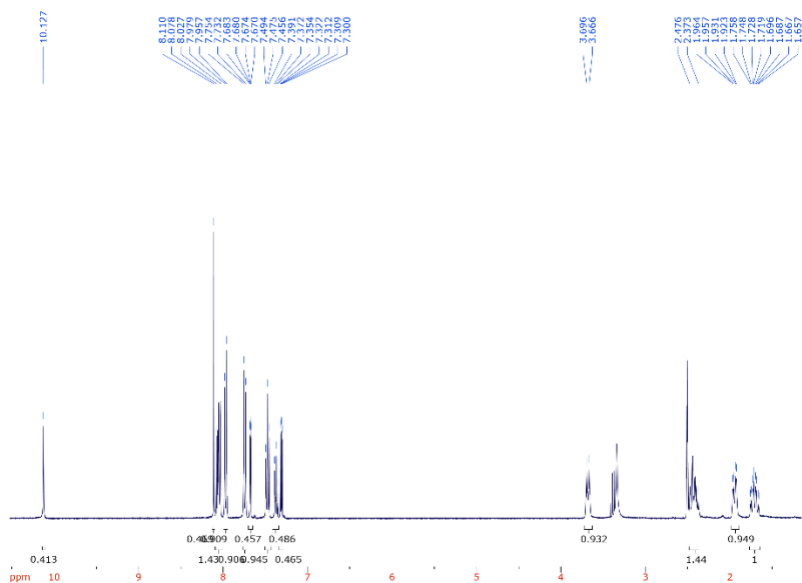




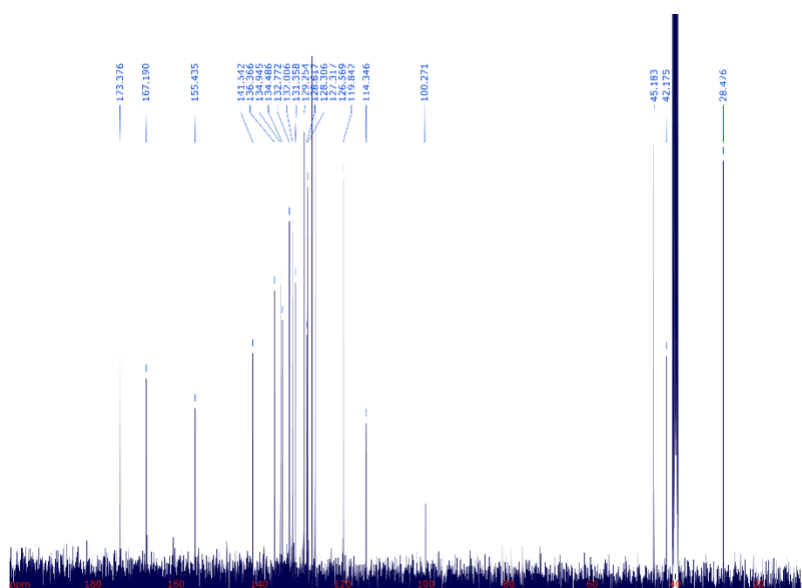
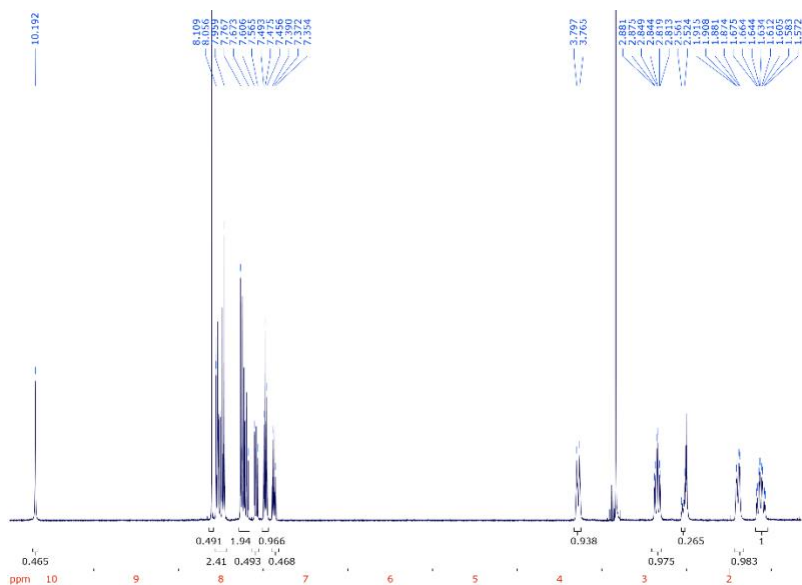
*N*-(naphthalen-2-yl)-1-(phenylsulfonyl)piperidine-4-carboxamide (**1-2**)



1-((2-fluorophenyl)sulfonyl)-N-(naphthalen-2-yl)piperidine-4-carboxamide (1-3)

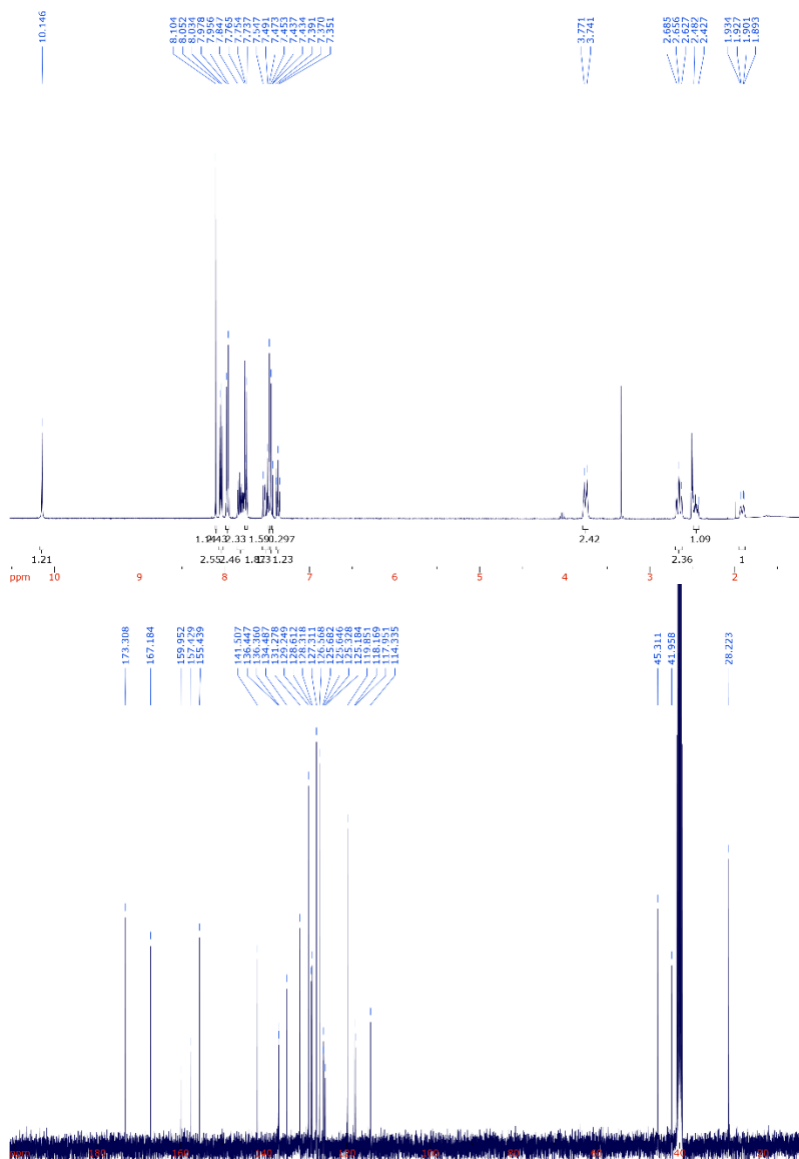


*N*-(4-(4-phenylthiazol-2-yl)phenyl)-1-(thiophen-2-ylsulfonyl)piperidine-4-carboxamide (**2-1**)

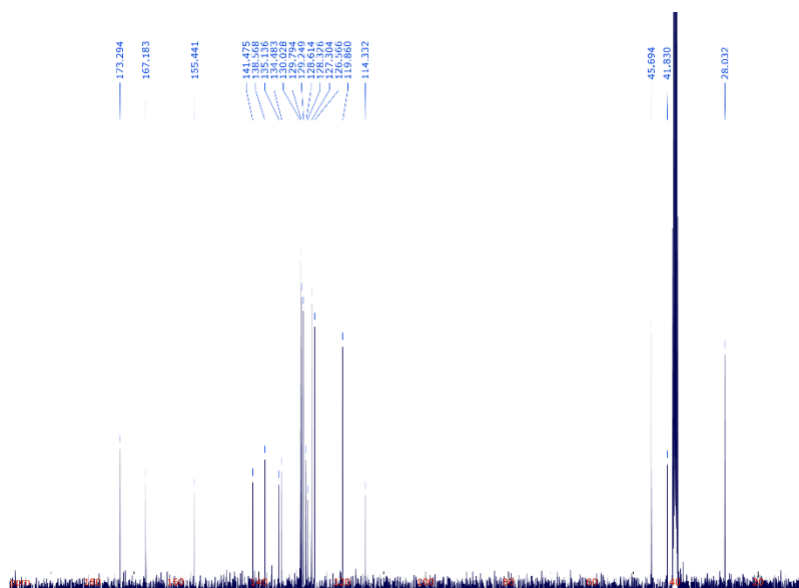
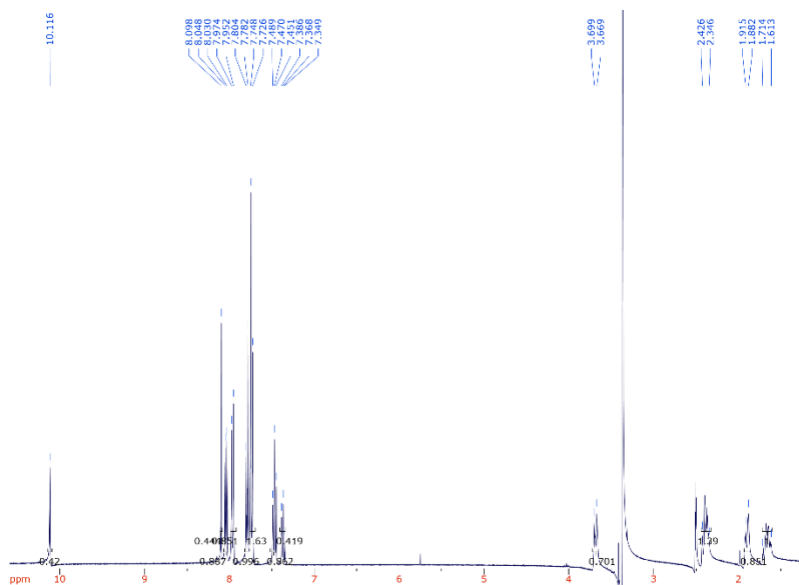


1-((2-fluorophenyl)sulfonyl)-*N*-(4-(4-phenylthiazol-2-yl)phenyl)piperidine-4-carboxamide (**2-2**)

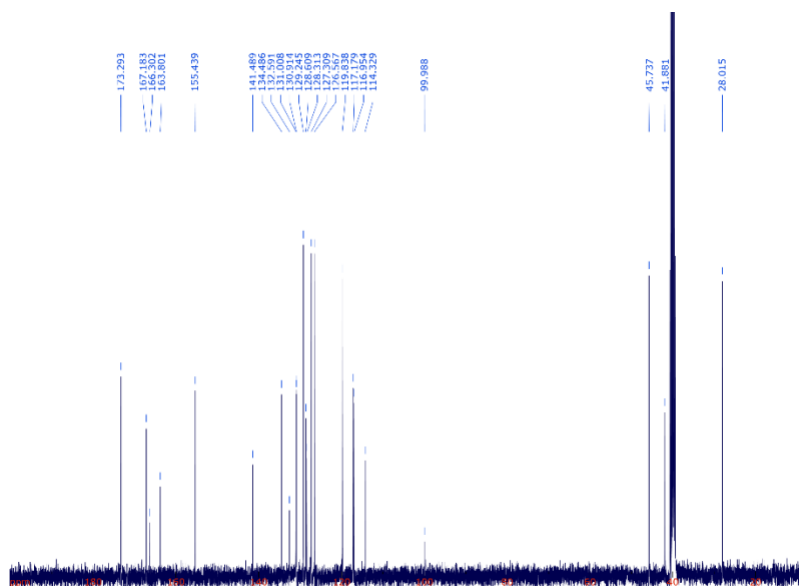
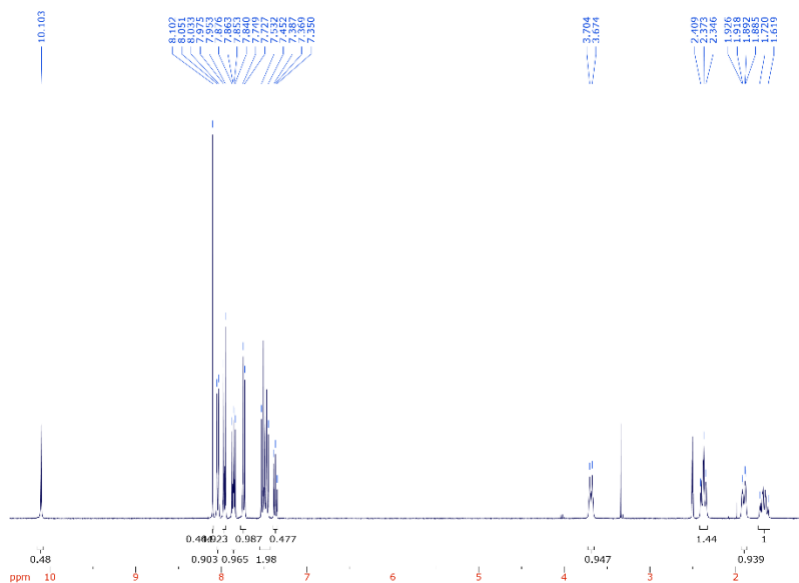




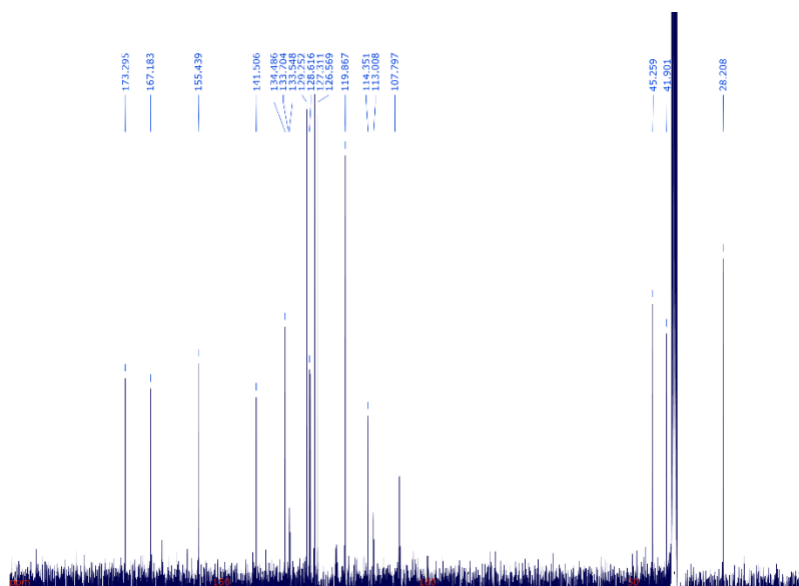
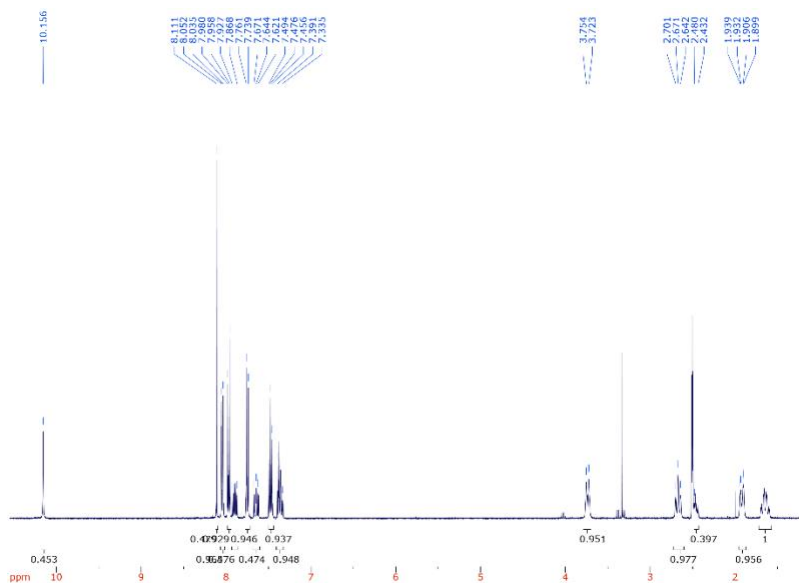
1-((2-chlorophenyl)sulfonyl)-*N*-(4-(4-phenylthiazol-2-yl)phenyl)piperidine-4-carboxamide (**2-3**)



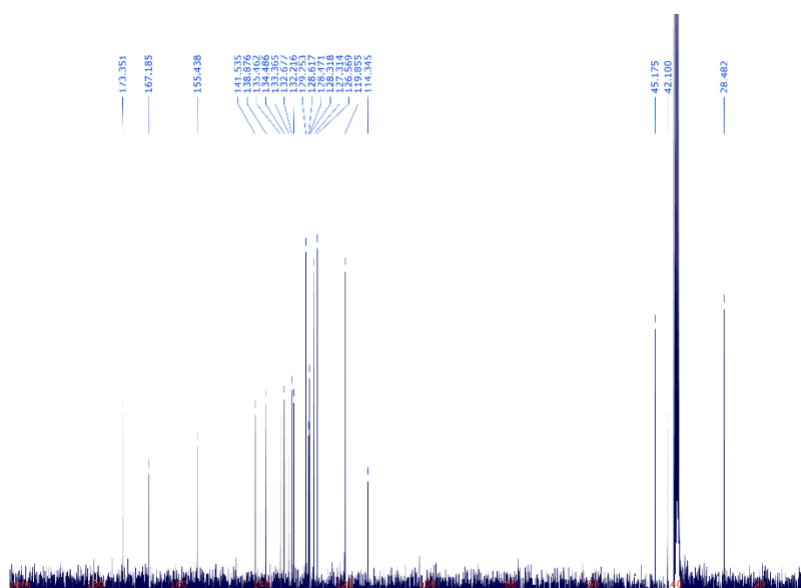
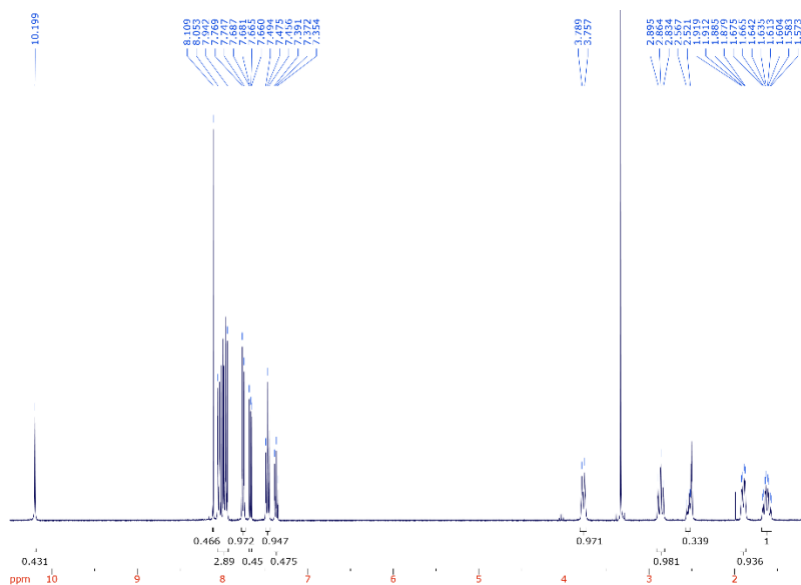
1-((4-fluorophenyl)sulfonyl)-*N*-(4-(4-phenylthiazol-2-yl)phenyl)piperidine-4-carboxamide (**2-4**)



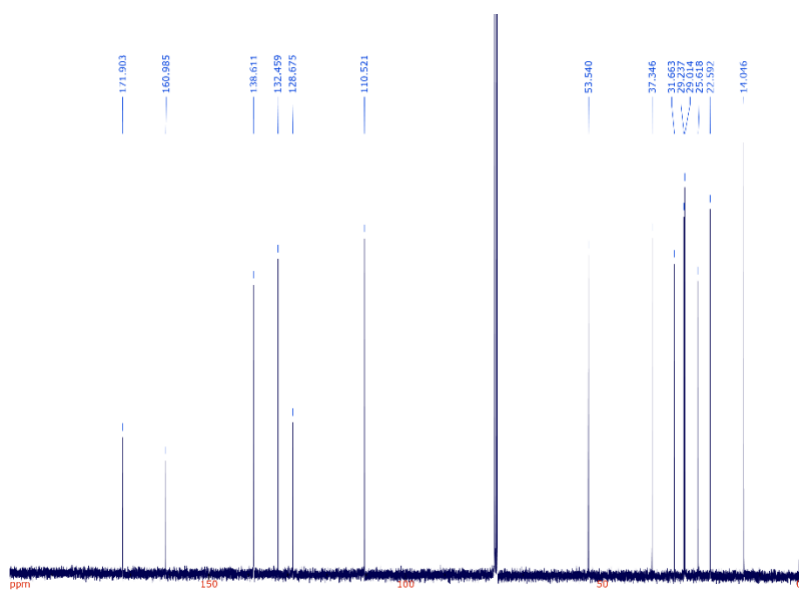
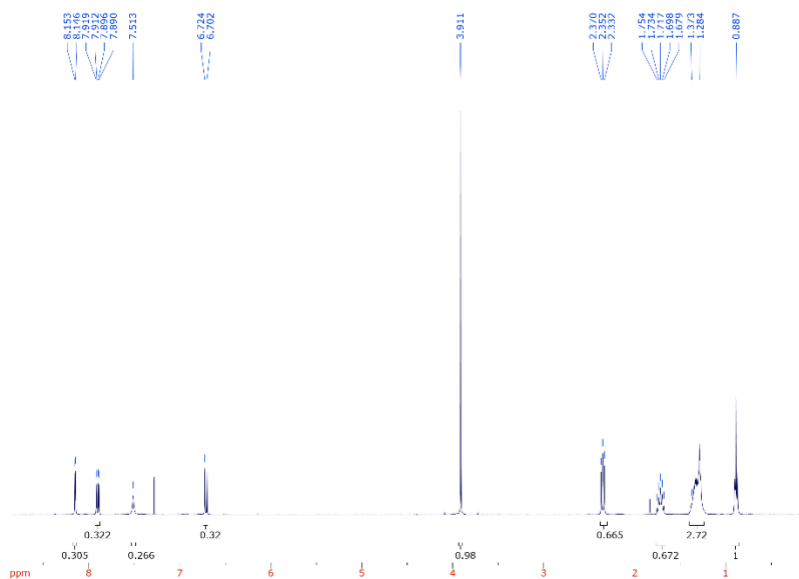
1-((4-chlorophenyl)sulfonyl)-N-(4-(4-phenylthiazol-2-yl)phenyl)piperidine-4-carboxamide (**2-5**)



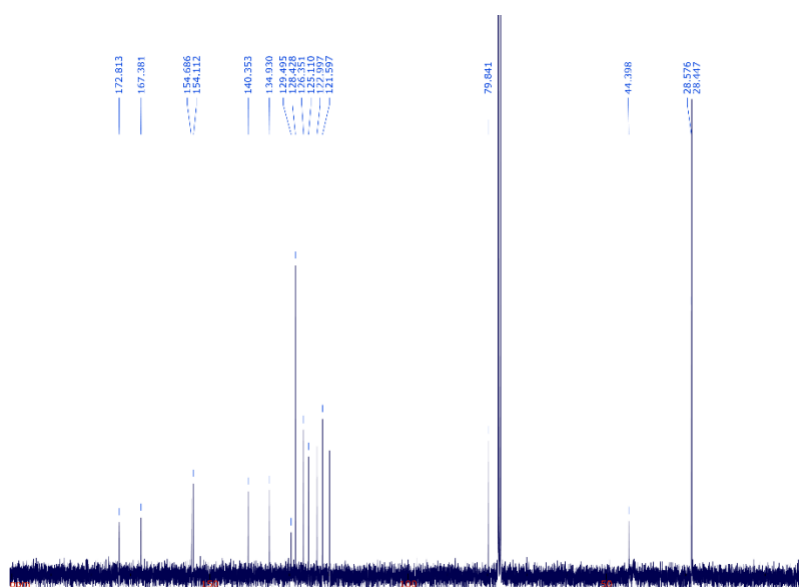
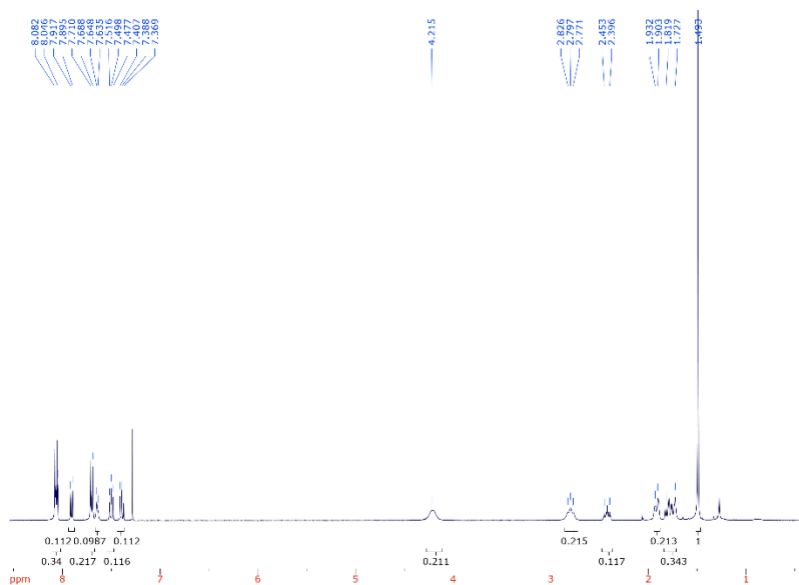
1-((2,4-difluorophenyl)sulfonyl)-*N*-(4-(4-phenylthiazol-2-yl)phenyl)piperidine-4-carboxamide (**2-6**)



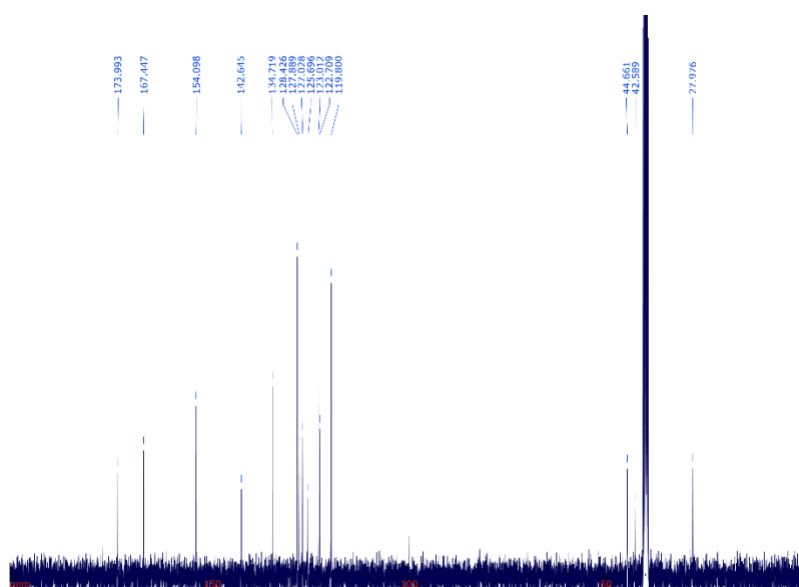
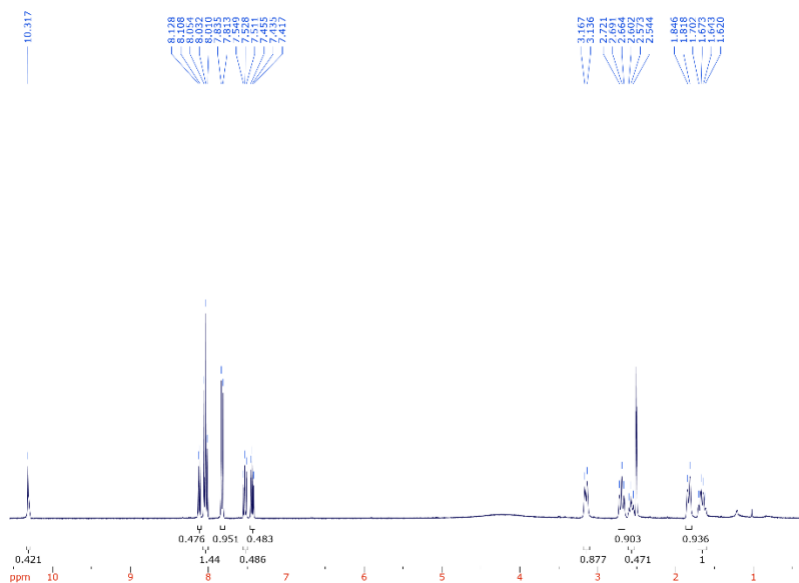
1-((2,4-dichlorophenyl)sulfonyl)-*N*-(4-(4-phenylthiazol-2-yl)phenyl)piperidine-4-carboxamide (**2-7**)



*N*-(6-methoxypyridin-3-yl) octanamide (OMP)

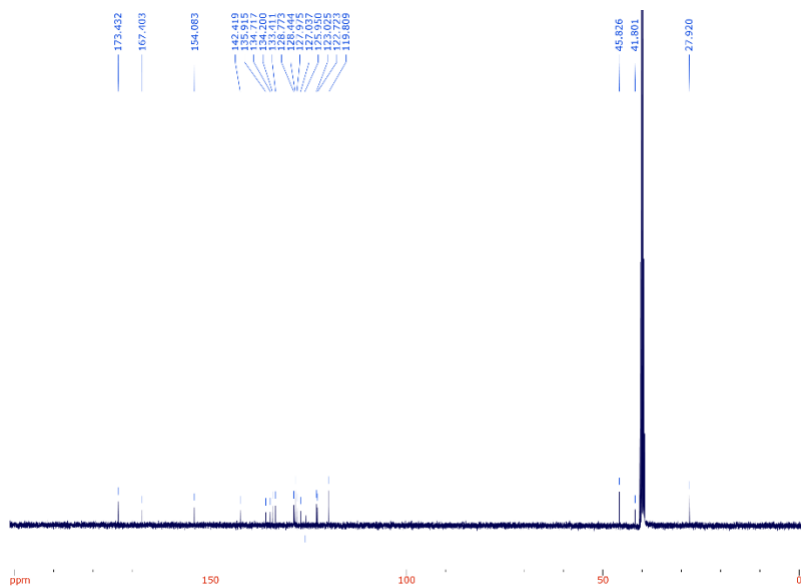
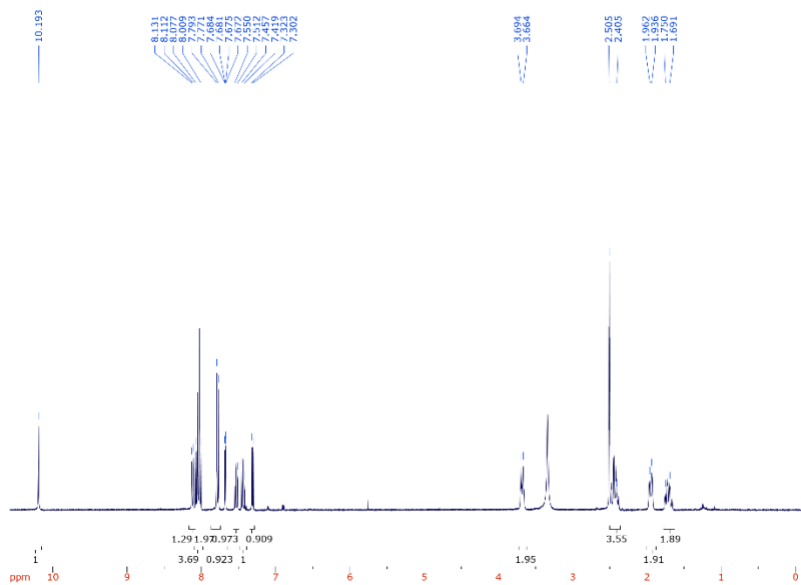


*tert*-butyl 4-((4-(benzo[*d*]thiazol-2-yl)phenyl)carbamoyl)piperidine-1-carboxylate, (d)

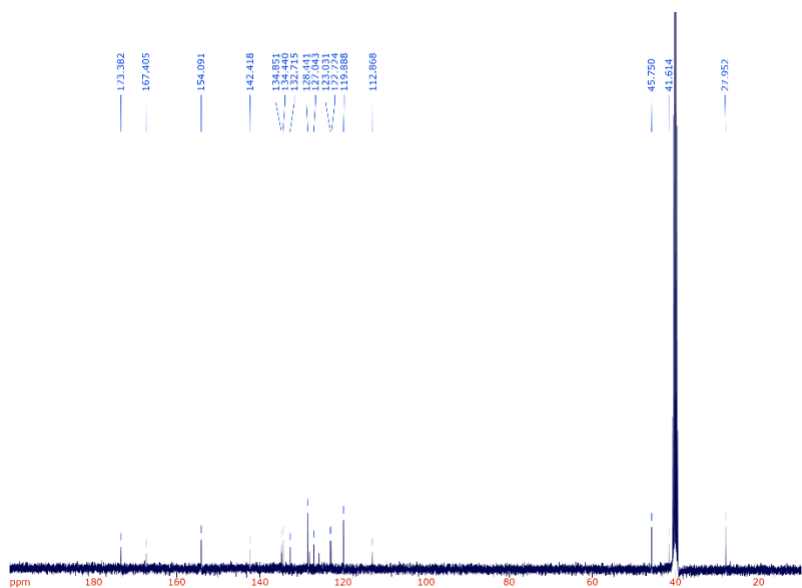
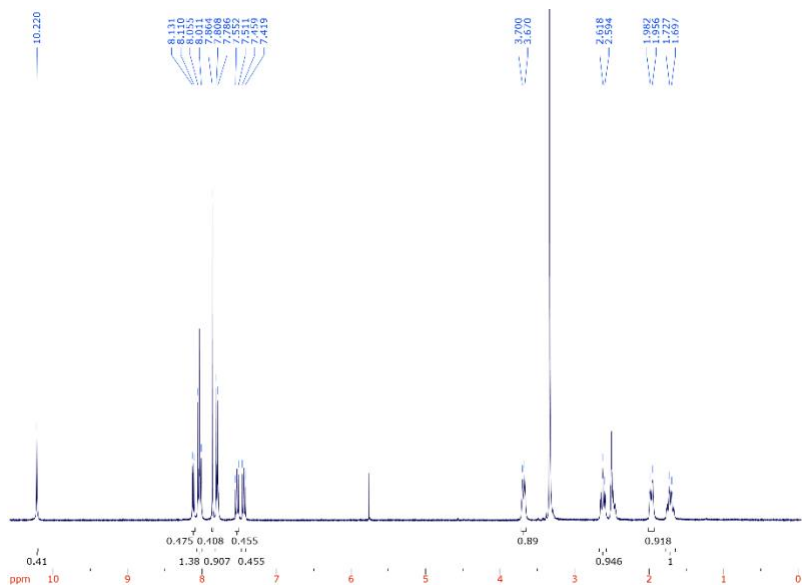


*N*-(4-(benzo[*d*]thiazol-2-yl)phenyl)piperidine-4-carboxamide, (e)

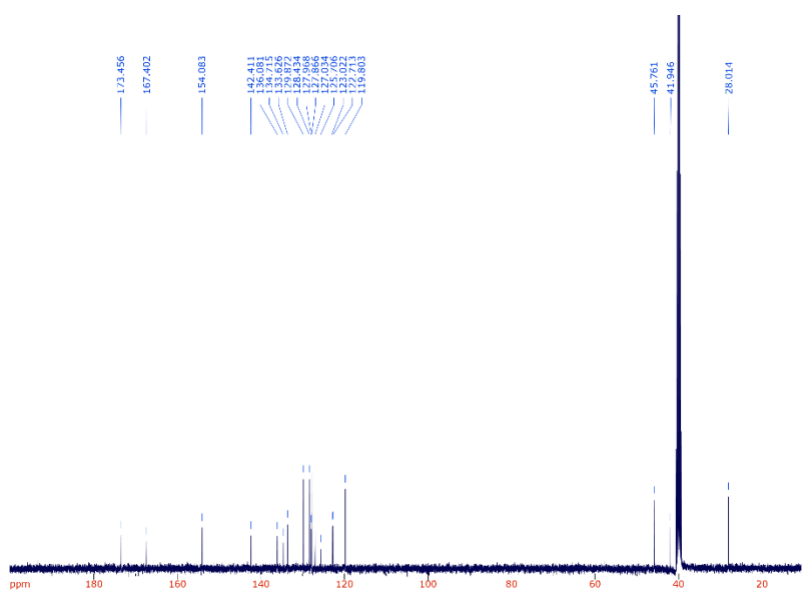
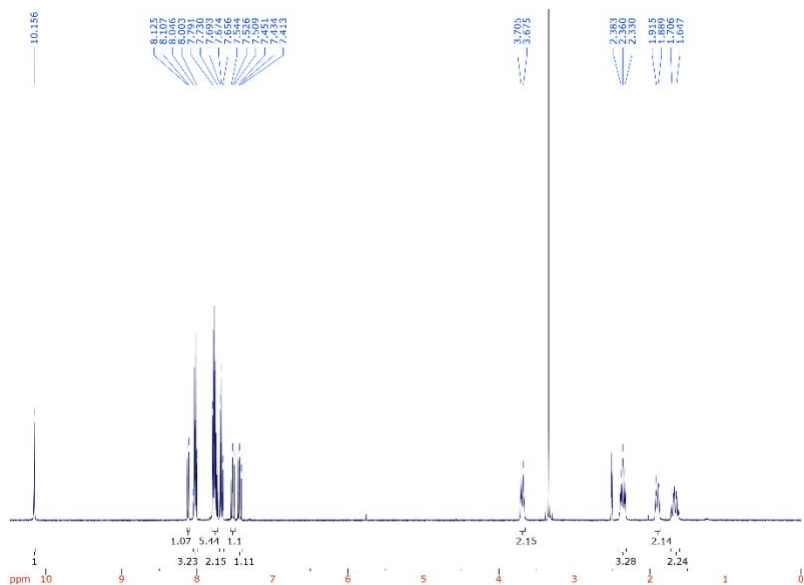




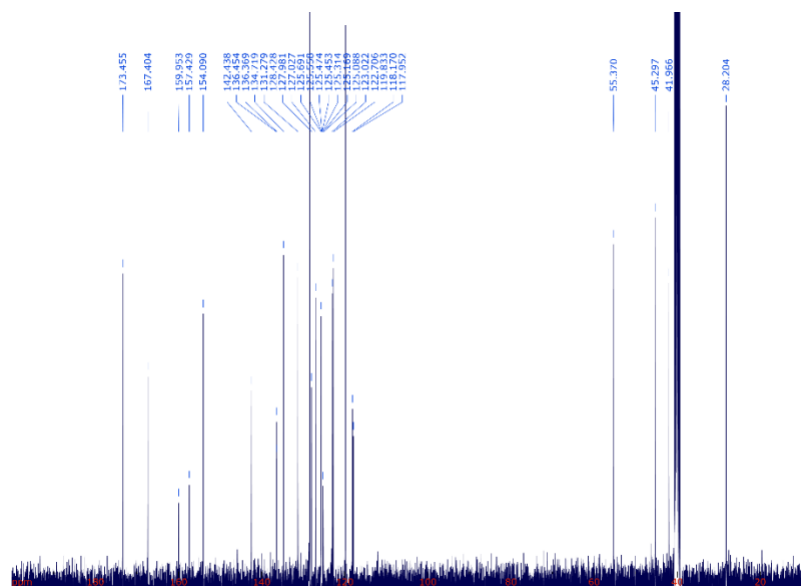
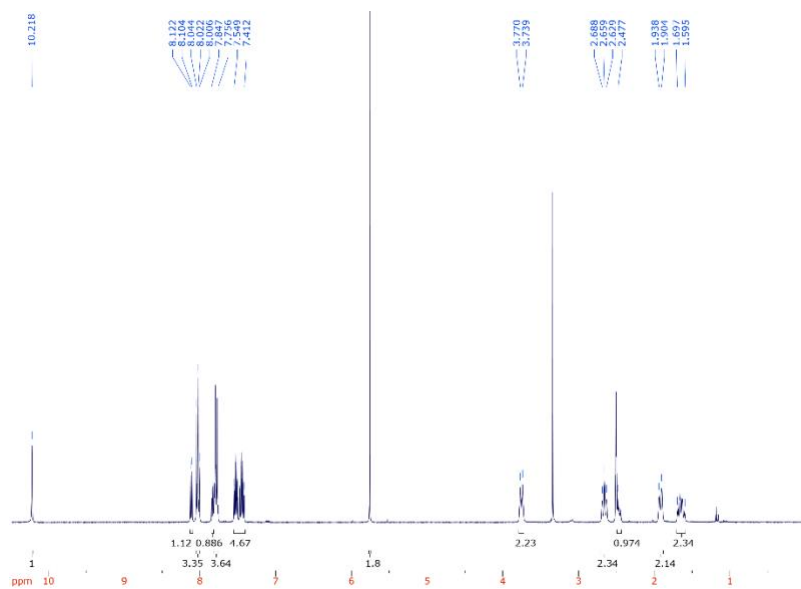
*N*-(4-(benzo[d]thiazol-2-yl)phenyl)-1-(thiophen-2-ylsulfonyl)piperidine-4-carboxamide (**3-1**)



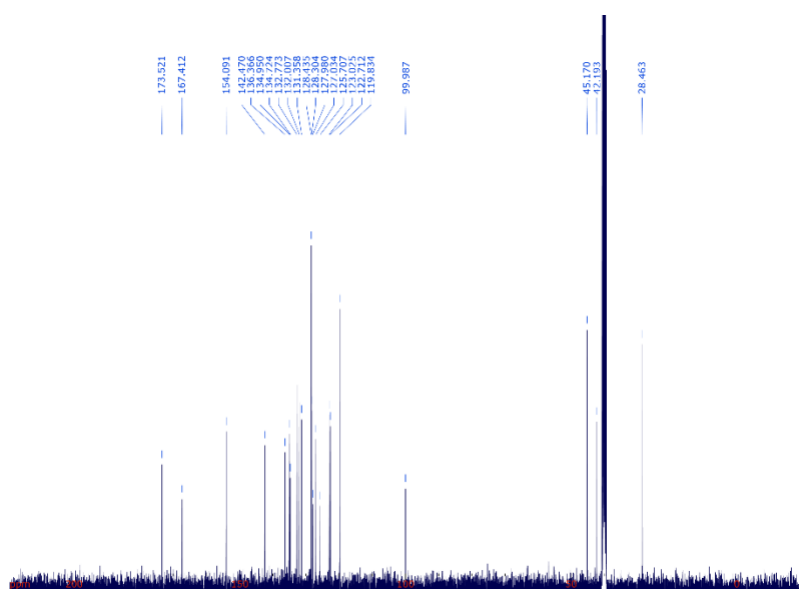
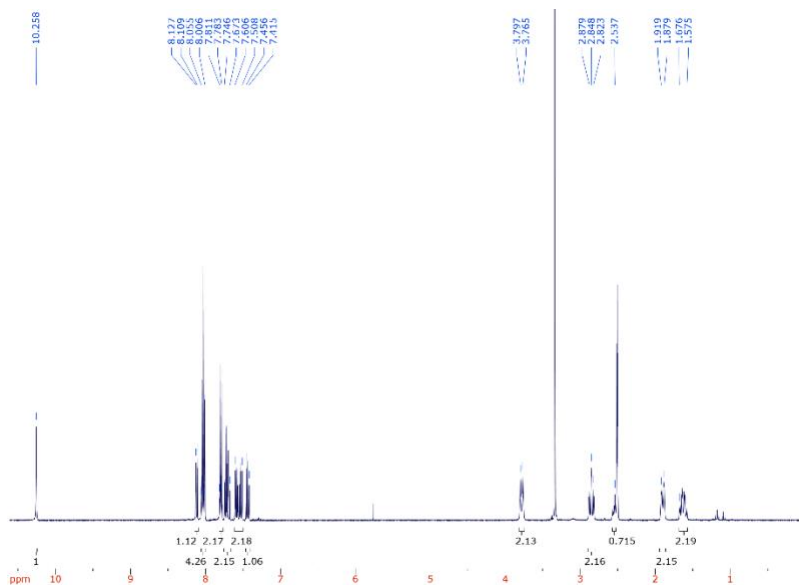
*N*-(4-(benzo[*d*]thiazol-2-yl)phenyl)-1-((4-bromo-5-chlorothiophen-2-yl)sulfonyl)piperidine-4-carboxamide (**3-2**)



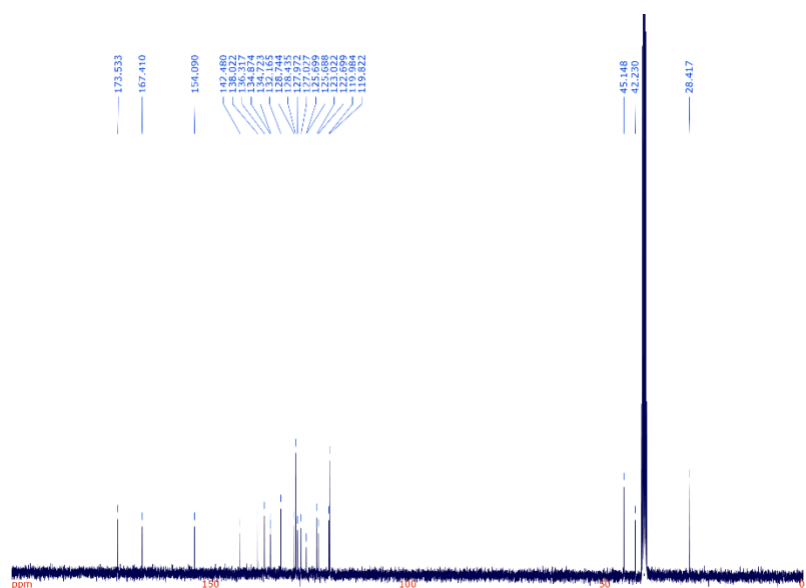
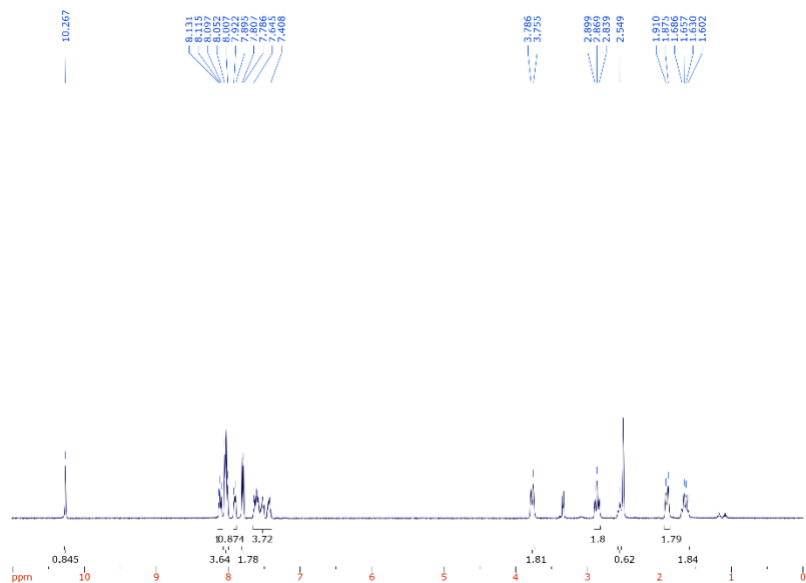
*N*-(4-(benzo[*d*]thiazol-2-yl)phenyl)-1-(phenylsulfonyl)piperidine-4-carboxamide (**3-3**)



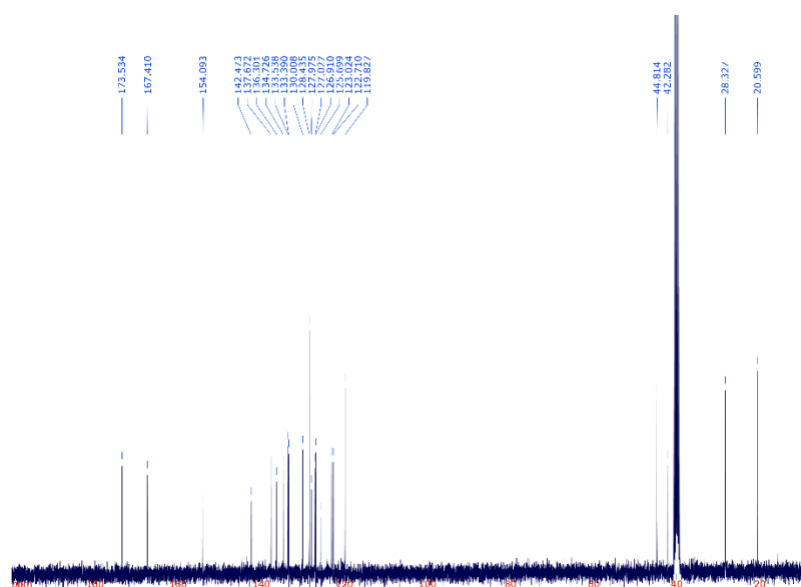
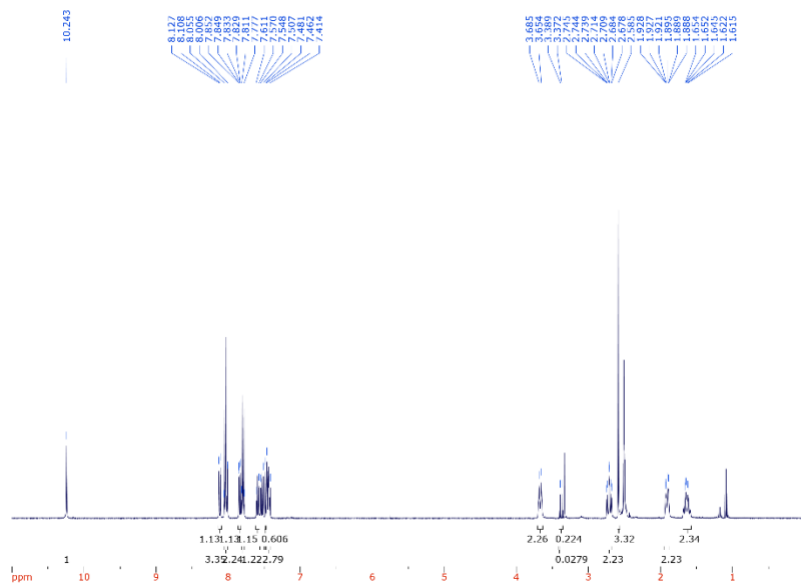
*N*-(4-(benzo[d]thiazol-2-yl)phenyl)-1-((2-fluorophenyl)sulfonyl)piperidine-4-carboxamide (**3-4**)



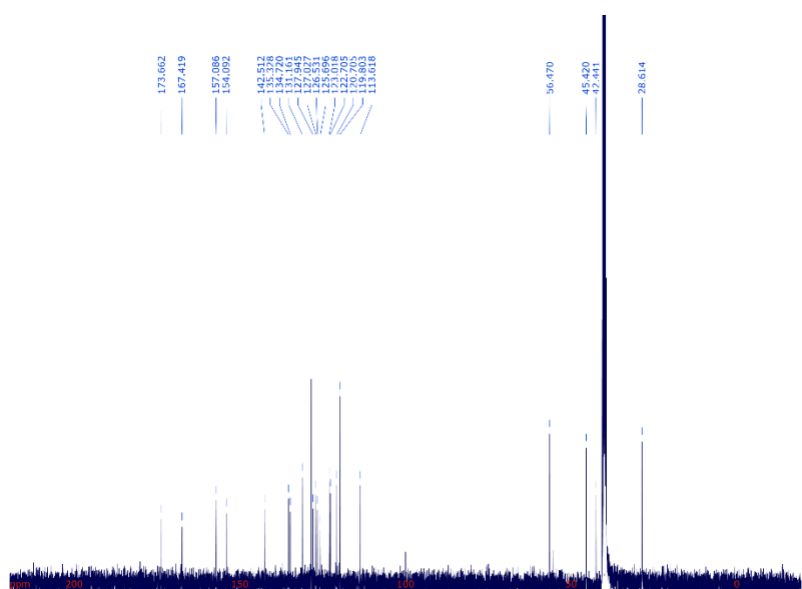
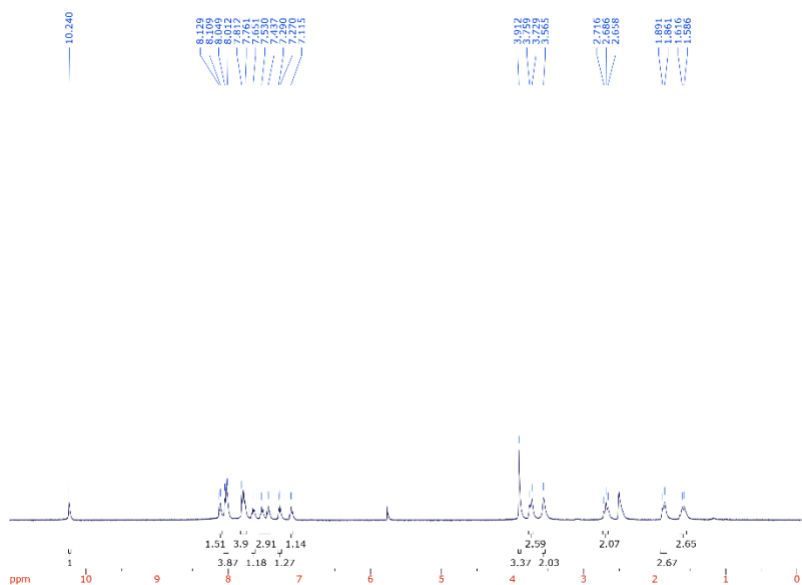
*N*-(4-(benzo[*d*]thiazol-2-yl)phenyl)-1-((2-chlorophenyl)sulfonyl)piperidine-4-carboxamide (3-5)



*N*-(4-(benzo[*d*]thiazol-2-yl)phenyl)-1-((2-bromophenyl)sulfonyl)piperidine-4-carboxamide (**3-6**)

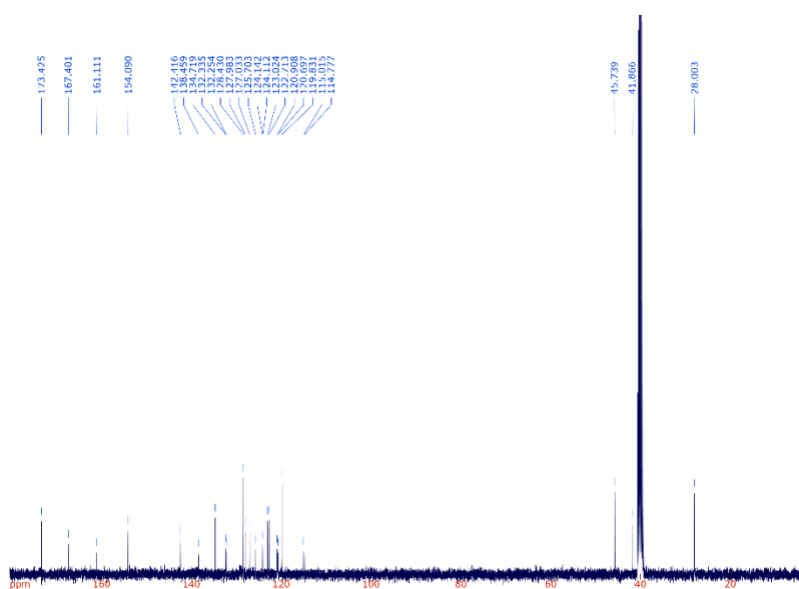
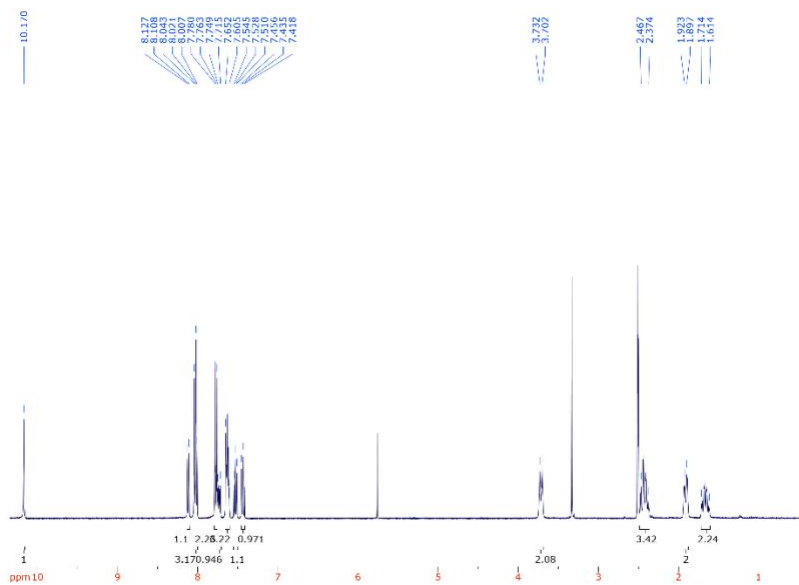


*N*-(4-(benzo[*d*]thiazol-2-yl)phenyl)-1-(*o*-tolylsulfonyl)piperidine-4-carboxamide (**3-7**)

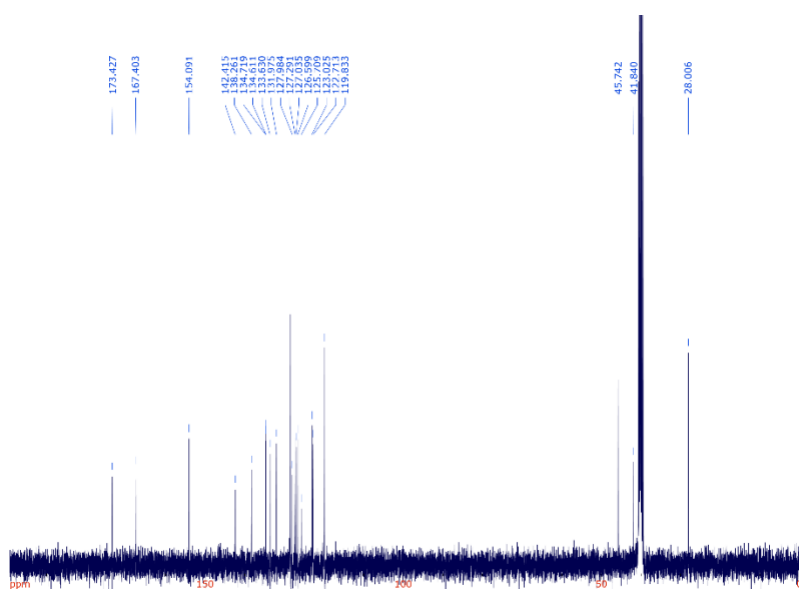
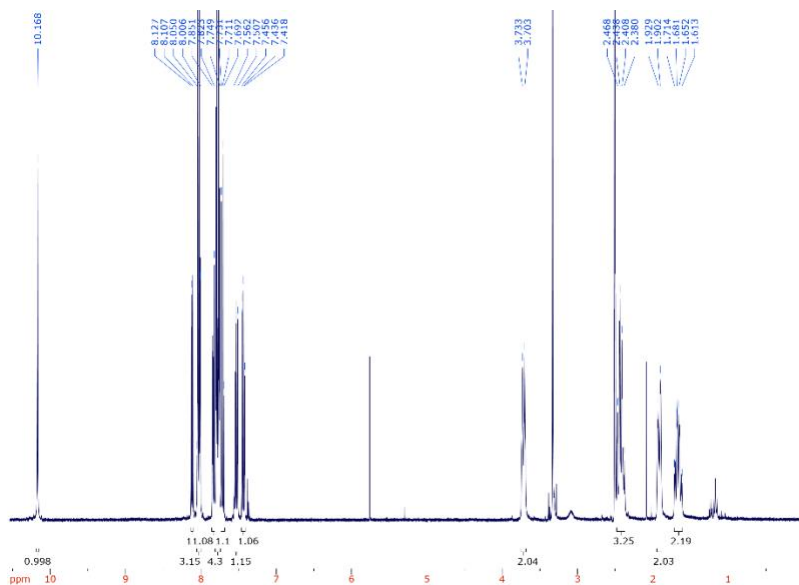


*N*-(4-(benzo[*d*]thiazol-2-yl)phenyl)-1-((2-methoxyphenyl)sulfonyl)piperidine-4-carboxamide (3-8)

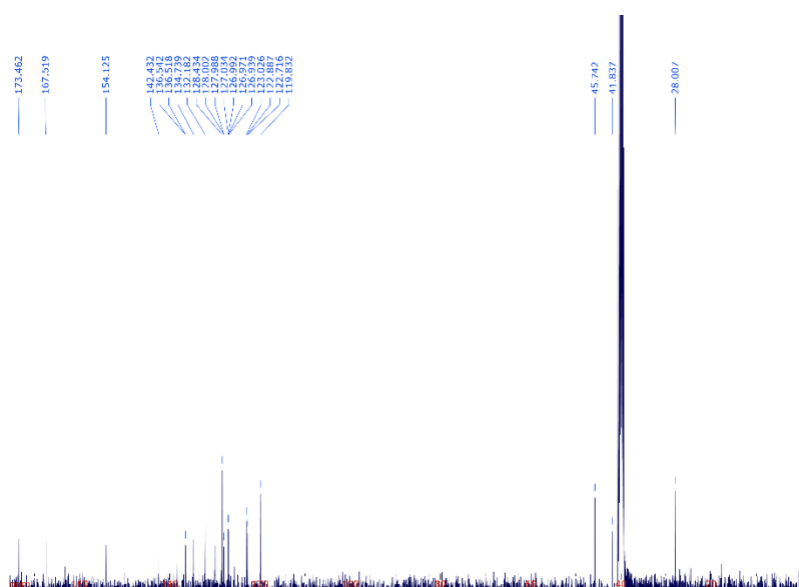
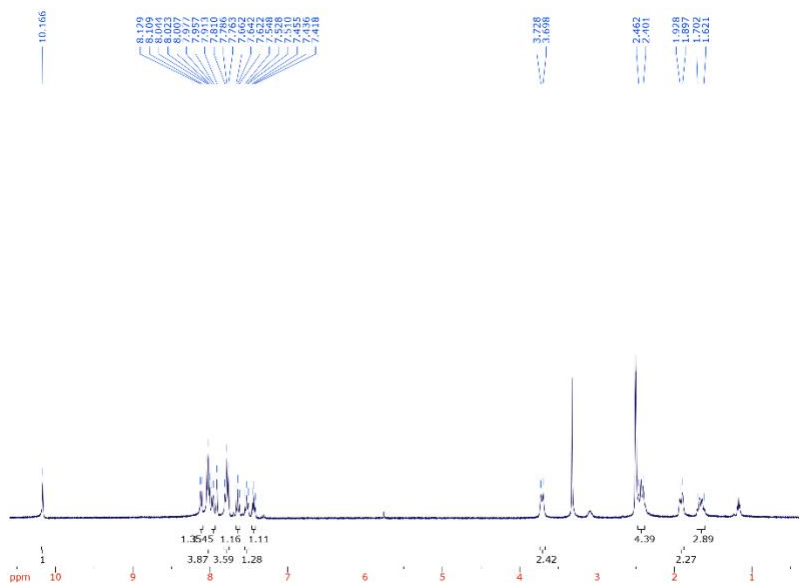




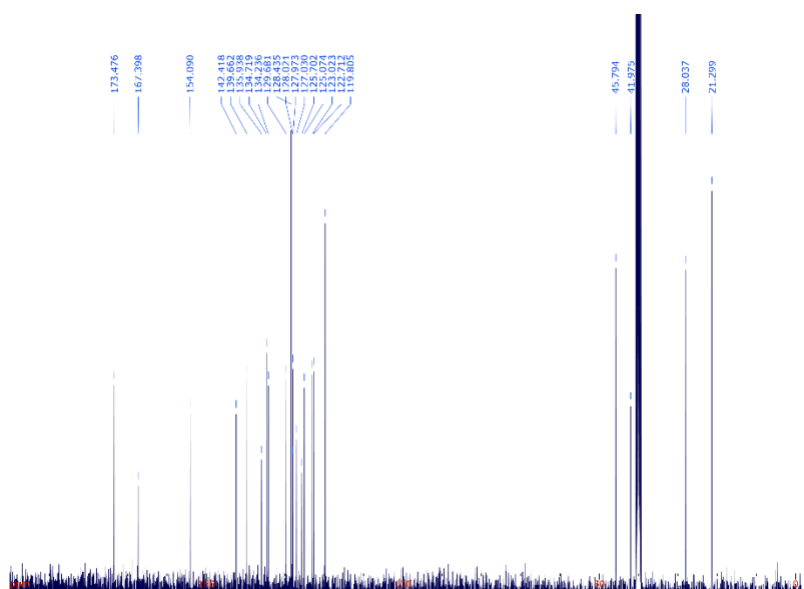
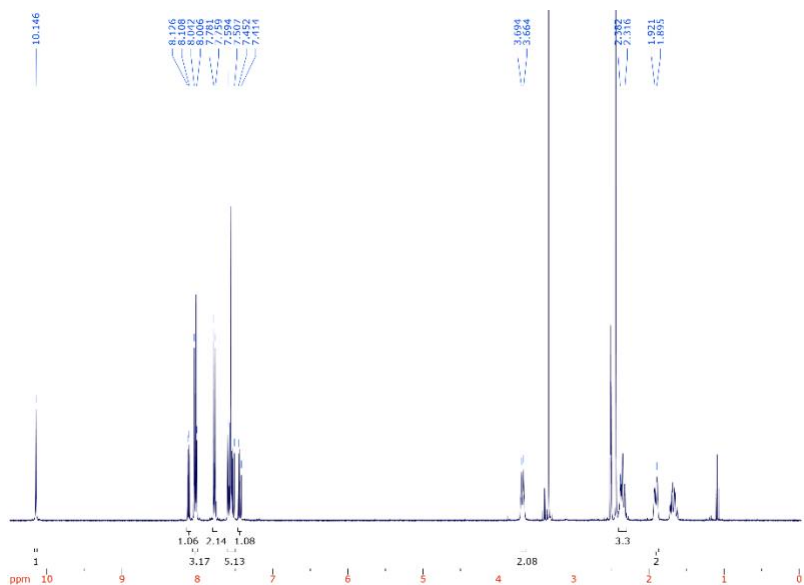
*N*-(4-(benzo[*d*]thiazol-2-yl)phenyl)-1-((3-fluorophenyl)sulfonyl)piperidine-4-carboxamide (**3-9**)



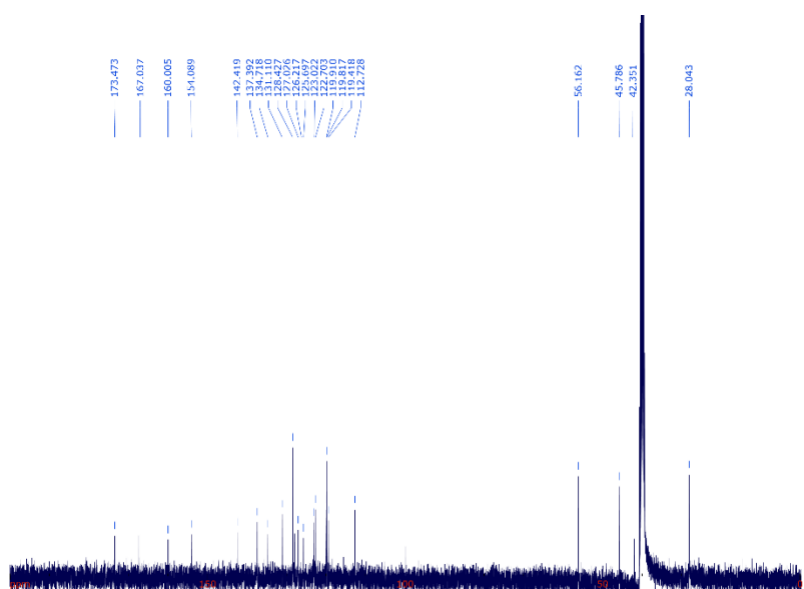
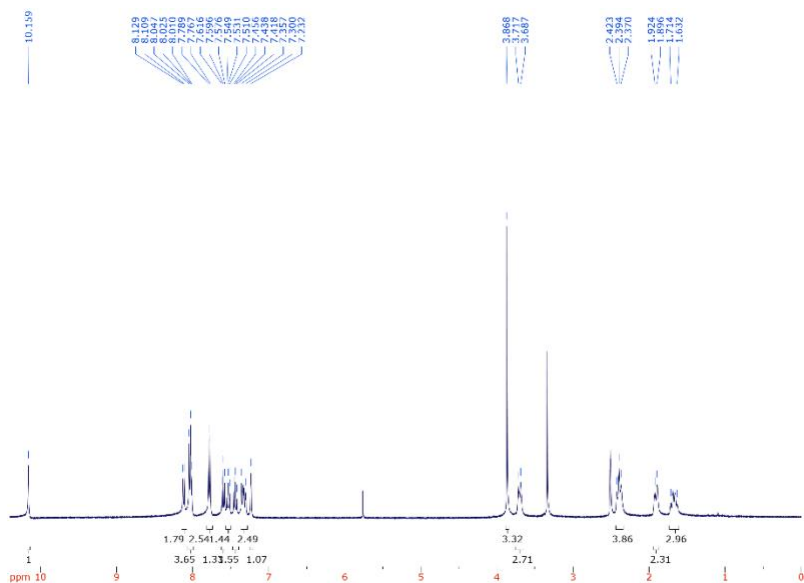
*N*-(4-(benzo[*d*]thiazol-2-yl)phenyl)-1-((3-chlorophenyl)sulfonyl)piperidine-4-carboxamide  
(3-10)



*N*-(4-(benzo[*d*]thiazol-2-yl)phenyl)-1-((3-bromophenyl)sulfonyl)piperidine-4-carboxamide  
**(3-11)**

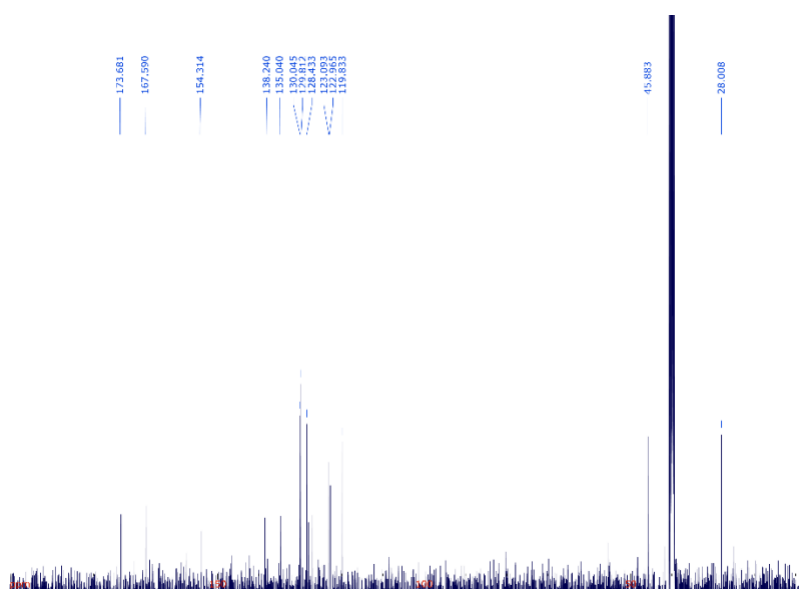
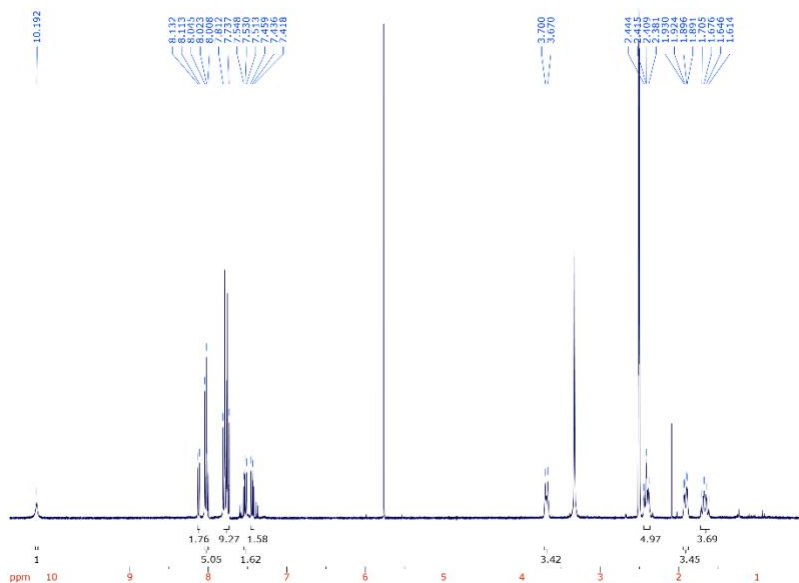


*N*-(4-(benzo[*d*]thiazol-2-yl)phenyl)-1-(*m*-tolylsulfonyl)piperidine-4-carboxamide (**3-12**)

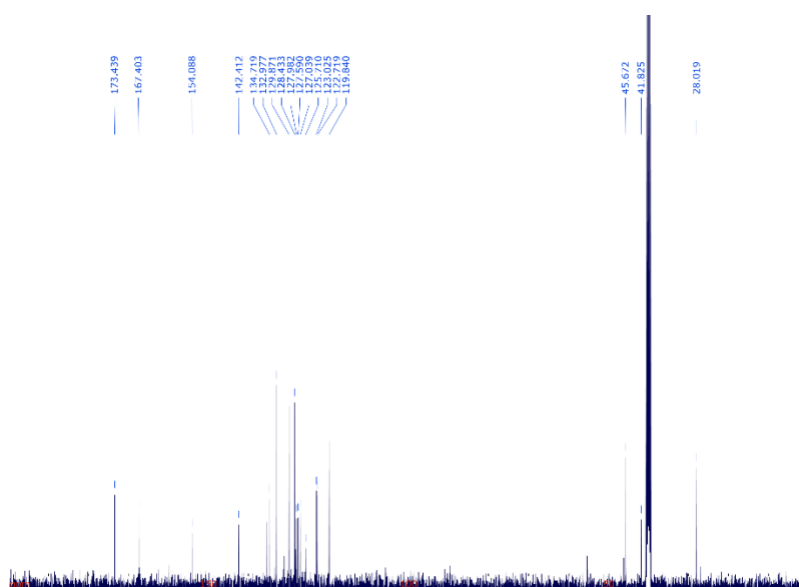
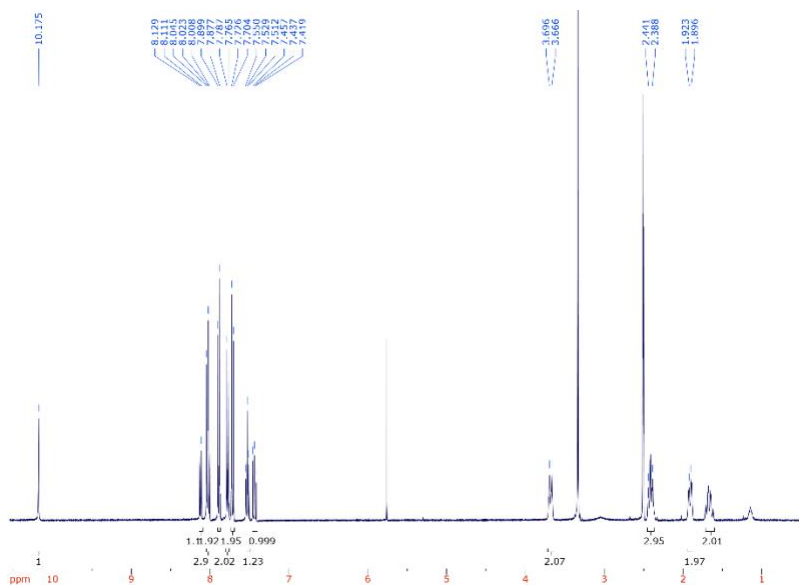


*N*-(4-(benzo[*d*]thiazol-2-yl)phenyl)-1-((3-methoxyphenyl)sulfonyl)piperidine-4-carboxamide  
(3-13)



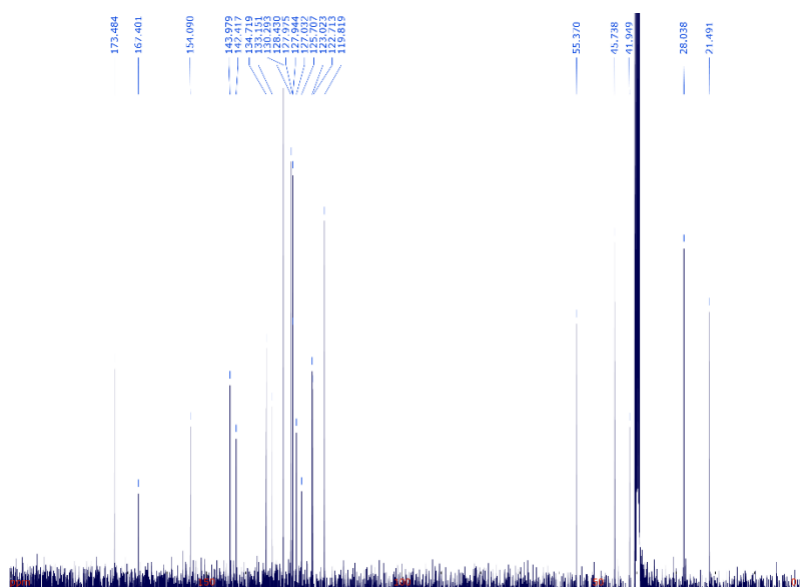
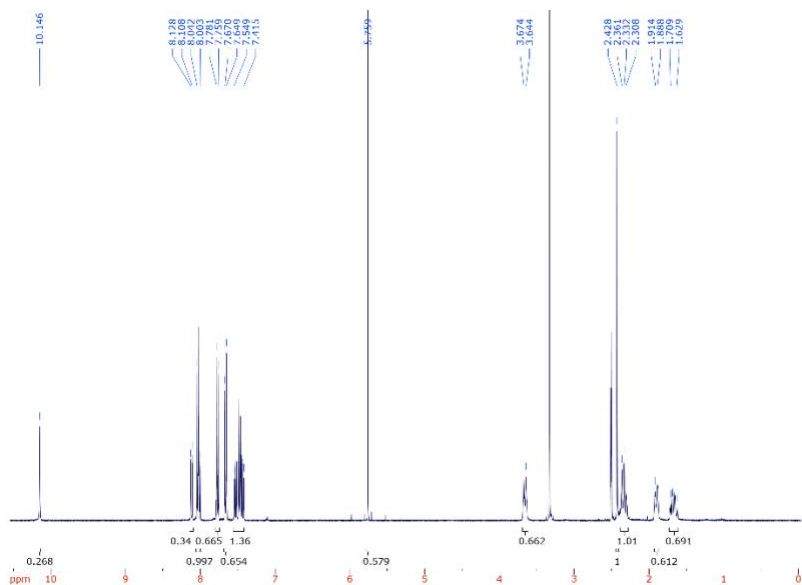


*N*-(4-(benzo[*d*]thiazol-2-yl)phenyl)-1-((4-chlorophenyl)sulfonyl)piperidine-4-carboxamide (3-15)

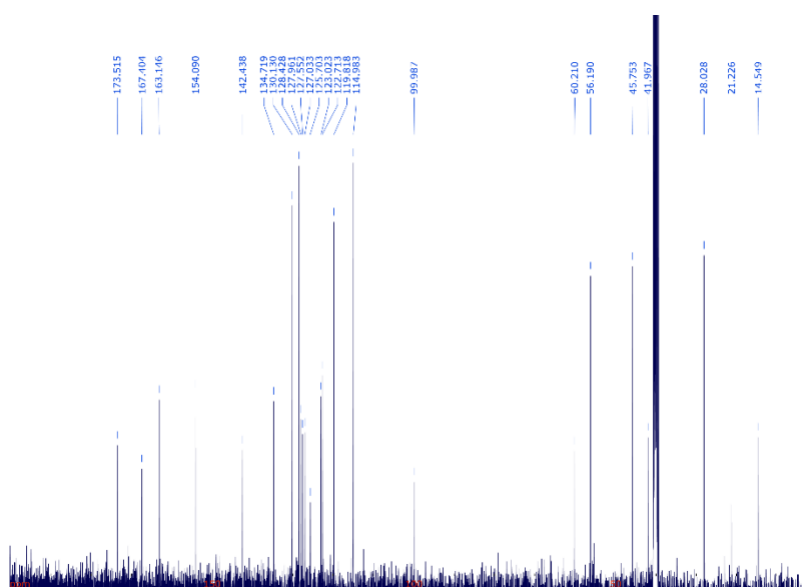
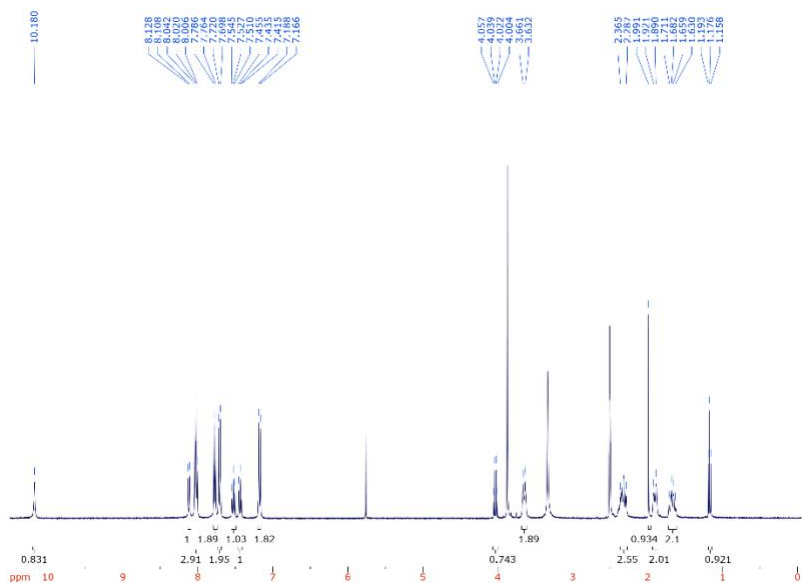


*N*-(4-(benzo[d]thiazol-2-yl)phenyl)-1-((4-bromophenyl)sulfonyl)piperidine-4-carboxamide  
**(3-16)**

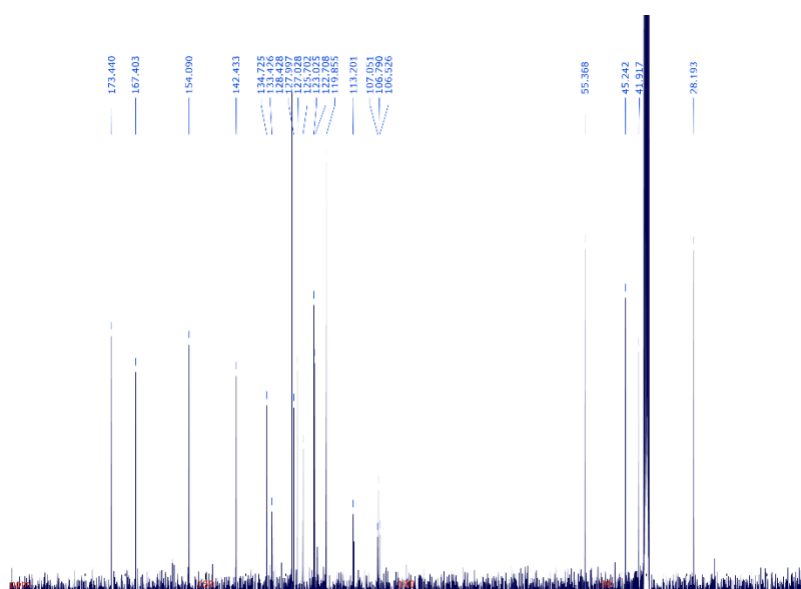
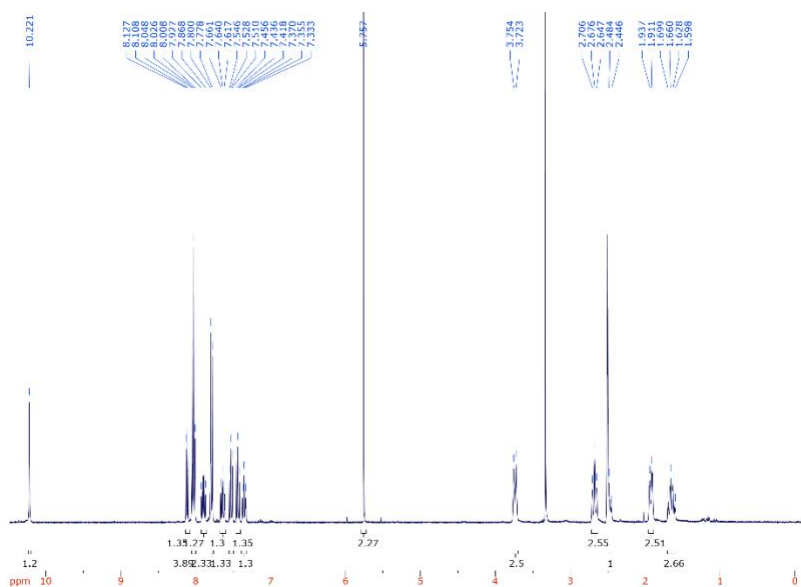




*N*-(4-(benzo[*d*]thiazol-2-yl)phenyl)-1-tosylpiperidine-4-carboxamide (3-17)

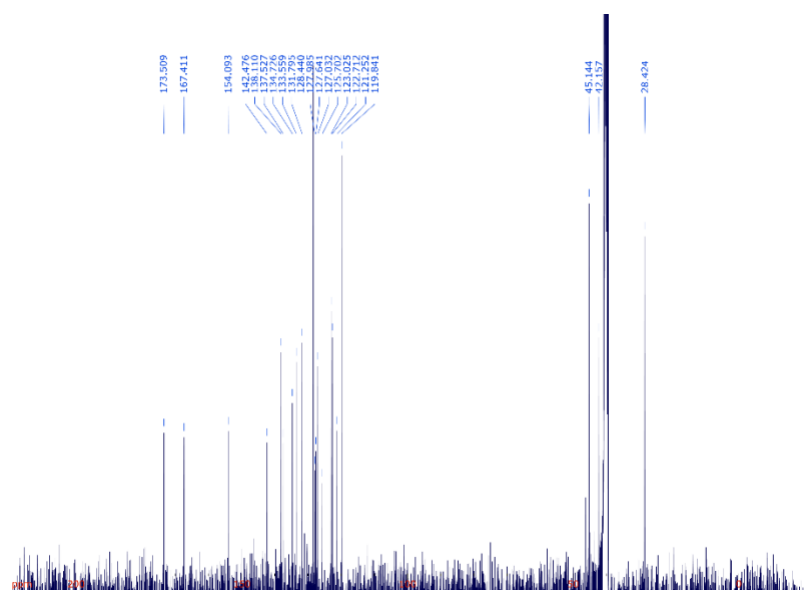
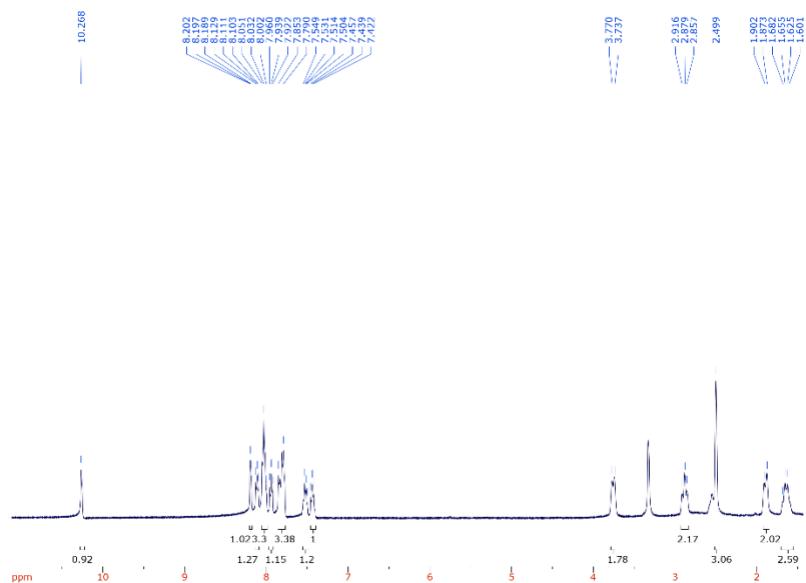


*N*-(4-(benzo[*d*]thiazol-2-yl)phenyl)-1-((4-methoxyphenyl)sulfonyl)piperidine-4-carboxamide  
(**3-18**)

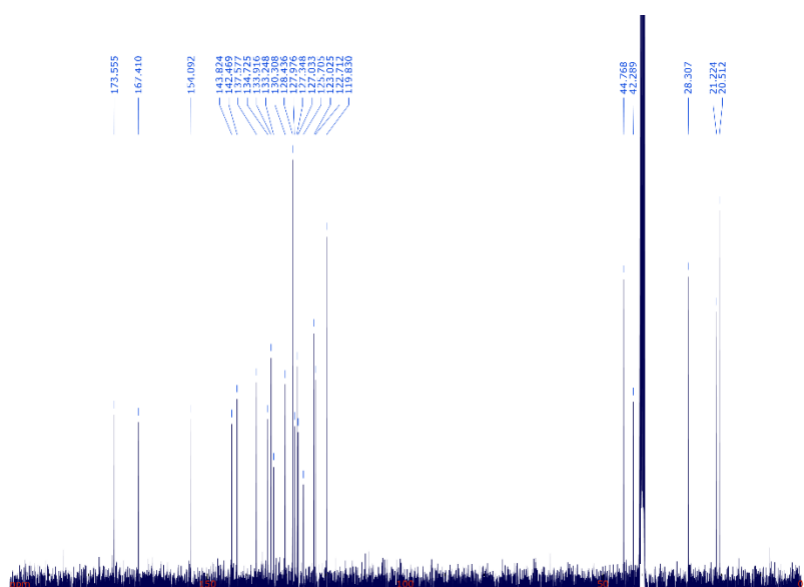
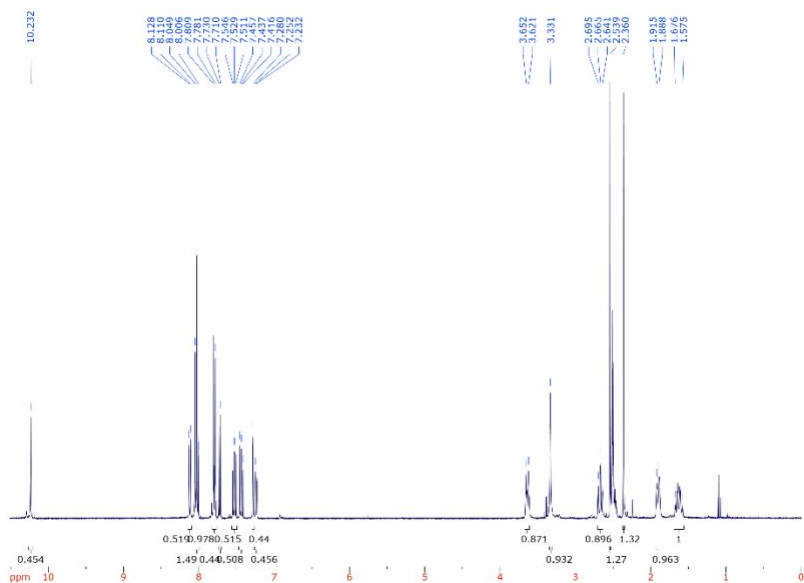


*N*-(4-(benzo[*d*]thiazol-2-yl)phenyl)-1-((2,4-difluorophenyl)sulfonyl)piperidine-4-carboxamide (**3-19**)

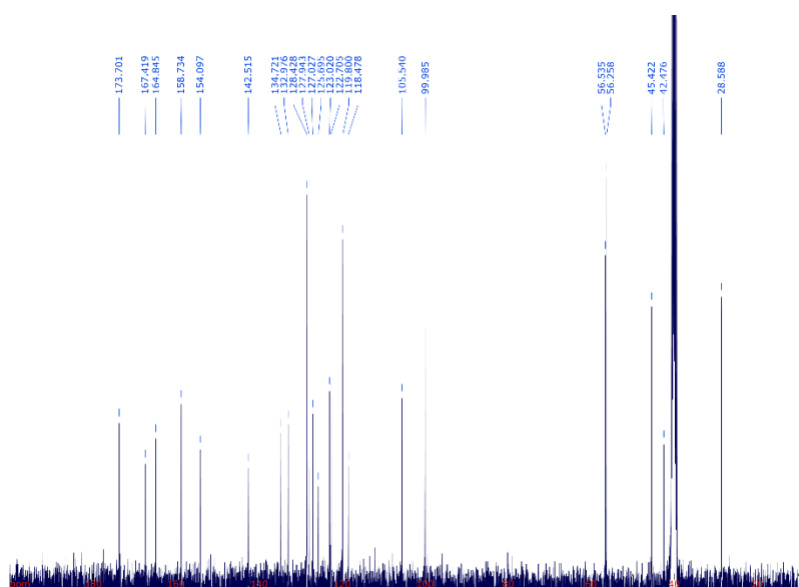
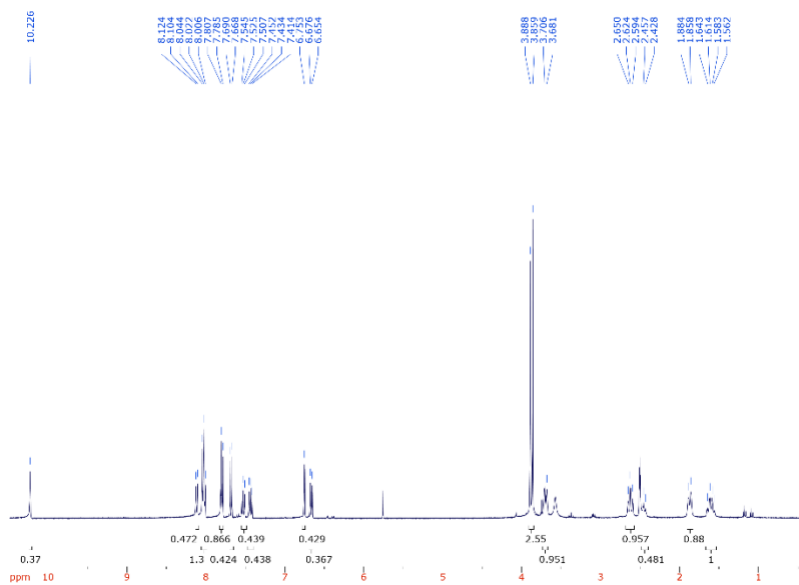




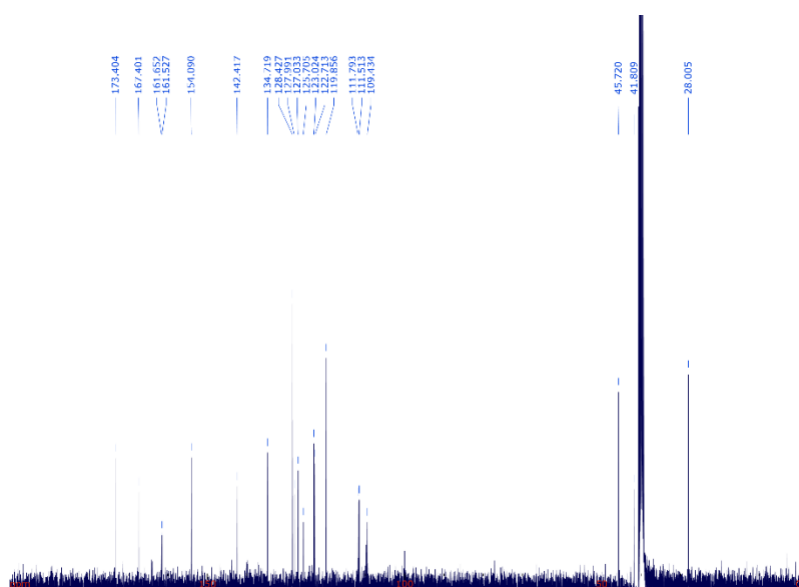
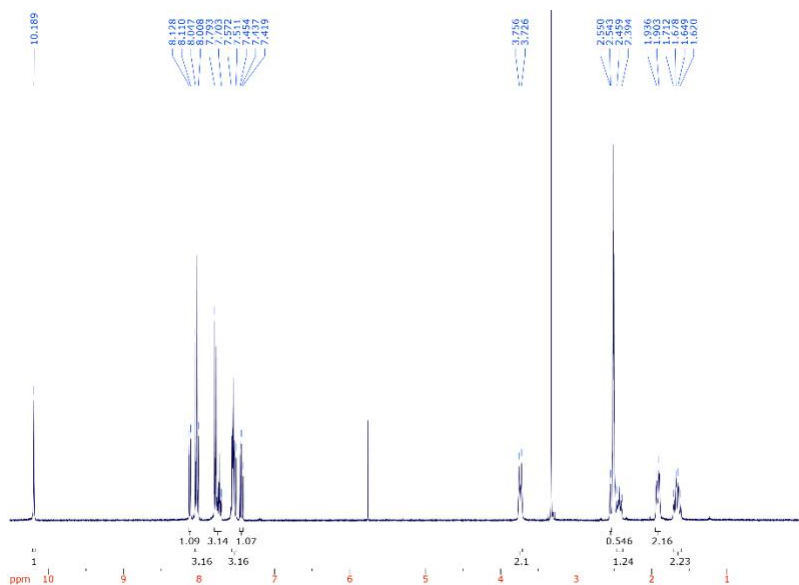
*N*-(4-(benzo[*d*]thiazol-2-yl)phenyl)-1-((2,4-dibromophenyl)sulfonyl)piperidine-4-carboxamide (**3-21**)



*N*-(4-(benzo[*d*]thiazol-2-yl)phenyl)-1-((2,4-dimethylphenyl)sulfonyl)piperidine-4-carboxamide (**3-22**)

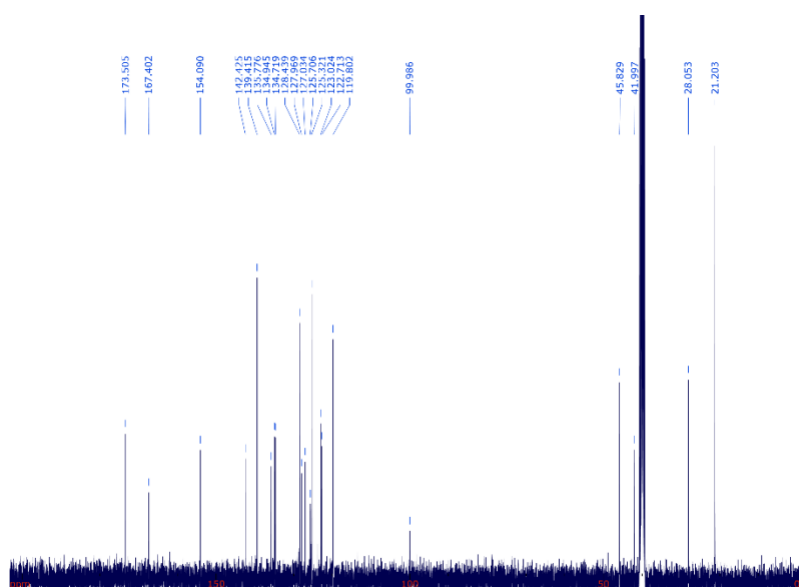
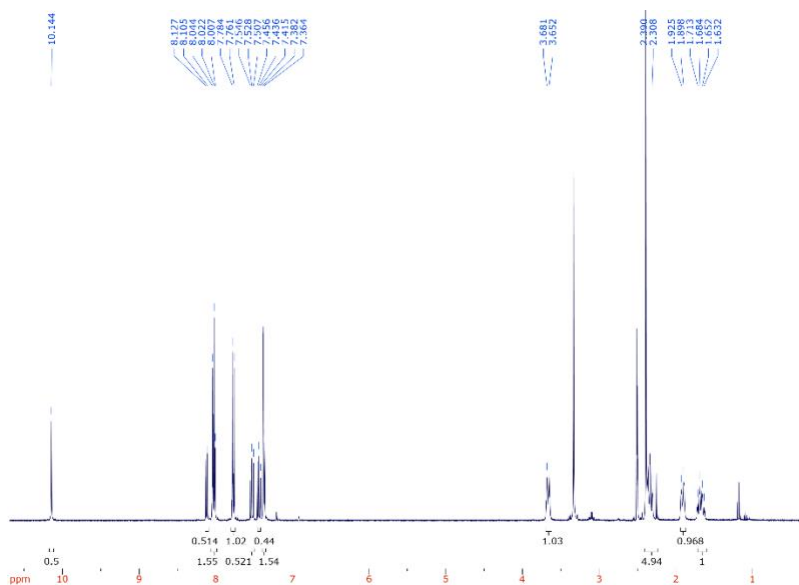


*N*-(4-(benzo[*d*]thiazol-2-yl)phenyl)-1-((2,4-dimethoxyphenyl)sulfonyl)piperidine-4-carboxamide (**3-23**)

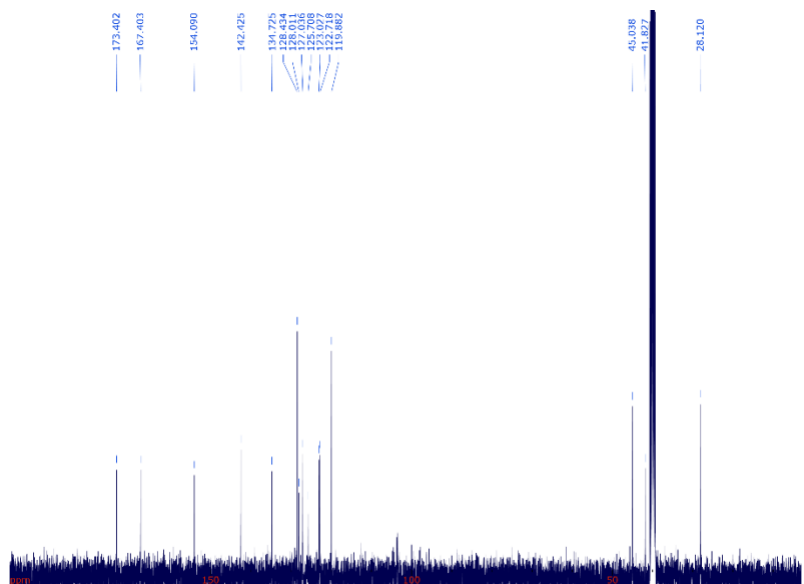
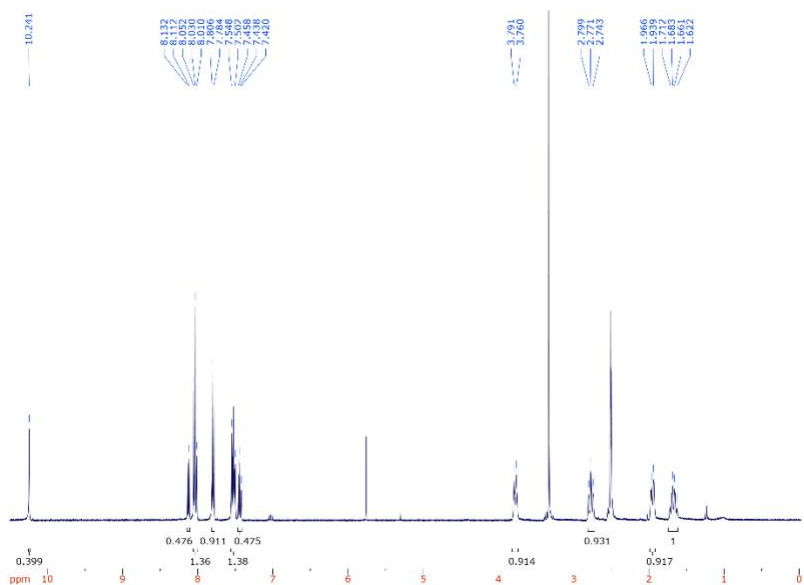


*N*-(4-(benzo[*d*]thiazol-2-yl)phenyl)-1-((3,5-difluorophenyl)sulfonyl)piperidine-4-carboxamide (**3-24**)

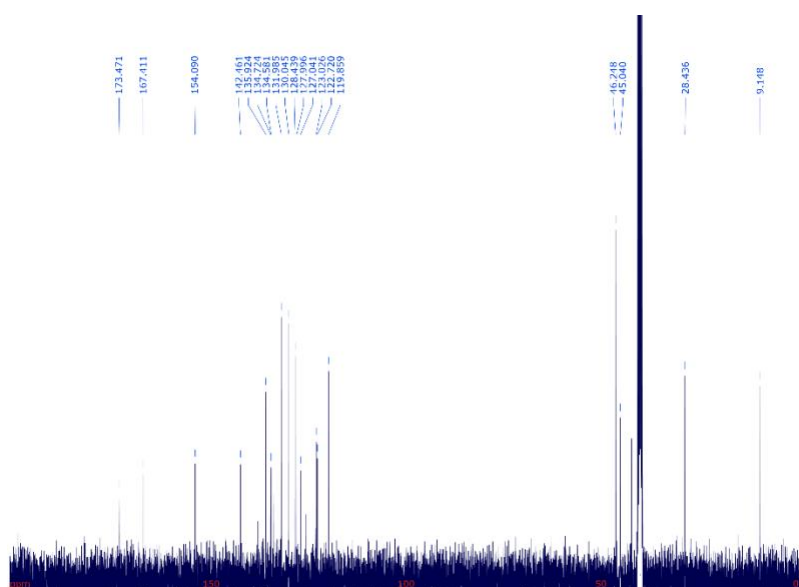
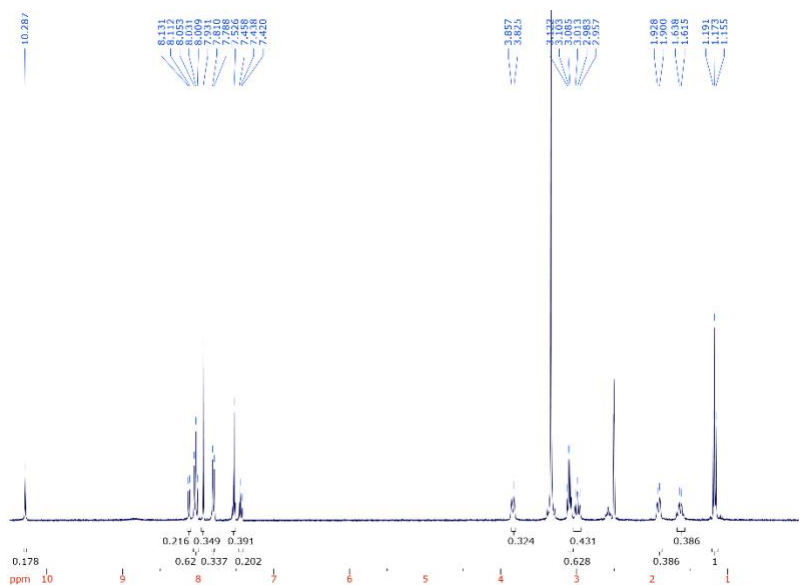




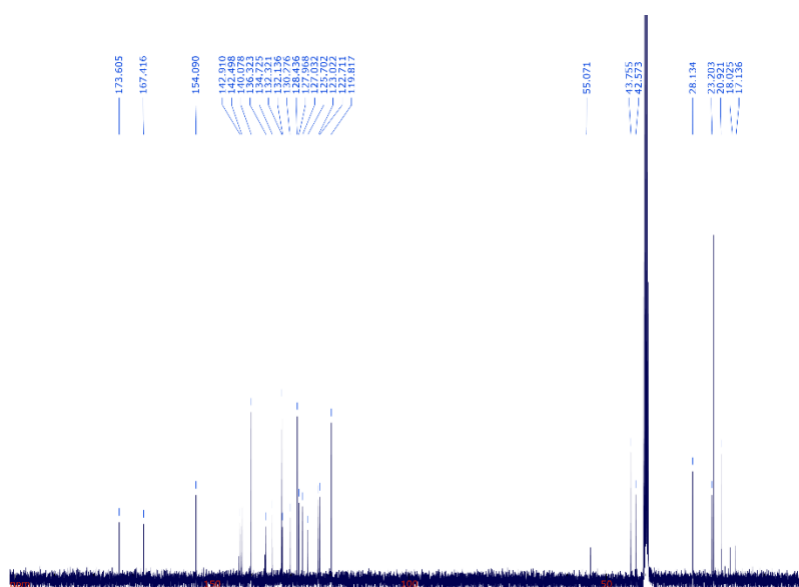
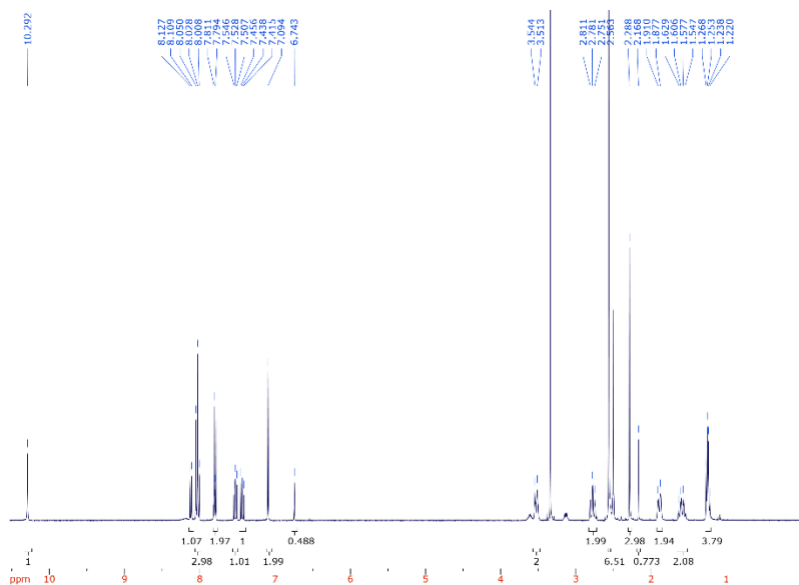
*N*-(4-(benzo[*d*]thiazol-2-yl)phenyl)-1-((3,5-dimethylphenyl)sulfonyl)piperidine-4-carboxamide (**3-25**)



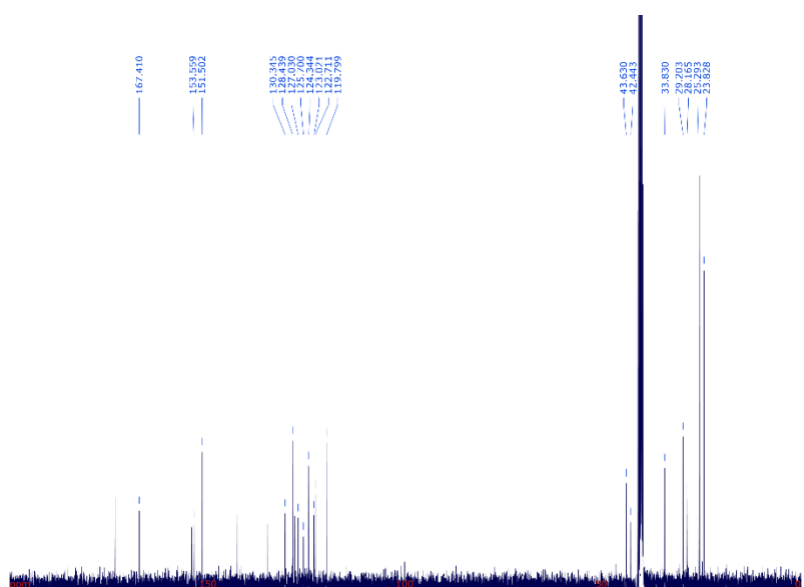
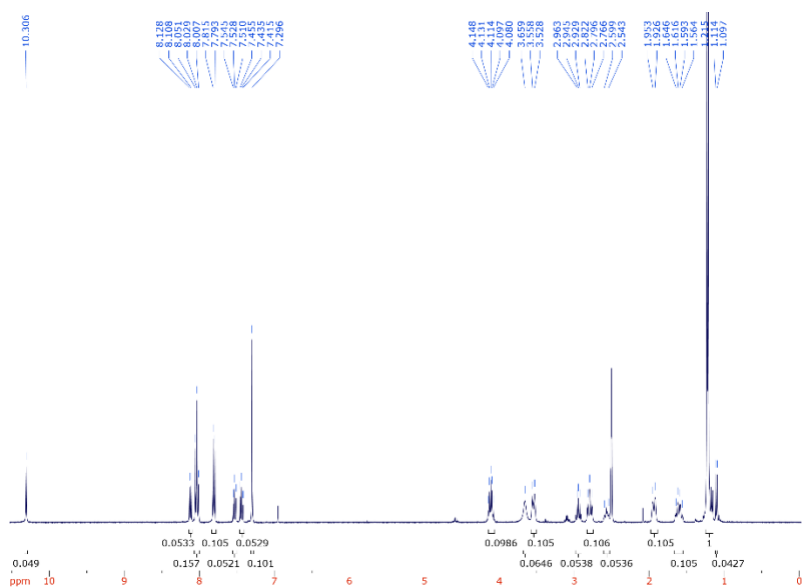
*N*-(4-(benzo[*d*]thiazol-2-yl)phenyl)-1-((2,4,6-trifluorophenyl)sulfonyl)piperidine-4-carboxamide (**3-26**)



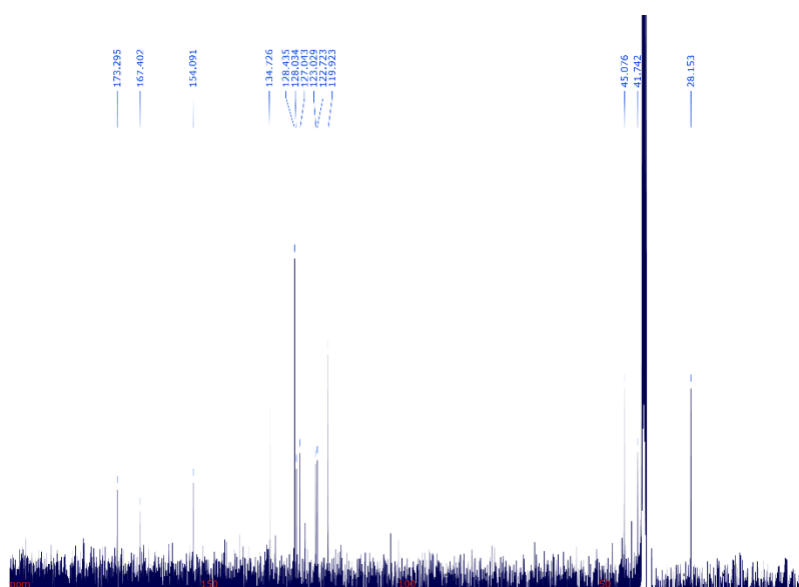
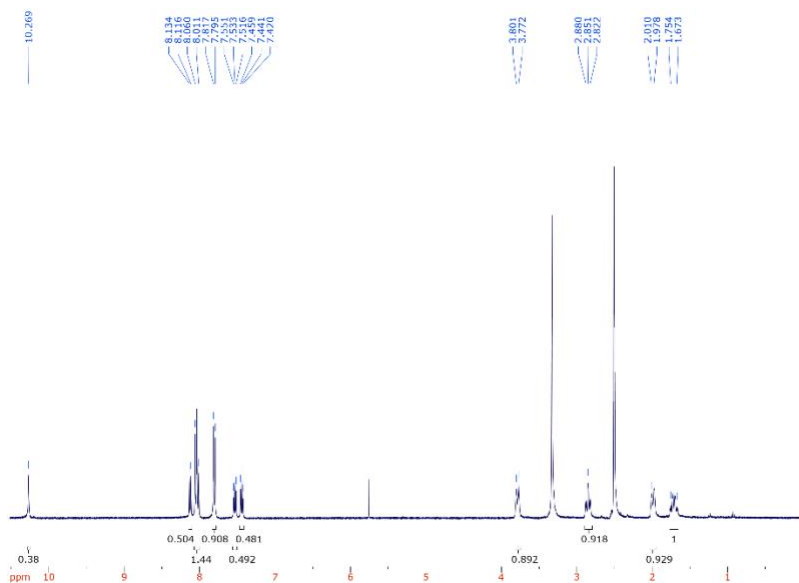
*N*-(4-(benzo[*d*]thiazol-2-yl)phenyl)-1-((2,4,6-trichlorophenyl)sulfonyl)piperidine-4-carboxamide (**3-27**)



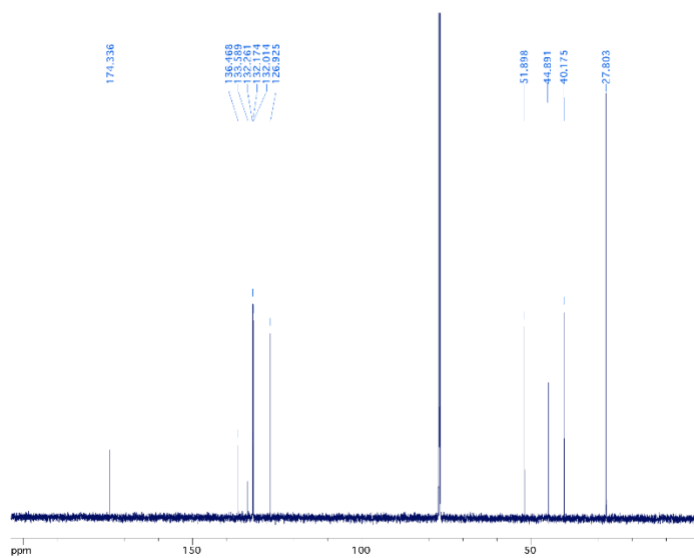
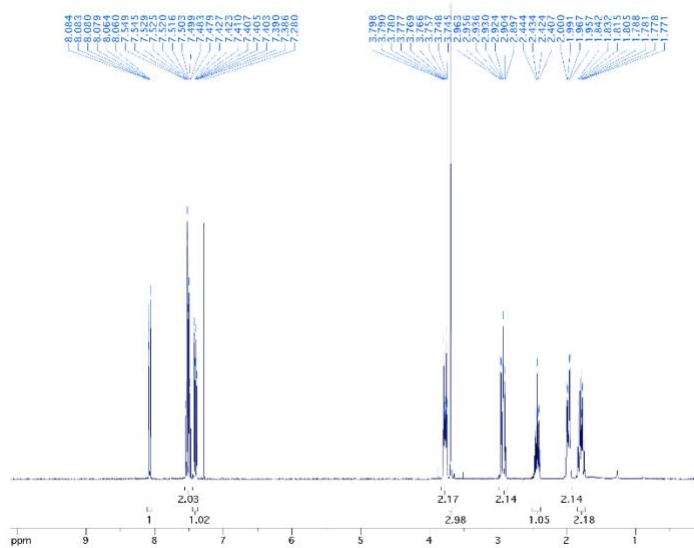
*N*-(4-(benzo[*d*]thiazol-2-yl)phenyl)-1-(mesitylsulfonyl)piperidine-4-carboxamide (**3-28**)



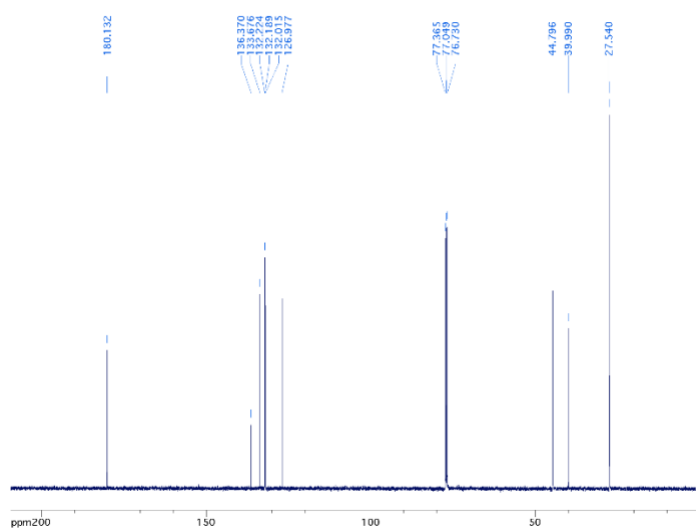
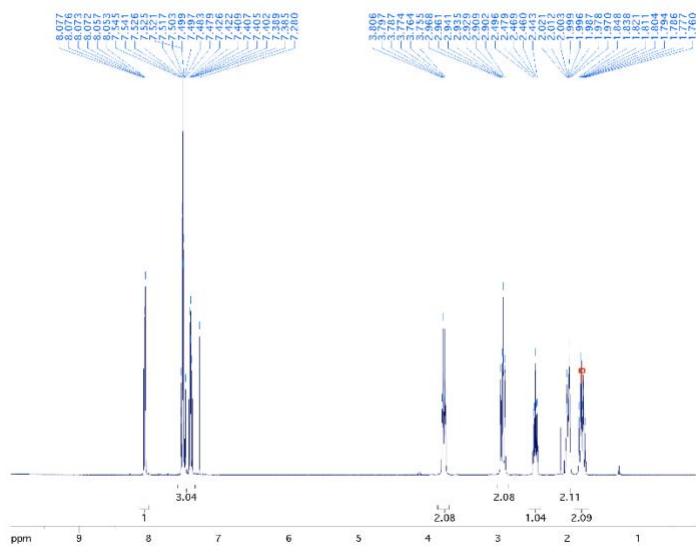
*N*-(4-(benzo[*d*]thiazol-2-yl)phenyl)-1-((2,4,6-triisopropylphenyl)sulfonyl)piperidine-4-carboxamide (**3-29**)



*N*-(4-(benzo[*d*]thiazol-2-yl)phenyl)-1-((perfluorophenyl)sulfonyl)piperidine-4-carboxamide (**3-30**)



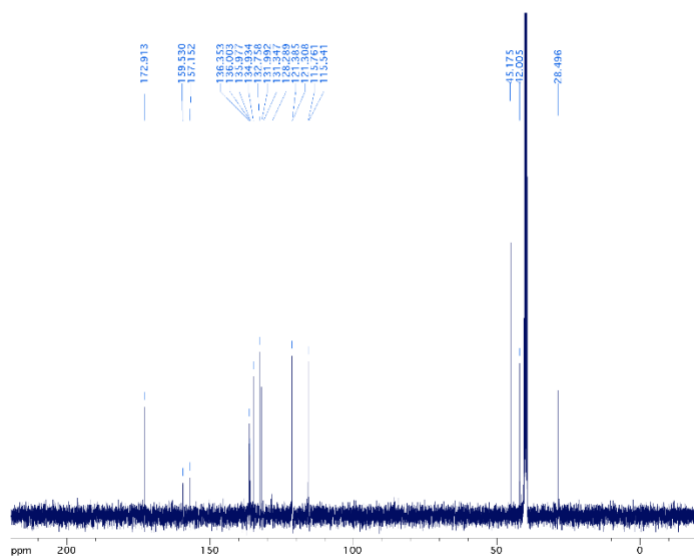
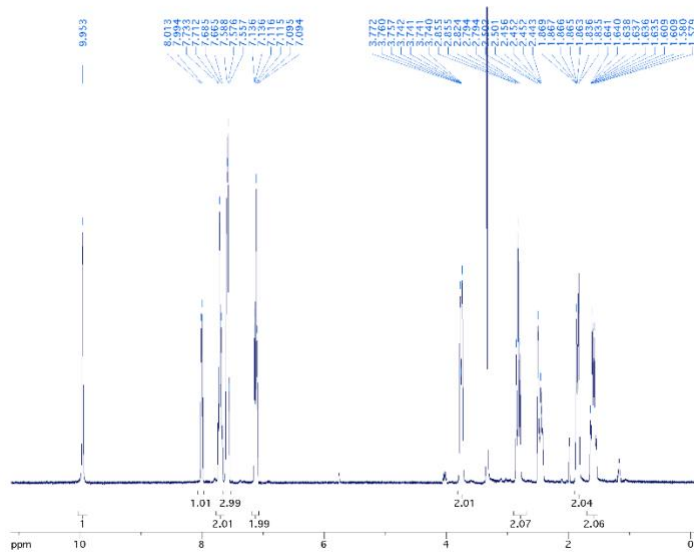
Methyl 1-((2-chlorophenyl)sulfonyl)piperidine-4-carboxylate (i)



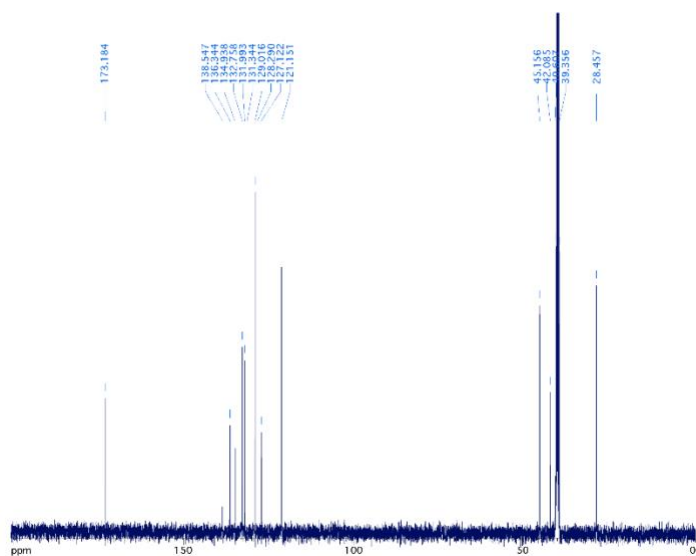
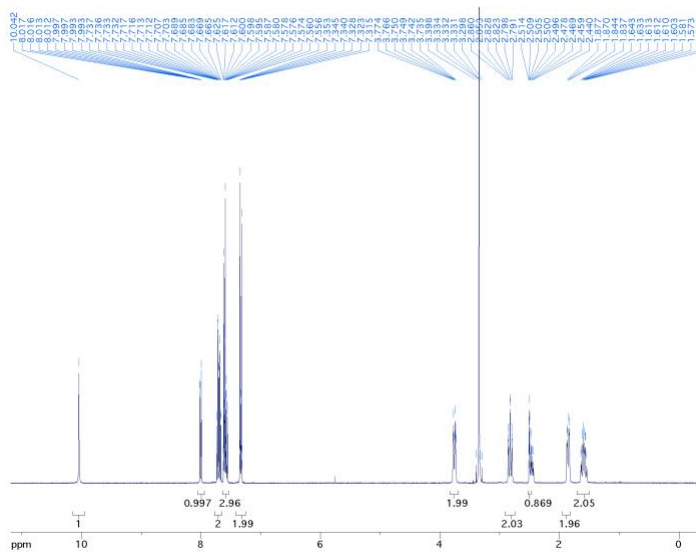
1-((2-chlorophenyl)sulfonyl)piperidine-4-carboxylic acid (j)



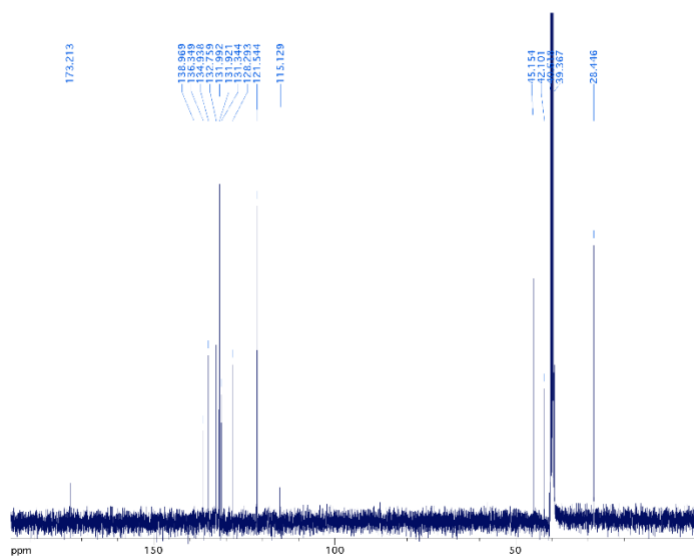
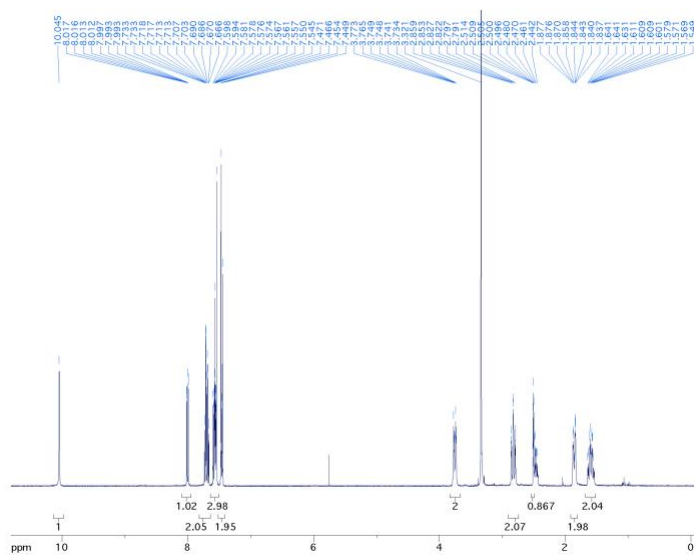




1-((2-chlorophenyl)sulfonyl)-N-(4-fluorophenyl)piperidine-4-carboxamide, **4-2**

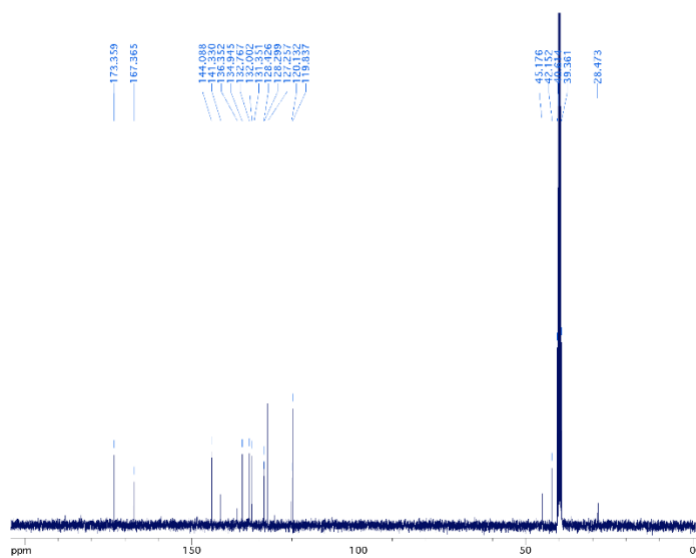
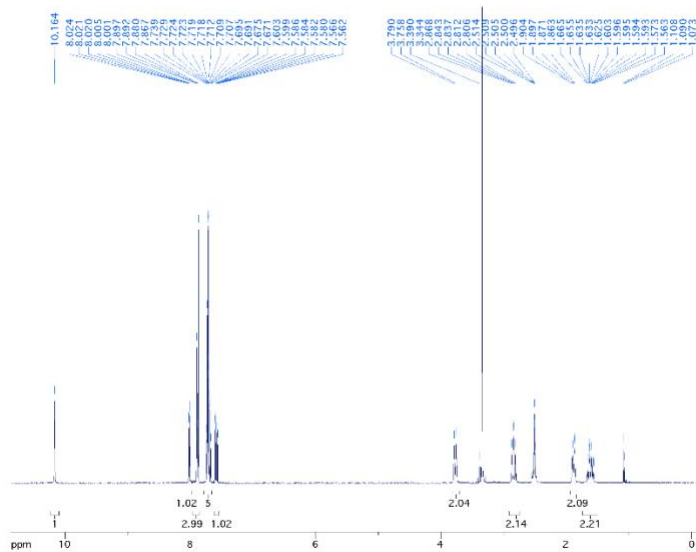


N-(4-chlorophenyl)-1-((2-chlorophenyl)sulfonyl)piperidine-4-carboxamide, **4-3**

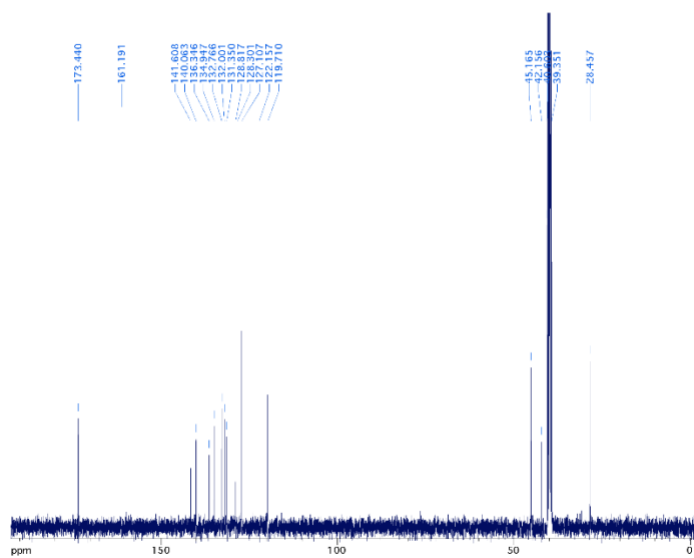
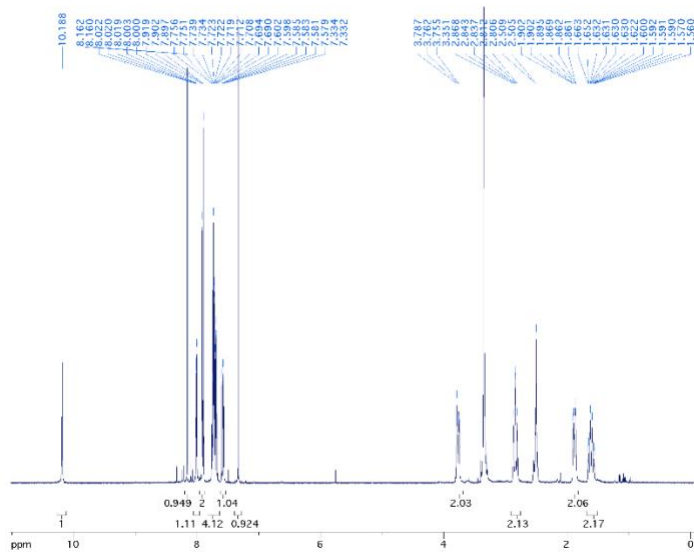


N-(4-bromophenyl)-1-((2-chlorophenyl)sulfonyl)piperidine-4-carboxamide, **4-4**





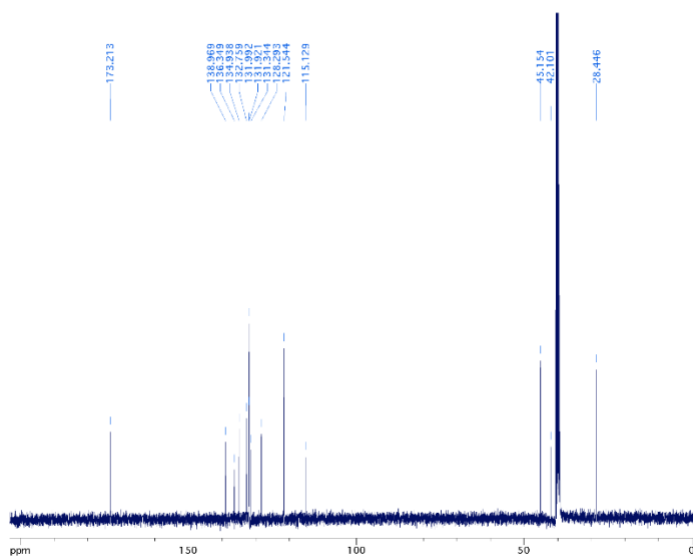
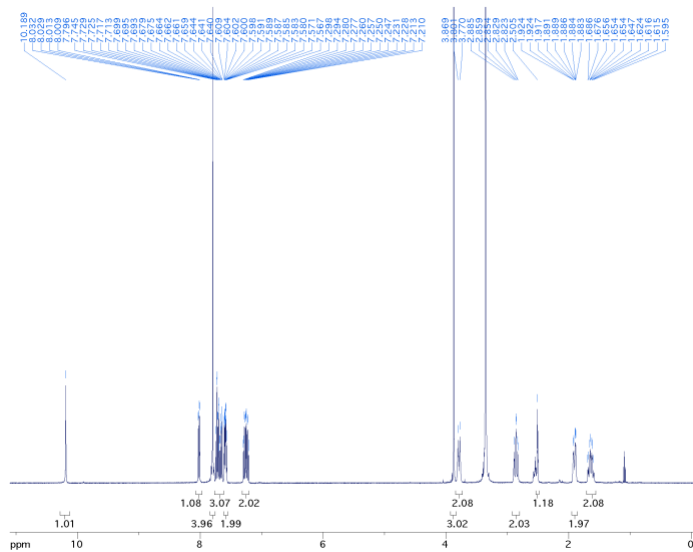
1-((2-chlorophenyl)sulfonyl)-N-(4-(thiazol-2-yl)phenyl)piperidine-4-carboxamide, **4-6**



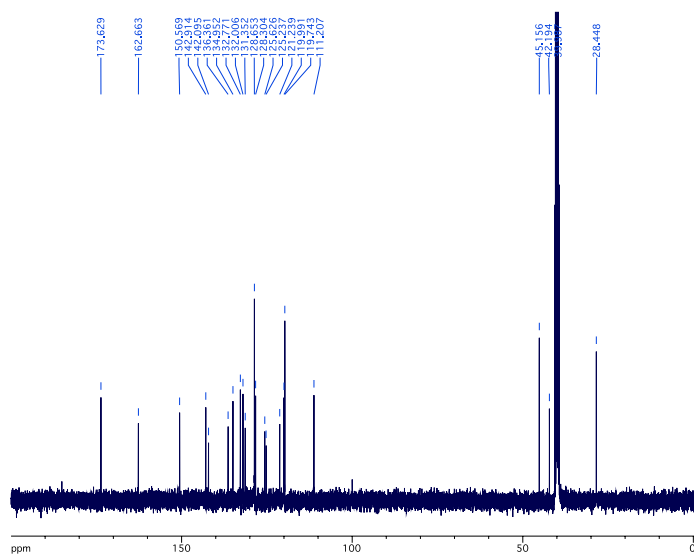
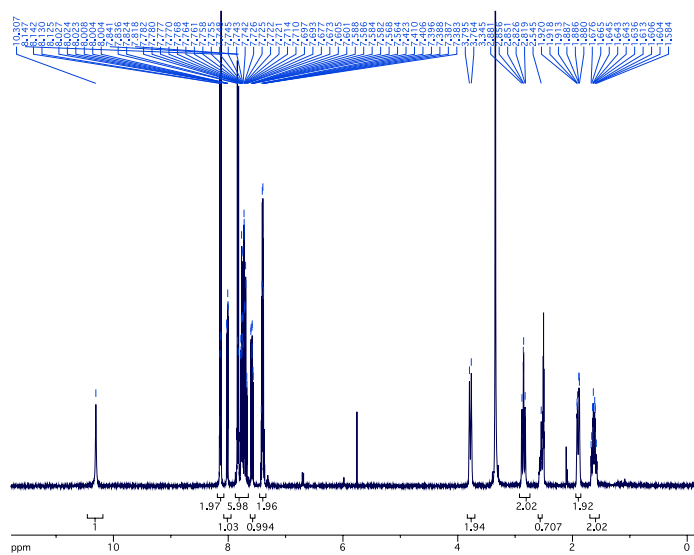
1-((2-chlorophenyl)sulfonyl)-N-(4-(oxazol-2-yl)phenyl)piperidine-4-carboxamide, **4-7**

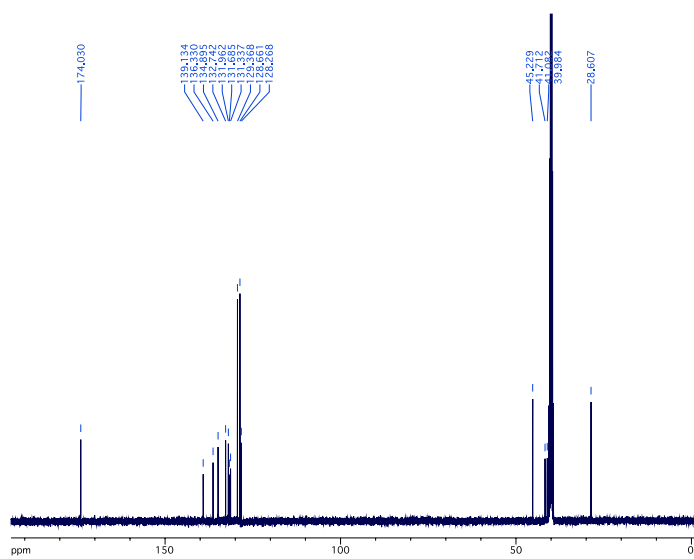
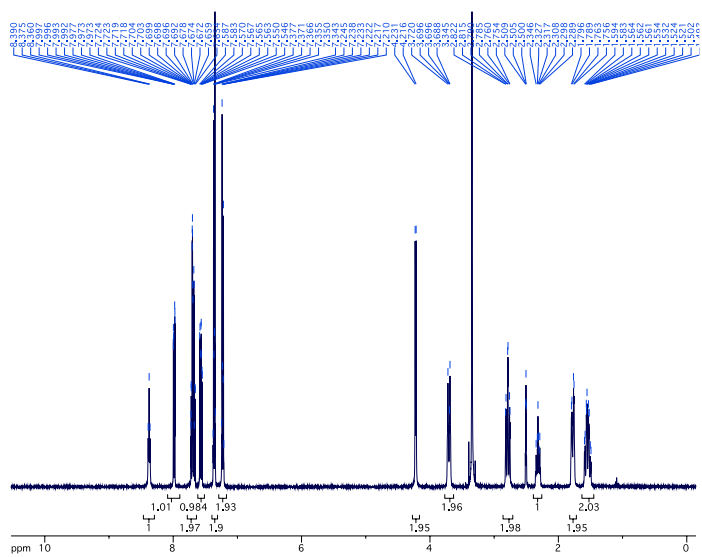






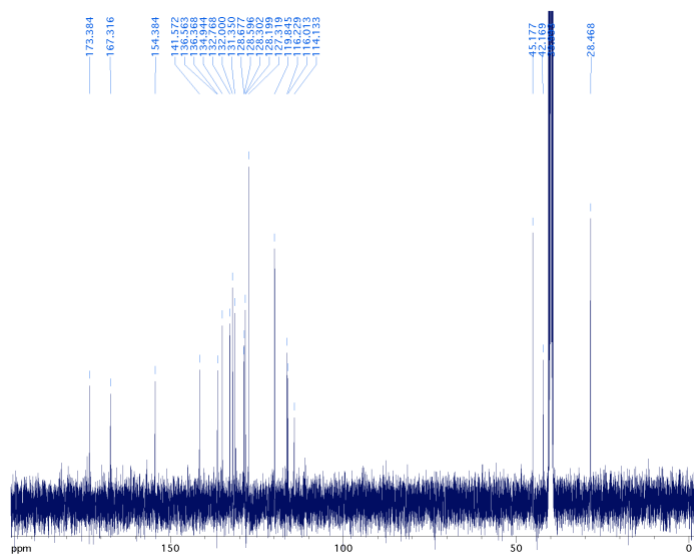
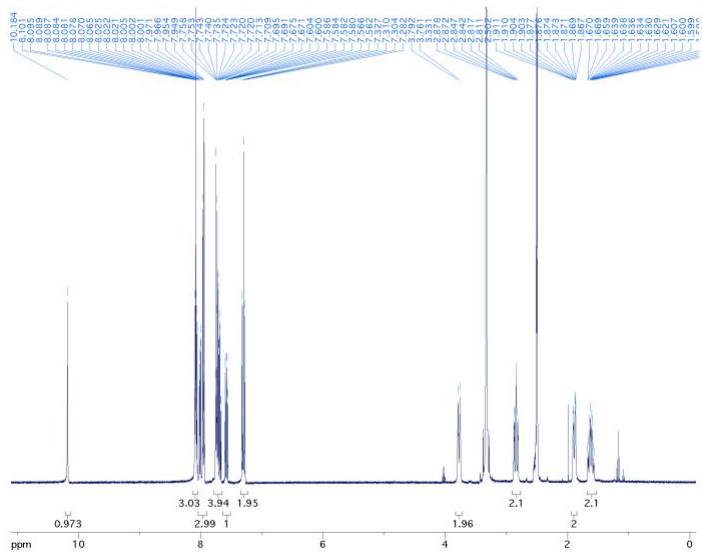
1-((2-chlorophenyl)sulfonyl)-N-(4-(1-methyl-1H-benzo[d]imidazol-2-yl)phenyl)piperidine-4-carboxamide, **4-9**



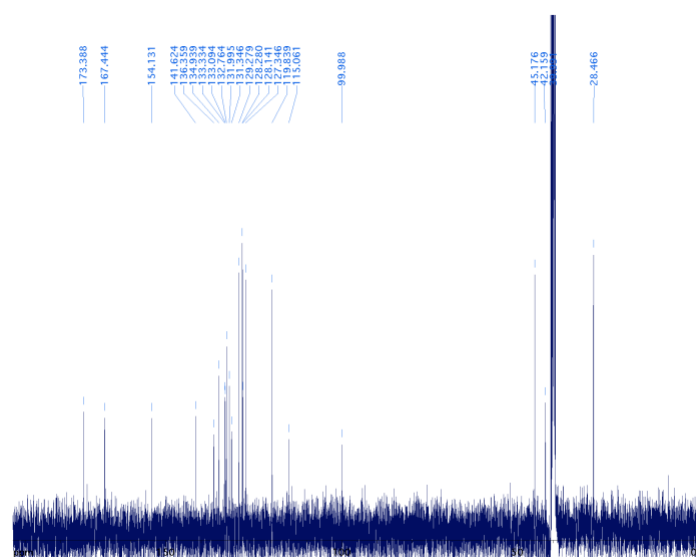
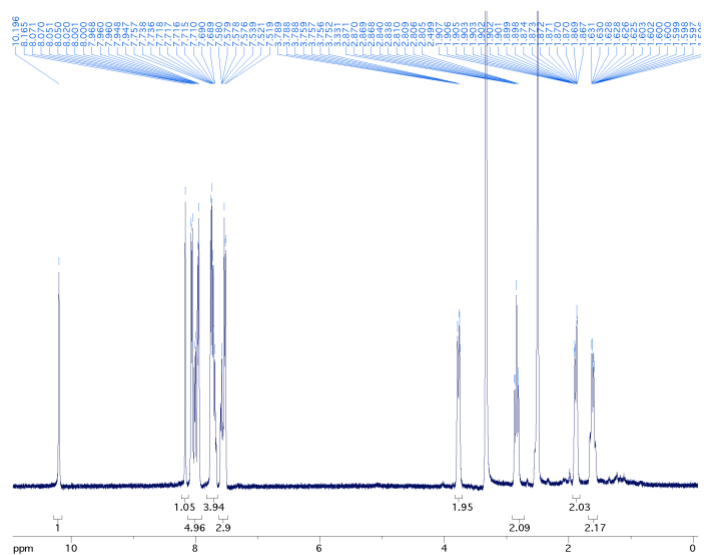


N-(4-(4-chlorobenzyl)phenyl)-1-((2-chlorophenyl)sulfonyl)piperidine-4-carboxamide, **4-11**

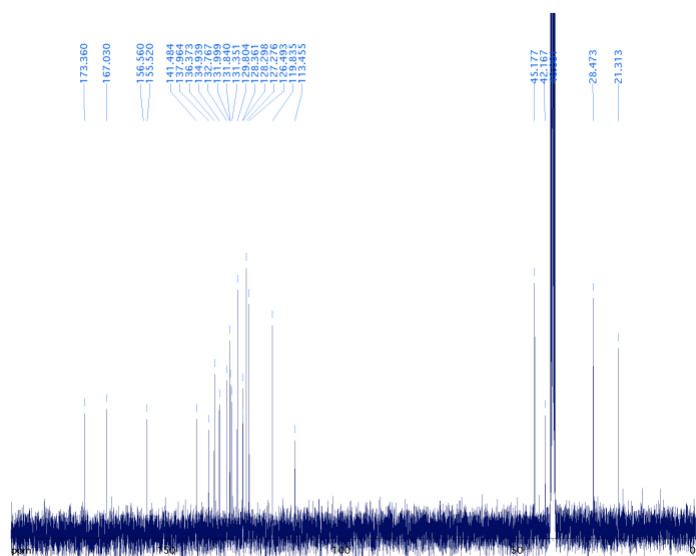
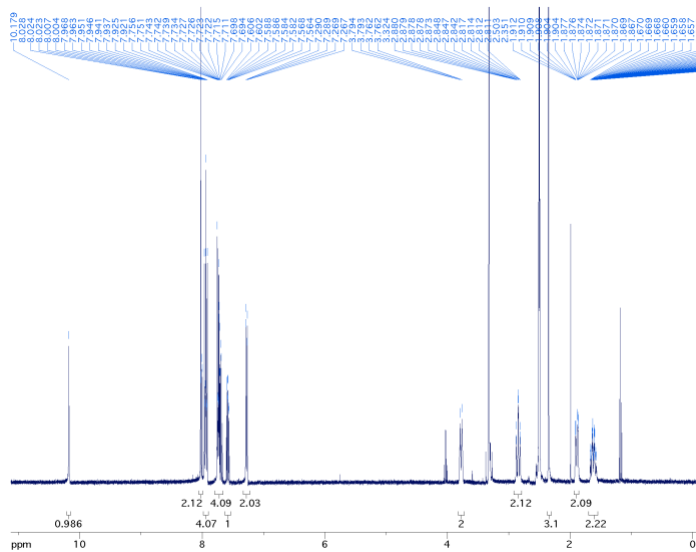




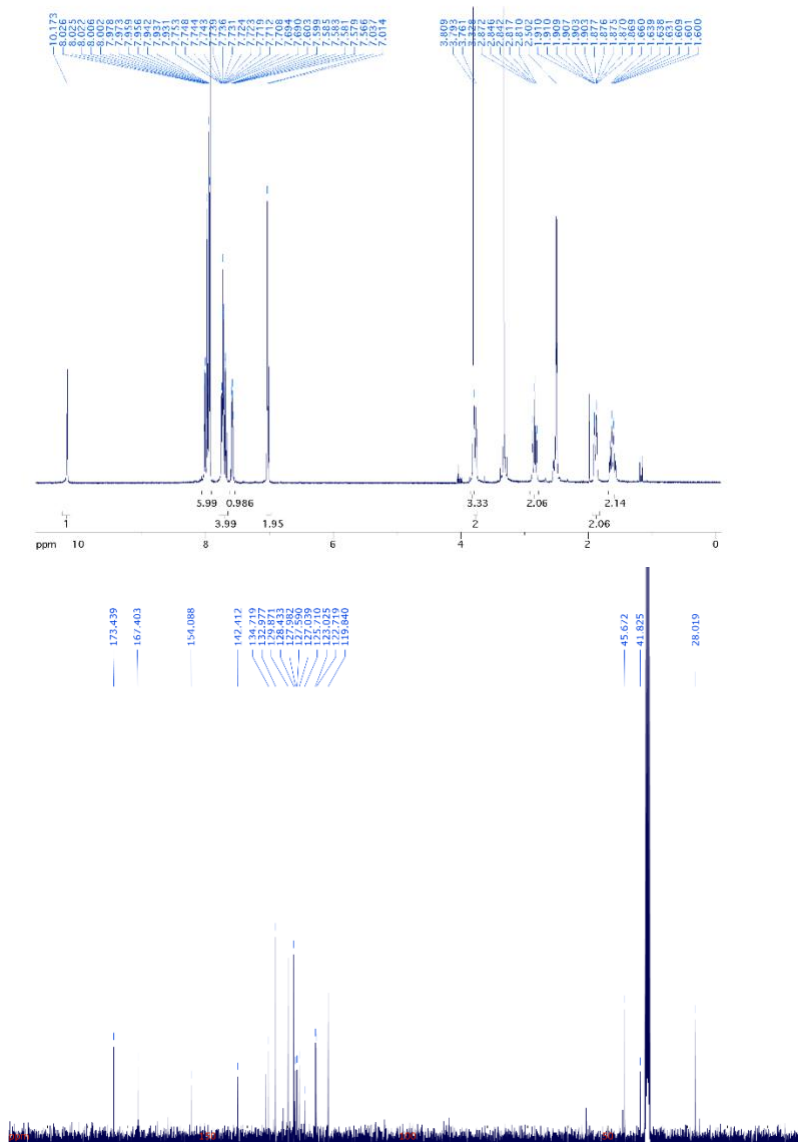
1-((2-chlorophenyl)sulfonyl)-N-(4-(4-(4-fluorophenyl)thiazol-2-yl)phenyl)piperidine-4-carboxamide, **4-13**



1-((2-chlorophenyl)sulfonyl)-N-(4-(4-(4-chlorophenyl)thiazol-2-yl)phenyl)piperidine-4-carboxamide, **4-14**



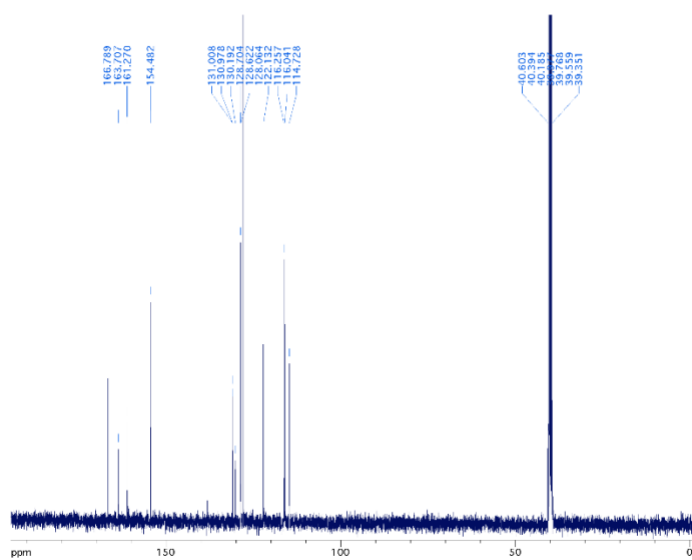
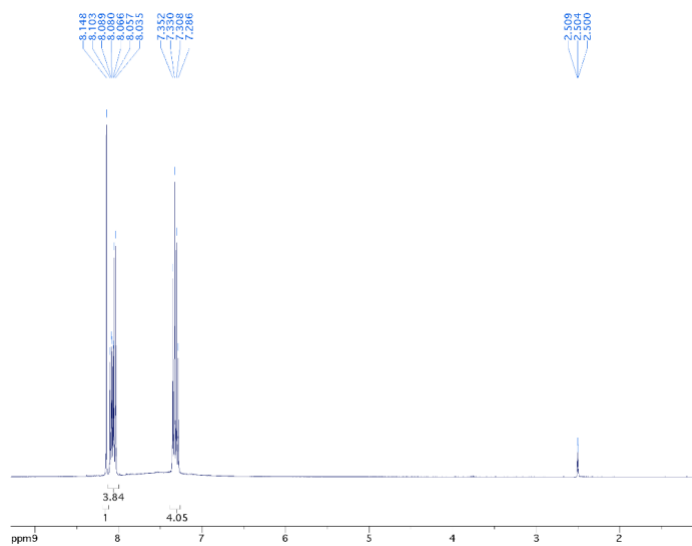
1-((2-chlorophenyl)sulfonyl)-N-(4-(4-(p-tolyl)thiazol-2-yl)phenyl)piperidine-4-carboxamide, **4-15**



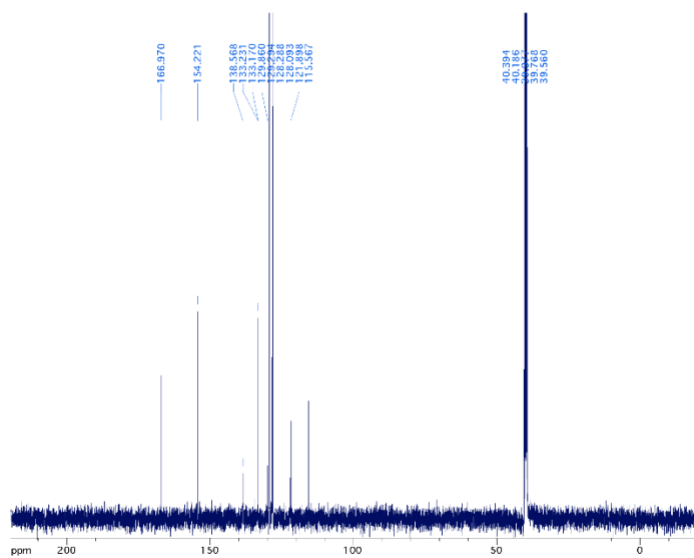
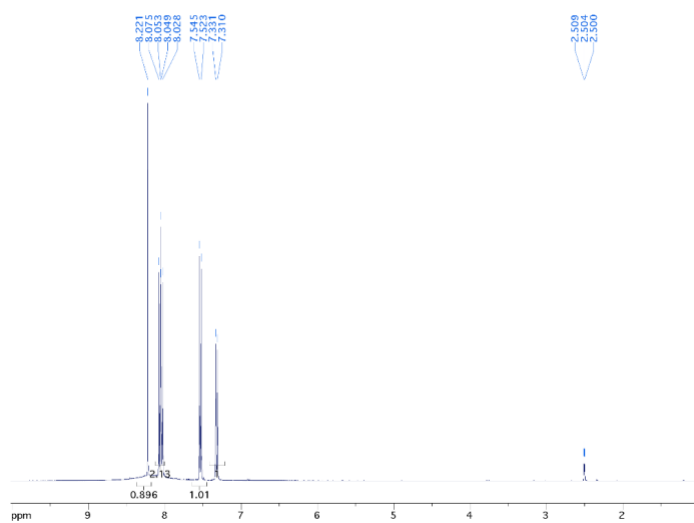
1-((2-chlorophenyl)sulfonyl)-N-(4-(4-(4-methoxyphenyl)thiazol-2-yl)phenyl)piperidine-4-carboxamide, **4-16**



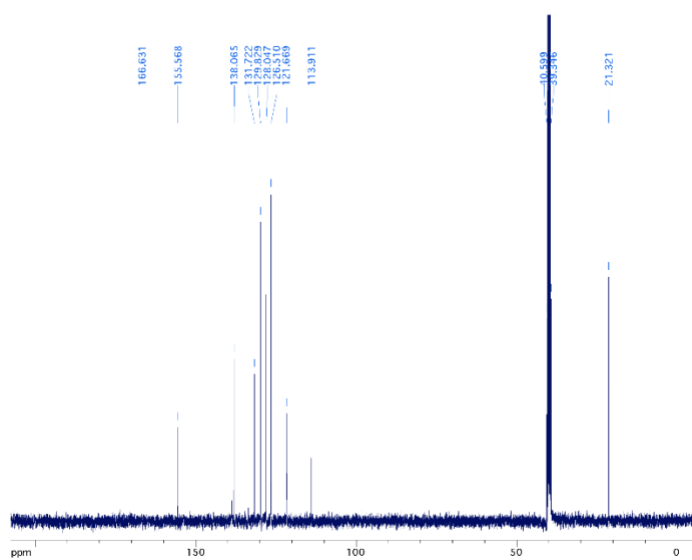
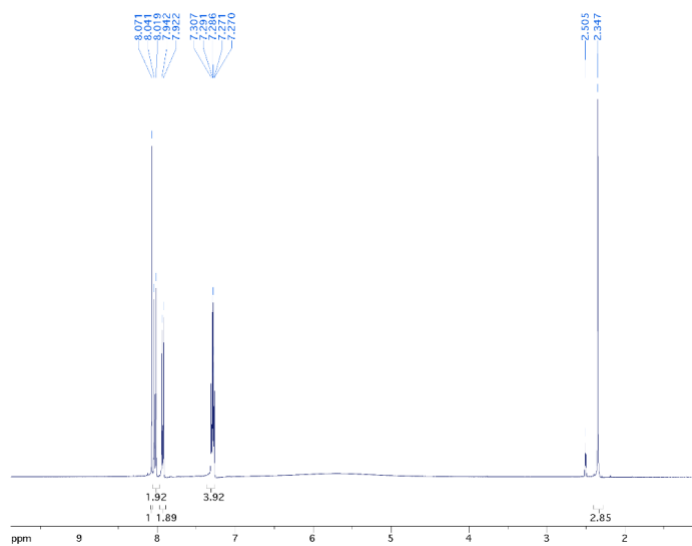




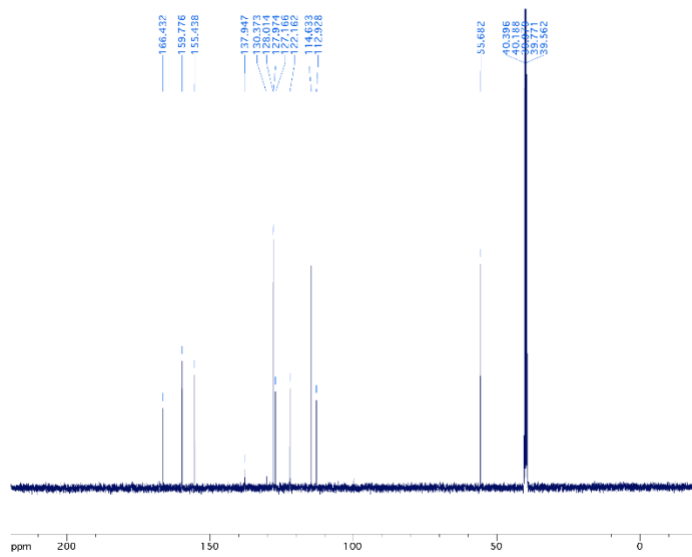
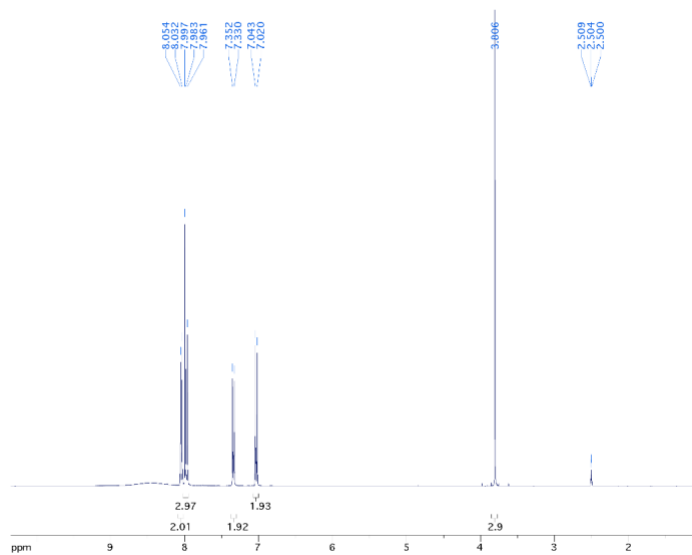
4-(4-(4-fluorophenyl)thiazol-2-yl)aniline (5-13)



4-(4-(4-chlorophenyl)thiazol-2-yl)aniline (**5-14**)



4-(4-(*p*-tolyl)thiazol-2-yl)aniline (5-15)



4-(4-(4-methoxyphenyl)thiazol-2-yl)aniline (5-16)

## REFERENCES

- Abagyan, R., & Totrov, M. (1994). Biased probability Monte Carlo conformational searches and electrostatic calculations for peptides and proteins. *Journal of Molecular Biology*, 235(3), 983-1002. doi:<https://doi.org/10.1006/jmbi.1994.1052>
- Aceto, M. D., Harris, L. S., Negus, S. S., Banks, M. L., Hughes, L. D., Akgun, E., & Portoghesi, P. S. (2012). MDAN-21: A Bivalent opioid ligand containing mu-agonist and delta-antagonist pharmacophores and its effects in Rhesus monkeys. *International Journal of Medicinal Chemistry*, 2012, 327257. doi:10.1155/2012/327257
- Ahn, K., Johnson, D. S., & Cravatt, B. F. (2009). Fatty acid amide hydrolase as a potential therapeutic target for the treatment of pain and CNS disorders. *Expert Opinion Drug Discovery*, 4(7), 763-784. doi:10.1517/17460440903018857
- Ahn, K., Johnson, D. S., Mileni, M., Beidler, D., Long, J. Z., McKinney, M. K., Weerapana, E., Sadagopan, N., Liimatta, M., Smith, S. E., Lazerwith, S., Stiff, C., Kamtekar, S., Bhattacharya, K., Zhang, Y., Swaney, S., Van Becelaere, K., Stevens, R. C., & Cravatt, B. F. (2009). Discovery and characterization of a highly selective FAAH inhibitor that reduces inflammatory pain. *Chemistry and Biology*, 16(4), 411-420. doi:10.1016/j.chembiol.2009.02.013
- Alhouayek, M., Masquelier, J., & Muccioli, G. G. (2014). Controlling 2-arachidonoylglycerol metabolism as an anti-inflammatory strategy. *Drug Discovery Today*, 19(3), 295-304. doi:10.1016/j.drudis.2013.07.009
- Antoniou, K. M., Margaritopoulos, G. A., Tomassetti, S., Bonella, F., Costabel, U., & Poletti, V. (2014). Interstitial lung disease. *European Respiratory Review*, 23(131), 40-54. doi:10.1183/09059180.00009113
- Arand, M., Wagner, H., & Oesch, F. (1996). Asp333, Asp495, and His523 form the catalytic triad of rat soluble epoxide hydrolase. *Journal of Biological Chemistry*, 271(8), 4223-4229. doi:10.1074/jbc.271.8.4223
- Ashton, J. C., Wright, J. L., McPartland, J. M., & Tyndall, J. D. (2008). Cannabinoid CB1 and CB2 receptor ligand specificity and the development of CB2-selective agonists. *Current Medicinal Chemistry*, 15(14), 1428-1443. doi:10.2174/092986708784567716
- Barratt, S. L., Creamer, A., Hayton, C., & Chaudhuri, N. (2018). Idiopathic Pulmonary Fibrosis (IPF): An Overview. *Journal of Clinical Medicine*, 7(8). doi:10.3390/jcm7080201
- Behl, T., Kaur, G., Bungau, S., Jhanji, R., Kumar, A., Mehta, V., Zengin, G., Brata, R., Hassan, S. S. u., & Fratila, O. (2020). Distinctive evidence involved in the role of endocannabinoid signalling in Parkinson's Disease: A Perspective on Associated Therapeutic Interventions. *International Journal of Molecular Sciences*, 21(17), 6235. Retrieved from <https://www.mdpi.com/1422-0067/21/17/6235>
- Benet, L. Z., Hosey, C. M., Ursu, O., & Oprea, T. I. (2016). BDDCS, the Rule of 5 and drugability. *Advanced Drug Delivery Reviews*, 101, 89-98. doi:<https://doi.org/10.1016/j.addr.2016.05.007>
- Berry, A. J., Zubko, O., Reeves, S. J., & Howard, R. J. (2020). Endocannabinoid system alterations in Alzheimer's disease: A systematic review of human studies. *Brain Research*, 1749, 147135. doi:<https://doi.org/10.1016/j.brainres.2020.147135>

- Bisogno, T., & Maccarrone, M. (2013). Latest advances in the discovery of fatty acid amide hydrolase inhibitors. *Expert Opinion Drug Discovery*, 8(5), 509-522. doi:10.1517/17460441.2013.780021
- Bjoraker, J. A., Ryu, J. H., Edwin, M. K., Myers, J. L., Tazelaar, H. D., Schroeder, D. R., & Offord, K. P. (1998). Prognostic significance of histopathologic subsets in idiopathic pulmonary fibrosis. *American Journal of Respiratory and Critical Care Medicine*, 157(1), 199-203. doi:10.1164/ajrccm.157.1.9704130
- Boger, D. L., Miyauchi, H., Du, W., Hardouin, C., Fecik, R. A., Cheng, H., Hwang, I., Hedrick, M. P., Leung, D., Acevedo, O., Guimaraes, C. R., Jorgensen, W. L., & Cravatt, B. F. (2005). Discovery of a potent, selective, and efficacious class of reversible alpha-ketoheterocycle inhibitors of fatty acid amide hydrolase effective as analgesics. *Journal of Medicinal Chemistry*, 48(6), 1849-1856. doi:10.1021/jm049614v
- Boger, D. L., Sato, H., Lerner, A. E., Austin, B. J., Patterson, J. E., Patricelli, M. P., & Cravatt, B. F. (1999). Trifluoromethyl ketone inhibitors of fatty acid amide hydrolase: a probe of structural and conformational features contributing to inhibition. *Bioorganic & Medicinal Chemistry Letters*, 9(2), 265-270. doi:10.1016/s0960-894x(98)00734-3
- Bozkurt, T. E. (2019). Endocannabinoid system in the airways. *Molecules*, 24(24). doi:10.3390/molecules24244626
- Brown, D. G., & Wobst, H. J. (2021). A decade of FDA-Approved drugs (2010-2019): trends and future directions. *Journal of Medicinal Chemistry*, 64(5), 2312-2338. doi:10.1021/acs.jmedchem.0c01516
- Centonze, D., Finazzi-Agrò, A., Bernardi, G., & Maccarrone, M. (2007). The endocannabinoid system in targeting inflammatory neurodegenerative diseases. *Trends in Pharmacological Sciences*, 28(4), 180-187. doi:https://doi.org/10.1016/j.tips.2007.02.004
- Cha, H. J., Song, Y. J., Lee, D. E., Kim, Y.-H., Shin, J., Jang, C.-G., Suh, S. K., Kim, S. J., & Yun, J. (2019). Receptor binding affinities of synthetic cannabinoids determined by non-isotopic receptor binding assay. *Toxicological Research*, 35(1), 37-44. doi:10.5487/TR.2019.35.1.037
- Cinar, R., Gochuico, B. R., Iyer, M. R., Jourdan, T., Yokoyama, T., Park, J. K., . . . Kunos, G. (2017). Cannabinoid CB1 receptor overactivity contributes to the pathogenesis of idiopathic pulmonary fibrosis. *Journal of Clinical Investigation*, 2(8). doi:10.1172/jci.insight.92281
- Clapper, J. R., Moreno-Sanz, G., Russo, R., Guijarro, A., Vacondio, F., Duranti, A., . . . Piomelli, D. (2010). Anandamide suppresses pain initiation through a peripheral endocannabinoid mechanism. *Nature Neuroscience*, 13(10), 1265-1270. doi:10.1038/nn.2632
- Clark, D. E. (2003). In silico prediction of blood-brain barrier permeation. *Drug Discovery Today*, 8(20), 927-933. doi:https://doi.org/10.1016/S1359-6446(03)02827-7
- Clayton, N., Marshall, F. H., Bountra, C., & O'Shaughnessy, C. T. (2002). CB1 and CB2 cannabinoid receptors are implicated in inflammatory pain. *Pain*, 96(3), 253-260. doi:10.1016/S0304-3959(01)00454-7
- Colovos, C., & Yeates, T. O. (1993). Verification of protein structures: patterns of nonbonded atomic interactions. *Protein Science*, 2(9), 1511-1519. doi:10.1002/pro.5560020916

- Connor, J., Rafter, N., & Rodgers, A. (2004). Do fixed-dose combination pills or unit-of-use packaging improve adherence? A systematic review. *Bulletin of the World Health Organization*, *82*, 935-939.
- Deng, Y., Edin, M. L., Theken, K. N., Schuck, R. N., Flake, G. P., Kannon, M. A., . . . Lee, C. R. (2011). Endothelial CYP epoxygenase overexpression and soluble epoxide hydrolase disruption attenuate acute vascular inflammatory responses in mice. *Federation of American Societies for Experimental Biology*, *25*(2), 703-713. doi:10.1096/fj.10-171488
- Di Marzo, V. (2008). Targeting the endocannabinoid system: to enhance or reduce? *Nature Review Drug Discovery*, *7*(5), 438-455. doi:10.1038/nrd2553
- Dowden, H., & Munro, J. (2019). Trends in clinical success rates and therapeutic focus. *Nature Review Drug Discovery*, *18*(7), 495-496. doi:10.1038/d41573-019-00074-z
- du Bois, R. M. (2012). An earlier and more confident diagnosis of idiopathic pulmonary fibrosis. *European Respiratory Review*, *21*(124), 141-146. doi:10.1183/09059180.00000812
- Dubuisson, D., & Dennis, S. G. (1977). The formalin test: a quantitative study of the analgesic effects of morphine, meperidine, and brain stem stimulation in rats and cats. *Pain*, *4*(2), 161-174. doi:10.1016/0304-3959(77)90130-0
- Eisenberg, D., Luthy, R., & Bowie, J. U. (1997). VERIFY3D: assessment of protein models with three-dimensional profiles. *Methods Enzymology*, *277*, 396-404. doi:10.1016/s0076-6879(97)77022-8
- Esposito, D. B., Lanes, S., Donneyong, M., Holick, C. N., Lasky, J. A., Lederer, D., . . . Tran, T. N. (2015). Idiopathic Pulmonary Fibrosis in United States automated claims. Incidence, prevalence, and algorithm validation. *American Journal of Respiratory and Critical Care Medicine*, *192*(10), 1200-1207. doi:10.1164/rccm.201504-0818OC
- Finn, D. P., Haroutounian, S., Hohmann, A. G., Krane, E., Soliman, N., & Rice, A. S. C. (2021). Cannabinoids, the endocannabinoid system, and pain: a review of preclinical studies. *Pain*, *162*(Suppl 1), S5-s25. doi:10.1097/j.pain.0000000000002268
- Gattrell, W., Johnstone, C., Patel, S., Smith, C. S., Scheel, A., & Schindler, M. (2013). Designed multiple ligands in metabolic disease research: from concept to platform. *Drug Discovery Today*, *18*(15-16), 692-696. doi:10.1016/j.drudis.2013.02.006
- Gattrell, W. T., Sambrook Smith, C. P., & Smith, A. J. (2012). An example of designed multiple ligands spanning protein classes: Dual MCH-1R antagonists/DPPIV inhibitors. *Bioorganic & Medicinal Chemistry Letters*, *22*(7), 2464-2469. doi:https://doi.org/10.1016/j.bmcl.2012.02.010
- Geldenhuys, W. J., Youdim, M. B., Carroll, R. T., & Van der Schyf, C. J. (2011). The emergence of designed multiple ligands for neurodegenerative disorders. *Progress in Neurobiology*, *94*(4), 347-359. doi:10.1016/j.pneurobio.2011.04.010
- George, P. M., Wells, A. U., & Jenkins, R. G. (2020). Pulmonary fibrosis and COVID-19: the potential role for antifibrotic therapy. *Lancet Respiratory Medicine*, *8*(8), 807-815. doi:10.1016/S2213-2600(20)30225-3



- Gomez, G. A., Morisseau, C., Hammock, B. D., & Christianson, D. W. (2006). Human soluble epoxide hydrolase: structural basis of inhibition by 4-(3-cyclohexylureido)-carboxylic acids. *Protein Science*, 15(1), 58-64. doi:10.1110/ps.051720206
- Guindon, J., & Beaulieu, P. (2009). The role of the endogenous cannabinoid system in peripheral analgesia. *Current Molecular Pharmacology*, 2(1), 134-139. doi:10.2174/1874467210902010134
- Guindon, J., & Hohmann, A. G. (2009). The endocannabinoid system and pain. *CNS & Neurological Disorders - Drug Targets*, 8(6), 403-421. doi:10.2174/187152709789824660
- Gustin, D. J., Ma, Z., Min, X., Li, Y., Hedberg, C., Guimaraes, C., Porter, A. C., Lindstrom, M., Lester-Zeiner, D., Xu, G., Carlson, T. J., Xiao, S., Meleza, C., Connors, R., Wang, Z., & Kayser, F. (2011). Identification of potent, noncovalent fatty acid amide hydrolase (FAAH) inhibitors. *Bioorganic Medicinal Chemistry Letters*, 21(8), 2492-2496. doi:10.1016/j.bmcl.2011.02.052
- Hopkins, R. B., Burke, N., Fell, C., Dion, G., & Kolb, M. (2016). Epidemiology and survival of idiopathic pulmonary fibrosis from national data in Canada. *European Respiratory Journal*, 48(1), 187-195. doi:10.1183/13993003.01504-2015
- Hopmann, K. H., & Himo, F. (2006). Theoretical study of the full reaction mechanism of human soluble epoxide hydrolase. *Chemistry*, 12(26), 6898-6909. doi:10.1002/chem.200501519
- Howlett, A. C., Barth, F., Bonner, T. I., Cabral, G., Casellas, P., Devane, W. A., Felder, C. C., Herkenham, M., Mackie, K., Martin, B. R., Mechoulam, R., & Pertwee, R. G. (2002). International Union of Pharmacology. XXVII. Classification of cannabinoid receptors. *Pharmacological Reviews*, 54(2), 161. doi:10.1124/pr.54.2.161
- Hunnskaar, S., & Hole, K. (1987). The formalin test in mice: dissociation between inflammatory and non-inflammatory pain. *Pain*, 30(1), 103-114. doi:10.1016/0304-3959(87)90088-1
- Idiopathic Pulmonary Fibrosis Clinical Research, N., Raghu, G., Anstrom, K. J., King, T. E., Jr., Lasky, J. A., & Martinez, F. J. (2012). Prednisone, azathioprine, and N-acetylcysteine for pulmonary fibrosis. *New England Journal of Medicine*, 366(21), 1968-1977. doi:10.1056/NEJMoa1113354
- Imig, J. D., & Hammock, B. D. (2009). Soluble epoxide hydrolase as a therapeutic target for cardiovascular diseases. *Nature Review Drug Discovery*, 8(10), 794-805. doi:10.1038/nrd2875
- Inceoglu, B., Schmelzer, K. R., Morisseau, C., Jinks, S. L., & Hammock, B. D. (2007). Soluble epoxide hydrolase inhibition reveals novel biological functions of epoxyeicosatrienoic acids (EETs). *Prostaglandins & Other Lipid Mediators*, 82(1), 42-49. doi:https://doi.org/10.1016/j.prostaglandins.2006.05.004
- Jing, Y., Easter, A., Peters, D., Kim, N., & Enyedy, I. J. (2015). In silico prediction of hERG inhibition. *Future Medicinal Chemistry*, 7(5), 571-586. doi:10.4155/fmc.15.18
- Jones, P. D., Tsai, H. J., Do, Z. N., Morisseau, C., & Hammock, B. D. (2006). Synthesis and SAR of conformationally restricted inhibitors of soluble epoxide hydrolase. *Bioorganic & Medicinal Chemistry Letters*, 16(19), 5212-5216. doi:10.1016/j.bmcl.2006.07.009

- Jones, P. D., Wolf, N. M., Morisseau, C., Whetstone, P., Hock, B., & Hammock, B. D. (2005). Fluorescent substrates for soluble epoxide hydrolase and application to inhibition studies. *Analytical Biochemistry*, *343*(1), 66-75. doi:10.1016/j.ab.2005.03.041
- Jourdan, D., Ardid, D., Bardin, L., Bardin, M., Neuzeret, D., Lanphouthacoul, L., & Eschalier, A. (1997). A new automated method of pain scoring in the formalin test in rats. *Pain*, *71*(3), 265-270. doi:10.1016/s0304-3959(97)03366-6
- Keith, J. M., Jones, W., Pierce, J. M., Seierstad, M., Palmer, J. A., Webb, M., Karbarz, M., Scott, B. P., Wilson, S. J., Luo, L., Wennerholm, M., Chang, L., Rizzolio, M., Rynberg, R., Chaplan, S., & Guy Breitenbucher, J. (2020). Heteroaryureas with fused bicyclic diamine cores as inhibitors of fatty acid amide hydrolase. *Bioorganic and Medicinal Chemistry Letters*, *30*(20), 127463. doi:https://doi.org/10.1016/j.bmcl.2020.127463
- Kelder, J., Grootenhuis, P. D., Bayada, D. M., Delbressine, L. P., & Ploemen, J. P. (1999). Polar molecular surface as a dominating determinant for oral absorption and brain penetration of drugs. *Pharmaceutical Research*, *16*(10), 1514-1519. doi:10.1023/a:1015040217741
- Kim, H. S., Moon, S.-J., Lee, S. E., Hwang, G. W., Yoo, H. J., & Song, J. W. (2021). The arachidonic acid metabolite 11,12-epoxyeicosatrienoic acid alleviates pulmonary fibrosis. *Experimental & Molecular Medicine*, *53*(5), 864-874. doi:10.1038/s12276-021-00618-7
- Kim, I. H., Morisseau, C., Watanabe, T., & Hammock, B. D. (2004). Design, synthesis, and biological activity of 1,3-disubstituted ureas as potent inhibitors of the soluble epoxide hydrolase of increased water solubility. *Journal of Medicinal Chemistry*, *47*(8), 2110-2122. doi:10.1021/jm030514j
- King, T. E., Jr., Pardo, A., & Selman, M. (2011). Idiopathic pulmonary fibrosis. *Lancet*, *378*(9807), 1949-1961. doi:10.1016/S0140-6736(11)60052-4
- Kodani, S. D., Bhakta, S., Hwang, S. H., Pakhomova, S., Newcomer, M. E., Morisseau, C., & Hammock, B. D. (2018). Identification and optimization of soluble epoxide hydrolase inhibitors with dual potency towards fatty acid amide hydrolase. *Bioorganic & Medicinal Chemistry Letters*, *28*(4), 762-768. doi:https://doi.org/10.1016/j.bmcl.2018.01.003
- Lam, P. C. H., Abagyan, R., & Totrov, M. (2018). Ligand-biased ensemble receptor docking (LigBEnD): a hybrid ligand/receptor structure-based approach. *Journal of Computer-Aided Molecular Design*, *32*(1), 187-198. doi:10.1007/s10822-017-0058-x
- Lam, P. C. H., Abagyan, R., & Totrov, M. (2019). Hybrid receptor structure/ligand-based docking and activity prediction in ICM: development and evaluation in D3R Grand Challenge 3. *Journal of Computer-Aided Molecular Design*, *33*(1), 35-46. doi:10.1007/s10822-018-0139-5
- Laskowski, R. A., Rullmann, J. A., MacArthur, M. W., Kaptein, R., & Thornton, J. M. (1996). AQUA and PROCHECK-NMR: programs for checking the quality of protein structures solved by NMR. *Journal of Biomolecular NMR*, *8*(4), 477-486. doi:10.1007/BF00228148
- Lederer, D. J., & Martinez, F. J. (2018). Idiopathic Pulmonary Fibrosis. *New England Journal of Medicine*, *378*(19), 1811-1823. doi:10.1056/NEJMra1705751

- Lee, H. M., Yu, M. S., Kazmi, S. R., Oh, S. Y., Rhee, K. H., Bae, M. A., Lee, B. H., Shin, D. S., Oh, K. S., Ceong, H., Lee, D., & Na, D. (2019). Computational determination of hERG-related cardiotoxicity of drug candidates. *BioMedCentral Bioinformatics*, *20*(Suppl 10), 250. doi:10.1186/s12859-019-2814-5
- Leleu-Chavain, N., Desreumaux, P., Chavatte, P., & Millet, R. (2013). Therapeutical potential of CB(2) receptors in immune-related diseases. *Current Molecular Pharmacology*, *6*(3), 183-203. doi:10.2174/1874467207666140219122337
- Ley, B., Collard, H. R., & King, T. E., Jr. (2011). Clinical course and prediction of survival in idiopathic pulmonary fibrosis. *American Journal of Respiratory and Critical Care Medicine*, *183*(4), 431-440. doi:10.1164/rccm.201006-0894CI
- Li, R., Chen, G., Zhou, L., Xu, H., Tang, F., Lan, J., Tong, R., Deng, L., Xue, J., & Lu, Y. (2017). The fatty acid amide hydrolase inhibitor URB937 ameliorates radiation-induced lung injury in a mouse model. *Inflammation*, *40*(4), 1254-1263. doi:10.1007/s10753-017-0568-7
- Li, Y., Su, M., Liu, Z., Li, J., Liu, J., Han, L., & Wang, R. (2018). Assessing protein–ligand interaction scoring functions with the CASF-2013 benchmark. *Nature Protocols*, *13*(4), 666-680. doi:10.1038/nprot.2017.114
- Lichtman, A. H., Leung, D., Shelton, C. C., Saghatelian, A., Hardouin, C., Boger, D. L., & Cravatt, B. F. (2004). Reversible inhibitors of fatty acid amide hydrolase that promote analgesia: evidence for an unprecedented combination of potency and selectivity. *Journal of Pharmacology and Experimental Therapeutics*, *311*(2), 441-448. doi:10.1124/jpet.104.069401
- Lipinski, C. A. (2000). Drug-like properties and the causes of poor solubility and poor permeability. *Journal of Pharmacological and Toxicological Methods*, *44*(1), 235-249. doi:10.1016/s1056-8719(00)00107-6
- Lipinski, C. A., Lombardo, F., Dominy, B. W., & Feeney, P. J. (1997). Experimental and computational approaches to estimate solubility and permeability in drug discovery and development settings. *Advanced Drug Delivery Reviews*, *23*(1), 3-25. doi:https://doi.org/10.1016/S0169-409X(96)00423-1
- Liu, T., De Los Santos, F. G., & Phan, S. H. (2017). The Bleomycin Model of Pulmonary Fibrosis. *Methods in Molecular Biology*, *1627*, 27-42. doi:10.1007/978-1-4939-7113-8\_2
- Lombardo, F., Desai, P. V., Arimoto, R., Desino, K. E., Fischer, H., Keefer, C. E., Petersson, C., Winiwarter, S., & Broccatelli, F. (2017). In silico absorption, distribution, metabolism, excretion, and pharmacokinetics (ADME-PK): Utility and best practices. An industry perspective from the International Consortium for Innovation through quality in pharmaceutical development. *Journal of Medicinal Chemistry*, *60*(22), 9097-9113. doi:10.1021/acs.jmedchem.7b00487
- Malkowski, M. G., Ginell, S. L., Smith, W. L., & Garavito, R. M. (2000). The productive conformation of arachidonic acid bound to prostaglandin synthase. *Science*, *289*(5486), 1933-1937. doi:10.1126/science.289.5486.1933
- Martín Giménez, V. M., Noriega, S. E., Kassuha, D. E., Fuentes, L. B., & Manucha, W. (2018). Anandamide and endocannabinoid system: an attractive therapeutic approach for cardiovascular disease. *Therapeutic Advances in Cardiovascular Disease*, *12*(7), 177-190. doi:10.1177/1753944718773690

- McAllister, S. D., Rizvi, G., Anavi-Goffer, S., Hurst, D. P., Barnett-Norris, J., Lynch, D. L., Reggio, P. H., & Abood, M. E. (2003). An aromatic microdomain at the cannabinoid CB(1) receptor constitutes an agonist/inverse agonist binding region. *Journal of Medicinal Chemistry*, *46*(24), 5139-5152. doi:10.1021/jm0302647
- McKinney, M. K., & Cravatt, B. F. (2003). Evidence for distinct roles in catalysis for residues of the serine-serine-lysine catalytic triad of fatty acid amide hydrolase. *Journal of Biological Chemistry*, *278*(39), 37393-37399. doi:10.1074/jbc.M303922200
- McKinney, M. K., & Cravatt, B. F. (2005). Structure and function of fatty acid amide hydrolase. *Annual Review Biochemistry*, *74*, 411-432. doi:10.1146/annurev.biochem.74.082803.133450
- McPhee, Kenny B.J. 25 July 2021, "ED50." *StatPearls*, <https://www.ncbi.nlm.nih.gov/books/NBK539699/>.
- Mileni, M., Kamtekar, S., Wood, D. C., Benson, T. E., Cravatt, B. F., & Stevens, R. C. (2010). Crystal structure of fatty acid amide hydrolase bound to the carbamate inhibitor URB597: Discovery of a deacylating water molecule and insight into enzyme inactivation. *Journal of Molecular Biology*, *400*(4), 743-754. doi:https://doi.org/10.1016/j.jmb.2010.05.034
- Mor, M., Rivara, S., Lodola, A., Plazzi, P. V., Tarzia, G., Duranti, A., Tontini, A., Piersanti, G., Kathuria, S., & Piomelli, D. (2004). Cyclohexylcarbamic acid 3'- or 4'-substituted biphenyl-3-yl esters as fatty acid amide hydrolase inhibitors: synthesis, quantitative structure-activity relationships, and molecular modeling studies. *Journal of Medicinal Chemistry*, *47*(21), 4998-5008. doi:10.1021/jm031140x
- Morales, P., Hurst, D. P., & Reggio, P. H. (2017). Molecular targets of the phytocannabinoids: A Complex Picture. *Progress in the Chemistry of Organic Natural Products*, *103*, 103-131. doi:10.1007/978-3-319-45541-9\_4
- Morisseau, C., Goodrow, M. H., Dowdy, D., Zheng, J., Greene, J. F., Sanborn, J. R., & Hammock, B. D. (1999). Potent urea and carbamate inhibitors of soluble epoxide hydrolases. *Proceedings of the National Academy of Sciences of the United States of America*, *96*(16), 8849-8854. doi:10.1073/pnas.96.16.8849
- Morisseau, C., Goodrow, M. H., Newman, J. W., Wheelock, C. E., Dowdy, D. L., & Hammock, B. D. (2002). Structural refinement of inhibitors of urea-based soluble epoxide hydrolases. *Biochemical Pharmacology*, *63*(9), 1599-1608. doi:10.1016/s0006-2952(02)00952-8
- Morisseau, C., & Hammock, B. D. (2008). Gerry Brooks and epoxide hydrolases: four decades to a pharmaceutical. *Pest Management Science*, *64*(6), 594-609. doi:10.1002/ps.1583
- Morisseau, C., & Hammock, B. D. (2013). Impact of soluble epoxide hydrolase and epoxyeicosanoids on human health. *Annual Review of Pharmacology and Toxicology*, *53*, 37-58. doi:10.1146/annurev-pharmtox-011112-140244
- Morphy, R., Kay, C., & Rankovic, Z. (2004). From magic bullets to designed multiple ligands. *Drug Discovery Today*, *9*(15), 641-651. doi:10.1016/S1359-6446(04)03163-0
- Morphy, R., & Rankovic, Z. (2005). Designed multiple ligands. An emerging drug discovery paradigm. *Journal of Medicinal Chemistry*, *48*(21), 6523-6543. doi:10.1021/jm058225d

- Mouratis, M. A., & Aidinis, V. (2011). Modeling pulmonary fibrosis with bleomycin. *Current Opinion in Pulmonary Medicine*, 17(5), 355-361. doi:10.1097/MCP.0b013e328349ac2b
- Navaratnam, V., Fleming, K. M., West, J., Smith, C. J., Jenkins, R. G., Fogarty, A., & Hubbard, R. B. (2011). The rising incidence of idiopathic pulmonary fibrosis in the U.K. *Thorax*, 66(6), 462-467. doi:10.1136/thx.2010.148031
- NIH. (2021). Idiopathic Pulmonary Fibrosis Phase 3 Trials. Retrieved from [https://clinicaltrials.gov/ct2/results?cond=Idiopathic+Pulmonary+Fibrosis&cntry=US&age\\_v=&ndr=&type=&rslt=&phase=2&Search=Apply](https://clinicaltrials.gov/ct2/results?cond=Idiopathic+Pulmonary+Fibrosis&cntry=US&age_v=&ndr=&type=&rslt=&phase=2&Search=Apply)
- Node, K., Huo, Y., Ruan, X., Yang, B., Spiecker, M., Ley, K., Zeldin, D. C., & Liao, J. K. (1999). Anti-inflammatory properties of cytochrome P450 epoxygenase-derived eicosanoids. *Science*, 285(5431), 1276-1279. doi:10.1126/science.285.5431.1276
- O'Boyle, N. M., & Meegan, M. J. (2011). Designed multiple ligands for cancer therapy. *Current Medicinal Chemistry*, 18(31), 4722-4737. doi:10.2174/092986711797535344
- Otrubova, K., Ezzili, C., & Boger, D. L. (2011). The discovery and development of inhibitors of fatty acid amide hydrolase (FAAH). *Bioorganic & Medicinal Chemistry Letters*, 21(16), 4674-4685. doi:https://doi.org/10.1016/j.bmcl.2011.06.096
- Palumbo-Zerr, K., Horn, A., Distler, A., Zerr, P., Dees, C., Beyer, C., Selvi, E., Cravatt, B. F., Distler, O., Schett, G., & Distler, J. H. (2012). Inactivation of fatty acid amide hydrolase exacerbates experimental fibrosis by enhanced endocannabinoid-mediated activation of CB1. *Annals of the Rheumatic Diseases*, 71(12), 2051-2054. doi:10.1136/annrheumdis-2012-201823
- Patsenker, E., Sachse, P., Chicca, A., Gachet, M. S., Schneider, V., Mattsson, J., Lanz, C., Worni, M., de Gottardi, A., Semmo, M., Hampe, J., Schafmayer, C., Brenneisen, R., Gertsch, J., Stickel, F., & Semmo, N. (2015). Elevated levels of endocannabinoids in chronic hepatitis C may modulate cellular immune response and hepatic stellate cell activation. *International Journal of Molecular Sciences*, 16(4), 7057-7076. doi:10.3390/ijms16047057
- Pecic, S., Deng, S.-X., Morisseau, C., Hammock, B. D., & Landry, D. W. (2012). Design, synthesis and evaluation of non-urea inhibitors of soluble epoxide hydrolase. *Bioorganic and Medicinal Chemistry Letters*, 22(1), 601-605. doi:https://doi.org/10.1016/j.bmcl.2011.10.074
- Pecic, S., Pakhomova, S., Newcomer, M. E., Morisseau, C., Hammock, B. D., Zhu, Z., Rinderspacher, A., & Deng, S.-X. (2013). Synthesis and structure–activity relationship of piperidine-derived non-urea soluble epoxide hydrolase inhibitors. *Bioorganic and Medicinal Chemistry Letters*, 23(2), 417-421. doi:https://doi.org/10.1016/j.bmcl.2012.11.084
- Pecic, S., Zeki, A. A., Xu, X., Jin, G. Y., Zhang, S., Kodani, S., Halim, M., Morisseau, C., Hammock, B. D., & Deng, S.-X. (2018). Novel piperidine-derived amide sEH inhibitors as mediators of lipid metabolism with improved stability. *Prostaglandins and Other Lipid Mediators*, 136, 90-95. doi:https://doi.org/10.1016/j.prostaglandins.2018.02.004
- Pertwee, R. G. (2010). Receptors and channels targeted by synthetic cannabinoid receptor agonists and antagonists. *Current Medicinal Chemistry*, 17(14), 1360-1381. doi:10.2174/092986710790980050
- Peters, J. U. (2013). Polypharmacology - foe or friend? *Journal of Medicinal Chemistry*, 56(22), 8955-8971. doi:10.1021/jm400856t

- Piomelli, D. (2003). The molecular logic of endocannabinoid signalling. *Nature Reviews Neuroscience*, 4(11), 873-884. doi:10.1038/nrn1247
- Piomelli, D., & Sasso, O. (2014). Peripheral gating of pain signals by endogenous lipid mediators. *Nature Neuroscience*, 17(2), 164-174. doi:10.1038/nn.3612
- Pontius, J., Richelle, J., & Wodak, S. J. (1996). Deviations from standard atomic volumes as a quality measure for protein crystal structures. *Journal of Molecular Biology*, 264(1), 121-136. doi:10.1006/jmbi.1996.0628
- Portoghese, P. S., Larson, D. L., Sayre, L. M., Yim, C. B., Ronsisvalle, G., Tam, S. W., & Takemori, A. E. (1986). Opioid agonist and antagonist bivalent ligands. The relationship between spacer length and selectivity at multiple opioid receptors. *Journal of Medicinal Chemistry*, 29(10), 1855-1861. doi:10.1021/jm00160a010
- Prevention, C. f. D. C. a. (2021). People with Certain Medical Conditions. Retrieved from <https://www.cdc.gov/coronavirus/2019-ncov/need-extra-precautions/people-with-medical-conditions.html>
- Proschak, E., Stark, H., & Merk, D. (2019). Polypharmacology by Design: A Medicinal Chemist's Perspective on Multitargeting Compounds. *Journal of Medicinal Chemistry*, 62(2), 420-444. doi:10.1021/acs.jmedchem.8b00760
- Raghu, G., Chen, S. Y., Hou, Q., Yeh, W. S., & Collard, H. R. (2016). Incidence and prevalence of idiopathic pulmonary fibrosis in US adults 18-64 years old. *European Respiratory Journal*, 48(1), 179-186. doi:10.1183/13993003.01653-2015
- Raghu, G., Chen, S. Y., Yeh, W. S., Maroni, B., Li, Q., Lee, Y. C., & Collard, H. R. (2014). Idiopathic pulmonary fibrosis in US Medicare beneficiaries aged 65 years and older: incidence, prevalence, and survival, 2001-11. *Lancet Respiratory Medicine*, 2(7), 566-572. doi:10.1016/S2213-2600(14)70101-8
- Reggio, P. H. (2010). Endocannabinoid binding to the cannabinoid receptors: what is known and what remains unknown. *Current Medicinal Chemistry*, 17(14), 1468-1486. doi:10.2174/092986710790980005
- Rossi, A., Pergola, C., Koeberle, A., Hoffmann, M., Dehm, F., Bramanti, P., Cuzzocrea, S., Werz, O., & Sautebin, L. (2010). The 5-lipoxygenase inhibitor, zileuton, suppresses prostaglandin biosynthesis by inhibition of arachidonic acid release in macrophages. *British Journal of Pharmacology*, 161(3), 555-570. doi:10.1111/j.1476-5381.2010.00930.x
- Sasso, O., Wagner, K., Morisseau, C., Inceoglu, B., Hammock, B. D., & Piomelli, D. (2015). Peripheral FAAH and soluble epoxide hydrolase inhibitors are synergistically antinociceptive. *Pharmacological Research*, 97, 7-15. doi:https://doi.org/10.1016/j.phrs.2015.04.001
- Savage, S. A., & Alter, B. P. (2009). Dyskeratosis congenita. *Hematology/Oncology Clinics of North America*, 23(2), 215-231. doi:10.1016/j.hoc.2009.01.003
- Scarpino, A., Ferenczy, G. G., & Keserű, G. M. (2018). Comparative evaluation of covalent docking tools. *Journal of Chemical Information and Modeling*, 58(7), 1441-1458. doi:10.1021/acs.jcim.8b00228

- Schapira, M., Totrov, M., & Abagyan, R. (1999). Prediction of the binding energy for small molecules, peptides and proteins. *Journal of Molecular Recognition*, 12(3), 177-190. doi:10.1002/(SICI)1099-1352(199905/06)12:3<177::AID-JMR451>3.0.CO;2-Z
- Scotter, E. L., Abood, M. E., & Glass, M. (2010). The endocannabinoid system as a target for the treatment of neurodegenerative disease. *British Journal of Pharmacology*, 160(3), 480-498. doi:https://doi.org/10.1111/j.1476-5381.2010.00735.x
- Shammas, M. A. (2011). Telomeres, lifestyle, cancer, and aging. *Current Opinion in Clinical Nutrition and Metabolic Care*, 14(1), 28-34. doi:10.1097/MCO.0b013e32834121b1
- Shen, H. C., Ding, F. X., Deng, Q., Xu, S., Chen, H. S., Tong, X., Tong, V., Zhang, X., Chen, Y., Zhou, G., Pai, L. Y., Alonso-Galicia, M., Zhang, B., Roy, S., Tata, J. R., Berger, J. P., & Colletti, S. L. (2009). Discovery of 3,3-disubstituted piperidine-derived trisubstituted ureas as highly potent soluble epoxide hydrolase inhibitors. *Bioorganic & Medicinal Chemistry Letters*, 19(18), 5314-5320. doi:10.1016/j.bmcl.2009.07.138
- Somogyi, V., Chaudhuri, N., Torrissi, S. E., Kahn, N., Muller, V., & Kreuter, M. (2019). The therapy of idiopathic pulmonary fibrosis: what is next? *European Respiratory Review*, 28(153). doi:10.1183/16000617.0021-2019
- Spagnolo, P., Balestro, E., Aliberti, S., Cocconcelli, E., Biondini, D., Casa, G. D., Sverzellati, N., & Maher, T. M. (2020). Pulmonary fibrosis secondary to COVID-19: a call to arms? *Lancet Respiratory Medicine*, 8(8), 750-752. doi:10.1016/S2213-2600(20)30222-8
- Spector, A. A., Fang, X., Snyder, G. D., & Weintraub, N. L. (2004). Epoxyeicosatrienoic acids (EETs): metabolism and biochemical function. *Progress in Lipid Research*, 43(1), 55-90. doi:10.1016/s0163-7827(03)00049-3
- Tait, R. J., Caldicott, D., Mountain, D., Hill, S. L., & Lenton, S. (2016). A systematic review of adverse events arising from the use of synthetic cannabinoids and their associated treatment. *Clinical Toxicology (Phila)*, 54(1), 1-13. doi:10.3109/15563650.2015.1110590
- Takebe, T., Imai, R., & Ono, S. (2018). The current status of drug discovery and development as originated in United States academia: The influence of industrial and academic collaboration on drug discovery and development. *Clinical and Translational Science*, 11(6), 597-606. doi:https://doi.org/10.1111/cts.12577
- van Breemen, R. B., & Li, Y. (2005). Caco-2 cell permeability assays to measure drug absorption. *Expert Opinion on Drug Metabolism & Toxicology*, 1(2), 175-185. doi:10.1517/17425255.1.2.175
- Veber, D. F., Johnson, S. R., Cheng, H. Y., Smith, B. R., Ward, K. W., & Kopple, K. D. (2002). Molecular properties that influence the oral bioavailability of drug candidates. *Journal of Medicinal Chemistry*, 45(12), 2615-2623. doi:10.1021/jm020017n
- Verma, A. A., Khuu, W., Tadrous, M., Gomes, T., & Mamdani, M. M. (2018). Fixed-dose combination antihypertensive medications, adherence, and clinical outcomes: a population-based retrospective cohort study. *Public Library of Science Medicine*, 15(6), e1002584.
- Vriend, G., & Sander, C. (1993). Quality control of protein models : directional atomic contact analysis. *Journal of Applied Crystallography*, 26, 47-60.

- Wagner, K., Inceoglu, B., Gill, S. S., & Hammock, B. D. (2011). Epoxygenated fatty acids and soluble epoxide hydrolase Inhibition: Novel mediators of pain reduction. *Journal of Agricultural and Food Chemistry*, *59*(7), 2816-2824. doi:10.1021/jf102559q
- Wagner, K. M., McReynolds, C. B., Schmidt, W. K., & Hammock, B. D. (2017). Soluble epoxide hydrolase as a therapeutic target for pain, inflammatory and neurodegenerative diseases. *Pharmacology & Therapeutics*, *180*, 62-76. doi:10.1016/j.pharmthera.2017.06.006
- Walker, J. M., Huang, S. M., Strangman, N. M., Tsou, K., & Sañudo-Peña, M. C. (1999). Pain modulation by release of the endogenous cannabinoid anandamide. *Proceedings of the National Academy of Sciences of the United States of America*, *96*(21), 12198-12203. doi:10.1073/pnas.96.21.12198
- Wan, D., Yang, J., McReynolds, C. B., Barnych, B., Wagner, K. M., Morisseau, C., Hwang, S. H., Sun, J., Blöcher, R., & Hammock, B. D. (2019). In vitro and in vivo Metabolism of a Potent Inhibitor of Soluble Epoxide Hydrolase, 1-(1-Propionylpiperidin-4-yl)-3-(4-(trifluoromethoxy)phenyl)urea. *Frontiers in Pharmacology*, *10*, 464-464. doi:10.3389/fphar.2019.00464
- Wang, X., Sarris, K., Kage, K., Zhang, D., Brown, S. P., Kolasa, T., . . . Stewart, A. O. (2009). Synthesis and evaluation of benzothiazole-based analogues as novel, potent, and selective fatty acid amide hydrolase inhibitors. *Journal of Medicinal Chemistry*, *52*(1), 170-180. doi:10.1021/jm801042a
- Wang, Y., Wagner, K. M., Morisseau, C., & Hammock, B. D. (2021). Inhibition of the soluble epoxide hydrolase as an analgesic strategy: A review of preclinical evidence. *Journal of Pain Research*, *14*, 61-72. doi:10.2147/jpr.S241893
- Wenzel, D., Matthey, M., Bindila, L., Lerner, R., Lutz, B., Zimmer, A., & Fleischmann, B. K. (2013). Endocannabinoid anandamide mediates hypoxic pulmonary vasoconstriction. *Proceedings of the National Academy of Sciences of the United States of America*, *110*(46), 18710-18715. doi:10.1073/pnas.1308130110
- Wills, T. J., & Lipkus, A. H. (2020). Structural approach to assessing the innovativeness of new drugs finds accelerating rate of innovation. *ACS Medicinal Chemistry Letters*, *11*(11), 2114-2119. doi:10.1021/acsmchemlett.0c00319
- Wilt, S. R., Rodriguez, M., Le, T. N. H., Baltodano, E. V., Salas, A., & Pecic, S. (2020). Design, microwave-assisted synthesis, biological evaluation and molecular modeling studies of 4-phenylthiazoles as potent fatty acid amide hydrolase inhibitors. *Chemical Biology & Drug Design*, *95*(5), 534-547. doi:10.1111/cbdd.13670
- Wolters, P. J., Blackwell, T. S., Eickelberg, O., Loyd, J. E., Kaminski, N., Jenkins, G., . . . Schwartz, D. A. (2018). Time for a change: is idiopathic pulmonary fibrosis still idiopathic and only fibrotic? *Lancet Respiratory Medicine*, *6*(2), 154-160. doi:10.1016/S2213-2600(18)30007-9
- Xie, Y., Liu, Y., Gong, G., Smith, D. H., Yan, F., Rinderspacher, A., Feng, Y., Zhu, Z., Li, X., Deng, S.-X., Branden, L., Vidović, D., Chung, C., Schürer, S., Morisseau, C., Hammock, B. D., & Landry, D. W. (2009). Discovery of potent non-urea inhibitors of soluble epoxide hydrolase. *Bioorganic and Medicinal Chemistry Letters*, *19*(8), 2354-2359. doi:https://doi.org/10.1016/j.bmcl.2008.09.066



- Xu, W., Lucke, A. J., & Fairlie, D. P. (2015). Comparing sixteen scoring functions for predicting biological activities of ligands for protein targets. *Journal of Molecular Graphics and Modelling*, 57, 76-88. doi:<https://doi.org/10.1016/j.jmglm.2015.01.009>
- Zhou, Y., Yang, J., Sun, G. Y., Liu, T., Duan, J. X., Zhou, H. F., Lee, K. S., Hammock, B. D., Fang, X., Jiang, J. X., & Guan, C. X. (2016). Soluble epoxide hydrolase inhibitor 1-trifluoromethoxyphenyl-3-(1-propionylpiperidin-4-yl) urea attenuates bleomycin-induced pulmonary fibrosis in mice. *Cell and Tissue Research*, 363(2), 399-409. doi:10.1007/s00441-015-2262-0
- Zurier, R. B., & Burstein, S. H. (2016). Cannabinoids, inflammation, and fibrosis. *Federation of American Societies for Experimental Biology*, 30(11), 3682-3689. doi:10.1096/fj.201600646R